PROGRAM OF THE CONFERENCE

Wednesday, September 26

9.00 *Opening*
9.15 P. Kroupa
10.00 M. López-Corredoira
10.45 *Coffee Break*
11.15 S. Capozziello
12.00 M. S. Pawlowski
12.20 *Lunch Break*
14.00 F. Lelli
14.45 I. Goldman
15.30 W. Oehm
15.50 *Coffee Break*
16.20 J. Dabringhausen
16.40 M. Haslbauer
17.00 Y. V. Dumin
17.20 M. Feldman
17.40 E. J. Lerner
18.00 M. Křížek

Thursday, September 27

9.00 A. A. Starobinsky
9.45 L. Marochnik
10.30 *Coffee Break*
10.55 Y. V. Dumin
11.15 S. J. Roblez-Perez
12.00 K. Morawetz
12.20 *Lunch Break*
14.00 B. Famaey
14.45 I. Karachentsev
15.30 L. Makarova
16.00 D. Makarov
16.30 *Coffee Break*
17.00 A. Maeder

Friday, September 28

9.00 A. D. A. M. Spallicci
9.45 Ł. Bratek
10.30 *Coffee Break*
11.00 A. Maeder
12.00 P. Magain
12.15 *Lunch Break*
14.00 S. McGaugh
14.45 O. Tsupko
15.15 T. Prevenslik
15.30 R. J. Wojtak
15.45 A. Mészáros
16.00 *Coffee Break*
16.30 *Short Communications*

Saturday, September 29

9.00 – 12.00 Excursion to the astronomical and cosmological sights of Prague

Prague's Horologe: Cosmological model from the 15th century

ISBN 978-80-85823-68-4

COSMOLOGY ON SMALL SCALES 2018

Proceedings of the International Conference

Cosmology on Small Scales 2018

Dark Matter Problem and Selected Controversies in Cosmology

Prague, September 26–29, 2018

Edited by
Michal Křížek and Yurii V. Dumin

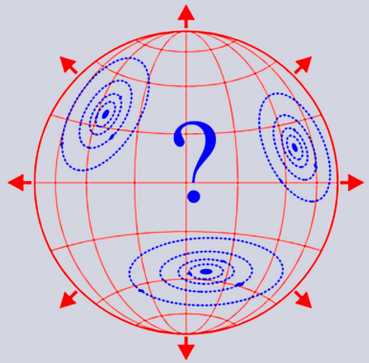

Institute of Mathematics
Czech Academy of Sciences

Proceedings of the International Conference

COSMOLOGY ON SMALL SCALES 2018

Dark Matter Problem and Selected Controversies in Cosmology

Prague, September 26–29, 2018

Edited by
Michal Křížek and Yurii V. Dumin

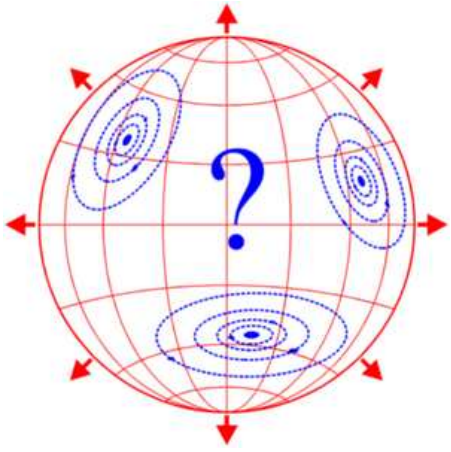

Institute of Mathematics
Czech Academy of Sciences
Prague 2018

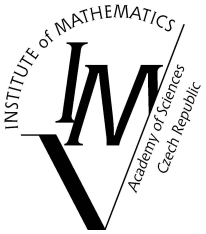

ISBN 978-80-85823-68-4
Institute of Mathematics
Czech Academy of Sciences
Prague 2018
LaTeX typesetting prepared by Hana Bílková

Dedicated to Prof. Lawrence Somer on his 70th birthday

CONTENTS

Alternative cosmological theories

Preface

Whoever claims to understand cosmology
only proves he has not understood anything at all.

Antonín Vrba
(Paraphrased quotation of Richard Feynman)

According to the standard cosmological model, our Universe needs a significant amount of dark matter, about six times more than that of the usual baryonic matter, besides an even larger amount of dark energy. But to date, both dark matter and dark energy have remained conceptually elusive, without concrete evidence based on direct physical measurements. Yet another subtle issue is that the Friedmann equation – the cornerstone of modern cosmology – was derived from the system of ten Einstein's equations applied to a perfectly symmetric universe, which is homogeneous and isotropic for every fixed time instant. So, the question is whether one can perform such excessive extrapolations and, in particular, at which scale the effect of Hubble expansion is manifested.

Therefore, it is timely to gather specialists from different disciplines – ranging from galaxy evolution to planetology and from empirical statistics to quantum field theory – to discuss the problem of existence and observable manifestations of dark matter and dark energy at various scales (particularly, in our local cosmic neighborhood), both from the theoretical and observational points of view. To bring more light into these topics, we decided to organize the International Conference *Cosmology on Small Scales 2018: Dark Matter Problem and Selected Controversies in Cosmology*. It was held at the Institute of Mathematics of the Czech Academy of Sciences in Žitná 25, Prague 1, from 26 to 29 September 2018 (see `css2018.math.cas.cz`). This was a continuation of our previous conference *Cosmology on Small Scales 2016: Local Hubble Expansion and Selected Controversies in Cosmology*, which took place two years ago (see `css2016.math.cas.cz`).

The main topics of the new conference "Cosmology on Small Scales 2018" were: mathematical aspects of cosmological phenomena at various scales; arguments for and against dark matter, and revisiting the foundations of physics; alternative models for dark matter and dark energy; a systematic discord in the value of the Hubble constant at various scales; complementary redshifts of non-cosmological nature; quantum effects on the early universe and their observational imprints nowadays. In particular, in these Proceedings we present several papers showing that the claimed amount of dark matter can be a result of vast overestimation and does not conform to reality.

In fact, only a fraction of the presented reports is included into these Proceedings; another part has been already published elsewhere, and their authors preferred to avoid duplicate publication. At the end of the Proceedings, there are several papers on "alternative cosmological theories". Although they may be questionable and

the Scientific Committee is not responsible for their content, we believe that it is reasonable to present them to the wide audience.

The Scientific Committee consisted of

Dr. Yurii Dumin (Moscow State University & Russian Academy of Sciences, Russia)
Prof. Itzhak Goldman (Afeka College, Israel)
Prof. Igor Karachentsev (Special Astrophysical Observatory of RAS, Russia)
Prof. Jaroslav Klokočník (Astronomical Institute of CAS, Czech Republic)
Prof. Sergei Kopeikin (University of Missouri, USA)
Prof. Pavel Kroupa (University of Bonn, Germany)
Prof. André Maeder (Geneva Observatory, Switzerland)
Assoc. Prof. Attila Mészáros (Charles University, Czech Republic)
Prof. Marek Nowakowski (Universidad de los Andes, Colombia)
Prof. Jan Palouš (Astronomical Institute of CAS, Czech Republic)
Prof. Alessandro Spallicci (University of Orleans, CNRS, France)

Local Organizing Committee consisted of

Prof. Michal Křížek — Chair (Czech Academy of Sciences, Czech Republic)
Dr. Yurii Dumin — Vice-Chair (Moscow State University & Russian Academy of Sciences, Russia)
Assoc. Prof. Tomáš Vejchodský (Czech Academy of Sciences, Czech Republic)
Hana Bílková (Institute of Computer Science of CAS, Czech Republic)

The Local Organizing Committee is deeply grateful to all authors for their contributions and the support of RVO 67985840 (Institute of Mathematics of the Czech Academy of Sciences). Out sincere thanks go also to all active members of the Cosmological Section of the Czech Astronomical Society for their continual help. Finally, we are indebted to Hana Bílková for technical assistance in the final typesetting and Tomáš Vejchodský for his helpful cooperation.

These Proceedings can be downloaded from the website:

`http://users.math.cas.cz/~krizek/list.html`

Michal Křížek and Yurii V. Dumin

Conference *Cosmology on Small Scales 2018*
Michal Křížek and Yurii Dumin (Eds.)
Institute of Mathematics CAS, Prague

SEVEN DECADES OF PROFESSOR LAWRENCE SOMER

Michal Křížek

Institute of Mathematics, Czech Academy of Sciences, Žitná 25,
CZ-115 67 Prague 1, Czech Republic, krizek@math.cas.cz

We do not count a man's years, until he has nothing else to count.

Ralph Waldo Emerson, 1803–1882

Days, hours, minutes, seconds, ... how many of them are there? A man full of scientific idealism arose from a boy. He established his direction of research and set off on a journey to find the unknown. He lived, worked, and published. His knowledge and experience reached a very high level. He has a large range of vision, bird's-eye view, and clearly sees all circumstances. He knows how and where to tackle the problem. He feels the enthusiasm of his colleagues and includes his own, spiced by knowledge and practice. He stands at the birth of new theories, he is young, really young ... This is Professor Lawrence Somer, Larry, as his friends call him.

The first time I met Larry was in 1999 at the Institute of Mathematics of the Czech Academy of Sciences. We immediately found that our interests have many intersections. From that time we wrote over 30 scientific papers on number theory, and also astronomy and cosmology, see e.g. [8]–[20], six monographs [2]–[7], and over 20 papers popularizing exact sciences. The monograph [2] appeared in the prestigious publishing house Springer-Verlag in New York in 2001. Its second edition was published in 2011. Our second monograph [3] even got a third edition. It contains many applications of number theory to solve real-life technical problems. Recently we have published also two monographs [4] and [6] on cosmology.

Professor Lawrence Somer, PhD., was born on October 10, 1948, in New York City. He has been fascinated by astronomy since his youth. He considers astronomy to be like a secular religion, since astronomical events take place on an almost inconceivably vast scale. He has read popular journals on astronomy such as Scientific American and Astronomy Magazine since his teenage years. In 1966–1970 he studied mathematics at Cornell University in Ithaca in New York State and got a B.A. degree cum laude in mathematics. In 1972 he received his M.A. in mathematics from the University of Illinois. During the period 1970–1975 Larry worked as Graduate Teaching Assistant in Mathematics at the University of Illinois, Champaign-Urbana. Then he was a mathematical statistician in the U.S. Department of Agriculture in Washington, D.C. In 1985 he received his PhD. degree from the University of Illinois. The title of his doctoral dissertation is: *The divisibility and modular properties of kth-order linear recurrences over the ring of integers of an algebraic number field with respect to prime ideals.* His supervisor was Professor Ernest Tilder Parker. During the period 1984–1986 Lawrence Somer was visiting Assistant Professor of Mathematics at George Washington University in Washington, D.C. From 1986 to 2009 he taught mathematics at the Catholic University of America, Washington, D. C., and became full Professor in 1995. At present, he is Professor Emeritus of Mathematics there.

Our long-term collaboration started on problems in number theory. Some of our main results are surveyed in [1]. Then we concentrated on the mathematical model of the astronomical clock in Prague in connection with its 600 year anniversary, see [12]. In [8] we introduced the term *Šindel sequence* named after Jan Šindel who invented the mathematical model of the Prague horologe around 1410. Now this term appears also in the On-line Encyclopedia of Integer Sequences (A028355, A028356). We also derived a necessary and sufficient condition for a periodic sequence to be a Šindel sequence.

In Washington, D.C., Larry Somer visited an astrophysical seminar for 10 years. This enabled him to employ mathematical methods in astronomy and cosmology. This seminar was also visited by Vera Rubin whose revolutionary ideas essentially changed the theory of flat rotational curves of spiral galaxies. Later we wrote the paper [17] on this topic. We calculated the gravitational potential of a flat disk with symmetric distribution of mass density. Then we showed that the observed flat rotational curves of spiral galaxies can also be explained without hypothetical nonbaryonic dark matter.

Ten years ago, I showed Larry how to derive the Friedmann equation from Einstein's equations. Then I introduced to him the cosmological parameters $\Omega_{\rm M}$ and Ω_Λ that represent the density of dark matter and dark energy. These parameters are obtained from the Friedmann equation. He looked at me and said:

Oh I see, dark matter and dark energy exist by definition.

I think he is right. Larry as a mathematician is able to disregard inessential things. His clear thinking allows to penetrate into the heart of the matter. From that time we seek for various controversies of the standard cosmological model.

Professor Somer is a member of the Editorial Board of the journal The Fibonacci Quarterly. The *Somer pseudoprimes* and *Somer–Lucas pseudoprimes* are called after him (see e.g. Wikipedia, Wolfram Mathworld, or the famous 1996 Ribenboim monograph, or CRC Concise Encyclopedia of Mathematics, 2003, p. 2756). Lawrence Somer wrote over 100 scientific papers (88 of them are recorded in the database of Mathematical Reviews). His Erdős number is 2 (he wrote a paper with the outstanding Polish mathematician Professor Andrzej Schinzel who is a coauthor of Paul Erdős). Lawrence has also a paper with Peter Hilton who collaborated with Alan Turing and several papers with Florian Luca who has over 600 records in Mathematical Reviews.

In January 2018, Prof. L. Somer was elected a foreign member of the Cosmological Section of the Czech Astronomical Society (see `users.math.cas.cz/~krizek/cosmol/seznam.html`). He has been a member of the American Mathematical Society, the Mathematical Association of America, and the Union of Czech Mathematicians and Physicists. He has also been a member of Phi Kappa Phi National Honor Society, Treasurer of the Catholic University of America Chapter of Sigma Xi Scientific Research Society, the Chair of Undergraduate Committee of the Mathematics Department at the Catholic University of America, and the Chair of Senate Faculty and Economic Welfare Committee of the Catholic University of America. In 2009 he was awarded the Josef Hlávka Literary Prize for the best scientific book published in the Czech Republic in the category of the science of inanimate nature for the monograph [3].

Felicitations: It is my privilege and honor to congratulate Professor Lawrence Somer sincerely on his 70th birthday. I wish him good health and happiness for many years to come. Meeting him was my great life luck.

Acknowledgement. The author is indebted to Jan Brandts and Jana Žďárská for careful reading and valuable suggestions. The paper was supported by RVO 67985840 of the Czech Republic.

References

Proceedings

[1] Somer, L.: My twelve years of collaboration with Michal Křížek on number theory. Prof. Conf. Appl. Math. 2012, Eds. J. Brandts et al., Inst. of Math., Prague, 2012, 267–277.

Monographs

[2] Křížek, M., Luca, F., Somer, L.: *17 lectures on Fermat numbers. From number theory to geometry*, CMS Books in Mathematics, vol. 9, Springer-Verlag, New York, 2001, xxiv+257 pp., second edition 2011.

[3] Křížek, M., Somer, L., Šolcová, A.: *The magic of numbers. From great discoveries to applications*. Edice Galileo, vol. 39, Academia, Prague, 2009, 365 + VIII pp., second edition 2011, third edition 2018. (In Czech.)

[4] Vishwakarma, R. G., Křížek, M., Brandts, J., Somer, L., Greben, J. M., Lee, S., Mitsou, V. A., Mavromatos, N. E., Shalyt-Margolin, A. E.: *Dark energy. Theory, implications and roles in cosmology*. Eds. C. A. Del Valle, D. F. Longoria, Nova Sci. Publ., New York, 2012, 170 pp.

[5] Křížek, M., Somer, L., Markl, M., Kowalski, O., Pudlák, P., Vrkoč, I.: *The first ten Abel prizes for mathematics*. Union of Czech Mathematicians and Physicists, Prague, 2013, 88 pp. (In Czech.)

[6] Křížek, M., Křížek, F., Somer, L.: *Antigravity — Its origin and manifestations*. Lambert Acad. Publ., Saarbrücken, 2015, xiv + 348 pp.

[7] Křížek, M., Somer, L., Markl, M., Kowalski, O., Pudlák, P., Vrkoč, I.: *The Abel Prize — the highest achievement in mathematics*. Academia, Prague, 2018, 219 pp. (In Czech.)

Some Papers on Astronomy and Cosmology

[8] Křížek, M., Šolcová, A., Somer, L.: Construction of Šindel sequences. Comment. Math. Univ. Carolin. 48 (2007), 373–388.

[9] Křížek, M., Šolcová, A., Somer, L.: What mathematics is hidden behind the astronomical clock of Prague? Highlights of Astronomy, vol. 14, SPS2 - Innovation in Teaching and Learning Astronomy (eds. R. M. Ros and J. M. Pasachoff), Proc. of the IAU XXVIth General Assembly in Prague, August 2006, Cambridge Univ. Press, 2007, p. 575, also in: J. M. Pasachoff, R. M. Ros, and N. Pasachoff, Innovation in Astronomy Education, Cambridge Univ. Press, 2008, 142–143.

[10] Křížek, M., Somer, L., Šolcová, A.: Ten mathematical theorems on the Prague horologe. Pokroky Mat. Fyz. Astronom. 54 (2009), 281–300.

[11] Křížek, M., Šolcová, A., Somer, L.: The mathematics behind Prague's horologe (in Chinese and English). Math. Culture 1 (2010), No. 2, 69–77.

[12] Křížek, M., Šolcová, A., Somer, L.: 600 years of Prague's horologe and the mathematics behind it. Math. Spectrum 44 (2011/2012), 28–33.

[13] Křížek, M., Somer, L.: Antigravity – its manifestations and origin. Internat. J. Astron. Astrophys. 3 (2013), 227–235.

[14] Křížek, M., Křížek, F., Somer, L.: Which effects of galaxy clusters can reduce the amount of dark matter. Bulg. Astron. J. 21 (2014), 43–65.

[15] Křížek, M., Somer, L.: A critique of the standard cosmological model. Neural Netw. World 24 (2014), 435–461.

[16] Křížek, M., Somer, L.: Manifestations of dark energy in the Solar system. Gravit. Cosmol. 21 (2015), 59–72.

[17] Křížek, M., Křížek, F., Somer, L.: Dark matter and rotation curves of spiral galaxies. Bulg. Astron. J. 25 (2016), 64–77.

[18] Křížek, M., Somer, L.: Excessive extrapolations in cosmology. Gravit. Cosmol. 22 (2016), 270–280.

[19] Křížek, M., Somer, L.: Anthropic principle and the local Hubble expansion. Proc. Conf. Cosmology on Small Scales 2016, Local Hubble Expansion and Selected Controversies in Cosmology (eds. M. Křížek, Y. V. Dumin), Inst. of Math., Prague, 2016, 65–94.

[20] Křížek, M., Somer, L.: Neglected gravitational redshift in detections of gravitational waves. Proc. Conf. Cosmology on Small Scales 2018, Dark Matter Problem and Selected Controversies in Cosmology (eds. M. Křížek, Y. V. Dumin), Inst. of Math., Prague, 2018, 173–179.

Conference *Cosmology on Small Scales 2018*
Michal Křížek and Yurii Dumin (Eds.)
Institute of Mathematics CAS, Prague

PROBLEMS WITH THE DARK MATTER AND DARK ENERGY HYPOTHESES, AND ALTERNATIVE IDEAS

Martín López-Corredoira[1,2]

[1] Instituto de Astrofísica de Canarias
C/.Vía Láctea, s/n, E-38205 La Laguna, Tenerife, Spain
martinlc@iac.es
[2] Department of Astrophysics, University of La Laguna
E-38206 La Laguna, Tenerife, Spain

Abstract: Two exotic elements have been introduced into the standard cosmological model: non-baryonic dark matter and dark energy. The success in converting a hypothesis into a solid theory depends strongly on whether we are able to solve the problems in explaining observations with these dark elements and whether the solutions of these problems are unique within the standard paradigm without recourse to alternative scenarios. We have not achieved that success yet because of numerous inconsistencies, mainly on galactic scales, the non-detection so far of candidate particles for dark matter, and the existence of many alternative hypotheses that might substitute the standard picture to explain the cosmological observations. A review of some ideas and facts is given here.

Keywords: dark matter, dark energy

PACS: 95.35.+d, 95.36.+x

1. History of the idea of dark matter

The existence of dark or invisible matter detectable through its gravitational influence has been known by astronomers for a long time now [14]. Bessel [15] in 1844 argued that the observed proper motions of the stars Sirius and Procyon could be explained only in terms of the presence of faint companion stars. In 1846, Le Verrier and Adams independently predicted the existence of Neptune based on calculations of the anomalous motions of Uranus. Le Verrier later proposed the existence of the planet Vulcan to explain anomalies in the orbit of Mercury, but he failed this time because the solution was not invisible matter but a change of gravitational laws, as was solved years later by Einstein with General Relativity. The dynamical analysis of dark matter in form of faint stars in the Milky Way using the motion of stars was

carried out by Lord Kelvin in 1904, Poincaré in 1906, Öpik in 1915, Kapteyn in 1922, Jeans in 1922, Lindblad in 1926, and Oort in 1932 with different results [14].

With regard to extragalactic astronomy, Zwicky's [100] 1933 paper on dark matter in rich clusters applied the virial theorem to these data and found a mass-to-light ratio of ∼60 in solar units (rescaled to the present-day value of the Hubble constant). In 1959 Kahn & Woltjer [39] determined the mass of the Local Group and obtained a mass-to-light ratio of 43 in solar units. In the 1950s, Page [71], [72] also found that pairs of elliptical galaxies had a mass-to-light ratio of 66 in solar units. This showed that such binaries must have massive envelopes or be embedded in a massive common envelope. Similar results were obtained in the 1950s from 26 binary galaxies by Holmberg [36]. In 1939 Babcock [5] first showed the need for dark matter for an individual galaxy by measuring the rotation curve of the outer regions of M31 out to 100 arcminutes (≈ 20 kpc) from its center. However, the majority of astronomers did not become convinced of the need for dark matter halos in galaxies until the publication of theoretical papers in the 1970s, such as the one on the stability of galactic disks by Ostriker & Peebles [69]. Later, rotation curves in the radio by Albert Bosma [18] and in the visible by Vera Rubin, Kent Ford, and Nortbert Thonnard [79] easily convinced the community. This shows the typical mentality of astrophysicists: accepting facts only when there is a theory to support them with an explanation, a not-so-empirical approach that dominates the development of cosmology.

Cosmology has indeed played a very important role in the idea of dark matter on galactic scales. The first predictions based on Cosmic Microwave Background Radiation (CMBR) anisotropies were wrong. It was predicted in the 1960s that $\Delta T/T$ should be one part in a hundred or a thousand [80]; however, fluctuations with this amplitude could not be found from observations in the 1970s. In order to solve this problem, non-baryonic dark matter was introduced *ad hoc* and was thought to be composed of certain mysterious particles different from known matter. In a short time, the connection between particle physics and the missing mass problem in galaxies arose. Many astrophysicists considered dark matter halos surrounding galaxies and galaxy clusters possibly to consist of a gas of non-baryonic particles rather than faint stars or other astrophysical objects. This was a happy idea without any proof; there is no proof that directly connects the problem of the amplitude of CMBR anisotropies with the rotation curves of galaxies or the missing mass in clusters, but the idea was pushed by leading cosmologists, who made the idea fashionable among the rest of the astrophysical community.

Part of the success of these non-baryonic dark matter scenarios in the halos of the galaxies was due to the good agreement of simulations of large scale structure with the observed distributions of galaxies. At first, in the 1980s, with the attempt to fit the data using hot dark matter composed of neutrinos, the simulations showed that very large structures should be formed first and only later go on to form galaxy-sized halos through fragmentation, which did not match the observations [99], whereas cold dark matter (CDM) models were more successful, at least on large scales ($> 1\,\mathrm{Mpc}$).

This tendency towards selling a prediction of failure as a success for a model

via the *ad hoc* introduction of some convenient form of unknown dark matter still prevails. An instance of this predilection is the introduction in 2018 of some peculiar form of dark matter [8] in order to cool the gas at $z \approx 18$ and solving the discrepancies in the measurements of 21 cm line amplitude with respect to the *a priori* predictions [19].

2. Dark matter and inconsistencies of the theory at galactic scales

That there is some dark matter, either baryonic or non-baryonic, is clear, but how much, and what is its nature? The success of the standard model in converting a hypothesis into a solid theory depends strongly on the answer to these open questions. Stellar and cold gas in galaxies sum to baryonic matter content that is $8^{+4}_{-5}\%$ of the total amount of the predicted Big Bang baryonic matter [10]. Where is the rest of the baryonic material? What is the nature of the putative non-baryonic dark matter required to achieve the current value of $\Omega_m \approx 0.3$?

Current CDM models predict the existence of dark matter haloes for each galaxy whose density profile falls approximately as r^{-2}, although the original idea [98] concerning hierarchical structures with CDM, which gave birth to the present models, was that the dark matter was distributed without internal substructure, more like a halo with galaxies than galaxies with a halo [9], something similar to the scenario in References [51], [52].

Some authors have been led to question the very existence of this dark matter on galactic scales since its evidence is weak [9], [59], [29], [90] and the predictions do not fit the observations: CDM has a "small scale crisis" since there are some features of the galaxies that are very different from the predictions of the cosmological model. Nonetheless, many researchers are eagerly trying to find solutions that make data and model compatible, assuming a priori that the model "must be" correct. Some of the problems are the following.

There is a problem with an observed lower density of the halo in the inner galaxy than predicted. ΛCDM (CDM including a Λ term for the cosmological constant; see §5) predicts halo mass profiles with cuspy cores and low outer density, while lensing and dynamical observations indicate a central core of constant density and a flattish high dark mass density outer profile [74]. The possible solutions of core-cusp problem without abandoning the standard model are: bar-halo friction, which reduces the density of the halo in the inner galaxy [85]; haloes around galaxies may have undergone a compression by the stellar disc [33] or/and suffered from the effects of baryonic physics [23].

Another problem is that the predicted angular momentum is much less than the observed one. Binney et al. [16] claim that the problem of an excess of predicted dark matter within the optical bodies and the fact that the observed discs are much larger than expected can be solved if a considerable mass of low angular momentum baryons is ejected (massive galactic outflows) and the discs are formed later from the high angular momentum baryons which fell in the galaxy. The conspiracy problem

is also solved if the ejection begins only once $M_{\text{baryons}}(r) \sim M_{\text{dark matter}}(r)$. Another solution within the standard cosmological model for the angular momentum problem is the tidal interaction of objects populating the primordial voids together with the Coriolis force due to void rotation [21].

Another fact that could cast doubt upon the existence of very massive halos of dark matter is that strong bars rotating in dense halos should generally slow down as they lose angular momentum to the halo through dynamical friction [22], whereas the observed pattern speed of galactic bars indicates that almost all of them rotate quite fast [1]. There should be a net transference of angular momentum from bars to halos, although friction can be avoided under some special conditions [86].

The enclosed dynamical mass-to-light ratio increases with decreasing galaxy luminosity and surface brightness, which is not predicted by dark matter scenarios [60].

Galaxies dominate the halo with little substructure whereas the model predicts that galaxies should be scaled versions of galaxy clusters with abundant substructure [25], [43]. Moreover, ΛCDM simulations predict that the majority of the most massive subhalos of the Milky Way are too dense to host any of its bright satellites ($L_V > 10^5$ $L_\odot$) [20]. Also, the distribution of satellites is in a plane, incompatible with ΛCDM [43], [42], [73]. Kroupa [44] says that these are arguments against the standard model in which one cannot make the typical rebuff of incompleteness of knowledge of baryonic physics. Furthermore, there is a correlation between bulge mass and the number of luminous satellites in tidal streams [43], [55] that is not predicted by the standard model, and it is predicted by models of modified gravity without dark matter. The disc of satellites and bulge-satellite correlation suggest that dissipational events forming bulges are related to the processes forming phase-space correlated satellite populations. These events are well known to occur, since in galaxy encounters energy and angular momentum are expelled in the form of tidal tails, which can fragment to form populations of tidal-dwarf galaxies and associated star clusters. If Local Group satellite galaxies are to be interpreted as Tidal Dwarf galaxies then the substructure predictions of the standard cosmological model are internally in conflict [43].

Perhaps, that most severe caveat to retain the hypothesis of dark matter is that, after a long time looking for it, it has not yet been found, although non-discovery does not mean that it does not exist. Microlensing surveys [45], [92] constrain the mass of the halo in our Galaxy in the form of dim stars and brown dwarfs to be much less than that necessary for dark matter halos. In any case, as already mentioned, the primordial nucleosynthesis model constrains baryonic matter to be around 10 % of the total mass [10], so these objects could not be compatible with the preferred cosmological model. Some observations are inconsistent with the dominant dark matter component being dissipationless [67]. Neither massive black hole halos [66] nor intermediate-mass primordial black holes [61] provide a consistent scenario. The nature of dark matter has been investigated and there are no suitable candidates among astrophysical objects.

3. Dark matter particles

The other possibility is that dark matter is not concentrated in any kind of astrophysical object but in a gas of exotic non-baryonic particles. There are three possible types of candidates [14]: 1) particles predicted by the supersymmetry hypothesis, which are electrically neutral and not strongly interacting, including superpartners of neutrinos, photons, Z bosons, Higgs bosons, gravitons, and others (neutralinos have been the most recently studied candidates in the last decades); 2) axions, typically with masses between 10^{-6} and 10^{-4} eV, predicted to resolve certain problems in quantum chromodynamics; and 3) Weakly Interacting Massive Particles (WIMPs), which are those particles that interact through the weak force.

The latest attempts to search for exotic particles have also finished without success. Technologies used to directly detect a dark matter particle have failed to obtain any positive result [57], [49]. Attempts have also been made to detect neutralinos with the MAGIC and HESS Cerenkov telescope systems for very high energy gamma rays through their Cherenkov radiation, but so far without success and only emission associated with the Galaxy has been found [3].Dwarf galaxies are expected to have high ratios of dark matter and low gamma ray emission due to other astrophysical processes so the search is focussed on these galaxies, but without positive results. As usual, the scientists involved in these projects attribute their failure of detection to the inability of the detectors to reach the necessary lower cross section of the interaction, or to tbe possibility that they may be 3–4 orders of magnitude below the possible flux of gamma rays emitted by dark matter [83], and ask for more funding to continue to feed their illusions: a never-ending story. As pointed out by David Merritt [63], this will never constitute a falsification of the CDM model because although success of detection will confirm the standard paradigm, non-detection is not used to discard it.

4. Scenarios without non-baryonic cold dark matter

Note also that some other dynamical problems in which dark matter has been claimed as necessary can indeed be solved without dark matter: galactic stability [93] or warp creation [52], for instance. Rotation curves in spiral galaxies can be explained without non-baryonic dark matter with magnetic fields [9], or modified gravity [81], or baryonic dark matter in the outer disc [31] or non-circular orbits in the outer disc [13]. Velocities in galaxy pairs and satellites might also measure the mass of the intergalactic medium filling the space between the members of the pairs [51], [52] rather than the mass of dark haloes associated with the galaxies.

The most popular alternative to dark matter is the modification of gravity laws proposed in MOND (Modified Newtonian Dynamics; [82]), which modifies the Newtonian law for accelerations lower than 1×10^{-10} m/s^2. This was in principle a phenomenological approach. It was attempted to incorporate elements that make it compatible with more general gravitation theories. The AQUAdratic Lagrangian theory (AUQAL) [11] expanded MOND to preserve the conservation of momen-

tum, angular momentum, and energy, and follow the weak equivalence principle. Later, a relativistic gravitation theory of MOND would be developed under the name Tensor-Vector-Scalar (TeVeS) [12], which also tried to provide consistency with certain cosmological observations, including gravitational lensing. However, the successes of MOND and its relativistic version are mostly limited to galactic scales and cannot compete with ΛCDM to explain the large-scale structure and other cosmological predictions. Moreover, a search was made for evidence of the MOND statement in a terrestrial laboratory: a sensitive torsion balance was employed to measure small accelerations due to gravity, and no deviations from the predictions of Newton's law were found down to 1×10^{-12} m/s^2 [48]. Therefore, unless these experiments are wrong, or we interpret the transition regime acceleration of 1×10^{-10} m/s^2 in terms of total absolute acceleration (including the acceleration of the Earth, Sun, etc.) rather than the relative one, MOND/TeVes is falsified by this experiment.

There are also proposals that the dark matter necessary to solve many problems may be baryonic: positively charged, baryonic (protons and helium nuclei) particles [26], which are massive and weakly interacting, but only when moving at relativistic velocities; simple composite systems that include nucleons but are still bound together by comparable electric and magnetic forces [58], making up a three-body system "tresinos" or four -body system "quatrinos"; antiparticles which have negative gravitational charge [35], etc.

In my opinion, the problem of 'dark matter' is not only one problem but many different problems within astrophysics that might have different solutions. The idea that the same non-baryonic dark matter necessary to explain the low anisotropies in the CMBR is going to solve the large-scale structure distribution, the lack of visible matter in clusters, the dispersion of velocities of their galaxies, the measurements of gravitational lensing, the rotation curves, etc., is a happy fantasy that has dominated astrophysics for the last 40 years. It would be wonderful if we also get a happy ending with the discovery of the particles of dark matter that constitute the dark halos of galaxies, but, in absence of that outcome, maybe it would be prudent to bet on a combination of different elements to explain the entire set of unexplained phenomena: possibly some baryonic dark matter in some cases, possibly a modification of gravity is part of the explanation for a wide set of events, and maybe cold dark matter dominates some phenomena and hot dark matter other phenomena. Certainly, a unified picture of a unique non-baryonic type of cold dark matter to explain everything would be a simpler and more elegant hypothesis; the question, however, is not one of simplicity but one of ascertaining how reality is, whether simple or complex.

5. Dark energy and the cosmological constant or quintessence

The question of the cosmological constant to maintain a static universe [70] was considered Einstein's biggest blunder, and it was introduced by Lemaître [46] in his equations for the evolution of the expanding universe. Indeed, it is equivalent to

positing an attractive gravitational acceleration $a(r) = -\frac{GM}{r^2} + Br$, already proposed by Newton for $B < 0$, but with $B > 0$ instead [41]. It is not usual physics but an exotic suggestion, since the usual thermodynamics for fluids with positive heat capacity and positive compressibility is not appliable to dark energy with negative pressure [7].

Twenty-five years ago, most cosmologists did not favour the scenarios dominated by the cosmological constant [32]. In the eighties, the cosmological constant was many times disregarded as an unnecessary encumbrance, or its value was set at zero [50], and all the observations gave a null or almost null value. However, since other problems in cosmology have risen, many cosmologists at the beginning of the '90s realized that an Ω_Λ ranging from 0.70 to 0.80 could solve many problems in CDM cosmology [28]. Years later, evidence for such a value of the cosmological constant began to arrive. A brilliant prediction or a prejudice which conditions the actual measurements?

All present claims about the existence of dark energy have measured Ω_Λ through its dependence on the luminosity distance vs. redshift dependence [27]. In the mid-1990s the position of the first peak in the power spectrum of the CMBR was determined to be at $\ell \approx 200$. White et al. in 1996 [97] realized that the preferred standard model at that time (an open universe with $\Omega = \Omega_m \approx 0.2$ and without dark energy) did not fit the observations, so that they needed a larger Ω. Between 1997 and 2000 a change of mentality in standard cosmology occurred. This was one of the elements, together with Type Ia Supernovae (SN Ia) observations and the age problem of the universe, that would encourage cosmologists to include a new ad hoc element: dark energy.

One measurement of the cosmological constant comes nowadays from supernovae, whose fainter-than-expected luminosity in distant galaxies can be explained with the introduction of the cosmological constant. It was criticized as being due possibly to intergalactic dust [2], [34], [64]. The presence of grey dust isnot necessarily inconsistent with the measure of a supernova at $z = 1.7$ (SN 1997ff) [34]. Dimming by dust along the line of sight, predominantly in the host galaxy of the SN explosion, is one of the main sources of systematic uncertainties [40]. Also, there was an underestimate of the effects of host galaxy extinction: a factor which may contribute to apparent faintness of high-z supernovae is the evolution of the host galaxy extinction with z [78]; therefore, with a consistent treatment of host galaxy extinction and the elimination of supernovae not observed before maximum, the evidence for a positive Λ is not very significant. Fitting the corrected luminosity distances (corrected for internal extinctions) with cosmological models Balazs et al. [6] concluded that the SNIa data alone did not exclude the possibility of the $\Lambda = 0$ solution.

SNe Ia also possibly have a metallicity dependence and this would imply that the evidence for a non-zero cosmological constant from the SNIa Hubble Diagram may be subject to corrections for metallicity that are as big as the effects of cosmology [87]. The old supernovae might be intrinsically fainter than the local ones, and the cosmological constant would not be needed [24]. As a matter of fact, some cases,

such as SNLS-03D3bb, have an exceptionally high luminosity [37]. Claims have been made about the possible existence of two classes of Normal-Bright SNe Ia [76]. If there is a systematic evolution in the metallicity of SN Ia progenitors, this could affect the determination of cosmological parameters. This metallicity effect could be substantially larger than has been estimated previously and could quantitatively evaluate the importance of metallicity evolution for determining cosmological parameters [75]. In principle, a moderate and plausible amount of metallicity evolution could mimic a Λ-dominated, a flat universe in an open, Λ-free universe. However, the effect of metallicity evolution appears not to be large enough to explain the high-z SNIa data in a flat universe, for which there is strong independent evidence, without a cosmological constant.

Furthermore, our limited knowledge of the SN properties in the U-band has been identified as another main source of uncertainty in the determination of cosmological parameters [40]. And the standard technique with SNe Ia consists in using spectroscopic templates, built by averaging spectra of well observed (mostly nearby) SNe Ia. Thus, the uncertainty in K-corrections depends primarily on the spectroscopic diversity of SNe Ia.

Even if we accept the present-day SN Ia analyses as correct and without any bias or selection effect, other cosmologies may explain the apparent cosmic acceleration of SNe Ia without introducing a cosmological constant into the standard Einstein field equation, thus negating the necessity for the existence of dark energy [88]. There are four distinguishing features of these models: 1) the speed of light and the gravitational "constant" are not constant, but vary with the evolution of the universe, 2) time has no beginning and no end, 3) the spatial section of the universe is a 3-sphere, and 4) the universe experiences phases of both acceleration and deceleration. An inhomogeneous isotropic universe described by a Lemaître–Tolman–Bondi solution of Einstein's fields equations can also provide a positive acceleration of the expansion without dark energy [77]. Quasi-Steady-State theory predicts a decelerating universe at the present era, it explains successfully the recent SNe Ia observations [95]. Carmeli's cosmology fits data for an accelerating and decelerating universe without dark matter or dark energy [68]. Thompson [91] used available measurement for the constrainst on the variation the proton to mass electron with redshift, and with $\Delta\alpha/\alpha = 7 \times 10^{-6}$ he finds that almost all of the dark energy models using the commonly expected values or parameters are excluded. A static universe can also fit the supernovae data without dark energy [89], [47], [54], [30], [56].

There are other sources of Ω_Λ measurement such as the anisotropies of the CMBR, but they are not free of inaccuracies owing to contamination and anomalies found in it [53], [84]. In the last two decades, many proofs have been presented to the community to convince us that the definitive cosmology has $\Omega_\Lambda \approx 0.7$, which is surprising taking into account that in the rest of the history of the observational cosmology proofs have been presented for $\Omega_\Lambda \approx 0$. Furthermore, recent tests indicate that other values are available in the literature. For instance, from the test angular size vs. redshift for ultracompact radio sources, it is obtained that Λ is negative [38].

Using the brightest galaxies in clusters, the fit in the Hubble diagram is compatible with a non-accelerated universe instead of $\Omega_\Lambda = 0.7$ [94], [4]. Concordance models produce far more high redshift massive clusters than observed in all existing X-ray surveys [17].

The actual values of Ω_Λ have some consistency problem in the standard scenario of the inflationary Big Bang. The cosmological constant predicted by quantum field theory has a value much larger than those derived from observational cosmology. This is because the vacuum energy in quantum field theory takes the form of the cosmological constant in Einstein's equations. If inflation took place at the Grand Unified Theory epoch, the present value would be too low by a factor $\sim 10^{-108}$, and if the inflation took place at the quantum gravity epoch, the above factor would be lower still at $\sim 10^{-120}$ [96]. The intrinsic absence of pressure in the "Big Bang Model" also rules out the concept of "Dark Energy", according to some opinions [65].

Furthermore, the standard model has some surprising coincidences. There is the coincidence that now the deceleration of the Hubble flow is compensated by the acceleration of the dark energy; the average acceleration throughout the history of the universe is almost null [62]. Again, everything is far from being properly understood.

Acknowledgements

Thanks are given to the language editor Terence J. Mahoney (IAC, Tenerife, Spain) for proof-reading of the text. The author was supported by the grant AYA2015-66506-P of the Spanish Ministry of Economy and Competitiveness (MINECO).

References

[1] Aguerri, J. A. L., Méndez-Abreu, J., Falcón-Barroso, J., et al.: Bar pattern speeds in CALIFA galaxies. I. Fast bars across the Hubble sequence. Hierarchic models for laminated composites. Astron. Astrophys. **576** (2015), A102, 17 pp.

[2] Aguirre, A., and Haiman, Z.: Cosmological Constant or Intergalactic Dust? Constraints from the Cosmic Far-Infrared Background. Astrophys. J. **532** (2000), 28–36.

[3] Aharonian, F., Akhperjanian, A. G., Bazer-Bachi, A. R., et al.: The H.E.S.S. survey of the inner galaxy in very high energy gamma rays. Astrophys. J. **636** (2006), 777–797.

[4] Andrews, T. B.: Falsification of the expanding universe model. In: E. J. Lerner and J. B. Almeida, (Eds.), *1st Crisis in Cosmology Conference, AIP Conf. Ser.* vol. 822(1), pp. 3–22. AIP, Melville, 2006.

[5] Babcock, H. W.: The rotation of the Andromeda Nebula. Lick Obs. Bull. **19 (498)** (1939), 41–51.

[6] Balázs, L. G., Hetesi, Zs., Regály, Zs., Csizmadia, Sz., Bagoly, Zs., Horváth, I., and Mészáros, A.: A possible interrelation between the estimated luminosity distances and internal extinctions of type Ia supernovae. Astron. Nachrichten **327** (2006), 917–924.

[7] Barboza, E. M. Jr., Nunes, R. da C., Abrey, E. M. C., and Neto J. A.: Is this the end of dark energy? arXiv.org, 1501.03491 (2015).

[8] Barkana, R.: Possible interaction between baryons and dark-matter particles revealed by the first stars. Nature **555** (2018), 71–74.

[9] Battaner, E. and Florido, E.: The rotation curve of spiral galaxies and its cosmological implications. Fund. Cosmic Phys. **21** (2000), 1–154.

[10] Bell, F. B., McIntosh, D. H., Katz, N., and Weinberg, M. D.: A first estimate of the baryonic mass function of galaxies. Astrophys. J. Lett. **585** (2003), L117–L120.

[11] Bekenstein, J. and Milgrom, M.: Does the missing mass problem signal the breakdown of Newtonian gravity? Astrophys. J. **286** (1984), 7–14.

[12] Bekenstein, J. D.: Relativistic gravitation theory for the modified Newtonian dynamics paradigm. Phys. Rev. D **70** (2004), id. 083509.

[13] Benhaiem, D., Joyce, M., and Sylos Labini, F.: Transient spiral arms from far out-of-equilibrium gravitational evolution. Astrophys. J. **851** (2017), id. 19, 10 pp.

[14] Bertone, G., and Hooper, D.: A History of Dark Matter. arXiv.org, 1605.04909 (2016).

[15] Bessel, F. W. On the variations of the proper motions of Procyon and Sirius. Mon. Not. R. Astron. Soc. **6** (1844), 136–141.

[16] Binney, J., Gerhard, O., and Silk, J.: The dark matter problem in disc galaxies. Mon. Not. R. Astron. Soc. **321** (2001), 471–474.

[17] Blanchard, A.: Evidence for an accelerating universe or lack of? In: J.-C. Pecker and J. V. Narlikar (Eds.), *Current issues in Cosmology*, pp. 76–84, Cambridge University Press, Cambridge, 2006.

[18] Bosma, A.: *The distribution of kinematics of neutral hydrogen in spiral galaxies of various morphological types*. Ph.D. thesis, University of Groningen, 1978.

[19] Bowman, J. D., Rogers, A. E. E., Monsalve, R. A., Mozdzen, T. J., and Mahesh, N.: An absorption profile centred at 78 megahertz in the sky-averaged spectrum. Nature **555** (2018), 67–70.

[20] Boylan-Kolchin, M., Bullock, J. S., and Kaplinghat, M.: Too big to fail? The puzzling darkness of massive Milky Way subhaloes. Mon. Not. R. Astron. Soc. **415** (2011), L40–L44.

[21] Casuso E., and Beckman J. E.: On the origin of the angular momentum of galaxies: cosmological tidal torques and coriolis force. Mon. Not. R. Astron. Soc. **449** (2015), 2910–2918.

[22] Debattista, V. P. and Sellwood, J. A.: Constraints from dynamical friction on the dark matter content of barred galaxies. Astrophys. J. **543** (2000), 704–721.

[23] Di Cintio, A., Brook, C. B., Macciò, A. V., Stinson, G. S., Knebe, A., Dutton, A. A., and Wadsley, J.: The dependence of dark matter profiles on the stellar-to-halo mass ratio: a prediction for cusps versus cores. Mon. Not. R. Astron. Soc. **437** (2014), 415–423.

[24] Domínguez I., Höflich P., Straniero O., and Wheeler C.: Evolution of type Ia supernovae on cosmological time scales. Mem. Soc. Astron. Ital. **71** (2000), 449–460.

[25] D'Onguia, E., Lake, G.: Cold dark matter's small-scale crisis grows up. Astrophys. J. **612** (2004), 628–632.

[26] Drexler, J.: Identifying dark matter through the constraints imposed by fourteen astronomically based 'cosmic constituents'. arXiv.org, astro-ph/0504512 (2005).

[27] Durrer, R. What do we really know about dark energy? J. Cosmol. **15** (2011), 6065–6078.

[28] Efstathiou, G., Sutherland, W. J., and Maddox, S. J.: The cosmological constant and cold dark matter. Nature **348** (1990), 705–707.

[29] Evans, N. W.: No need for dark matter in galaxies? In: N. J. C. Spooner and V. Kudryavtsev (Eds.), *Proceedings of the 3rd International Workshop on the Identification of Dark Matter*, pp. 85–92. World Scientific, Singapore, 2001.

[30] Farley, F. J. M.: Does gravity operate between galaxies? Observational evidence re-examined. Proc. R. Soc. A **466** (2010), 3089–3096.

[31] Feng, J. Q. and Gallo, C. F.: Deficient reasoning for dark matter in galaxies. Phys. Int. **6** (2015), 11–22.

[32] Fukugita, M. and Lahav, O.: Ly-alpha clouds at low redshift and the cosmological constant. Mon. Not. R. Astron. Soc. **253** (1991), 17P–20P.

[33] Gnedin, O. Y., Kravtsov, A. V., Klypin, A. A., and Nagai, D.: Response of dark matter halos to condensation of baryons: cosmological simulations and improved adiabatic contraction model. Astrophys. J. **616** (2004), 16–26.

[34] Goobar, A., Bergström, L., and Mörtsell, E.: Measuring the properties of extragalactic dust and implications for the Hubble diagram. Astron. Astrophys. **384** (2002), 1–10.

[35] Hajdukovic, D. S.: Virtual gravitational dipoles: The key for the understanding of the universe? Physics of the Dark Universe **3** (2014), 34–40.

[36] Holmberg, E.: On the masses of double galaxies. Meddelanden fran Lunds Astronomiska Observatorium Series I **186** (1954), 1–20.

[37] Howell, D. A., Sullivan, M., Nugent, P. E., et al.: The type Ia supernova SNLS-03D3bb from a super-Chandrasekhar-mass white dwarf star. Nature **443** (2006), 308–311.

[38] Jackson, J. C., and Dodgson, M.: Deceleration without dark matter. Mon. Not. R. Astron. Soc. **285** (1997), 806–810.

[39] Kahn F. D., and Woltjer L.: Intergalactic matter and the galaxy. Astrophys. J. **130** (1959), 705–717.

[40] Knop, R. A., Aldering, G., Amanullah, R., et al.: New constraints on Ω_M, Ω_Λ, and w from an independent set of 11 high-redshift supernovae observed with the Hubble space telescope. Astrophys. J. **598** (2003), 102–137.

[41] Komatsu, E.: What every dynamicist should know about ... Cosmology. In: *American Astronomical Society, DDA meeting #42*, Bull. Am. Astron. Soc. 43, id.4.01, 2011.

[42] Kroupa, P., Theis, C., and Boily, C. M.: The great disk of Milky-Way satellites and cosmological sub-structures. Astron. Astrophys. **431** (2005), 517–521.

[43] Kroupa, P., Famaey, B., de Boer, K. S., et al.: Local-group tests of dark-matter concordance cosmology . Towards a new paradigm for structure formation. Astron. Astrophys. **523** (2010), id. A32, 22 pp.

[44] Kroupa, P.: The dark matter crisis: falsification of the current standard model of cosmology. Publ. Astron. Soc. Australia **29** (2012), 395–433.

[45] Lasserre, T., Afonso, C., Albert, J. N., et al.: Not enough stellar mass Machos in the Galactic halo. Astron. Astrophys. **355** (2000), L39–L42.

[46] Lemaître, G.: Evolution of the Expanding Universe. Proc. Nat. Acad. Sci. USA **20** (1934), 12–17

[47] Lerner, E. J.: Tolman test from $z = 0.1$ to $z = 5.5$: preliminary results challenge the expanding universe model. In: F. Potter (Ed.), *Second Crisis in Cosmology Conference* (ASP Conf. Ser. 413), pp. 12–23. ASP, S. Francisco, 2009.

[48] Little, S. and Little, M.: Laboratory test of Newton's law of gravity for small accelerations. Class. Quantum Grav. **31** (2014), id. 195008.

[49] Liu, J., Chen, X., Ji, X.: Current status of direct dark matter detection experiments. Nature Physics **13** (2017), 212–216.

[50] Longair, M. S.: Observational cosmology 1986. In: A. Hewitt, G. Burbidge, and L. Z. Fang (Eds.) *Observational Cosmology* (IAU Symp. 124), pp. 823–840. Reidel, Dordrecht, 1987.

[51] López-Corredoira, M., Beckman, J. E., and Casuso E.: High-velocity clouds as dark matter in the local group. Astron. Astrophys. **351** (1999), 920–924.

[52] López-Corredoira, M., Betancort-Rijo, J., and Beckman, J. E.: Generation of galactic disc warps due to intergalactic accretion flows onto the disc. Astron. Astrophys. **386** (2002), 169–186.

[53] López-Corredoira, M.: Some doubts on the validity of the foreground Galactic contribution subtraction from microwave anisotropies. J. Astrophys. Astron. **28** (2007), 101–116.

[54] López-Corredoira, M.: Angular-size test on the expansion of the Universe. Int. J. Mod. Phys. D **19** (2010), 245–291.

[55] López-Corredoira, M., and Kroupa, P.: The number of tidal dwarf satellite galaxies in dependence of bulge index. Astrophys. J. **817** (2016), id. 75, 7 pp.

[56] Marosi, L. A.: Hubble diagram test of expanding and static cosmological models: the case for a slowly expanding flat universe. Advances in Astronomy **2013**, id. 917104.

[57] Marrodán Undagoitia, T. and Rauch, L.: Dark matter direct-detection experiments. Journal of Physics G: Nuclear and Particle Physics **43** (2016), id. 013001.

[58] Mayer, F. J. and Reitz, J. R.: Electromagnetic composites at the compton scale. Int. J. Theor. Phys. **51** (2012), 322–330.

[59] McGaugh, S. S.: Boomerang data suggest a purely baryonic universe. Astrophys. J. Lett. **541** (2000), L33–L36.

[60] McGaugh, S.: The third law of galactic rotation. Galaxies **2** (2014), 601–622.

[61] Mediavilla, E., Jiménez-Vicente, J., Muñoz, J. A., Vives-Arias, H., and Calderón-Infante, J.: Limits on the mass and abundance of primordial black holes from quasar gravitational microlensing. Astrophys. J. Lett. **836** (2017), id. L18, 5 pp.

[62] Melia, F. and Shevchuk, A. S.: The $R_h = ct$ universe. Mon. Not. R. Astron. Soc. **419** (2012), 2579–2586.

[63] Merritt, D.: Cosmology and convention. Studies in History and Philosophy of Modern Physics **57** (2017), 41–52.

[64] Milne, P. A., Foley, R. J., Brown, P. J., and Narayan, G.: The changing fractions of type Ia spernova NUV–optical subclasses with redshift. Astrophys. J. **803** (2015), id. 20, 15 pp.

[65] Mitra, A.: Why Friedmann cosmology cannot describe the observed universe having pressure and radiation. J. Mod. Phys. **2** (2011), 1436–1442.

[66] Moore, B.: An upper limit to the mass of black holes in the halo of the galaxy. Astrophys. J. Lett. **413** (1993), L93–L96.

[67] Moore, B.: Evidence against dissipation-less dark matter from observations of galaxy haloes. Nature **370** (1994), 629–631.

[68] Oliveira, F. J. and Hartnett, J. G.: Carmeli's cosmology fits data for an accelerating and decelerating universe without dark matter or dark energy. Foundations of Physics Letters **19** (2006), 519–535.

[69] Ostriker, J. P., and Peebles, J. P. E.: A numerical study of the stability of flattened galaxies: or, can cold galaxies survive? Astrophys. J. **186** (1973), 467–480.

[70] Padmanabhan, T.: Cosmological constant-the weight of the vacuum. Phys. Reports **380** (2003), 235–320.

[71] Page, T.: Radial velocities and masses of double galaxies. Astrophys. J. **116** (1952), 63–84.

[72] Page, T.: Average masses and mass-luminosity ratios of the double galaxies. Astrophys. J. **132** (1960), 910–912.

[73] Pawlowski, M. S. and Kroupa, P.: The rotationally stabilized VPOS and predicted proper motions of the Milky Way satellite galaxies. Mon. Not. R. Astron. Soc. **435** (2013), 2116–2131.

[74] Perivolaropoulos, L.: Six puzzles for LCDM cosmology. arXiv.org, 0811.4684 (2008).

[75] Podsiadlowski, P., Mazzali, P. A., Lesaffre, P., Wolf, C., and Forster, F.: Cosmological implications of the second parameter of type Ia supernovae. arXiv.org, astro-ph/0608324 (2006).

[76] Quimby, R., Höflich, P., and Craig Wheeler, J.: SN 2005hj: Evidence for two classes of normal-bright sne ia and implications for cosmology. Astrophys. J. **666** (2007), 1083–1092.

[77] Romano, A. E.: Lemaitre-Tolman-Bondi universes as alternatives to dark energy: Does positive averaged acceleration imply positive cosmic acceleration? Phys. Rev. D **75** (2007), id. 043509.

[78] Rowan-Robinson, M.: Do Type Ia supernovae prove $\Lambda > 0$? Mon. Not. R. Astron. Soc. **332**(2002), 352–360.

[79] Rubin, V. and Ford, W. K. Jr., and Thonnard, N.: Rotational properties of 21 Sc galaxies with a large range of luminosities and radii from NGC 4605 (R=4 kpc) to UGC 2885 (R=122 kpc). Astrophys. J. **238** (1980), 471–487.

[80] Sachs, R. K. and Wolfe, A. M.: Perturbations of a cosmological model and angular variations of the microwave background. Astrophys. J. **147** (1967), 73–90.

[81] Sanders, R. H. and McGaugh, S. S.: Modified Newtonian dynamics as an alternative to dark matter. Ann. Rev. Astron. Astrophys. **40** (2002), 263–317.

[82] Sanders, R. H.: A historical perspective on modified Newtonian dynamics. Canadian J. Phys. **93** (2015), 126–138.

[83] Sánchez-Conde, M. A.: Gamma-ray dark matter searches in the Milky Way. Oral presentation in: *Distribution of Mass in the Milky Way*, Leiden, Netherlands, 13-17 July 2009.

[84] Schwarz, D. J, Copi, C. J., Huterer, D., and Starkman G. D.: CMB anomalies after Planck. Classical and Quantum Gravity **3**3 (2016), id. 184001.

[85] Sellwood, J. A.: Bar-Halo friction in Galaxies. III. Halo Density Changes. Astrophys. J. **679** (2008), 379–396.

[86] Sellwood, J. A., and Debattista, V P.: Bar-Halo friction in galaxies. II. Metastability. Astrophys. J. **639** (2006), 868–878.

[87] Shanks, T., Allen, P. D., Hoyle, F., and Tanvir, N. R.: Cepheid, Tully-Fisher and SNIa distances. arXiv.org, astro-ph/0102450 (2001).

[88] Shu, W.-Y.: The Geometry of the universe. arXiv.org, 1007.1750 (2010).

[89] Sorrell, W. H.: Misconceptions about the Hubble recession law. Astrophys. Space Sci. **323** (2009), 205–211. Erratum: Astrophys. Space Sci. **323** (2009), 213.

[90] Tasitsiomi, A.: The state of the cold dark matter models on galactic and subgalactic scales. Int. J. Mod. Phys. D **12** (2003), 1157–1196.

[91] Thompson, R. I.: Constraints on quintessence and new physics from fundamental constants. Mon. Not. R. Astron. Soc. **422** (2012), L67–L71.

[92] Tisserand, P., Le Guilou, L., Afonso, C., et al.: Limits on the Macho content of the Galactic Halo from the EROS-2 Survey of the Magellanic Clouds. Astron. Astrophys **469** (2007), 387–404.

[93] Toomre, A.: What amplifies the spirals. In: S. M., Fall, and D. Lynden-Bell (Eds.), *The Structure and Evolution of Normal Galaxies*, pp. 111–136. Cambridge University Press, Cambridge U.K., 1981.

[94] Vauclair, S. C., Blanchard, A., Sadat, R., et al.: The XMM-Omega project. II. Cosmological implications from the high redshift L – T relation of X-ray clusters. Astron. Astrophys. **412** (2003), L37–L41.

[95] Vishwakarma, R. G. and Narlikar, J. V.: Modeling repulsive gravity with creation. J. Astrophys. Astr. **28** (2007), 17–27.

[96] Weinberg, S.: The cosmological constant problem. Rev. Mod. Phys. **61** (1989), 1–23.

[97] White, M., Viana, P. T. P., Liddle, A. R., and Scott, D.: Primeval adiabatic perturbation in an expanding universe. Mon. Not. R. Astron. Soc. **283** (1996), 107–118.

[98] White, S. D. M. and Rees, M. J.: Core condensation in heavy halos - a two-stage theory for galaxy formation and clustering. Mon. Not. R. Astron. Soc. **183** (1978), 341–358.

[99] White, S. D. M., Frenk, C. S., and Davis, M.: Clustering in a neutrino-dominated universe. Astrophys. J. **274** (1983), L1–L5.

[100] Zwicky, F.: Die Rotverschiebung von extragalaktischen Nebeln Helvetica Phys. Acta **6** (1933), 110–127.

Conference *Cosmology on Small Scales 2018*
Michal Křížek and Yurii Dumin (Eds.)
Institute of Mathematics CAS, Prague

CONSTRAINTS ON THE EXISTENCE OF DARK MATTER HALOES BY THE M81 GROUP AND THE HICKSON COMPACT GROUPS OF GALAXIES

W. Oehm[1], P. Kroupa[2,3]

[1] Bonn, Germany
physik@wolfgang-oehm.com
[2] Helmholtz Institut für Strahlen und Kernphysik
Universität Bonn, Nussallee 14 - 16, 53115 Bonn, Germany
pavel@astro.uni-bonn.de
[3] Astronomical Institute, Faculty of Mathematics and Physics, Charles University
V Holešovičkách 2, CZ-180 00 Prague 8, Czech Republic

Abstract: According to the standard model of cosmology, the visible baryonic matter of galaxies is embedded in dark matter haloes, thus extending the mass and the size of galaxies by one to two orders of magnitude. Taking into account dynamical friction between the dark matter haloes, the nearby located M81 group of galaxies as well as the Hickson compact groups of galaxies are here investigated with regard to their dynamical behaviour. The results of the employment of the Markov Chain Monte Carlo method and the genetic algorithm show statistically substantial merger rates between galaxies, and long living constelllations without merging galaxies comprise — apart from very few instances — initially unbound systems only. This result is derived based on three- and four-body calculations for a model of rigid Navarro–Frenk–White profiles for the dark matter haloes, but verified by the comparison to randomly choosen individual solutions for the M81 galaxy group with high-resolution simulations of live self-consistent systems (N-body calculations). In consequence, the observed compact configurations of major galaxies are a very unlikely occurence if dark matter haloes exist.

Keywords: dark matter, dynamics of galaxy groups, statistical methods
PACS: 98.65.Cw

1. Introduction

Radioastronomical observations (see [9], [10], [22], [1], [23], [24]) established the fact that the M81 companions M82 and NGC 3077 are connected with the central galaxy M81 by intergalactic clouds of H_I emitting gas, namely the north and the south tidal bridge. Attempting to reproduce those morphological structures by

numerical simulations, based on the dark matter hypothesis underlying the cosmological model, Yun [25] couldn't find solutions for the dynamic development of the inner M81 group of galaxies without the occurence of merging galaxies due to dynamical dissipation. Employing full N-body calculations, Thomson et al. [21] did not find appropriate solutions without a merger either. Although more recent observational work exists, the dynamical evolution of the inner M81 group has not been investigated theoretically since then, until Oehm et al. [18] investigated the inner M81 group regarding their dynamical behaviour including the effects of dynamical friction between the dark matter haloes from a statistical point of view. The results obtained there disfavour the existence of dark matter haloes according to the model, and are summarized in Chapter 3.

Currently we transfer the methodology applied to the M81 Group to the Hickson compact groups of galaxies (see [11], [12], [13], [14]), based on investigations recently published by Sohn et al. [20]. Comparably to the M81 group, the preliminary results obtained for a subset of 100 compact groups also disfavour the existence of dark matter haloes because of significant merger probabilities. The approach and the preliminary results are presented in Chapter 4.

At first, the underlying physical model for the statistical evaluations is explained in Chapter 2.

2. The model

The DM halo of either galaxy is treated as a rigid halo with a density profile according to Navarro, Frenk and White [17] (NFW-profile), truncated at the radius R_{200}:

$$\rho(r) = \frac{\rho_0}{r/R_s \left(1 + r/R_s\right)^2} \ , \tag{1}$$

with $R_s = R_{200}/c$, R_{200} denoting the radius yielding an average density of the halo of 200 times the cosmological critical density

$$\rho_{crit} = \frac{3H^2}{8\pi G} \ , \tag{2}$$

and the concentration parameter c

$$\log_{10} c = 1.02 - 0.109 \left(\log_{10} \frac{M_{\rm vir}}{10^{12} M_\odot} \right) , \tag{3}$$

see [16].

The DM halo masses are derived from the luminosities of the galaxies available at the NASA/IPAC Extragalactic Database for the M81 group (query submitted on 2014 February 8), and in [20] for the Hickson compact groups. In a first step the stellar masses are determined by means of Eq. 6 of [3], and based on the stellar masses the DM halo masses are extracted from Fig. 7 of [2] thereafter.

Exploring the dynamics of bodies travelling along paths in the interior of DM haloes implies that the effects of dynamical friction have to be taken into account in an appropriate manner [5]. For isotropic distribution functions the decelaration of an intruding point mass due to dynamical friction is described by Chandrasekhar's formula [6], which reads for a Maxwellian velocity distribution with dispersion σ (for details see [4], Chap. 8.1):

$$\frac{d\vec{\mathbf{v}}_M}{dt} = -\frac{4\pi G^2 M \rho}{{\mathrm{v}_M}^3} \ln\Lambda \left[\mathrm{erf}(X) - \frac{2X}{\sqrt{\pi}}\mathrm{e}^{-X^2}\right] \vec{\mathbf{v}}_M \ , \tag{4}$$

with $X = \mathrm{v}_M/(\sqrt{2}\sigma)$. The intruder of mass M and relative velocity $\vec{\mathbf{v}}_M$ is decelareted by $d\vec{\mathbf{v}}_M/dt$ in the background density ρ of the DM halo.

Simulating galaxy-galaxy encounters Petsch and Theis [19] showed that a modified model for the Coulomb logarithm lnΛ, originally proposed by Jiang et al. [15], describes the effects of dynamical friction in a realistic manner. This mass- and distance-dependent model reads:

$$\ln\Lambda = \ln\left[1 + \frac{M_{halo}(r)}{M}\right] \ , \tag{5}$$

where $M_{halo}(r)$ is the mass of the host dark matter halo within the radial distance r of the intruding point mass.

So far Eq. 4 describes the dynamical friction of a point mass in halo i with a Maxwellian velocity distribution. The approach how to calculate the dynamical friction between two overlapping haloes i and j using NFW-profiles is described in detail in Appendix C of [18].

Chandrasekhar's formula only gives an estimate at hand. However, for the sake of establishing statistical statements about merger rates between galaxies, high-resolution simulations of live self-consistent systems presented in [18] (especially refer to Figures 13 and 14) confirm our approach of employing this semi-analytical formula in our three- and four-body calculations.

The equations of motion and the numerical approach of their integration are presented in Appendix C of [18].

3. M81 review

We briefly present the methodology and the results obtained for the galaxy group M81 (see [18]).

The fact that the three core members, M81, M82, and NGC 3077, are enshrouded by intergalactic clouds of H_I emitting gas (north and south tidal bridge) implies that either companion M82 and NGC 3077 must have encountered the central galaxy M81 closely within the recent cosmological past (for a review see [25]).

The plane-of-sky coordinates, the line-of-sight velocities, and the DM-halo masses are at our disposal. However, the plane-of-sky velocities are unknown, and the radial

(line-of-sight) distances are only roughly established. Therefore, within the reference frame of the central galaxy M81, we are confronted with six open parameters: The radial distances and the plane-of-sky velocities of the companions M82 and NGC 3077.

The possible values of those open parameters were investigated from a statistical point of view:

At first, calculating three-body orbits backwards up to -7 Gyr, statistical populations for the open parameters were generated by means of the Markov Chain Monte Carlo method (MCMC) and the genetic algorithm (GA). Following the results of [25] we added, additionally to the known initial conditions at present, the rather general condition that

both companions M82 and NGC 3077 encountered M81
within the recent 500 Myr at a pericentre distance below 30 kpc.

Each three-body orbit of those statistical populations is fully determined by all the known and the open parameters provided by either MCMC or GA. Starting at time -7 Gyr and calculating the corresponding three-body orbits forward in time up to $+7$ Gyr, the behaviour of the inner group has been investigated with respect to the question of possibly ocurring mergers in the future.

The details of applying the Metropolis-Hastings algorithm based on a methodology proposed by Goodman and Weare ([8]) for MCMC are presented in Section 4 and Appendix D of [18], and, based on the proposal by Charbonneau [7] for GA in Section 5 of [18]. Basically both methods deliver comparable results. However, as discussed in Section 6 of [18], due to the structure of the likelyhood function applied for MCMC in our case, the genetic algorithm has been proved to deliver more stable results.

In Table 1 (which is Table 4 in [18]) we present the basic results of our statistical evaluations which can be summarized as follows:

- Long living solutions without mergers comprise constellations only where the three galaxies are unbound and — arriving from a far distance — happen to simultaneously encounter each other within the previous 500 Myr.

- Cases where all three galaxies are bound at -7 Gyr represent only 7% of either statistical population of the MCMC and GA solutions, respectively. And those originally bound systems would be merging within the near cosmological future.

4. The Hickson compact groups

Upon having established our methods for the galaxy group M81, we transferred this methodology to the Hickson compact groups with three and four members based on the observational data summarized by Sohn et al. [20]. The aim is to achieve statistical results for the merger rates for a subset of 188 compact groups extracted

	MCMC	GA
solutions not merging within next 7 Gyr	118	278
solutions not merging within next 7 Gyr and: neither M82 nor N3077 bound to M81 7 Gyr ago	117	276
solutions not merging within next 7 Gyr and: one companion bound to M81 7 Gyr ago	1	2
solutions for: M82 and N3077 bound to M81 7 Gyr ago	66	70
longest lifetime from today for: M82 and N3077 bound to M81 7 Gyr ago	2.7 Gyr	2.8 Gyr
average lifetime from today for: M82 and N3077 bound to M81 7 Gyr ago	1.7 Gyr	1.3 Gyr

Table 1: *Galaxy group M81:* Key numbers for both statistical methods MCMC and GA, based on populations of 1000 solutions in either case. Actually, the three solutions not merging within the next 7 Gyr, where one companion is bound to M81 (third position) merge after 7.3 Gyr (MCMC), and 7.8 and 8.2 Gyr (GA).

from the list of originally 332 compact groups presented in [20]. The reasons for the non-consideration of 144 groups are:

- There are groups where the true membership of at least one galaxy is not clarified (52 cases).
- We do not consider groups consisting of more than four true members (28 cases).
- Some groups are omitted due to only inaccurately known line-of-sight velocities (spread of redshifts, $\Delta z = 0.001$ being too large) (9 cases).
- Groups consisting of galaxies with a DM-halo mass exceeding $10^{15} M_\odot$ are not taken into account, because the determination of the DM-halo masses based on the stellar masses according to Behroozi et al. [2] is confined to the interval $[10^{10} M_\odot, 10^{15} M_\odot]$ for the DM-halo masses (94 cases).

Of course two ore more criteria can simultaneously apply to one compact group, therefore ending up with 188 groups to be considered, which is 57% of the original set. However, as the investigations were still in process when creating this article, the preliminary results presented here are based on a subset of the nearest 100 compact goups (see Appendix A) from this set of 188 objects. The range of distances for our preliminary set of 100 groups is [65 Mpc, 308 Mpc].

The average plane-of-sky distance between two galaxies for our final set of 188 compact groups is 92.7 kpc. The assumption of isotropy yields an average spatial distance between two galaxies of 113 kpc. Physical intuition already implies that dynamical

friction between DM-haloes with radii of hundreds of kpc plays an important role regarding the dynamical behaviour of the groups.

Following our methodology established for the M81 group, we specify the general condition for the compact groups that

the minimal value for the hyper radius does not exceed a certain ceiling value within the recent Gyr, i.e. $[-1\ Gyr, today]$.

To be precise, the hyper radius ρ defined by

$$\rho^2 = \sum_{i<j}^{n} r_{ij}^2 \quad , \tag{6}$$

for the n members of each group shall fullfil the following condition for the minimal value ρ_{min}

$$\rho_{min}^2 < \rho_0^2 = \frac{n(n-1)}{2}\, r_0^2 \quad \text{within } [-1 \text{ Gyr, today}] \tag{7}$$

with ceiling value ρ_0. Concerning r_0, we consider three different values:

$$r_0 = \begin{cases} 75 \text{ kpc} & (\text{model } A), \\ 100 \text{ kpc} & (\text{model } B), \\ 113 \text{ kpc} & (\text{model } C), \end{cases} \tag{8}$$

the models A and B being motivated by the statement that the compact groups have recently gone through a configuration where the average distance between the individual members does not exceed two to three times the value of the visible, baryonic diameter of the galaxies. Model C refers to the above mentioned observed average spatial distance between two galaxies within a group.

Employing the genetic algorithm we confine, within the reference frame of the most massive galaxy of each group, for the remaining members the hardly known line-of-sight distances to $[-1$ Mpc, $+1$ Mpc$]$, and the unknown plane-of-sky Cartesian velocity components to realistic values of $[-500$ pc/Myr, $+500$ pc/Myr$]$. The range for the line-of-sight distances is obviously justified by the average spatial distance of 113 kpc between galaxies, and the constraints for the velocity components are actually in agreement with the results obtained by Sohn et al. (see [20], Figures 5 and 6).

As a matter of fact, according to Hickson [14] and Sohn et al. this choice of ranges for the unknown entities could be confined even more drastically. However, in order not to influence the statistics by "whishful" a priori constraints, we take our decision for this choice of ranges.

The fitness function — which corresponds to the likelyhood function of MCMC — is defined by referring to the ceiling values ρ_0 from Eq. 7 for the various models of Eq. 8:

$$f(\rho_{\min}) = \begin{cases} 1 & \rho_{\min} \leq \rho_0, \\ \exp\left(-\dfrac{(\rho_{\min} - \rho_0)^2}{2 \cdot (25 \text{ kpc})^2}\right) & \rho_{min} > \rho_0. \end{cases} \tag{9}$$

Model	0-1 Gyr	0-2 Gyr	0-3 Gyr	0-4 Gyr	0-5 Gyr	0-6 Gyr	0-7 Gyr
A	38%	68%	79%	83%	86%	87%	88%
B	31%	63%	76%	81%	84%	85%	86%
C	28%	61%	74%	79%	82%	84%	85%
$C-3$	23%	53%	66%	73%	76%	78%	80%
$C-4$	36%	72%	84%	88%	90%	91%	92%

Table 2: *Compact groups:* Percentages of mergers for selected periods of time from the present until maximally 7 Gyr, cumulated over our preliminary set of 100 selected groups. The numbers refer to the first occurence of a merging pair of galaxies for each group and are based on populations of 100 solutions per group, yielding in total a set of 10 000 solutions. The first three rows show the total percentages for the three models of the fitness function, while the fourth and the fifth row refer to 56 three-galaxy groups and 44 four-galaxy groups, respectively, for model C.

Model	0-1 Gyr	0-2 Gyr	0-3 Gyr	0-4 Gyr	0-5 Gyr	0-6 Gyr	0-7 Gyr
A	4%	24%	37%	45%	51%	55%	58%
B	3%	21%	33%	41%	46%	50%	54%
C	2%	19%	31%	39%	44%	49%	53%
$C-3$	3%	23%	34%	41%	46%	50%	53%
$C-4$	1%	14%	26%	36%	42%	48%	52%

Table 3: *Compact groups:* Same as for Table 2, but the numbers refer to complete mergers (all individual galaxies of a group will have merged to one object).

The results obtained are presented in Tables 2 and 3 as well as in Figures 1 and 2.

- Although the models A, B, and C cover a substantial variation of r_0, the long term merger percentages show absolutely comparable numbers (see Tables 2 and 3). Each model delivers the result that more than half of the considered preliminary set of compact groups will totally be merged to one galaxy within the next 7 Gyr (Table 3), as well as that for about 2/3 of the groups at least one pair of galaxies will be merging within the next 2 Gyr (Table 2). The major difference between the models is just a slight delay for merging galaxies caused by a higher value of r_0, thus above all affecting the percentages for 0-1 Gyr.

- Apart from very few exceptions, the hyper radii at -7 Gyr shown in Fig. 1 clearly indicate that non-merging long living solutions comprise unbound systems only. Actually, instances with hyper radii less than 1 Mpc for the three-galaxy groups concern only three out of 56 compact groups, namely SDSS-CGA00488, 01220, and 01446. For the four-galaxy groups only two out of 44 compact groups comprise solutions with hyper radii less than 2 Mpc, namely

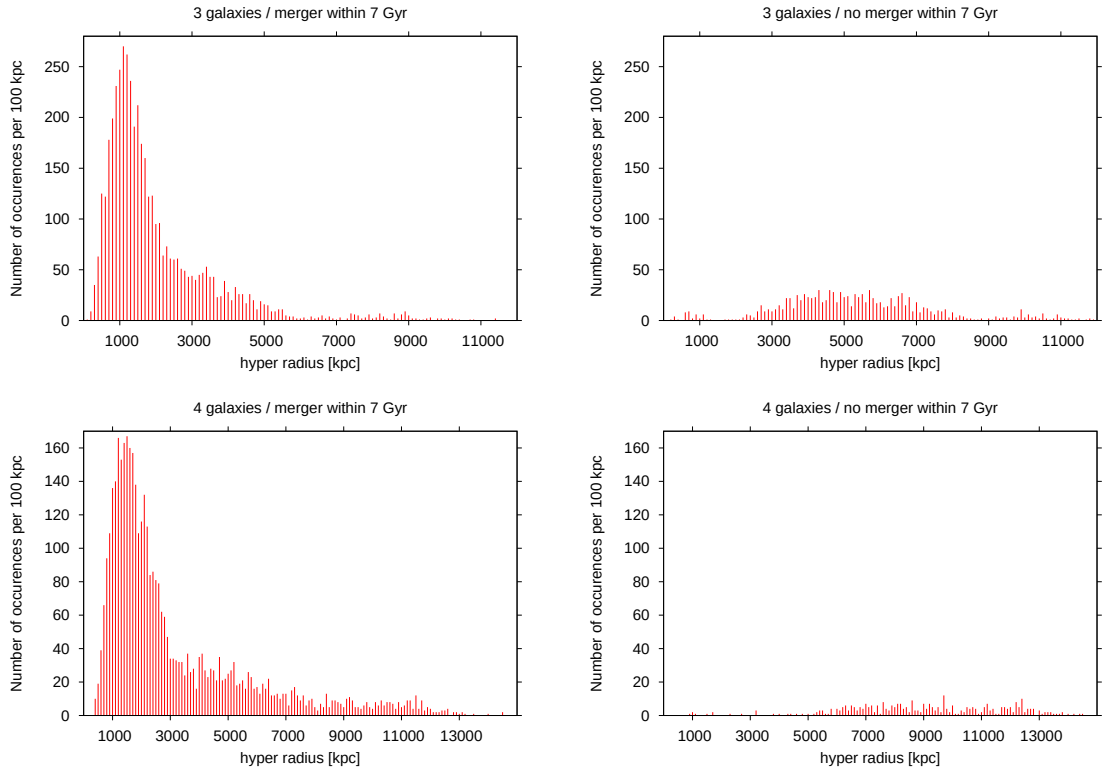

Figure 1: *Compact groups:* Hyper radii at -7 Gyr for the three-galaxy groups (top panel) and the four-galaxy groups (bottom panel). The left panel shows the number of ocurrences for intervals of 10 kpc for solutions, where at least one pair of galaxies will be merging within the next 7 Gyr, while the right panel refers to solutions without a merger within the next 7 Gyr. The data are extracted from the results for Model C.

SDSSCGA00425 and 00800. Emphasizing our statement, Fig. 2 shows that the non-merging solutions almost completely comprise instances where the individual galaxies are, at -7 Gyr, moving towards the centre of mass of their group with linearly increasing radial velocities in dependence of the centre of mass distance.

5. Conclusions

We apprehend the statistically elaborated merger percentages for the M81 group and the Hickson compact groups of galaxies as a *merger probability per time unit* for those systems. The solutions of the configuration of these groups 7 Gyr ago obtained under the condition that the groups have not merged by the present time comprise virtually only cases, where the galaxies making-up the present-day groups are moving towards each other from large distances ($>$ 1 Mpc). It appears unlikely for this correlated motion to be realistic.

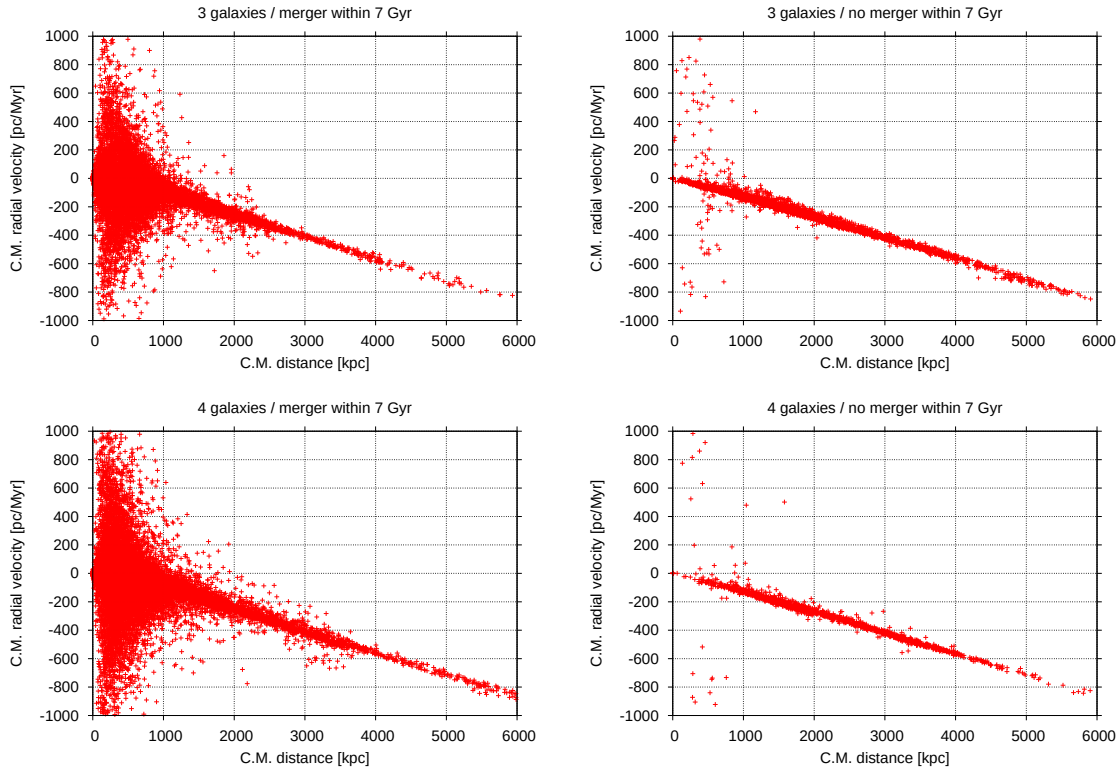

Figure 2: *Compact groups:* The centre of mass radial velocities of the galaxies in dependence of the centre of mass distances at -7 Gyr for the three-galaxy groups (top panel) and the four-galaxy groups (bottom panel). Similar to Fig. 1, the left panel refers to solutions where at least one pair of galaxies will be merging within the next 7 Gyr, while the right panel refers to solutions without a merger within the next 7 Gyr. The data are extracted from the results for Model *C*.

Appendix

The 100 compact groups from the *SDSS* catalogue considered in this publication are (56 groups with three and 44 with four members):

SDSSCGA00027, 00029, 00037, 00110, 00113, 00131, 00132, 00177, 00240, 00275, 00309, 00345, 00355, 00375, 00397, 00407, 00418, 00425, 00435, 00483, 00488, 00510, 00539, 00621, 00630, 00673, 00676, 00711, 00728, 00735, 00736, 00752, 00755, 00798, 00800, 00811, 00820, 00895, 00902, 00912, 00916, 00933, 00934, 00954, 00960, 01012, 01020, 01036, 01056, 01059, 01065, 01076, 01136, 01139, 01184, 01220, 01244, 01251, 01264, 01265, 01277, 01300, 01303, 01327, 01344, 01372, 01383, 01391, 01428, 01434, 01446, 01458, 01485, 01503, 01512, 01528, 01557, 01563, 01568, 01605, 01616, 01667, 01713, 01724, 01784, 01841, 01874, 01932, 02022, 02037, 02056, 02188, 02191, 02192, 02206, 02237, 02257, 02270, 02273, 02277.

Acknowledgements

W. Oehm would like to express his gratitude for the support of scdsoft AG in providing a SAP system environment for the numerical calculations. Without the support of scdsoft's executives *P. Pfeifer* and *U. Temmer* the innovative approach of programming the numerical tasks in SAP's language ABAP would not have been possible.

References

[1] Appleton, P. N., Davies, R. D., Stephenson, R.: The neutral hydrogen content of the M81/M82 group of galaxies I. The observations. Monthly Not. Roy. Astron. Soc. **195** (1981), 327–352.

[2] Behroozi, P. S., Wechsler, R. H., Conroy, C.: The average star fromation histories of galaxies in dark matter halos from z = 0–8. Astrophys. J. **770** (2013), 57–92.

[3] Bernardi, M. et al.: Galaxy luminosities, stellar masses, sizes, velocity dispersions as a function of morphologocal type. Monthly Not. Roy. Astron. Soc. **404** (2010), 2087–2122.

[4] Binney, J., Tremaine, S.: *Galactic Dynamics*. Princeton University Press, New Jersey, 2008.

[5] Chandrasekhar, S.: *Principles of Stellar Dynamics*. University of Chicago Press, Chiccago, 1942.

[6] Chandrasekhar, S.: Dynamical Friction. I. General Considerations: the Coefficient of Dynamical Friction. Astrophys. J. **97** (1943), 255–262.

[7] Charbonneau, P.: Genetic algorithms in Astronomy and Astrophysics. Astrophys. J. Supplement Series **101** (1995), 309–334.

[8] Goodman, J., Weare, J.: Ensemble samplers with affine invariance. Communications in Applied Mathematics and Computationel Science **5 (1)** (2010), 65–80.

[9] Cottrell, G. A.: 21-cm observations of the interacting galaxies M81 and M82. Monthly Not. Roy. Astron. Soc. **178** (1977), 577–589.

[10] Gottesman, S. T., Weliachev, L.: A high angular resolution study of the neutral hydrogen in the IRR II galaxy M82. Astrophys. J. **211** (1977), 47–61.

[11] Hickson, P.: Systematic properties of compact groups of galaxies. Astrophys. J. **255** (1982), 382–391.

[12] Hickson, P., Kindl, E., Huchra, J. P.: Morphology of galaxies in compact groups. Astrophys. J. **331** (1988), 64–70.

[13] Hickson, P., Mendes de Oliveira, C., Huchra, J. P., Palumbo, G. G.: Dynamical properties of compact groups of galaxies. Astrophys. J. **399** (1992), 353–367.

[14] Hickson, P.: Compact groups of galaxies. Annual Review of Astronomy and Astrophysics **35** (1997), 357–388.

[15] Jiang, C. Y. et al.: A fitting formula for the merger timescale of galaxies in hierarchical clustering. Astrophys. J. **675** (2008), 1095–1105.

[16] Macciò, A. V. et al.: Concentration, spin and shape of dark matter haloes: scatter and the dependence on mass and environment. Monthly Not. Roy. Astron. Soc. **378** (2007), 55–71.

[17] Navarro, J. F., Frenk, C. S., White, S. D. M.: Simulations of X-ray clusters. Monthly Not. Roy. Astron. Soc. **275** (1995), 720–740.

[18] Oehm, W., Thies, I., Kroupa, P.: Constraints on the dynamical evolution of the galaxy group M81. Monthly Not. Roy. Astron. Soc. **467** (2017), 273–289.

[19] Petsch, H. P., Theis, C.: Modeling merging galaxies using MINGA: Improving restricted N-body by dynamical friction. Astronomische Nachrichten **329** (2008), 1046–1049.

[20] Sohn, J. et al.: Compact groups of galaxies with complete spectroscopic redshifts in the local universe. J. Korean Astron. Soc. **48** (2015), 381–398.

[21] Thomson, R. C., Laine, S., Turnbull, A.: Towards an Interaction Model of M81, M82 and NGC 3077. In: J. E. Barnes, D. B. Sanders (Eds.), *Galaxy Interactions at Low and High Redshift*, *Proc. IAU Symp.*, vol. 186, pp. 135. Kluwer, Dordrecht, 1999.

[22] van der Hulst, J. M.: The structure and kinematics of the neutral hydrogen bridge between M81 and NGC 3077. Astron. Astrophys. **75** (1979), 97–111.

[23] Yun, M. S., Ho, P. T. P., Lo, K. Y.: H I streamers around M82 - Tidally disrupted outer gas disk. Astrophys. J. **411** (1993), L17–L20.

[24] Yun, M. S., Ho, P. T. P., Lo, K. Y.: A high-resolution image of atomic hydrogen in the M81 group of galaxies. Nature **372** (1994), 530–532.

[25] Yun, M. S.: Tidal interactions in M81 group. In: J. E. Barnes, D. B. Sanders (Eds.), *Galaxy Interactions at Low and High Redshift*, *Proc. IAU Symp.*, vol. 186, pp. 81–88. Kluwer, Dordrecht, 1999.

Conference *Cosmology on Small Scales 2018*
Michal Křížek and Yurii Dumin (Eds.)
Institute of Mathematics CAS, Prague

CAN THE DARK-MATTER DEFICIT IN THE HIGH-REDSHIFT GALAXIES EXPLAIN THE PERSISTENT DISCREPANCY IN HUBBLE CONSTANTS?

Yurii V. Dumin[1,2]

[1]P.K. Sternberg Astronomical Institute of M.V. Lomonosov Moscow State University
Universitetskii prosp., 13, 119234, Moscow, Russia
[2]Space Research Institute of the Russian Academy of Sciences
Profsoyuznaya str. 84/32, 117997, Moscow, Russia
dumin@yahoo.com, dumin@sai.msu.ru

Abstract: One of hot topics in the last years is a systematic discrepancy in the determination of Hubble parameter by various methods. Namely, the values derived "directly" from the distance scale based on Cepheids and supernovae — and referring to the relatively "local" part of the Universe — are about 10% greater than the ones following from the analysis of the cosmic microwave background (CMB) radiation, which refers to the "global" scales. The most popular interpretation of this discord, widely discussed nowadays, is variation of the dark-energy equation-of-state parameter w. However, there might be a much simpler explanation, following from the recent observations of the rotation curves in the high-redshift galaxies. Namely, it was found that they have much smaller dark-matter halos than galaxies in the vicinity of us [5]. Since both the dark and luminous matter possess the same dust-like equation of state and, therefore, their average cosmological densities evolve by the same way, our local neighborhood is not quite typical but rather overfilled with the dark matter. Then, the local value of the Hubble constant should be greater than the global one. Roughly speaking, a twofold excess of the dark matter in our local Universe would give just the above-mentioned 10% increase in the value of Hubble parameter.

Keywords: Hubble constant, dark matter, high-redshift galaxies

PACS: 98.80.Es, 95.35.+d, 95.36.+x, 98.62.Gq

Determination of the Hubble parameter H_0 is a long-standing problem in cosmology, lasting for almost a century; and the corresponding values varied in this period by an order of magnitude, 50 to 500 $\mathrm{km\,s^{-1}\,Mpc^{-1}}$ (see, for example, [4], [13] and references therein). Despite of considerable improvements, some discrepancies persist till now. The most notable of them is that the value of H_0 derived from

the distance scale based on Cepheids and supernovae is $73.24\pm1.74\,\mathrm{km\,s^{-1}\,Mpc^{-1}}$ and, for some calibration, can even be as large as $76.18\pm2.37\,\mathrm{km\,s^{-1}\,Mpc^{-1}}$ [12]. On the other hand, the analysis based on measurements of the cosmic microwave background (CMB) by *Planck* satellite under assumption of the ΛCDM cosmological model leads to the values $H_0 = 66.88\pm0.91$ to $67.31\pm0.96\,\mathrm{km\,s^{-1}\,Mpc^{-1}}$, depending on the method of data processing [1]. So, these numbers are about 10% less than in the first case.

The above-mentioned discrepancy between the "local" (by Cepheids) and "global" (by CMB) measurements of H_0 was clearly recognized in the recent years, and it is commonly attributed now either to the systematic errors (such as degeneracy between different quantities in the analysis of CMB) or to the uncertainty in the fitting parameters (e.g., the number and masses of neutrinos, etc.) [2], [15]. Yet another popular explanation is a modification of the dark-energy equation-of-state parameter w (where $p = w\rho$) [3], [6], [9], [16]; though the resulting values $w < -1$ look quite suspicious from the viewpoint of general physical principles.[1]

However, from our point of view, the spread in values of H_0 can have a much more straightforward explanation, following from the recent observations of the rotation curves in distant galaxies [5], [14]: it was found that the amount of dark matter is considerably less in the vicinity of galaxies located at large redshifts, $z = 0.6{-}2.6$. Next, it should be kept in mind that due to the same dust-like equation of state ($w \approx 0$) both for the luminous and dark matter, the ratio of their densities does not change with cosmological time. So, we have to conclude that this ratio should be substantially variable in space and, thereby, the Hubble parameter should be scale-dependent.

Really, according to the standard Friedmann equation [11]:

$$H_0 = \left[\frac{8\pi G}{3}\right]^{1/2} \Big[\rho_{\mathrm{de}} + \langle\rho_{\mathrm{dm}}\rangle + \langle\rho_{\mathrm{lm}}\rangle\Big]^{1/2}, \tag{1}$$

where ρ_{de} is density of the dark energy, which is assumed to be perfectly uniform in space (i.e., described by the Λ-term), ρ_{dm} and ρ_{lm} are densities of the dark and luminous (baryonic) matter, and the angular brackets denote averaging over the given spatial scale. Then, ratio of the Hubble parameters at the local and global scales should be:[2]

$$\frac{H_0^{(\mathrm{loc})}}{H_0^{(\mathrm{glob})}} = \left[\frac{\Omega_{\mathrm{de}} + \langle\Omega_{\mathrm{dm}}\rangle^{(\mathrm{loc})} + \langle\Omega_{\mathrm{lm}}\rangle}{\Omega_{\mathrm{de}} + \langle\Omega_{\mathrm{dm}}\rangle^{(\mathrm{glob})} + \langle\Omega_{\mathrm{lm}}\rangle}\right]^{1/2}, \tag{2}$$

where $\Omega_i = \rho_i/\rho_{\mathrm{c}}$ are the corresponding densities normalized to the critical density at

[1] For example, the values of w somewhat greater than -1 (i.e., $|w| < 1$) could be easily attributed to the small-scale irregularities of the scalar field representing the "dynamic" dark energy [8], but such an effect cannot result in $w < -1$.

[2] For simplicity, we ignore here the curvature term that might appear at the local scales due to the non-uniform dark matter distribution.

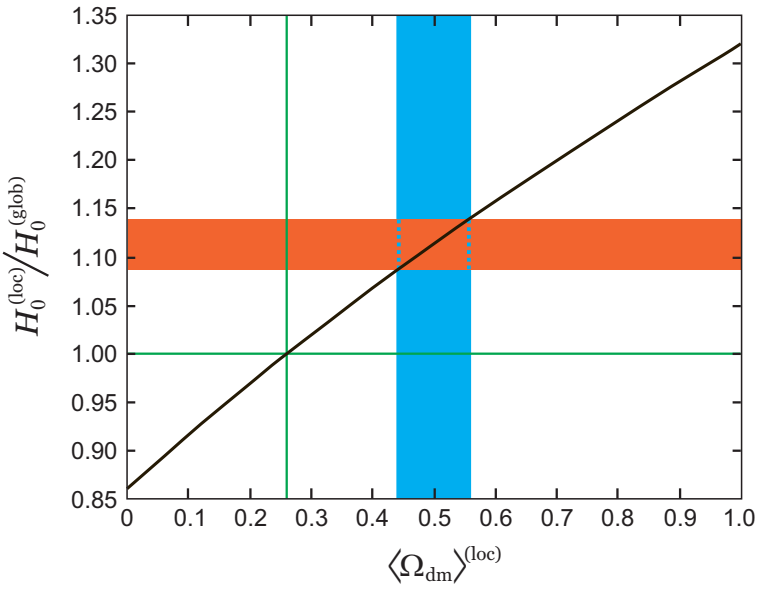

Figure 1: Ratio of the Hubble parameters at the local and global scales $H_0^{(\mathrm{loc})}/H_0^{(\mathrm{glob})}$ as function of the local dark-matter density normalized to the global critical density $\langle\Omega_{\mathrm{dm}}\rangle^{(\mathrm{loc})}$ (diagonal black curve). Horizontal red and vertical blue strips show the range of observable values. Horizontal and vertical green lines correspond to the trivial case when $\langle\Omega_{\mathrm{dm}}\rangle^{(\mathrm{loc})} = \langle\Omega_{\mathrm{dm}}\rangle^{(\mathrm{glob})}$.

the global scale; and we assume that the luminous matter distribution is sufficiently uniform.

This ratio of the Hubble parameters is plotted in Fig. 1 as function of the local dark-matter density at the standard cosmological parameters: $\Omega_{\mathrm{de}} = 0.69$, $\langle\Omega_{\mathrm{dm}}\rangle^{(\mathrm{glob})} = 0.26$, and $\langle\Omega_{\mathrm{lm}}\rangle = 0.05$. The range of observed values of $H_0^{(\mathrm{loc})}/H_0^{(\mathrm{glob})}$ is shown by the horizontal red strip. Then, the corresponding normalized densities of the dark matter in our local cosmological neighborhood should be in the range $\langle\Omega_{\mathrm{dm}}\rangle^{(\mathrm{loc})} = 0.44 - 0.56$ (vertical blue strip), i.e. about two times greater than globally.

In fact, Genzel, et al. [5] already emphasized that at the global scales the dark matter should play a smaller part than in the local Universe. So, from our point of view, the systematic discrepancy between the "local" and "global" values of the Hubble parameter is just a direct consequence of the above-mentioned fact.

Finally, let us mention that a number of papers published in the recent years made just the opposite statement as compared to [5]: namely, that there is a considerable deficit of luminous and dark matter in our local cosmological neighborhood. For example, Makarov & Karachentsev [10] and Karachentsev [7] found $\Omega_{\mathrm{dm}} + \Omega_{\mathrm{lm}} = 0.08 \pm 0.02$ in the sphere of radius $z \sim 0.01$ around us, which is over three times smaller than the standard value in the ΛCDM model. Unfortunately, their analysis

involved a lot of model assumptions. On the other hand, the work by Genzel, et al. [5], which is based solely on the galaxy rotation curves, seems to be much less model-dependent; and the corresponding results on the deficit of dark matter in the high-redshift (rather than local) galaxies look more reliable.

Acknowledgements

I am grateful to Yu.V. Baryshev, S.M. Kopeikin, M. Křížek, A. Maeder, and M. Nowakowski for valuable discussions of the problem of small-scale Hubble expansion, as well as to the referee for a few important remarks.

References

[1] Aghanim, N., Ashdown, M., Aumont, J., et al. (Planck Collaboration): Planck intermediate results: XLVI. Reduction of large-scale systematic effects in HFI polarization maps and estimation of the reionization optical depth. Astron. Astrophys. **596** (2016), A107.

[2] Bernal, J.L., Verde, L., and Riess, A.G.: The trouble with H_0. J. Cosmol. Astropart. Phys. **10** (2016), 019.

[3] Di Valentino, E.: Crack in the cosmological paradigm. Nature Astron. **1** (2017), 569.

[4] Freedman, W.L.: Cosmology at a crossroads. Nature Astron. **1** (2017), 0121.

[5] Genzel, R., Förster Schreiber, N.M., Übler, H., et al.: Strongly baryon-dominated disk galaxies at the peak of galaxy formation ten billion years ago. Nature **543** (2017), 397.

[6] Huang, Q.-G. and Wang, K.: How the dark energy can reconcile Planck with local determination of the Hubble constant. Eur. Phys. J. C **76** (2016), 506.

[7] Karachentsev, I.D.: Missing dark matter in the local Universe. Astrophys. Bull. **67** (2012), 123.

[8] Linde, A.D.: The inflationary Universe. Rep. Prog. Phys. **47** (1984), 925.

[9] Liu, Z.-E., Yu, H.-R., Zhang, T.-J., and Tang, Y.-K.: Direct reconstruction of dynamical dark energy from observational Hubble parameter data. Phys. Dark Univ. **14** (2016), 21.

[10] Makarov, D. and Karachentsev, I.: Galaxy groups and clouds in the local ($z \sim 0.01$) Universe. Mon. Not. R. Astron. Soc. **412** (2011), 2498.

[11] Olive, K.A. and Peacock, J.A.: Big-bang cosmology. In: Particle Data Group: *Review of Particle Physics.* Chin. Phys. C **40** (2016), 100001, p. 355.

[12] Riess, A.G., Macri, L.M., Hoffmann, S.L., et al.: A 2.4% determination of the local value of the Hubble constant. Astrophys. J. **826** (2016), 56.

[13] Ryden, B.: A constant conflict. Nature Phys. **13** (2017), 314.

[14] Swinbank, M.: Distant galaxies lack dark matter. Nature **543** (2017), 318.

[15] Verde, L., Protopapas, P., and Jimenez, R.: Planck and the local Universe: Quantifying the tension. Phys. Dark Univ. **2** (2013), 166.

[16] Zhao, G.-B., Raveri, M., Pogosian, L., et al.: Dynamical dark energy in light of the latest observations. Nature Astron. **1** (2017), 627.

Conference *Cosmology on Small Scales 2018*
Michal Křížek and Yurii Dumin (Eds.)
Institute of Mathematics CAS, Prague

STELLAR AND DARK MATTER DENSITY IN THE LOCAL UNIVERSE

I.D. Karachentsev[1], K.N. Telikova[2]

[1] Special Astrophysical Observatory RAS
Nizhnij Arkhyz, Karachai-Cherkessian Republic 369167, Russia
ikar@sao.ru
[2] Ioffe Institute
26 Politekhnicheskaya, St. Petersburg, 194021, Russia
ks.telikova@mail.ru

Abstract: We calculate the mean density profiles for luminous and dark matter on distance scales $D \sim (1-100)$ Mpc around us using recent all-sky catalogs of galaxy groups. Within the Local Volume ($D < 11$ Mpc) we derived the mean stellar density $\Omega_* = 0.44\,\%$ in the critical density units and the mean total matter density $\Omega_m = 0.17$. In the sphere with a radius of 40 Mpc these quantities drop to $\Omega_* = 0.24$–$0.32\,\%$ and $\Omega_m = 0.09$–0.14. In a larger volume within $D \sim 135$ Mpc the discussed densities become more uncertain: $\Omega_* = 0.20$–$0.24\,\%$ and $\Omega_m = 0.05$–0.16. We summarize that the major part of the cosmic dark matter locates outside the virial and collapsing zones of groups and clusters.

Keywords: cosmology, dark matter, galaxy formation

PACS: 4.20-q, 95.35+d, 95.30.Sf

1. Introduction

Observational data on the structure and kinematics of the Local Universe is the widely used base for checking cosmological models. On a number of occasions this fact was pointed by Peebles [29], [30]. The paucity information on galaxy distances was a serious hindrance for the observational cosmology of the Local Universe for a long time. The situation has changed dramatically with the Hubble Space Telescope (HTS) commissioning. The unique abilities of the HST let astronomers separate the individual stars in the nearby galaxies and estimate the galaxy distances by the tip of the red giant branch (TRGB) method with $\sim$(5–10) % accuracy. In the fast observational regime (one galaxy per unit orbit) it is available to measure distances for galaxies within 11 Mpc. At the present time the total number of galaxies with measured TRGB-distances in the Local Volume ($D < 11$ Mpc) is about 400. These

measurements are involved in the Updated Nearby Galaxy Catalog (UNGC) [19] and the Extragalactic Distance Database (EDD) [45].

Outside the Local Volume the galaxy distances were estimated by Cepheid variables, type Ia supernovae and surface brightness fluctuations with (5–10)% accuracy (see EDD and references therein). Distances for about 5 000 gas-rich galaxies were determined by Tully & Fisher relation [44] between galaxy's luminosity and 21-cm emission line width with $\sim$(20–25) % accuracy. Half of them locates within a distance of ~ 70 Mpc.

Courtois et al. [6] created maps of the large-scale distribution of galaxies in the Local Universe. These maps demonstrate the complicate density pattern produced by galaxy groups, clusters and empty areas. However, it is not easy to conclude from distribution of the attractors and voids surrounding the Milky Way whether our Galaxy is: in underdensity or overdensity region.

As far as we know, the first reconstruction of the mean density profile versus distance from the Milky Way was done by Makarov & Karachentsev [24]. The authors calculated the stellar and total (virial) mass density up to $D \simeq 45$ Mpc using a sample comprising 11 000 galaxies with Galactic latitudes $|b| > 15°$. On these scales the estimated mean stellar density is greater than its global value. Nevertheless, the mean total density Ω_m in the critical density units is systematically lower than the cosmological value $\Omega_m = 0.24$ from WMAP [37] or $\Omega_m = 0.315$ from Planck Collaboration [31].

The fact that the virial masses of nearby groups and clusters cannot provide the cosmological value of the matter density in the ΛCDM model has been already known. According to independent estimates by Vennik [46] and Tully [40], the mean virial mass density inside the Local Supercluster is $\Omega_m \simeq 0.08$, which 3–4 times less than its global value. Potential causes of this discrepancy were discussed in detail by Karachentsev [16]. Note that recent papers [41], [42], [23], [36] make an important contribution to "the missing dark matter" problem.

In the next sections we present estimations of the mean luminous and total (dark) matter density on different scales from nearby widely investigated volume to farther poorly known regions in the Local Universe.

2. Mean density profile in the Local Volume

The Updated Nearby Galaxy Catalog involves 869 galaxies with radial velocities $V_{LG} < 600\,\mathrm{km\,s^{-1}}$ or distances $D < 11$ Mpc. Regularly updated online version of this database[1] contains 1029 galaxies at the beginning of 2018 year [15].

Stellar masses in the UNGC were inferred from K-band luminosity of the galaxies as $M_* \approx (M_\odot/L_\odot)L_K$, see [2]. Majority of K-band magnitudes were measured in 2MASS Redshift Survey [12]. It is common knowledge that 2MASS misses low surface brightness galaxies, especially with predominantly blue stellar population because of

[1] http://www.sao.ru/lv/lvgdb

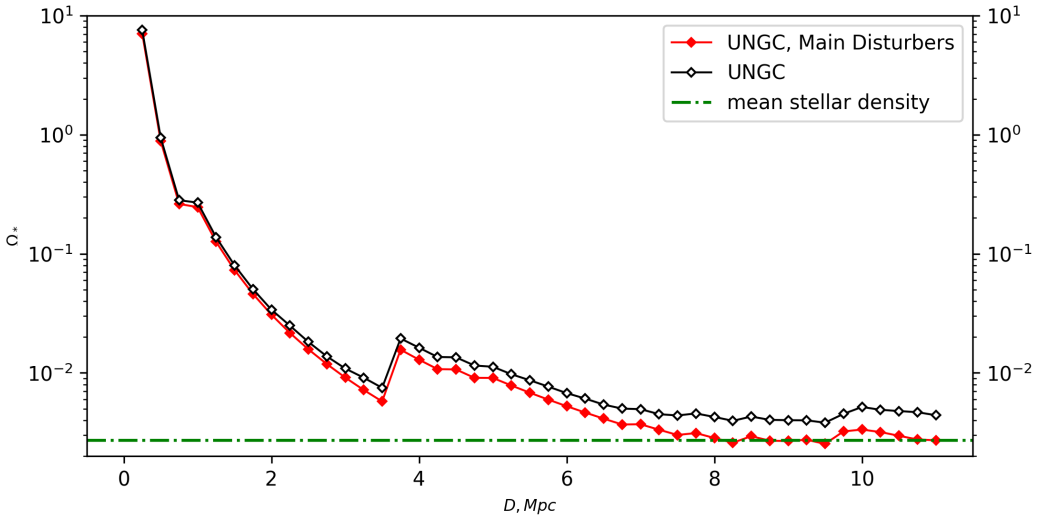

Figure 1: Mean density of stellar matter within a distance D in the Local Volume. Empty diamonds show the stellar density of all galaxies in the UNGC, filled diamonds correspond to the stellar density produced by 21 Main Disturbers seen in Table 1. Dash-dotted horizontal line shows the global cosmic stellar density from [9].

shot exposure time. For missing galaxies K-band magnitudes in UNGC were derived from B-magnitudes with respect to morphological types T as [13]

$$K = \begin{cases} B - 4.10 & \text{for } T < 3, \\ B - 4.60 + 0.25T & \text{for } 3 \leq T \leq 8, \\ B - 2.35 & \text{for } T > 8. \end{cases} \quad (1)$$

Two dozens high luminosity galaxies such as our Milky Way locate in the Local Volume. With respect to random orientation of the satellites' orbits and their mean eccentricity $\langle e^2 \rangle = 1/2$, the total mass of the parent galaxy halo can be defined as [17]

$$M_{tot} = (16/\pi) G^{-1} \langle \Delta V^2 \; R_p \rangle, \quad (2)$$

where R_p is the projected separation between the dominated galaxy and its companion, ΔV is their radial velocity difference and G is the gravitational constant. The sample of the luminous galaxies (Main Disturbers) with Galactic latitudes $|b| > 15^\circ$ in the Local Volume is seen in Table 1. Its columns contain: (1) galaxy name, (2) distance in Mpc, (3) radial velocity in the Local Group frame in $\mathrm{km\,s^{-1}}$, (4) logarithm of stellar mass in the solar mass units, (5) logarithm of halo mass, inferred from projected separation and radial velocity difference of the companions. Almost half of the galaxy population in the Local Volume belong to satellites of these luminous galaxies.

Galaxy	D	V_{LG}	$\log M_*$	$\log M_{tot}$
	Mpc	$\mathrm{km\,s^{-1}}$	$M_\odot$	$M_\odot$
Milky Way	0.01	−65	10.70	12.07
M31	0.77	−29	10.79	12.23
NGC5128	3.68	310	10.89	12.89
M81	3.70	104	10.95	12.69
NGC253	3.70	276	10.98	12.18
NGC4826	4.41	365	10.49	10.78
NGC4736	4.41	352	10.56	12.43
NGC5236	4.90	307	10.86	12.02
M101	6.95	378	10.79	12.17
NGC4258	7.66	506	10.92	12.50
NGC3627	8.32	579	10.82	12.16
M51	8.40	538	10.97	11.78
NGC2903	8.87	443	10.82	11.68
NGC5055	9.04	562	11.00	12.49
NGC4594	9.55	894	11.30	13.45
NGC6744	9.51	706	10.91	11.72
NGC3115	9.68	439	10.95	12.54
NGC2683	9.82	334	10.81	12.13
NGC891	9.95	736	10.98	11.90
NGC628	10.2	827	10.60	11.66
NGC3379	11.0	774	10.92	13.23

Table 1: Luminous galaxies at $|b| > 15^\circ$ in the Local Volume.

Figure 1 shows the mean stellar density in the Local Volume as a function of distance from the Milky Way. The global value of stellar density $\Omega_{*c} = 0.0027 \pm 0.0005$ (see [9]) in the critical density units in Figure 1 is in a good agreement with the mean K-luminosity density $j_K = (4.3 \pm 0.2) \times 10^8\ L_\odot\,\mathrm{Mpc^{-3}}$ from [14], [8]. The critical density can be expressed via the Hubble parameter H_0 as

$$\rho_C = \frac{3H_0^2}{8\pi G}, \tag{3}$$

consequently $\rho_C = 10^{-26}\ \mathrm{kg\,m^{-3}}$ or $1.46 \times 10^{11}\ M_\odot\,\mathrm{Mpc^{-3}}$ for $H_0 = 73\,\mathrm{km\,s^{-1}\,Mpc^{-1}}$. Here and in the sections below we use a prefactor $(1-\sin 15^\circ)^{-1} \simeq 1.35$ to compensate missed galaxies at $|b| < 15^\circ$. The total stellar mass of the 21 high luminosity galaxies is $1.6 \times 10^{12}\ M_\odot$ or 59% from the total stellar mass of the whole Local Volume sample. Notice that stellar density on all the scales $D < 11\,\mathrm{Mpc}$ is greater than its global cosmic value.

Figure 2 shows the mean dark matter density in the Local Volume within a distance D from the Milky Way. In the current cosmological scenarios the star formation process is the most efficient for stellar masses $M_* \simeq 10^{9-10}\ M_\odot$ [39]. This feature is

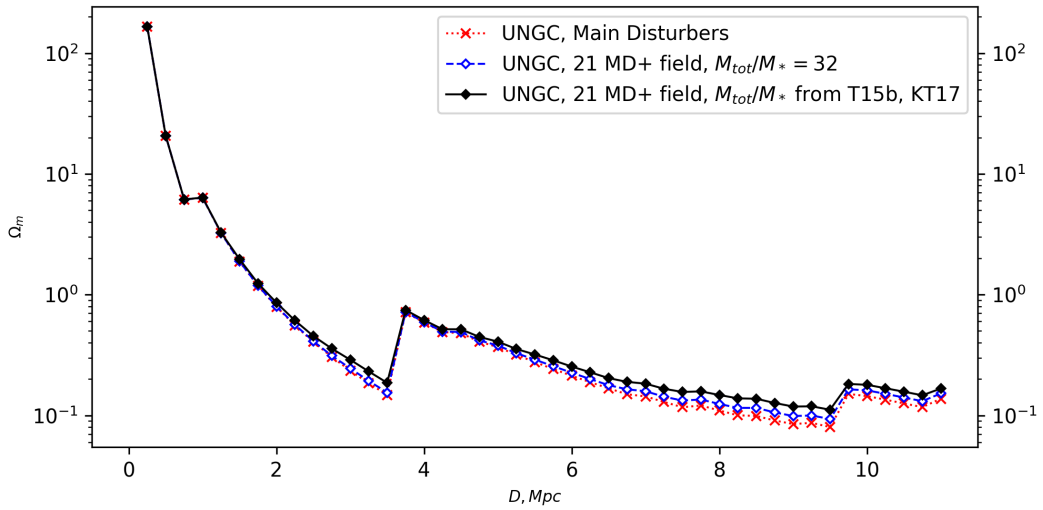

Figure 2: Mean density of dark matter within a distance D in the Local Volume. Crosses shows the dark matter density from 21 Main Disturbers. Filled and empty diamonds show the dark matter density with account of all galaxies in the UNGC. Here, the total masses of field galaxies were estimated under the assumption that $M_{tot}/M_* \simeq 32$ (see [17]) or using equation (4) (see [42], [23]) and shown as filled and empty diamonds, respectively.

accompanied with increase of the mass-to-light ratio, M_{tot}/M_*, towards luminous as well as faint galaxies. Kourkchi & Tully provided an analytical approximation for mass-to-light ratio with such two branches [23]:

$$\log(M_{tot}/M_*) = \begin{cases} \log(32) - 0.50\log(M_*/10^{10}) & \text{for } \log M_* < 8.97, \\ \log(32) + 0.15\log(M_*/10^{10}) & \text{for } \log M_* > 10.65. \end{cases} \quad (4)$$

The estimate of the dark matter density based on eq. (4) has a bit greater value than that based on $M_{tot}/M_* \simeq 32$ relation following from Table 1 data. The total mass of the Local Volume turns out to be $10^{14} M_\odot$ with the respective mean dark matter density $\Omega_m = 0.17$.

It can be seen from Figures 1 and 2 that the profile of $\Omega_m(D)$ is similar to $\Omega_*(D)$. Naturally, this result is expected because of the basic contribution of the 21 luminous galaxies to Ω_* and Ω_m.

3. Mean density profile in the Local Supercluster, z < 0.01

For 11 000 galaxies with radial velocities $V_{LG} < 3\,500\,\mathrm{km\,s^{-1}}$ at $|b| > 15°$ Makarov & Karachentsev applied a new group-finding algorithm. In contrast to "Friends of Friends" percolation algorithm [10], the authors took into account a vast luminosity difference existing among galaxies [24]. They assumed that virtual galaxy pair has

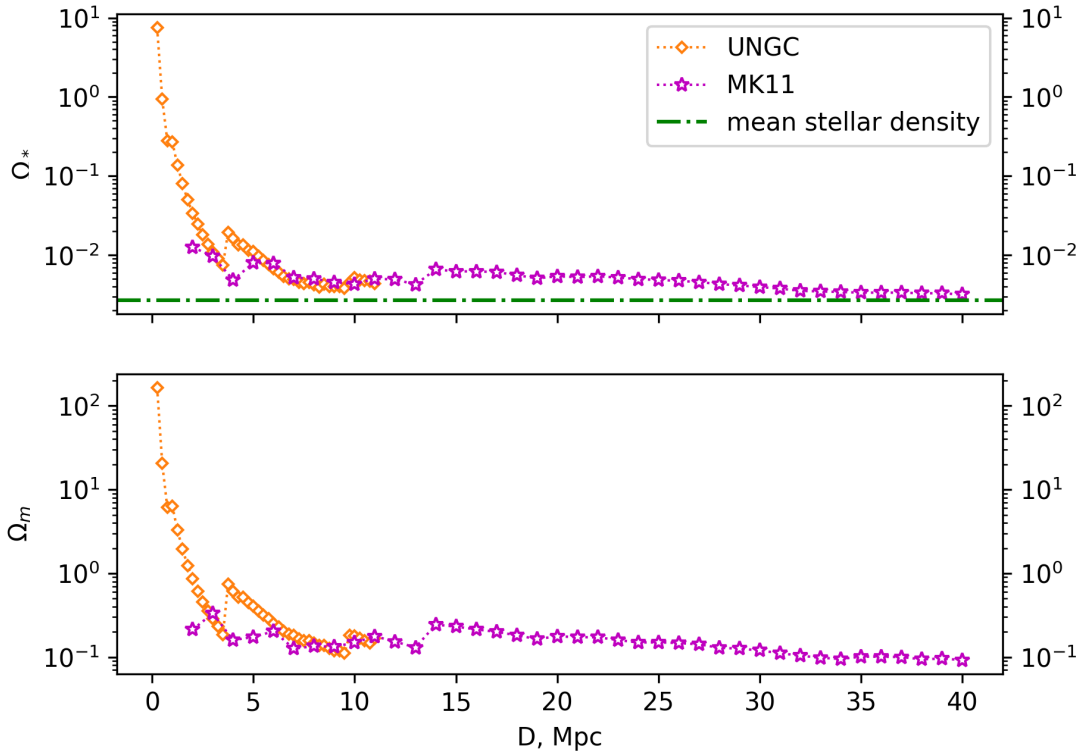

Figure 3: Mean density of the stellar matter (upper panel) and dark matter (lower panel) within a distance D up to 40 Mpc. Diamonds and stars show the mean density by UNGC (Local Volume) and MK11 data, respectively. Dash-dotted horizontal line in the upper panel shows the global cosmic stellar density.

negative total energy and pair's members have a crossing time less than the age of the Universe. The varying parameter of the clusterization was calibrated by nearby galaxy groups. Using this procedure the authors created catalogs of 509 galaxy pairs [18], 168 triplets [25] and 395 galaxy groups with more then 3 members [24]. As a result, the catalogs contain 54% of the initial galaxy sample or 82% of its total K-band luminosity.

Figure 3 shows profiles of the mean density of stellar matter (upper panel) and dark matter (lower panel) within different distances up to $D = 40$ Mpc calculated in the Local Volume (Figure 1 and 2) and by Makarov & Karachentsev [24] (hereinafter referred to as MK11). All density profiles in this paper are calibrated with the Hubble parameter $H_0 = 73\,\mathrm{km\,s^{-1}\,Mpc^{-1}}$. The mean stellar density on the distance scales $D < 40$ Mpc is systematically greater than that of global cosmic value. Estimated total stellar mass and mean stellar density within this volume are $9.2 \times 10^{13} M_\odot$ and 0.32 % in the critical density units, respectively. Taking into account that the galaxy

distances in MK11 were estimated simply by their radial velocities, we conclude a good agreement between these two independent Ω_* sequences within the Local Volume. In contrast to Ω_*, the mean density of the virial mass on the scales $D > 6\,\mathrm{Mpc}$ is lower than its cosmological value. Within a sphere of radius $D = 40\,\mathrm{Mpc}$, the total virial mass is $2.7 \times 10^{15} M_\odot$. The mean density on this scales decreases to $\Omega_m = 0.09$. The second peak in the both panels is the result of the Virgo cluster contribution with its virial mass of $6.3 \times 10^{14} M_\odot$, see [36].

Kourkchi & Tully (hereafter KT17) recently published a new catalog of galaxy groups with the same limits for radial velocity $V_{LG} < 3\,500\,\mathrm{km\,s^{-1}}$ and Galactic latitude $|b| > 15^\circ$ as in MK11 [23]. For clusterization algorithm KT17 used some empirical relations between the virial radius, velocity dispersion and the total mass of groups. The authors provided two types of estimations of the total group mass. Dynamic masses were inferred from radial velocity dispersion σ_p^2 and the mean harmonic radius of the group R_g:

$$M_{dyn} = (\alpha\pi/2G)\sigma_p^2 R_g, \tag{5}$$

where parameter $\alpha = 2.5$ is written to account for projection effects. Paucity of knowledge about the kinematics of distant galaxies implies significant uncertainties of M_{dyn}. That is why KT17 applied also another mass estimate. To determine the halo mass from a galaxy stellar mass (or L_K-luminosity) they used equation (4). All scaling relations were calibrated with 8 nearby galaxy groups. In the clusterization criterion authors took into account the significant difference of galaxies' luminosities. As a result, KT17 applied their algorithm to 15 004 galaxies and created the catalog of 1 536 galaxy groups which is presented in EDD[2]. About 49% of the total sample still remained as isolated galaxies. We used this catalog to investigate the stellar and virial mass distribution on the distance scales $D < 40\,\mathrm{Mpc}$. For unification we restate data from KT17 for the same Hubble parameter $H_0 = 73\,\mathrm{km\,s^{-1}\,Mpc^{-1}}$.

Figure 4 presents the mean stellar density profile up to $D = 40\,\mathrm{Mpc}$ based on KT17 catalog. As seen, the difference between the mean density within Northern and Southern Galactic hemispheres varies from factor 5 at the Virgo cluster distance to factor 2 at the edge of considered volume. In this figure we also added the MK11 results. In almost all the bins Ω_* from KT17 catalog is slightly lower than the mean density in MK11. The ratio $\Omega_*^{KT17}/\Omega_*^{MK11}$ is near 0.77 both at the edge of the Local Volume and at $D = 40\,\mathrm{Mpc}$. We suppose that the MK11 catalog infers the total flux from bluish diffuse galaxies, missed in 2MASS survy, more accurately.

The behavior of the dark matter's mean density within a sphere of radius D is shown in the Figure 5. Its upper and lower panels present the virial masses estimated by equation (4), M_{Lum}, and by galaxy group's kinematic properties, M_{dyn}, respectively. Note a significant difference between the Ω_m for Northern and Southern Galactic hemispheres at all distances $D < 40\,\mathrm{Mpc}$. For mass inferred from galaxy

[2]http://edd.ifa.hawaii.edu

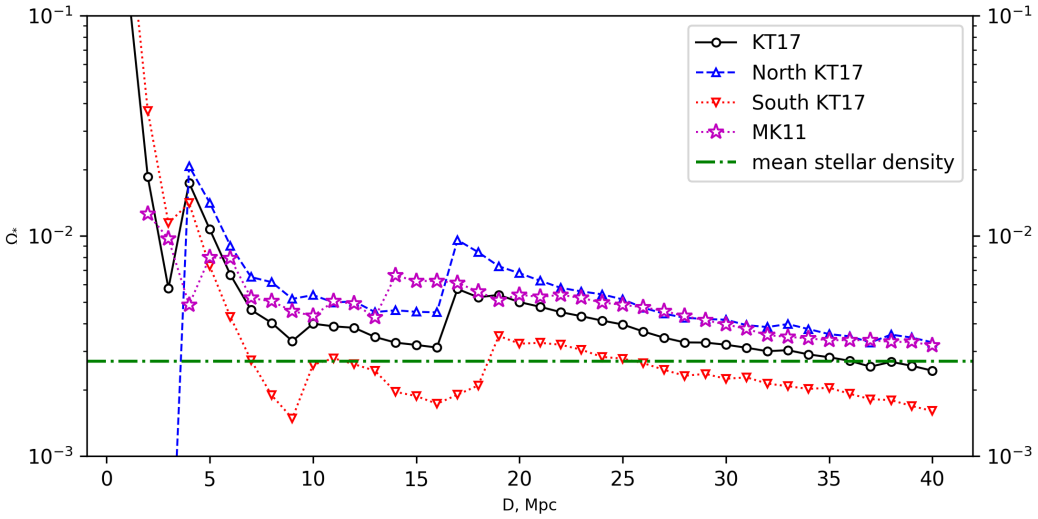

Figure 4: Stellar density within a sphere of radius D. Different symbols show the mean density based on KT17 catalog (circles for all sky, triangles for Northern and Southern hemispheres) and results by MK11 (stars). Dash-dotted horizontal line shows the global stellar density.

group's luminosity this difference is less distinct than for dynamic mass. We conclude that the Local Universe within ~ 40 Mpc does not fit still the size of cosmic homogeneity cell.

In Figure 6 we summarize three independent estimations of the virial mass' mean density within 40 Mpc. In MK11 catalog authors take into account also masses of triple, binary and isolated galaxies. At the $D < 20$ Mpc scales these estimations of Ω_m differ from each other significantly, but at the edge of considered volume the mean densities lie in the narrow range $\Omega_m = 0.09$–0.14, showing a tendency to further decreasing. The total mass within a sphere of radius $D = 40$ Mpc is $(2.7$–$4.0) \times 10^{15} M_\odot$ with the Virgo cluster contribution as (16–23) %.

4. Ω_* and Ω_m within 10000 km s^{-1}

Based on the 2MASS Redshift Survey [11] containing objects with magnitudes up to $K_s = 11.75^m$, Tully (hereafter T15b) created a catalog of galaxy groups with $V_{LG} = 3\,000$–$10\,000$ km s^{-1}, see [42]. The clusterization algorithm of galaxies was the same as in the closer volume [42]. About 58 % of the total sample accounting 24 044 galaxies were clusteried into 3461 groups with two or more members.

It is obvious that on long distances 2MASS Redshift Survey misses a significant number of galaxies because of the bright observational limit $K_s = 11.75^m$. Taking this fact into account, Tully calculated a correction factor (CF) for the total luminosity of a group. To estimate the CF, Tully assumed that galaxy luminosity

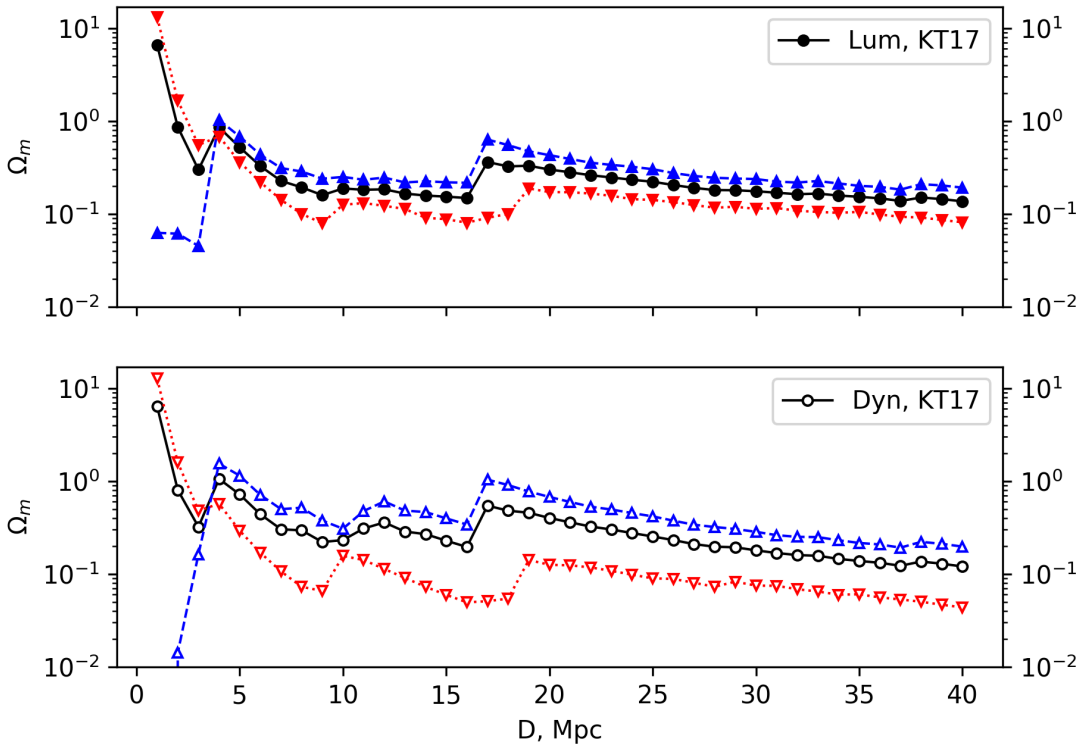

Figure 5: Mean density of the total mass, calculated by luminosity (upper panel) and by dynamic mass (lower panel) from KT17. Different symbols show the mean density for the whole sky (circles) and for Northern/Southern hemisphere (triangles).

function is well described by Schechter function [33] with parameters $\alpha_K = -1.0$ and $M_K^* = -24.23$ at $H_0 = 73\,\mathrm{km\,s^{-1}\,Mpc^{-1}}$. The resulted CF-factor is negligible at $V_{LG} < 1300\,\mathrm{km\,s^{-1}}$, but increases to 2.3 at $V_{LG} = 10000$.

Figure 7 shows the mean stellar density profile calculated on the distance scales $D < 135\,\mathrm{Mpc}$. To fill the nearby volume ($D < 40\,\mathrm{Mpc}$) we used KT17 catalog. For longer distances we used T15b catalog with the correction factor CF. Notice that values of Ω_* for Northern and Southern Galactic hemispheres are approximately equal each other, since $D > 70\,\mathrm{Mpc}$. At the volume edge ($D = 135\,\mathrm{Mpc}$) Ω_* is $(0.22 \pm 0.02)\,\%$ of the critical density, being slightly lower than its global value $(0.27 \pm 0.05)\,\%$ by [9]. The difference between these quantities looks quite expected because 2MASS Survey misses about 20–25 % of the total K-band luminosity.

Distribution of the $\Omega_m(D)$ based on KT17 and T15b catalogs is shown in Figure 8. Its upper and lower panels show the mean density of the total mass estimated by equation (4) with accounting the correction factor CF and by kinematic characteristics of the galaxy groups, respectively.

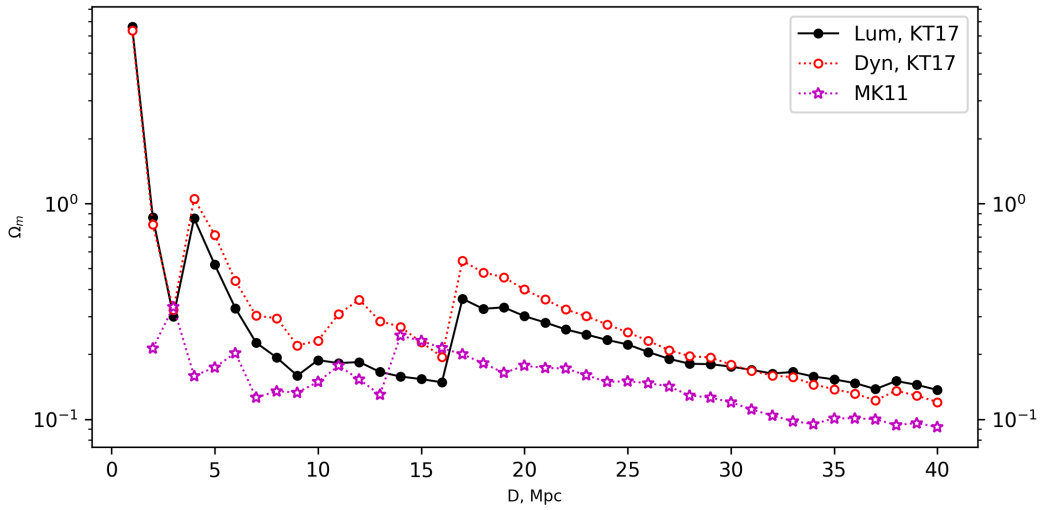

Figure 6: Mean density of the total mass inferred from luminosity of the galaxy groups (filled circles) and from dynamic masses (open circles). Data from MK11 catalog is shown by stars.

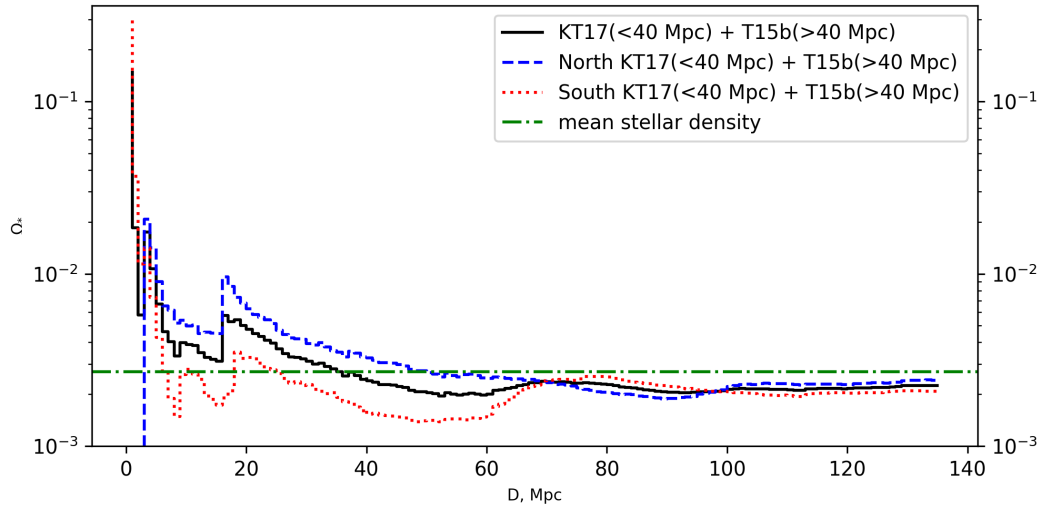

Figure 7: Mean stellar density calculated using KT17 catalog at $D < 40$ Mpc and T15b catalog at $D = 40$–135 Mpc. Middle curve corresponds to the stellar density for the whole sky, upper and lower curves match Northern and Southern hemispheres, respectively. The global stellar density is shown by dash-dotted horizontal line.

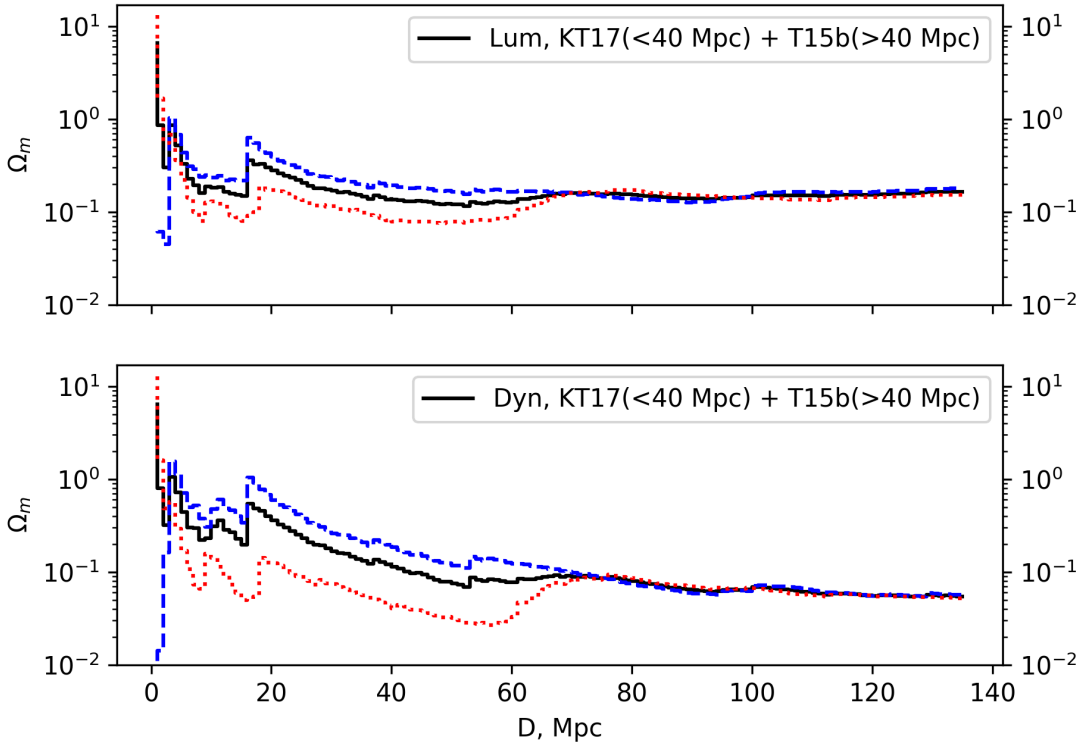

Figure 8: Mean density of the viral mass inferred from group's luminosity (upper panel) and from the dynamic mass (lower panel). Used catalogs are: KT17 at $D < 40$ Mpc and T15b at $D = 40$–135 Mpc. Middle curves correspond to the mean density for the whole sky, upper and lower curves match Northern and Southern hemispheres.

From the Figure 8 one can draw the following conclusions:

a. Difference between Ω_m for Northern and Southern Galactic hemispheres decreases with increasing D and at $D > 70$ Mpc it becomes within (10–15) % of the mean value.

b. Difference between mean densities of the total mass calculated by empirical relation (4) and by kinematic of galaxy groups increases with D and reaches a factor 2–3 at $D > 70$ Mpc.

c. Within a sphere of 135 Mpc radius, the mean density of matter amounts to $\Omega_m = 0.05 \pm 0.002$ via M_{dyn} and $\Omega_m = 0.16 \pm 0.01$ via M_{Lum}. The latter value is in a good agreement with the quantity $\Omega_{collapsed} = 0.16 \pm 0.02$ published by T15b.

5. Discussion and conclusions

For reliable measurements of the mean density of matter within a nearby Universe we need deep photometric and spectroscopic surveys covering a major part of the sky. Moreover, in the Local Volume (~ 10 Mpc) we need also individual estimates of galaxy distances, because their radial velocities are often distorted by a large peculiar component. Recent progress in the galaxy surveys like the Sloan Digital Sky Survey [1] and Pan-STARRS [5] gives astronomers hope to improve these measurements. According to observational data from HST, the mean stellar density within the Local Volume is 1.5–1.8 times greater than the global cosmic value. Consequently, we live inside the positive baryonic matter fluctuation. Alongside this, in the same volume the mean density of dark matter is $\Omega_m = 0.17$–0.18, i.e. less than its global value.

Within the volume of $D < 40$ Mpc including the Local Supercluster and neighboring clusters, the mean stellar density is approximately equal to the global stellar density. Wherein, three independent estimates of the virial masses give $\Omega_m = 0.09$–0.14, the value which is 2–3 times lower than Ω_m in the standard ΛCDM model.

Outside a sphere of radius ~ 50 Mpc, 2MASS photometric survey and 2MASS Redshift Survey miss a significant part of the galaxies. This fact makes the estimates of Ω_* and Ω_m less certain. Using the T15b catalog with the correction factor CF for missed galaxies leads to the mean stellar density within $D = 135$ Mpc nearly the same, 0.8 ± 0.2, as the mean global density. However, our calculations of the mean density of dark matter via dynamic masses of the groups or via the empirical halo-mass-to-luminosity relation yield the Ω_m value in the range from 0.05 to 0.16. Note that the latter value, 0.16, which is calculated from luminous mass, is more trustworthy than the first one.

Using 264 objects from Cosmicflows-3 [43] with accurately measured distances and radial velocities, Shaya et al. [36] applied Numerical Action Method to calculate 3D-trajectories for galaxies, groups and clusters within a distance of 40 Mpc. The authors conclude that their model with parameters $\Omega_m = 0.244$ (WMAP) and $H_0 = 75\,\mathrm{km\,s^{-1}\,Mpc^{-1}}$ is in a good agreement with the existing observational data if they add into their model a dispersed (orphan) dark matter component with $\Omega_{orphan} = 0.077 \pm 0.019$, distributed outside the virial zones of groups and clusters.

Nuza et al. presented distribution of matter in the Local Universe based on N-body simulations accounting for ΛCDM model with $\Omega_m = 0.27$, see [28]. They estimated a cosmic variance on the scale of 80 Mpc to be $\sim 3\,\%$. Such a level corresponds to the concept of homogeneous cosmic cell, but on the other hand, conflicts with the existence of huge structures like Shapley Supercluster [27]. Nuza et al. conclude that the predominant part of the cosmic matter is associated with filaments (34 % of the total mass), while knots (clusters) and walls and voids account for 22 % of the total mass each. Finally, the authors estimate the fraction of dark matter concentrated within the virial zones of groups and clusters in the Local Universe ($D < 40$ Mpc). Their value, $\Omega_m = 0.08$, is consistent with observational data by Karachentsev [16].

There are at least three ideas, which may explain the difference between the local density $\Omega_m \simeq 0.08$ and the global quantity $\Omega_m = 0.24$–0.31:

a. In recent years, we have been able to measure the total mass of nearby groups and clusters not only by internal (virial) galaxy motions, but also by motions of surrounding galaxies, which are retarding by overdensity. In this case the estimate of the total mass correspond to the zero-velocity radius R_0, which exceeds 3–4 times the virial radius R_{vir}. Analysis of the Hubble flow around the Virgo cluster shows that the total mass of the cluster inside R_0 is almost the same as its virial mass [20], [21]. Just similar result has been obtained by Kashibadze & Karachentsev [21] for the Local Group and other nearby groups from analysis of their Hubble flows. Consequently, the assumption about the existence of dark massive halos around local groups and clusters extending to $\sim (3\text{–}4)R_{vir}$ is not confirmed by observations.

b. Another idea is an assumption that we live inside the giant void [34], [32]. Some recent observations favour the existence of such extended zone ($\sim 200\,$Mpc) with the mean stellar density about 15–40 % less than that of the global value [22], [47], [4]. However, another observations in the K-band not proved a significant local underdensity [7], [3], [38]. Anyway, one needs the presence of a deep large void of $\sim 200\,$Mpc diameter to explain the observed threefold difference between the global and local Ω_m quantities. But the existence of such an extended structure disagrees with the common concept of the large-scale homogeneity of the Universe.

c. At present, the most promising explanation of the Ω_m-paradox is the assumption that the considerable fraction ($\sim 2/3$) of the dark matter is dispersed outside the virial and collapsing zones of galaxy groups and clusters. Diffuse non-virialized structures, like cosmic filaments and walls, can manifest themselves via effects of weak gravitational lensing. Methodology of searching for dark massive attractors by the weak gravitational lensing effects has been applied so far only to rich galaxy clusters [35], [26]. Apparently, the most easily observable can be the dark filaments oriented along the line-of-sight. Such kind of observational program needs wide-sky surveys with large telescopes having a high sub-arcsecond seeing.

Finally, one can presume the existence of two different components of the dark matter. The second component (of unknown nature) would be a medium uniformly filling the intergalactic space. However, this idea is not compatible with the established cosmological paradigm and hence will be rejected by "Occam's razor".

Acknowledgements

This work was supported by the Russian Foundation for Basic Research, grant 18-02-00005.

References

[1] Abazajian, K.N., Adelman-McCarthy, J.K., et al.: The Seventh Data Release of the Sloan Digital Sky Survey. Astroph. J. Suppl. Ser. **182** (2009) 543–558.

[2] Bell, E.F., McIntosh, D.H., Katz, N., and Weinberg, M.D.: The Optical and Near-Infrared Properties of Galaxies. I. Luminosity and Stellar Mass Functions. Astroph. J. Suppl. Ser. **149** (2003) 289–312.

[3] Bershady, M.A., Lowenthal, J.D., and Koo, D.C.: Near-Infrared Galaxy Counts to J and K $\sim$ 24 as a Function of Image Size. Astrophys. J. **505** (1998) 50–73.

[4] Böhringer, H., Chon, G., Bristow, M., and Collins, C.A.: The extended ROSAT-ESO Flux-Limited X-ray Galaxy Cluster Survey (REFLEX II). V. Exploring a local underdensity in the southern sky. Astron. Astrophys. **574** (2015) A26.

[5] Chambers, K.C., Magnier, E.A., et al.: The Pan-STARRS1 Surveys. ArXiv e-prints (2016). `astro-ph/1612.05560`.

[6] Courtois, H.M., Pomarède, D., Tully, R.B., Hoffman, Y., and Courtois, D.: Cosmography of the Local Universe. Astron. J. **146** (2013) 69.

[7] Djorgovski, S., Soifer, B.T., et al.: Deep galaxy counts in the K band with the Keck telescope. Astrophys. J. Lett. **438** (1995) L13–L16.

[8] Driver, S.P., Robotham, A.S.G., et al.: Galaxy And Mass Assembly (GAMA): the $0.013 < z < 0.1$ cosmic spectral energy distribution from 0.1 μm to 1 mm. Mon. Not. R. Astron. Soc. **427** (2012) 3244–3264.

[9] Fukugita, M. and Peebles, P.J.E.: The Cosmic Energy Inventory. Astrophys. J. **616** (2004) 643–668.

[10] Huchra, J.P. and Geller, M.J.: Groups of galaxies. I - Nearby groups. Astrophys. J. **257** (1982) 423–437.

[11] Huchra, J.P., Macri, L.M., et al.: The 2MASS Redshift Survey – Description and Data Release. Astroph. J. Suppl. Ser. **199** (2012) 26.

[12] Jarrett, T.H., Chester, T., Cutri, R., Schneider, S., Skrutskie, M., and Huchra, J.P.: 2MASS Extended Source Catalog: Overview and Algorithms. Astron. J. **119** (2000) 2498–2531.

[13] Jarrett, T.H., Chester, T., Cutri, R., Schneider, S.E., and Huchra, J.P.: The 2MASS Large Galaxy Atlas. Astron. J. **125** (2003) 525–554.

[14] Jones, D.H., Peterson, B.A., Colless, M., and Saunders, W.: Near-infrared and optical luminosity functions from the 6dF Galaxy Survey. Mon. Not. R. Astron. Soc. **369** (2006) 25–42.

[15] Kaisina, E.I., Makarov, D.I., Karachentsev, I.D., and Kaisin, S.S.: Observational database for studies of nearby universe. Astrophysical Bulletin **67** (2012) 115–122.

[16] Karachentsev, I.D.: Missing dark matter in the local universe. Astrophysical Bulletin **67** (2012) 123–134.

[17] Karachentsev, I.D. and Kudrya, Y.N.: Orbital Masses of Nearby Luminous Galaxies. Astron. J. **148** (2014) 50.

[18] Karachentsev, I.D. and Makarov, D.I.: Binary galaxies in the local supercluster and its neighborhood. Astrophysical Bulletin **63** (2008) 299–345.

[19] Karachentsev, I.D., Makarov, D.I., and Kaisina, E.I.: Updated Nearby Galaxy Catalog. Astron. J. **145** (2013) 101.

[20] Karachentsev, I.D., Tully, R.B., Wu, P.F., Shaya, E.J., and Dolphin, A.E.: Infall of Nearby Galaxies into the Virgo Cluster as Traced with Hubble Space Telescope. Astrophys. J. **782** (2014) 4.

[21] Kashibadze, O.G. and Karachentsev, I.D.: Cosmic flow around local massive galaxies. Astron. Astrophys. **609** (2018) A11.

[22] Keenan, R.C., Barger, A.J., and Cowie, L.L.: Evidence for a ~ 300 Megaparsec Scale Under-density in the Local Galaxy Distribution. Astrophys. J. **775** (2013) 62.

[23] Kourkchi, E. and Tully, R.B.: Galaxy Groups Within 3500 km s^{-1}. Astrophys. J. **843** (2017) 16.

[24] Makarov, D. and Karachentsev, I.: Galaxy groups and clouds in the local ($z \sim 0.01$) Universe. Mon. Not. R. Astron. Soc. **412** (2011) 2498–2520.

[25] Makarov, D.I. and Karachentsev, I.D.: Galaxy triplets in the local supercluster. Astrophysical Bulletin **64** (2009) 24–49.

[26] Miyazaki, S., Oguri, M., et al.: A large sample of shear-selected clusters from the Hyper Suprime-Cam Subaru Strategic Program S16A Wide field mass maps. Proc. Astron. Soc. Japan **70** (2018) S27.

[27] Muñoz, J.A. and Loeb, A.: The density contrast of the Shapley supercluster. Mon. Not. R. Astron. Soc. **391** (2008) 1341–1349.

[28] Nuza, S.E., Kitaura, F.S., Heß, S., Libeskind, N.I., and Müller, V.: The cosmic web of the Local Universe: cosmic variance, matter content and its relation to galaxy morphology. Mon. Not. R. Astron. Soc. **445** (2014) 988–1001.

[29] Peebles, P.J.E.: *The large-scale structure of the universe*. 1980.

[30] Peebles, P.J.E.: *Principles of Physical Cosmology*. 1993.

[31] Planck Collaboration, Ade, P.A.R., et al.: Planck 2013 results. XVI. Cosmological parameters. Astron. Astrophys. **571** (2014) A16.

[32] Romano, A.E., Starobinsky, A.A., and Sasaki, M.: Effects of inhomogeneities on apparent cosmological observables: "fake" evolving dark energy. European Physical Journal C **72** (2012) 2242.

[33] Schechter, P.: An analytic expression for the luminosity function for galaxies. Astrophys. J. **203** (1976) 297–306.

[34] Shafieloo, A., Sahni, V., and Starobinsky, A.A.: Is cosmic acceleration slowing down? Phys. Rev. D **80** (2009) 101301.

[35] Shan, H., Kneib, J.P., Tao, C., Fan, Z., Jauzac, M., Limousin, M., Massey, R., Rhodes, J., Thanjavur, K., and McCracken, H.J.: Weak Lensing Measurement of Galaxy Clusters in the CFHTLS-Wide Survey. Astrophys. J. **748** (2012) 56.

[36] Shaya, E.J., Tully, R.B., Hoffman, Y., and Pomarède, D.: Action Dynamics of the Local Supercluster. Astrophys. J. **850** (2017) 207.

[37] Spergel, D.N., Bean, R., et al.: Three-Year Wilkinson Microwave Anisotropy Probe (WMAP) Observations: Implications for Cosmology. Astroph. J. Suppl. Ser. **170** (2007) 377–408.

[38] Totani, T., Yoshii, Y., Maihara, T., Iwamuro, F., and Motohara, K.: Near-Infrared Faint Galaxies in the Subaru Deep Field: Comparing the Theory with Observations for Galaxy Counts, Colors, and Size Distributions to K $\sim$ 24.5. Astrophys. J. **559** (2001) 592–605.

[39] Trujillo-Gomez, S., Klypin, A., Primack, J., and Romanowsky, A.J.: Galaxies in ΛCDM with Halo Abundance Matching: Luminosity-Velocity Relation, Baryonic Mass-Velocity Relation, Velocity Function, and Clustering. Astrophys. J. **742** (2011) 16.

[40] Tully, R.B.: Nearby groups of galaxies. II – an all-sky survey within 3000 kilometers per second. Astrophys. J. **321** (1987) 280–304.

[41] Tully, R.B.: Galaxy Groups. Astron. J. **149** (2015) 54.

[42] Tully, R.B.: Galaxy Groups: A 2MASS Catalog. Astron. J. **149** (2015) 171.

[43] Tully, R.B., Courtois, H.M., and Sorce, J.G.: Cosmicflows-3. Astron. J. **152** (2016) 50.

[44] Tully, R.B. and Fisher, J.R.: A new method of determining distances to galaxies. Astron. Astrophys. **54** (1977) 661–673.

[45] Tully, R.B., Rizzi, L., Shaya, E.J., Courtois, H.M., Makarov, D.I., and Jacobs, B.A.: The Extragalactic Distance Database. Astron. J. **138** (2009) 323–331.

[46] Vennik, J.: A list of nearby groups of galaxies. Tartu Astrofuusika Observatoorium Teated **73** (1984).

[47] Whitbourn, J.R. and Shanks, T.: The local hole revealed by galaxy counts and redshifts. Mon. Not. R. Astron. Soc. **437** (2014) 2146–2162.

Conference *Cosmology on Small Scales 2018*
Michal Křížek and Yurii Dumin (Eds.)
Institute of Mathematics CAS, Prague

DWARF SATELLITES IN THE LOCAL UNIVERSE: INSIGHTS TO THE COSMOLOGY

L. N. Makarova[1], D. I. Makarov[1], A. V. Antipova[1],
I. D. Karachentsev[1], R. B. Tully[2]

[1] Special Astrophysical Observatory
Nizhniy Arkhyz, Karachai-Cherkessia 369167, Russia
lidia@sao.ru
[2] Institute for Astronomy, University of Hawaii
2680 Woodlawn Drive, HI 96822, USA

Abstract: The Local Volume of galaxies can be regarded as a unique laboratory to study the formation and evolution of dwarf galaxies in order to shed light on the unsolved questions of modern cosmological ΛCDM theory. The problem of 'lost satellites' is one of them. There are a number of approaches that could bring some success on the way of the solution of this problem in observational astrophysics. One of them is a search for new (missing) satellites in the nearby galaxy groups. It is including also discoveries of 'satellites of satellites'. A faint dwarf irregular galaxy has been discovered in the HST/ACS field of LV J1157+5638. The galaxy is resolved into individual stars, including the brightest magnitude of the red giant branch. The dwarf is very likely a physical satellite of LV J1157+5638. The distance modulus of LV J1157+5638 using the tip of the red giant branch (TRGB) distance indicator is 29.82 ± 0.09 mag ($D = 9.22 \pm 0.38$ Mpc). The TRGB distance modulus of LV J1157+5638 sat is 29.76 ± 0.11 mag ($D = 8.95 \pm 0.42$ Mpc). The distances to the two galaxies are consistent within the uncertainties. The projected separation between them is only 3.9 kpc. LV J1157+5638 has a total absolute V-magnitude of -13.26 ± 0.10 and linear Holmberg diameter of 1.36 kpc, whereas its faint satellite LV J1157+5638 sat has $M_V = -9.38 \pm 0.13$ mag and Holmberg diameter of 0.37 kpc. Such a faint dwarf was discovered for the first time beyond the nearest 4 Mpc from us. The presence of main sequence stars in both galaxies unambiguously indicates the classification of the objects as dwarf irregulars (dIrrs) with recent or ongoing star formation events in both galaxies.

Keywords: galaxies dwarf, galaxies distances and redshifts, galaxies stellar content, galaxies individual LV J1157+5638

PACS: 98.65.Cw, 98.80.-k

1. Introduction

Dwarfs are usually considered to be galaxies with a stellar mass of less than 10^8–$10^9\,M_\odot$ and absolute stellar magnitude fainter than $M_V = -17$. Dwarf galaxies are the most convenient objects for galaxy evolution study: they are most numerous galaxies in the Universe, and their structure is relatively simple. Nearest galaxies are resolving into individual stars, which can be studied photometrically and by spectroscopy. Thus, the Local Volume of galaxies can be regarded as a unique laboratory to study the formation and evolution of dwarf galaxies in order to shed light on the unsolved questions of modern cosmological ΛCDM theory. The problem of 'lost satellites' is one of them. The luminosity function of the galaxies in the Local Volume contains about an order of magnitude fewer dwarfs than predicted by the ΛCDM theory [13], [14]. There are a number of approaches that could bring some success on the way of the solution of this problem in observational astrophysics. One of them is a search for new (missing) satellites in the nearby galaxy groups. It is including also discoveries of 'satellites of satellites' (see below). And the other assumption is that a number of dwarf galaxies could form due to complex merging events, or suffer from tidal disruption events within the galaxy groups [20], [31].

1.1. The nearest galaxy groups as systems of dwarf satellites

There are several well-known large groups of galaxies in the Local Universe (named after their central galaxy): Milky Way, Andromeda, M 81, Centaurus A, M 83. Each of these groups is a system of a giant galaxy and a family of satellites. It is interesting, that all of the groups (with the exception of Centaurus A) have a giant siral as a central body. Milky Way and Andromeda (due to their proximity) forms the Local Group of galaxies, and Centaurus A and M 83 groups are also often considering as one galaxy complex. A kind of exception is Canes Venatici Cloud I, which is a large scattered cloud of mostly dwarf irregular galaxies.

1.2. New satellites in the Local Universe

Particularly rich families of faint satellites were discovered around Andromeda and the Milky Way [1], [9], [15], [16].

For more distant galaxy groups we naturally lose more faint satellites. Nevertheless, recent observations on ground-based telescopes, and follow-up observations with the Hubble Space Telescope, substantially reduce these gaps. Such a survey was performed for the M 81 group [4], where 12 new dwarf galaxies were found. Recently, searches for faint galaxies in the Centaurus A group were successfully carried out [6], [24], and these surveys led to the discovery of more than 60 new dwarf galaxy candidates. Even in more distant groups like, for example, the M 101 group at the distance of 7.2 Mpc [17], observational surveys bring the discovery of new dwarf satellites [7], [10], [25]. Park et al. [26] also recently reported the discovery of 22 dwarf members of the group around NGC 2784 (at the distance about 9.8 Mpc).

1.3. 'Satellites of satellites'

However, not only groups around giant galaxies should be taken into account. Karachentsev and Makarov [12] in the framework of a binary galaxy study in the Local Supercluster drew attention to the existence of a large number of systems consisting exclusively of dwarf galaxies. A similar claim was made by Tully et al. [32]. Dwarf galaxy groups account for about 5% of all groups in the Local Supercluster [21]. Taking into account the selection effects, the total number of multiple dwarf systems should be at least 5-6 times greater. The authors show that groups of dwarf galaxies are located in low density regions and evolve without the influence of massive neighbours.

Despite difficulties in finding of faint satellites of dwarf galaxies, a number of discoveries have recently been made [2], [3], [5], [30]. Although targeted hunts give us a substantial increase in the number of dwarf galaxies of the Local Volume, new objects can also be found in the analysis of serendipitously observed areas of sky. Here we present our work [22], where we report the discovery of an extremely small galaxy located near the LV J1157+5638 dwarf galaxy.

2. Observations and data reduction

LV J1157+5638 was observed on October 18, 2013 with HST/ACS in the course of the SNAP project 13442 (PI: R.B.Tully). Dithered images were obtained in the $F606W$ and $F814W$ filters with the exposures summing to 1100 s in each band. The $F606W$ image of the LV J1157+5638 field is shown in Fig. 1. This compact galaxy is very well resolved into individual stars. It is easily distinguished in the upper part of the ACS image. This region can be seen in detail on the enlarged image at the upper right panel. The off-centre knot of blue brighter stars is well resolved into individual stars, indicating ongoing star formation in LV J1157+5638. A newly discovered galaxy is situated about 1.5 arcmin to the south of LV J1157+5638 in the lower right corner of the image. It is shown at the lower right panel, and also visibly resolved into individual stars.

We use the ACS module of the DOLPHOT software package[1] by A. Dolphin for photometry of resolved stars. The resulting colour-magnitude diagrams (CMD) of the LV J1157+5638 and its satellite are presented in Fig. 2. We call this satellite LV J1157+5638 sat in this paper.

3. The colour-magnitude diagrams

Two colour-magnitude diagrams are presented in the Fig. 2. In the left panel we show stellar populations measured at the ACS/WFC field within the body of LV J1157+5638, and at the right panel are the stars within the tiny satellite LV J1157+5638 sat. Even the CMD of the 'main' dwarf looks sparsely populated. We can see upper main sequence at $(F606W - F814W) \leq 0.4$, red supergiant plus

[1] http://americano.dolphinsim.com/dolphot/

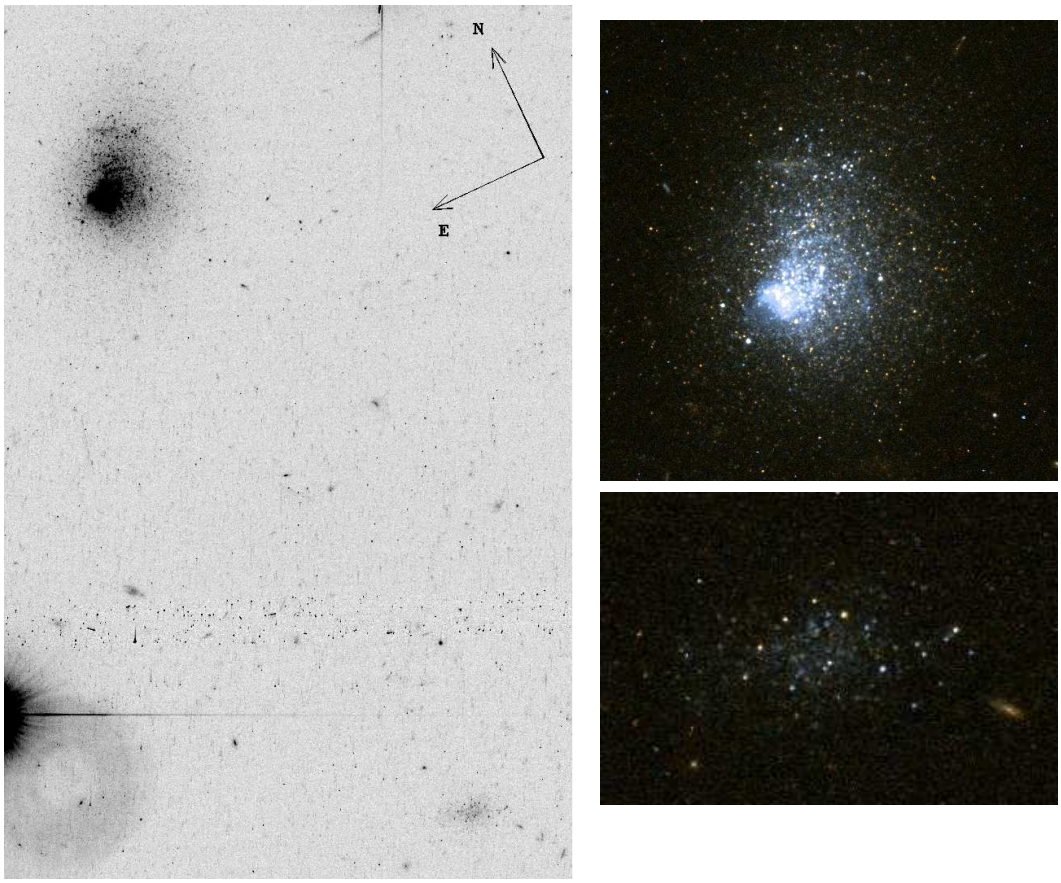

Figure 1: *HST*/ACS combined distortion-corrected mosaic image of the LV J1157+5638 field in the *F606W* filter (left panel). The image size is 1.2×1.8 arcmin. Enlarged combined $F606W + F814W$ images of LV J1157+5638 and the new dwarf satellite are shown at the right panel.

upper AGB (asymptotic giant branch) stars at $F814W \leq 25.7$ mag, and the rest are more abundant RGB (red giant branch). Only about 80 stars were resolved in the tiny satellite LV J1157+5638 sat. Nevertheless, clear signs of the upper main sequence at $(F606W - F814W) \leq 0.4$ are presented, and the RGB is well represented. Among brighter stars ($F814W \leq 25$ mag) we can distinguish a few red supergiants, but the main sequence only rises to roughly match the level of the TRGB at $F814W$. The presence of main sequence stars in both galaxies unambiguously indicate, that we can classify the objects as dwarf irregulars (dIrrs). Therefore, we can expect recent or ongoing star formation events in the galaxies. According to the GALEX and Hα data (see Table 1, where the general parameters and results are indicated), LV J1157+5638 has sufficient ongoing star formation, whereas its satellite is too faint to evince ongoing star formation activity with the data available.

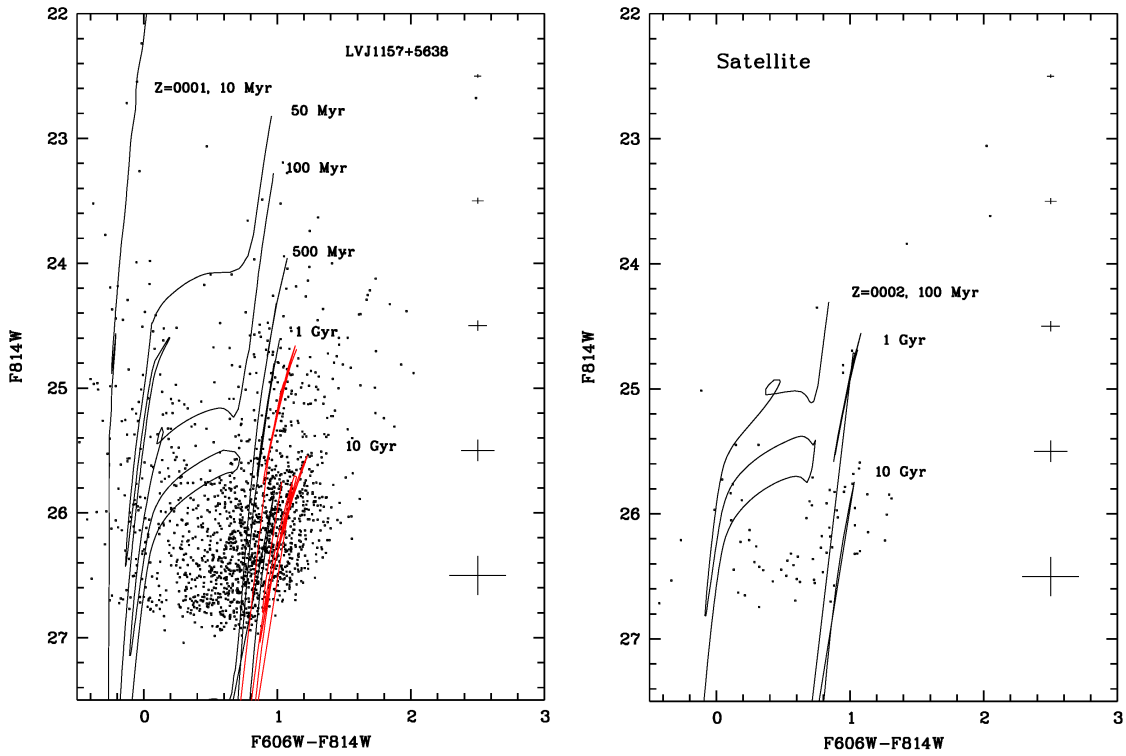

Figure 2: LV J1157+5638 and LV J1157+5638 sat colour-magnitude diagrams. Photometric errors are indicated by the bars at the right in the CMD. Padova theoretical stellar isochrones [23] of the different ages and metallicities are overplotted. The metallicity of the shown isochrones are: left panel, black Z=0001 ([Fe/H] = −2.36); left panel, red Z=0.0004 ([Fe/H] = −1.74); right panel Z=0.0002 ([Fe/H] = −2.05).

4. Distance measurement and star formation

We have determined a photometric TRGB distance of both LV J1157+5638 dwarf galaxy and its expected satellite with our TRGBTOOL program which uses a maximum-likelihood algorithm to obtain the magnitude of TRGB from the stellar luminosity function [18]. The measured TRGB magnitude of LV J1157+5638 is $F814W_{\rm TRGB} = 25.74 \pm 0.07$ mag in the ACS instrumental system. Using the calibration for the TRGB distance indicator by Rizzi et al. [27] and the Galactic extinction $E(B-V) = 0.017$ from Schlafly and Finkbeiner [28], we derived the true distance modulus for LV J1157+5638: 29.82 ± 0.09 mag ($D = 9.22 \pm 0.38$ Mpc). The CMD of the LV J1157+5638 sat is poorly populated, and the galaxy is distant which makes uncertainties of the distance estimation large. Nevertheless, the TRGBTOOL program is working quite well even in this case. The measured TRGB magnitude of LV J1157+5638 sat is $F814W_{\rm TRGB} = 25.68 \pm 0.09$ mag. We obtained the distance modulus for this dwarf 29.76 ± 0.11 mag ($D = 8.95 \pm 0.42$ Mpc). The distances to the both galaxies are consistent within the uncertainties. Therefore, we can claim,

that the considered dwarfs are very likely a physical pair with the projected separation 3.9 kpc between them.

The isochrones of these metallicities were superimposed on the CMDs of the studied dwarfs (see Fig. 2), so that we can approximately estimate the age of the resolved stars. In the LV J1157+5638 galaxy, we can assume the presence of a small number of stars ∼10 Myr old, which indicates an evident ongoing star formation, as can be seen also from Hα data (see section 3). At the same time, the upper main sequence of the dwarf is not densely populated, so we cannot expect a recent intense burst of star formation. Relatively young stars of the age of 50–100 Myr are also present in the galaxy. In addition, we can assume from the theoretical isochrones, that the age of the resolved red giants can be from 1 to 10–13 Gyr, i.e. the galaxy most likely includes the oldest RGB stars. As can be seen from the figure, we can not exclude somewhat higher metallicity of the RGB stars, [Fe/H] = −1.74. However, photometric errors play a significant role in this part of the CMD, that it is difficult to make certain conclusions.

Apparently, there are no stars younger than 100 Myr in the tiny satellite (see the right panel of Fig. 2). This agrees with the Hα and GALEX data, and indicates the absence of ongoing star formation. The isochrones of the metallicity estimated from the RGB colour well fit the CMD as a whole. LV J1157+5638 sat also most likely includes the oldest RGB stars up to about 13 Gyr old.

5. Discussion and concluding remarks

We discover a new faint dwarf irregular galaxy, detected in the HST/ACS images. The galaxy is resolved into individual stars, including the RGB, which allowed us to measure the TRGB distance to this galaxy. This dwarf is very likely a physical companion of LV J1157+5638. Thus, we were able to detect a satellite of a dwarf galaxy. The structure of the neighbourhood of our objects is demonstrated in the Fig. 3. It is obvious, that LV J1157+5638 is situated far away from any giant galaxies and their satellite families. The closest neighbour – dwarf irregular galaxy KKH 73 – is situated at the projected distance of 83 arcmin (220 kpc) from LV J1157+5638. The second nearest galaxy – dwarf irregular KDG 78 – is located at the projected distance of 352 arcmin (940 kpc) from LV J1157+5638 (see Fig. 3). Unfortunately, both neighbours, KKH 73 and KDG 78, do not have photometric distance estimations. Their heliocentric radial velocities V_h(KKH 73) = 596 ± 6 km s^{-1} and V_h(KDG 78) = 574.8 ± 1.7 km s^{-1}, from the LV database (http://www.sao.ru/lv/lvgdb) exceed the radial velocity of V_h(LV J1157+5638) = 416.3 ± 1.4 over 150 km s^{-1}. It is highly unlikely that they form a physically bounded system.

According to Klypin et al. [13], the LV galaxy sample is complete up to $M_B \sim -14$ mag. We can estimate the total number of fainter galaxies using the Schechter luminosity function approximation with the parameters $\phi_* = 1.25 \times 10^{-2} h^3\,\mathrm{Mpc}^3$, $\alpha = -1.3$ and $M_* = -20.0 + 5 * \log(h)$ in B filter, taking into account that $h = 0.73$. The absolute magnitude of LV J1157+5638 sat is approximately $M_B = -8.9$, assum-

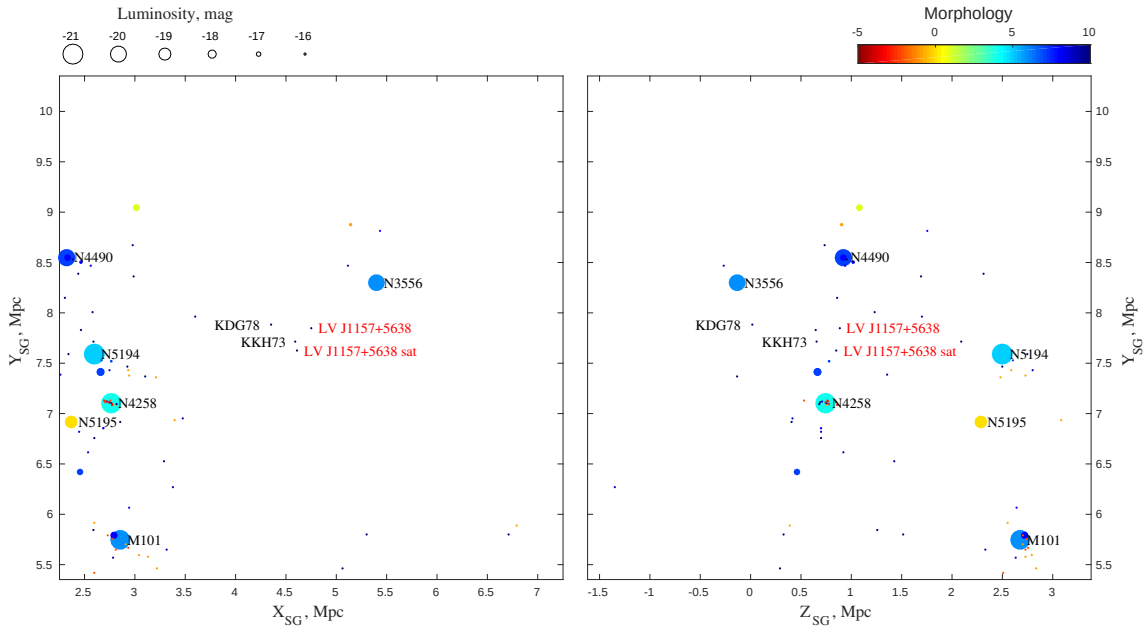

Figure 3: A panorama of the LV J1157+5638 neighbourhood in the supergalactic coordinates. The figure shows the projection of galaxies in a cube of ±2.5 Mpc size. The left panel is a projection on the supergalactic plane XY, while the right panel is the ZY view of the distribution of galaxies. The colour of a dot represents the morphology of the galaxy according to the colour bar. The size of a galaxy corresponds to its luminosity as shown in the legend panel.

ing the average colour of the LV dIrrs to be $\langle B-V\rangle = 0.48 \pm 0.2$ [29]. The resulting expected number of galaxies in the Local Volume ($D < 10$ Mpc) with luminosities from $M_B = -8$ to $M_B = -14$ is 1830. Assuming a random distribution of these galaxies, we can estimate the probability of random projection of one of these galaxies into a circle with a radius of 1.5 arcmin, which is approximately 0.017 per cent. Similarly, a random location of this galaxy inside a sphere with a radius of 0.3 Mpc is 4.9 per cent. Thus, there is a very small probability of accidental detection of two dwarf galaxies in such a small spatial area, i.e. the two studied dwarfs are very likely to be physically connected.

General parameters of the galaxies under study are presented in Table 1. Judging by the total and surface photometry data in the table, LV J1157+5638 sat is similar to extreme Local Group dwarfs. At the same time LV J1157+5638 sat looks quite faint and rather compact and could be similar to d1005+68, the satellite of a dwarf galaxy in the M 81 group discovered by Smercina et al. [30].

Fig. 4 represent total absolute V-magnitudes of the Local Volume dwarf galaxies versus their linear distances. The data were extracted from the HyperLeda database [19]. Here black dots are measurements from original works, and grey dots are the magnitudes originally measured in B and translated to the V-magnitudes ac-

	LV J1157+5638	LV J1157+5638 sat
Position (J2000)[a]	$11^{\rm h}57^{\rm m}53.9^{\rm s}+56°38'17''$	$11^{\rm h}57^{\rm m}53.0^{\rm s}+56°36'49''$
$E(B-V)$[b], mag	0.017	0.017
V_T, mag [c]	16.61 ± 0.04	20.43 ± 0.06
I_T, mag	16.05 ± 0.04	19.75 ± 0.06
M_V, mag	-13.26 ± 0.10	-9.38 ± 0.13
M_I, mag	-13.80 ± 0.10	-10.04 ± 0.13
Central surface brightness in V, mag arcsec^{-2}	21.15 ± 0.04	23.16 ± 0.06
Central surface brightness in I, mag arcsec^{-2}	21.02 ± 0.02	22.71 ± 0.06
Exponential scale length in V, arcsec	3.23 ± 0.02	1.39 ± 0.03
Exponential scale length in I, arcsec	3.96 ± 0.02	1.45 ± 0.04
Holmberg diameter in V, $a_{26.5}$, arcsec / kpc	30.0 / 1.36	8.4 / 0.37
Holmberg diameter in I, $a_{26.5}$, arcsec / kpc	39.8 / 1.79	10.2 / 0.44
Heliocentric radial velocity[d], km s^{-1}	416.3 ± 1.4	–
Radial velocity relative to the Local Group[e], km s^{-1}	514	–
Distance modulus, mag	29.82 ± 0.09	29.76 ± 0.11
Distance, Mpc	9.22 ± 0.38	8.95 ± 0.42
Mean metallicity of RGB, [Fe/H], dex [f]	-2.30 ± 0.07	-2.08 ± 0.10
F(Hα), erg/cm^2 sec [g]	9.33×10^{-14}	$< 0.4 \times 10^{-14}$
log(SFR)(Hα), $M_\odot$/yr	-2.10	< -3.50
m(FUV), mag[h]	18.49	22.71
log(SFR)(FUV), $M_\odot$/yr	-2.63	-4.35

[a] The measurements were made from the HST/ACS images.
[b] From [28]
[c] The total magnitudes and central surface brightness are not corrected for Galactic extinction, whereas absolute magnitudes are corrected for the Galactic extinction.
[d] from SDSS DR12
[e] from the Catalog & Atlas of the LV galaxies database: http://www.sao.ru/lv/lvgdb/
[f] The small [Fe/H] uncertainties are mostly reflect the formal errors of the estimate defined by expression given in the Section 4.
[g] Using data from [11] and our distances
[h] These GALEX magnitudes were obtained from the Mikulski Archive for Space Telescopes (MAST) (GALEX Public Release GR6/GR7). We estimate the respective SFR with the recipe given in the LV galaxies database for the similar data.

Table 1: General parameters of LV J1157+5638 and LV J1157+5638 sat

cording to the mean colours of the LV dwarf galaxies of different types from the work of Sharina et al. [29]. LV J1157+5638 is shown with red circle and LV J1157+5638 sat with red star. It is interesting to note, that the Local Group dwarf galaxy family is relatively well studied, a lot of really faint objects are discovered. A number of known faint dwarf galaxies is rapidly decreases with increasing distance. It is obvious, that LV J1157+5638 sat is extremely faint for its distance. It is highly possible, that most of faint satellites are still unknown at the distance of 5–10 Mpc.

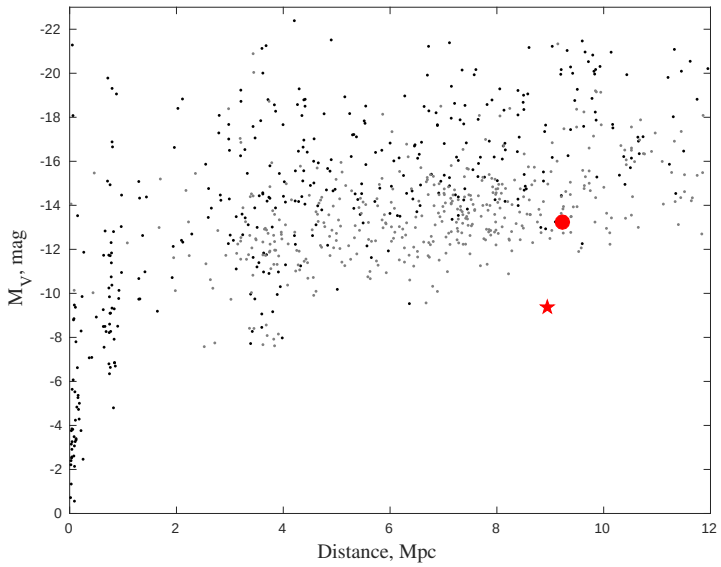

Figure 4: A relation between linear distance and total absolute V-magnitude for the Local Volume galaxies. The data are taken from the HyperLeda database. Black dots are represent original measurements, and grey dots are the magnitudes originally measured in B and translated to the V-magnitudes according to the mean colours from Sharina et al. [29]. LV J1157+5638 is shown with red circle and LV J1157+5638 sat with red star.

According to Makarov and Uklein [21], their groups of dwarf galaxies form a continuous sequence in the distribution of luminosities and masses with associations of dwarfs discovered by Tully et al. [32] in an analysis of the three-dimensional distribution of nearby galaxies. The dwarf companion LV J1157+5638 sat discovered by us, together with its 'main' irregular dwarf probably represents an example of a dwarf group of extremely low luminosity. This extends the sequence of dwarf galaxy groups to the faint and ultra-faint luminosities.

Wheeler et al. [33] carried out hydrodynamic zoom-in simulations of isolated dark matter halos. The authors demonstrate, that every halo is filled with subhalos, many of which form stars. The simulated dwarf galaxies with $M_* \simeq 10^6 M_\odot$ host 1–2 satellites with $M_* = 2{-}200 \times 10^3 M_\odot$. There is the implication that dwarf galaxies throughout the universe should host tiny satellite galaxies of their own. Dooley et al. [8] also predict 1–6 (2–12) satellites with $M_* > 10^5 M_\odot (M_* > 10^4 M_\odot)$ within the virial volume of LMC-sized galaxies, using Caterpillar simulations. The authors emphasize an importance of finding and observing of the faint satellites of dwarf galaxies for the determination of the galaxy mass function and an importance of searches for faint dwarf groups, which could test ΛCDM theory.

Acknowledgements

This study is supported by the Russian Science Foundation (grant 14–12–00965).

References

[1] K. Bechtol, et al. Eight New Milky Way Companions Discovered in First-year Dark Energy Survey Data. *ApJ*, 807:50, July 2015.

[2] J. L. Carlin, et al. First Results from the MADCASH Survey: A Faint Dwarf Galaxy Companion to the Low-mass Spiral Galaxy NGC 2403 at 3.2 Mpc. *ApJ*, 828:L5, September 2016.

[3] J. N. Chengalur, S. A. Pustilnik. Discovery of an extremely gas rich dwarf triplet near the centre of the Lynx-Cancer void. *MNRAS*, 428:1579–1586, January 2013.

[4] K. Chiboucas, I. D. Karachentsev, R. B. Tully. Discovery of New Dwarf Galaxies in the M81 Group. *AJ*, 137:3009–3037, February 2009.

[5] D. Crnojević, et al. Discovery of a Close Pair of Faint Dwarf Galaxies in the Halo of Centaurus A. *ApJ*, 795:L35, November 2014.

[6] D. Crnojević, et al. The Extended Halo of Centaurus A: Uncovering Satellites, Streams, and Substructures. *ApJ*, 823:19, May 2016.

[7] S. Danieli, et al. The Dragonfly Nearby Galaxies Survey. III. The Luminosity Function of the M101 Group. *ApJ*, 837:136, March 2017.

[8] G. A. Dooley, A. H. G. Peter, J. L. Carlin, A. Frebel, K. Bechtol, B. Willman. The predicted luminous satellite populations around SMC- and LMC-mass galaxies — a missing satellite problem around the LMC? *MNRAS*, 472:1060–1073, November 2017.

[9] D. Homma, et al. A New Milky Way Satellite Discovered in the Subaru/Hyper Suprime-Cam Survey. *ApJ*, 832:21, November 2016.

[10] B. Javanmardi, et al. DGSAT: Dwarf Galaxy Survey with Amateur Telescopes. I. Discovery of low surface brightness systems around nearby spiral galaxies. *A&A*, 588:A89, April 2016.

[11] I. D. Karachentsev, S. S. Kaisin, E. I. Kaisina. Extending the Hα Survey for the Local Volume Galaxies. *Astrophysics*, 58:453–470, December 2015.

[12] I. D. Karachentsev, D. I. Makarov. Binary galaxies in the local supercluster and its neighborhood. *Astrophysical Bulletin*, 63:299–345, December 2008.

[13] A. Klypin, I. D. Karachentsev, D. Makarov, O. Nasonova. Abundance of field galaxies. *MNRAS*, 454:1798–1810, December 2015.

[14] A. Klypin, A. V. Kravtsov, O. Valenzuela, F. Prada. Where Are the Missing Galactic Satellites? *ApJ*, 522:82–92, September 1999.

[15] S. E. Koposov, V. Belokurov, G. Torrealba, N. W. Evans. Beasts of the Southern Wild: Discovery of Nine Ultra Faint Satellites in the Vicinity of the Magellanic Clouds. *ApJ*, 805:130, June 2015.

[16] B. P. M. Laevens, et al. Sagittarius II, Draco II and Laevens 3: Three New Milky Way Satellites Discovered in the Pan-STARRS 1 3π Survey. *ApJ*, 813:44, November 2015.

[17] M. G. Lee, I. S. Jang. The Distance to M101 Hosting Type Ia Supernova 2011fe Based on the Tip of the Red Giant Branch. *ApJ*, 760:L14, November 2012.

[18] D. Makarov, L. Makarova, L. Rizzi, R. B. Tully, A. E. Dolphin, S. Sakai, E. J. Shaya. Tip of the Red Giant Branch Distances. I. Optimization of a Maximum Likelihood Algorithm. *AJ*, 132:2729–2742, December 2006.

[19] D. Makarov, P. Prugniel, N. Terekhova, H. Courtois, I. Vauglin. HyperLEDA. III. The catalogue of extragalactic distances. *A&A*, 570:A13, October 2014.

[20] D. I. Makarov, L. N. Makarova, S. A. Pustilnik, S. B. Borisov. Unusual void galaxy DDO 68: implications of the HST-resolved photometry. *MNRAS*, 466:556–563, April 2017.

[21] D. I. Makarov, R. I. Uklein. A list of groups of dwarf galaxies in the local supercluster. *Astrophysical Bulletin*, 67:135–146, April 2012.

[22] L. N. Makarova, D. I. Makarov, A V. Antipova, I. D. Karachentsev, R. B. Tully. Serendipitous discovery of a faint dwarf galaxy near a Local Volume dwarf. *MNRAS*, 474:3221–3227, March 2018.

[23] P. Marigo, et al. A New Generation of PARSEC-COLIBRI Stellar Isochrones Including the TP-AGB Phase. *ApJ*, 835:77, January 2017.

[24] O. Müller, H. Jerjen, B. Binggeli. New low surface brightness dwarf galaxies in the Centaurus group. *A&A*, 597:A7, January 2017.

[25] O. Müller, R. Scalera, B. Binggeli, H. Jerjen. The M 101 group complex: new dwarf galaxy candidates and spatial structure. *A&A*, 602:A119, June 2017.

[26] H. S. Park, D.-S. Moon, D. Zaritsky, M. Pak, J.-J. Lee, S. C. Kim, D.-J. Kim, S.-M. Cha. Dwarf Galaxy Discoveries from the KMTNet Supernova Program I. The NGC 2784 Galaxy Group. *ArXiv e-prints*, August 2017.

[27] L. Rizzi, R. B. Tully, D. Makarov, L. Makarova, A. E. Dolphin, S. Sakai, E. J. Shaya. Tip of the Red Giant Branch Distances. II. Zero-Point Calibration. *ApJ*, 661:815–829, June 2007.

[28] E. F. Schlafly, D. P. Finkbeiner. Measuring Reddening with Sloan Digital Sky Survey Stellar Spectra and Recalibrating SFD. *ApJ*, 737:103, August 2011.

[29] M. E. Sharina, V. E. Karachentseva, D. I. Makarov. Multiparametric scaling relations for dwarf irregular galaxies in different environments. In R. de Grijs, editor, *Advancing the Physics of Cosmic Distances*, volume 289 of *IAU Symposium*, pages 236–239, February 2013.

[30] A. Smercina, E. F. Bell, C. T. Slater, P. A. Price, J. Bailin, A. Monachesi. D1005+68: A New Faint Dwarf Galaxy in the M81 Group. *ApJ*, 843:L6, July 2017.

[31] T. Tepper-García, J. Bland-Hawthorn. The Sagittarius dwarf galaxy: Where did all the gas go? *MNRAS*, May 2018.

[32] R. B. Tully, L. Rizzi, A. E. Dolphin, I. D. Karachentsev, V. E. Karachentseva, D. I. Makarov, L. Makarova, S. Sakai, and E. J. Shaya. Associations of Dwarf Galaxies. *AJ*, 132:729–748, August 2006.

[33] C. Wheeler, J. Oñorbe, J. S. Bullock, M. Boylan-Kolchin, O. D. Elbert, S. Garrison-Kimmel, P. F. Hopkins, D. Kereš. Sweating the small stuff: simulating dwarf galaxies, ultra-faint dwarf galaxies, and their own tiny satellites. *MNRAS*, 453:1305–1316, October 2015.

Conference *Cosmology on Small Scales 2018*
Michal Křížek and Yurii Dumin (Eds.)
Institute of Mathematics CAS, Prague

MULTIPARAMETRIC TULLY-FISHER RELATION FOR LATE TYPE EDGE-ON GALAXIES

D. I. Makarov,[1] N. A. Zaitseva,[2] D. V. Bizyaev[3,2]
[1] Special Astrophysical Observatory of the Russian academy of sciences, Nizhnij Arkhyz, Karachai-Circassia 369167, Russia
dim@sao.ru (DIM)
[2] Sternberg Astronomical Institute, Moscow State University, Universitetskij pr. 13, 119991 Moscow, Russia
[3] Apache Point Observatory and New Mexico State University, Sunspot, NM 88349, USA

Abstract: We analyzed the influence of additional parameters on the Tully-Fisher (TF) relation, using a sample of edge-on galaxies from the Revised Flat Galaxy Catalog with precise HI data and photometry. Only the optical colors and HI-to-optical luminosity ratio are statistically significant in the multiparametric TF relation. It means that only terms directly related to the baryonic matter, the stellar populations and the gas fraction in galaxies, play significant role in the TF relation. The standard deviation of our multiparametric TF relation is 0.32 mag, which makes a sample of flat galaxies a good tool for studies of the bulk motion of galaxies in the Universe.

Keywords: flat galaxies, multiparametric Tully-Fisher relation

PACS: 98.52.Nr, 98.62.Py, 98.80.Es

1. Introduction

Modern surveys provide us with a huge set of high precision information about galaxies across the sky, such as photometry in different bandpasses, HI-flux, redshift and internal kinematics. The Tully-Fisher (TF) and the Baryonic Tully-Fisher (BTF) relations play a very important role in the study of the distribution and motion of matter in the Universe up to several hundreds Mpc, as well as in the understanding of formation and evolution of galaxies. In this study we concentrate on thin disk galaxies highly inclined, $\sim 90°$, to the line of sight. Usually, such "edge-on" galaxies are excluded from consideration to avoid the problems with inner extinction due to presence of a dust lane. However, "edge-on" galaxies have a number of observational advantages for the study of bulk motions in the Universe.

Karachentsev (13) proposed a very simple criterion on the axes ratio, $a/b \geq 7$, for the selection of flattest and most inclined galaxies. In Fig. 1 we show an example of

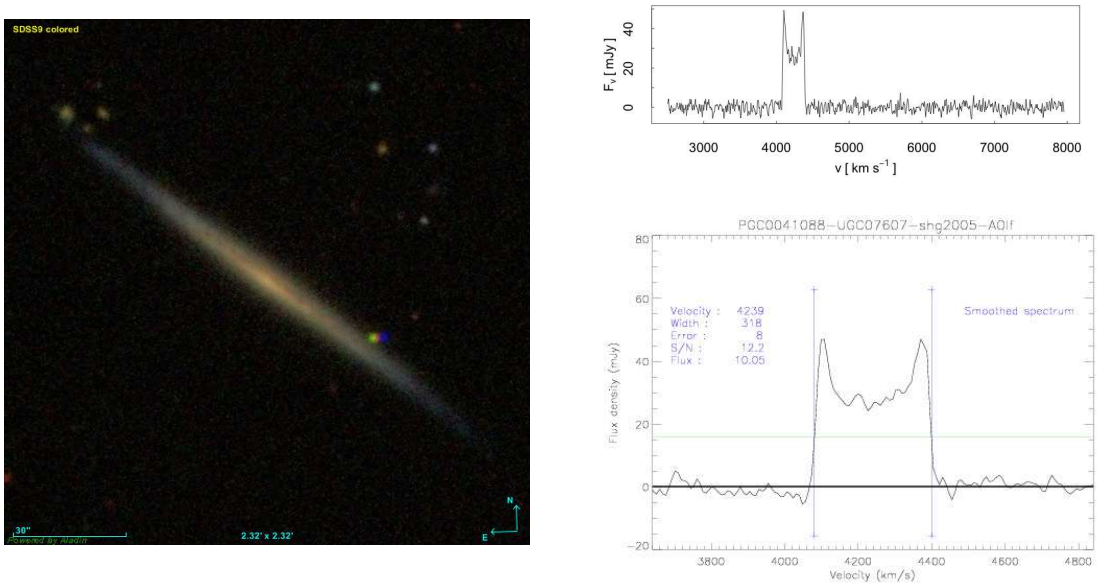

Figure 1: An example of very thin edge-on galaxy RFGC 2295. The left panel shows color SDSS image of the galaxy. The top right panel contains the HI-spectrum of the galaxy obtained in the ALFALFA survey (11). The bottom right panel shows the reduction of the spectrum in EDD HI catalog (7).

the flat and highly inclined galaxy RFGC 2295. This criterion excludes all early type galaxies as well as most of dwarf and irregular systems. The very first works (13), (14) show that the scatter of TF relation does not increase for edge-on galaxies and that the flat galaxies can be a good tool to study a large scale motion of galaxies up to 200 Mpc. Most the flat galaxies belong to the late morphological types Sc–Sd. Such galaxies show more uniform spatial distribution in the Universe comparable to early type objects. Since the flat galaxies are observed almost edge-on, they have a high surface brightness, making it easier to detect and classify even at large distances. What is really important, the edge-on galaxies do not require correction of their kinematics for the inclination. This correction is one of the main sources of uncertainties in the TF relation.

Only edge-on galaxies give us the opportunity for a direct study of the vertical distribution of luminous matter in the galactic disk. This can be important for the TF relation. Zasov et al. (49) show that the relative thickness of a gravitationally stable galactic disk depends on relative mass of a spherical component. The existence of superthin galaxies with $a/b \geq 10$ is possible only in the presence of massive dark halos around galaxies. N-body simulations (49), (42), (26) confirm that the lower limit of the dark halo mass can be estimated from the theoretical relationship between the disk thickness and the halo mass. This fact encourages us to consider an influence of the relative thickness of a galactic disk on the TF relation.

The revised version (RFGC) (18) of the Flat Galaxies Catalog (FGC) (19) covers whole the sky and contains 4236 galaxies with blue axes ratio $a/b \geq 7$ and maximal diameter $a \geq 0.6'$. These catalogs have been used to study the peculiar motions of galaxies in the Universe (17), (16), (15), (34), (28), (36), (25), (35) using different multiparametric modifications of the TF relation. The typical scatter of the TF relation for RFGC galaxies is about 0.6–0.7 mag (27), (20), (25).

In the last decade, new high-quality observational data on the photometry and kinematics of galaxies appeared. We supplemented the RFGC galaxies with homogeneous set of HI-linewidth measurements from the 'Cosmic Flows' project (8), and with structural parameters from the catalog of edge-on disk galaxies (EGIS) (2). The bottom right panel demonstrates the result of the reduction of HI spectrum of the flat edge-on galaxy RFGC 2295.

The goal of the Cosmic Flows project is to reconstruct the large scale motion of the matter in the Universe using the redshift independent distance measurements. The TF relation is one of the most convenient methods for distance determination to spiral galaxies over a large volume. In framework of the project a large sample of galaxies was observed with 100-meter Green Bank Telescope (GBT) at the National Radio Astronomy Observatory in north hemisphere and with the 64-m Parkes telescope in Australia for southern objects (8). The observations were performed for five subsamples of galaxies: the V3K sample provides a high-density mapping of the Universe within 3000 $\mathrm{km\,s^{-1}}$; the PSCz sample extends the volume up to 6000 $\mathrm{km\,s^{-1}}$ and gives a good coverage at low Galactic latitudes; the RFGC galaxies provides a sparse coverage over a large volume outside of clusters; the calibrator's sample allows authors to precise the TF relation; the SN Ia host galaxy sample is very important for absolute calibration of extragalactic ladder on large scales. These observations combined with archival radio data from Arecibo, Nançay, GBT, Parkes, the old NRAO 300 and the 140, and Effelsberg telescopes were processed in a uniform manner in order to obtain a homogeneous set of HI-linewidth with precision better than 20 $\mathrm{km\,s^{-1}}$ (7). The rotational velocity of galaxies is based on W_{m50} measurements of the width of an HI profile using new robust method developed in framework of the 'Cosmic Flows' project (7).

The EGIS catalog (2) based on the Sloan Digital Sky Survey images (1) provides us with aperture photometry and structural parameters for 5747 genuine edge-on galaxies in the optical g, r and i bands. The galaxies were selected based on the axial ratio, angular diameter, magnitude and color limits. After automatic selection all candidates underwent a visual inspection. Only galaxies with clearly seen dust layers or without signs of non-edge-on spiral arms were classified as true edge-on. The combination of high precision radio and optical data gives us opportunity to improve the TF relation for edge-on galaxies and minimize the scatter using additional terms.

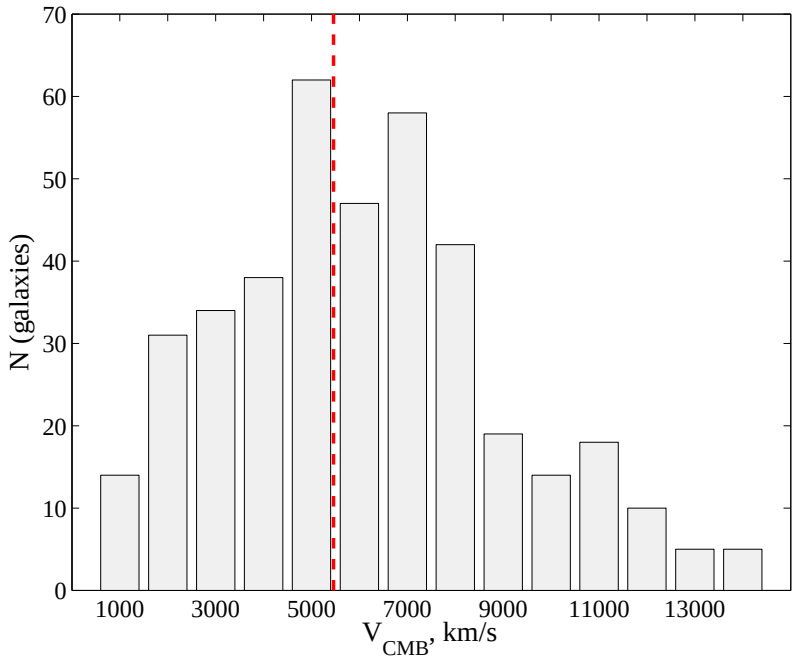

Figure 2: Distribution of RFGC galaxies with reliable photometry from the EGIS catalog and HI-data from EDD. The vertical dashed line indicates the effective depth of the sample.

2. The sample of flat galaxies

We selected 397 edge-on galaxies from the RFGC catalog (18) with precision of a linewidth measurement better than 20 km s^{-1} from the All Digital HI Profile Catalog (7) of the Extragalactic Distance Database (EDD) (47) and having photometry in the EGIS catalog (2). Fig. 2 shows the distribution of the selected galaxies in the cosmic microwave background (CMB) reference frame. The sample has en effective depth of 5458.5 km s^{-1}.

We excluded from the consideration 14 galaxies with small radial velocities, $V_{\rm LG} \leq 1000$ km s^{-1}, to avoid problems with distance estimation from the simple Hubble law. Also, we eliminated 15 objects within the 'zero-velocity surface' of the Virgo cluster, $R_0 = 7.2$ Mpc (23), and having radial velocity respect to the Local Group from -321 to 2679 km s^{-1}. This region is characterized by high peculiar and random motions of galaxies. Moreover, 12 galaxies were rejected because of high Galactic extinction, $A_B \geq 0.6$. Finally, we carried out visual inspection of all galaxies in the sample and excluded 14 galaxies with suspected photometry, sign of interaction and with neighbors which may contaminate the radio measurements. As a result, our list of good RFGC-galaxies consists of 331 objects.

We used the data from EDD HI catalog for analysis. The line width at the 50% of the mean flux level, W^c_{m50}, is corrected for a relativistic broadening and for finite spectral resolution as it is described by Courtois and Tully (6). We do not

apply a correction for the inclination because of all flat galaxies have $i > 86^\circ$ (2) and such correction is negligible.

The aperture photometry and structural parameters of the galaxies, the radial and vertical scales, central surface brightness and bulge-to-disk ratio, were determined by EGIS catalog (2). The data are available in three SDSS passbands: g, r and i. All magnitudes are corrected for Galactic foreground extinction using maps by Schlegel et al. (39) as described by Bizyaev et al. (2). Also we apply the K-correction according to the methodology[1] (4), (5). For comparison with literature data, we use the transformation from the SDSS-magnitudes to the Johnson-Cousins system by Lupton (2015) [2].

We did not apply any correction for internal extinction. Because we consider galaxies seen nearly edge-on, the effects of high and irregular absorption in the disk along a line of sight can be very complicated and difficult to account. It is far beyond the scope of the study. However, there are reasons to circumvent this difficulty. Typically, the dust is concentrated in a narrow layer in the plane of the galactic disk. Hence, in the edge-on galaxies significant part of light is not affected by dust. Moreover, RFGC-galaxies form very homogeneous sample by morphology, mostly of the late types, Sc–Sd (24). We can expect that the internal extinction varies smoothly with the galaxy properties such as total mass, stellar populations, relative thickness of the disk and so on. Thus, we expect that the effects of the internal extinction will be partially taken into account with usage of additional parameters in multiparametric TF relation, such as color, relative mass of hydrogen, relative thickness, and amplitude of rotation.

The distances are estimated from the radial velocities in the CMB reference frame using the linear Hubble law. Throughout this paper we use cosmology parameters $\Omega_\Lambda = 0.7$, $\Omega_m = 0.3$ and $H_0 = 73$ km s^{-1}.

3. The Tully-Fisher relation

The TF relations in g, i and r bands are shown in three panels of the Fig. 3. The behavior is similar in all filters. The dwarf galaxies with rotation velocity $V_{\rm rot} \lesssim 91$ km s^{-1} show a different slope respect to the giant ones. The galaxies with slow rotation lie systematically below the relation extrapolated from the fast rotators. We fit the data with a broken line:

$$M = \begin{cases} a + b \log V_{\rm rot} & \text{if } V_{\rm rot} > V_{\rm bp} \\ \hat{a} + c \log V_{\rm rot} & \text{if } V_{\rm rot} \le V_{\rm bp} \\ & \hat{a} = a + (b - c) \log V_{\rm bp}, \end{cases} \quad (1)$$

where a and b are the intercept and slope terms for the giant galaxies; $V_{\rm bp}$ is the break point of the relation; c is the slope term for the dwarf galaxies; and σ_s represent the scatter for the giant and whole-sample relation, respectively. The results are summarized in Table 1.

[1] http://kcor.sai.msu.ru/

[2] http://www.sdss.org/dr12/algorithms/sdssubvritransform/

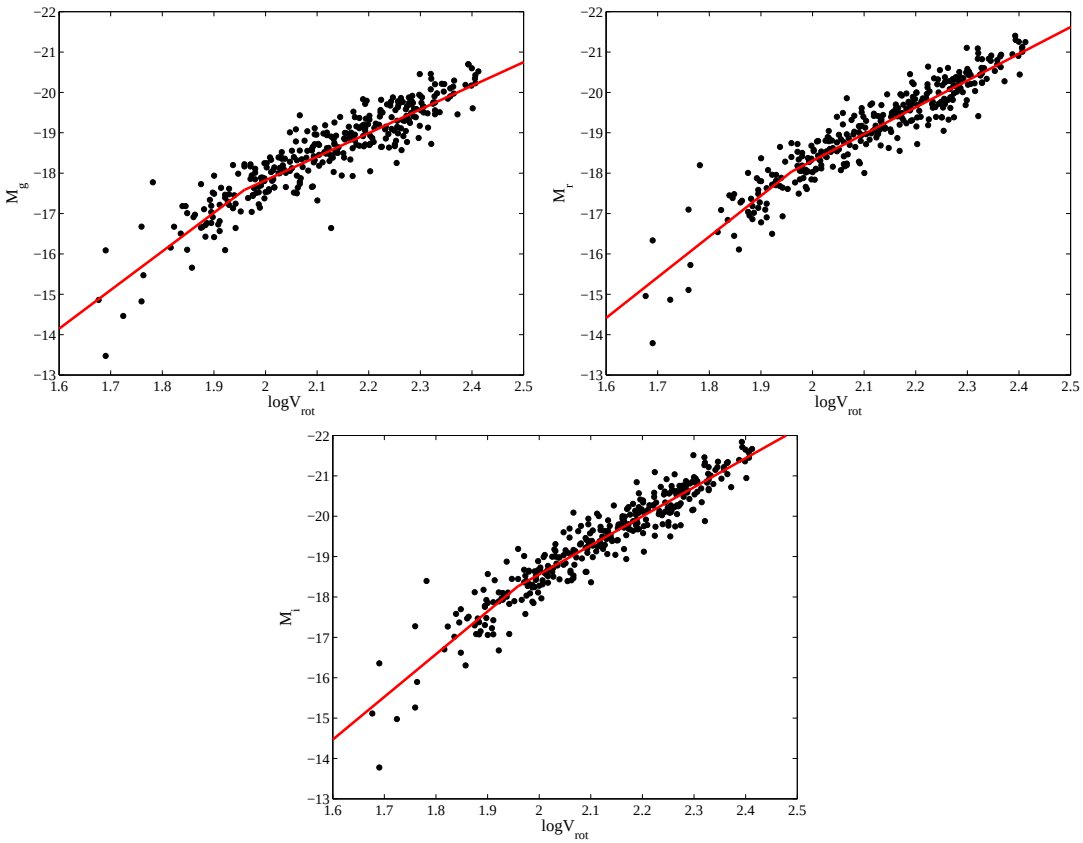

Figure 3: The TF relations for the selected RFGC-galaxies in the g, r and i bands. Trends look similar for all mentioned bands.

	g	r	i
a	-6.18 ± 0.10	-5.07 ± 0.07	-4.18 ± 0.04
b	-5.85 ± 0.10	-6.63 ± 0.10	-7.19 ± 0.06
$V_{\rm bp}$	91.0 ± 1.5	91.0 ± 1.3	91.0 ± 0.8
c	-9.57 ± 0.25	-10.09 ± 0.21	-10.58 ± 0.19
σ (giants)	0.40	0.35	0.34
σ (total)	0.44	0.41	0.40

Table 1: The Broken Line fitting coefficients of the TF relation

There are several reasons to explain such behavior of slow rotators on TF diagram. The sample of slow rotators $V_{\rm rot} < 91$ km s^{-1} is quite small (55 of 331). We can not exclude the influence of selection biases. The disks of dwarf galaxies are thicker in the comparison to regular spiral galaxies. Sánchez-Janssen et al. (38) found that below $\mathfrak{M}^* \approx 2 \times 10^9$ $\mathfrak{M}_\odot$ low-mass galaxies become systematically thicker. It corresponds to absolute magnitude $M_i \sim -18$ mag, which coincides with the break in our sample

(see Fig. 3). The strict cut of the axes ratio of $a/b \geq 7$ in RFGC catalog (18) selects the mostly thin, low surface brightness galaxies in our sample. These galaxies have lower luminosity comparable to the whole sample of dwarf galaxies.

However, the similar break in TF relation was found by McGaugh et al. (31) in a sample of galaxies with circular velocities ranging between $30 \lesssim V_c \lesssim 300$ km s^{-1}. The dwarfs galaxies with $V_c \lesssim 90$ km s^{-1} in a field are systematically less luminous with respect to the expectation from the faster spinning galaxies. McGaugh et al. (31) noted that these faint galaxies are very gas rich and the bulk of their baryonic material is still not converted into stars. This is the reason why the slowly rotating galaxies are underluminous with respect to the bright galaxies. Usage of the sum of the stellar and gas masses restores the linear relation over the entire observed range. McGaugh et al. (31) argue that the traditional TF relation is a particular case of more fundamental Baryonic Tully-Fisher (BTF) relation between the total mass of baryons and rotational velocity.

This explanation is also suitable in our case of thin and slowly rotating, gas-rich galaxies. As it is shown in section 4, the multiparametric TF relation restores a linear behavior when the HI mass and colors of stellar populations are taken into the analysis.

A simulations also show similar break in the TF relation. Guo et al. (10) applied a semi-analytic model of the galaxy formation to the Millennium (43) and Millennium-II simulations (3). Their predicted RF relation shows the break in the linear relation near $\log V_{\rm max} \simeq 2.0$ (see Fig. 13 from (10)). This value corresponds to $M_r - 5\log(h) \simeq -18$, which is in good agreement with our TF relation for the edge-on galaxies.

4. Multiparametric TF relation

Our goal is to improve the classical TF relation by including various distance independent terms in the regression. For the analysis we collected structural parameters from the EGIS photometry (2), the All Digital HI Profile Catalog (7) and the HyperLEDA database (29). The list of tested parameters includes the minor-to-major axes ratio, $\log(\frac{b}{a})_{o,e}$ in the blue and red POSS-I bands; the vertical-to-radial scale ratio $\log(\frac{z}{h})_{g,r,i}$, in the g, r and i bands; the HI color index, $m_{21} - \{g, r, i\}$, which corresponds to the HI-mass-to-light ratio, where $\{g, r, i\}$ is one of the galaxy visible magnitude in g, r, and i bands from EGIS, and m_{21} is the 21-cm line flux expressed in magnitude according to $m_{21} = -2.5\log F + 17.40$ (9); galactic colors in different bands using aperture photometry of SDSS images. Also we checked if the multiparametric TF relation depends on the Galactic extinction in B-band. In addition, we test if the ratios $\log V_{\rm rot}\log(\frac{b}{a})_{o,e}$ and $\log V_{\rm rot}\log(\frac{z}{h})_{g,r,i}$ are connected with the internal extinction in our edge-on galaxies.

The stepwise regression was used for selection of the significant parameters of the multiparametric TF relation. This iterative procedure adds and removes terms from multilinear model based on their statistical significance in a regression. At

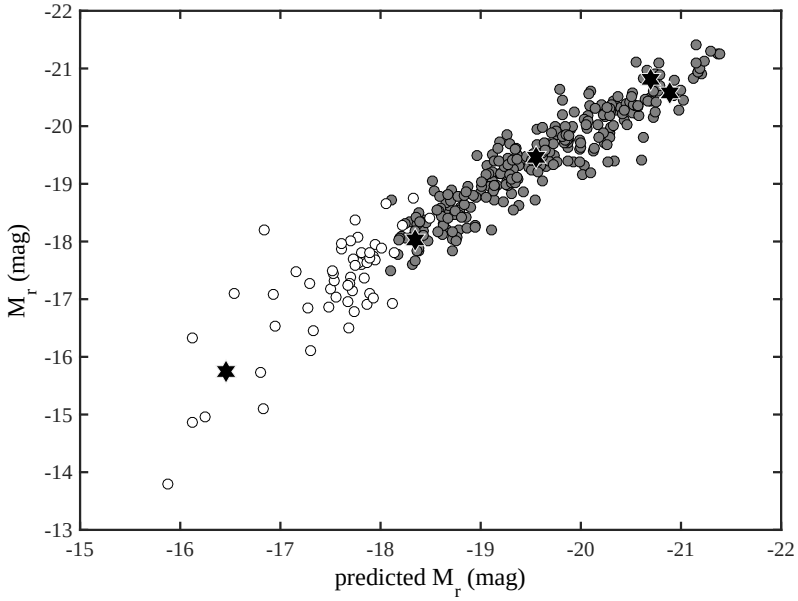

Figure 4: Multiparametric TF relation for RFGC-galaxies in the r-band. The relations in the g and i bands look similar. The regression is obtained for massive galaxies (filled circles) with $\log V_{\rm rot} > 1.96$. The open circles show the extrapolation to the slow rotating galaxies. The objects with known TRGB-distances are designated by filled hexagons.

each step, the p-value of the F-statistics is computed to test the models with and without a potential term. The term is added to corresponding model if there is an evidence that the term coefficient would significantly differ from zero. Conversely, the term is removed from the model if there is insufficient evidence that the coefficient differs from a zero. The iterations over the coefficients terminate when the coefficient additions do not improve the F-statistics anymore. We use MATLAB's realization of this algorithm with p-value of 0.001 as threshold for the including/excluding the parameters.

The regression coefficients for the sample of 276 massive, fast rotating galaxies with $\log V_{\rm rot} > 1.96$ are presented in Table 4. The last line shows the resulting scatter of the relation. The zero-point was calibrated through the galaxies with known, redshift-independent distances based on the tip of the red giant branch (TRGB; see Sect. 5). In addition to the rotation velocity, the most significant parameters are the optical and HI color indexes. It reflects the fact that only terms directly connected with baryonic matter, the stellar population and the fraction of the gas, play the most important role in the TF relation. These parameters have high confidence level with p-value less than 10^{-8}. No more considered parameters were included in the final relation because their p-value is greater than 0.04. Surprisingly, the multiparametric relation for giants improves the behavior of the whole sample including 55 slow rotators with $\log V_{\rm rot} < 1.96$. Thereby, taking into account the optical and

	M_g	M_r	M_i
$\log V_{\rm rot}$	-8.60 ± 0.32	-8.22 ± 0.28	-8.48 ± 0.30
$(m_{21} - \{g, r, i\})$	-0.23 ± 0.04	-0.23 ± 0.04	-0.22 ± 0.04
$(g - i)$	2.00 ± 0.19		1.19 ± 0.20
$(g - r)$		2.21 ± 0.28	
zero-point	-2.09 ± 0.10	-2.80 ± 0.09	-2.28 ± 0.10
σ	0.34	0.32	0.32

Table 2: Regression coefficients for multiparametric TF relation in different SDSS bands. Subsample of the massive galaxies contains those with $\log V_{\rm rot} > 1.96$.

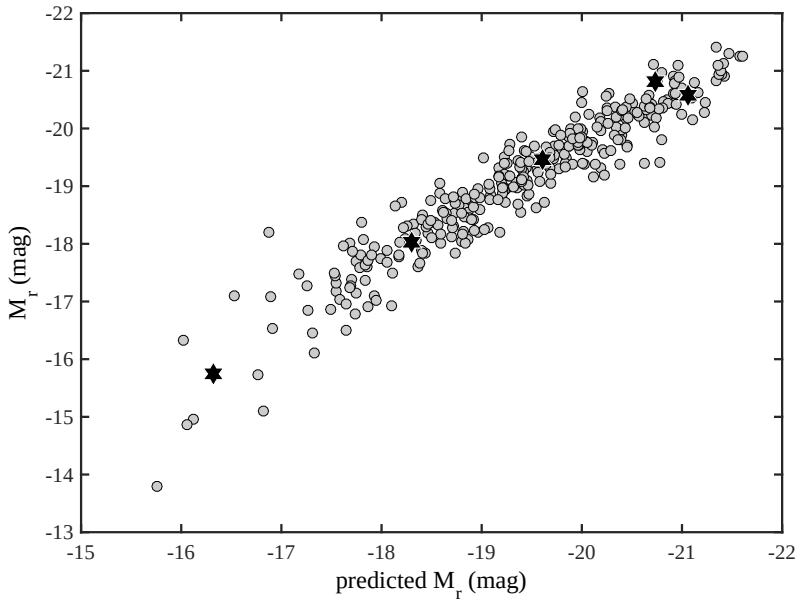

Figure 5: Multiparametric TF relation for the whole sample of 331 flat galaxies in the r-band. The hexagons shows the galaxies with known, TRGB-distances.

HI color indexes for giant galaxies removes the break and suppresses the dispersion for the dwarfs also. The comparison between the predicted and observed absolute r-magnitudes of galaxies is shown in Fig. 4.

Fig. 4 suggests that a simple, linear multiparametric regression can be constructed for the whole sample of 331 edge-on galaxies. The resulting relation is shown in Fig. 5 and the corresponding coefficients are reported in Table 3. Similar to the sample of giants-only, the most significant terms are the optical and HI color indexes, which show the the p-value less than 10^{-6}. As can be seen from the Table 3, a subsample of massive galaxies has the same scatter as in cases, when we analyzed only giant galaxies. Comparison of the standard deviations in Tables 1 and 3 shows that the multiparametric linear regression improves the TF relation by 10% with respect to the broken line approximation.

	M_g	M_r	M_i
$\log V_{\rm rot}$	-8.50 ± 0.26	-8.48 ± 0.25	-8.57 ± 0.28
$(m_{21} - \{g, r, i\})$	-0.30 ± 0.04	-0.30 ± 0.04	-0.29 ± 0.04
$(g - i)$			1.12 ± 0.21
$(g - r)$	2.88 ± 0.29	2.24 ± 0.30	
zero-point	-2.21 ± 0.09	-2.29 ± 0.09	-2.05 ± 0.11
σ (giants)	0.34	0.32	0.32
σ	0.40	0.38	0.39

Table 3: Regression coefficients for multiparametric TF relation in different SDSS bands.

5. Zero-point calibration

Our sample contains just few galaxies with precise distance estimates. There are no distance measurements from Cepheids for any FGC-galaxy. Only five of eleven RFGC-galaxies with precise TRGB-distances are included in our sample. Most of them have distance less than 10 Mpc. Distance of these galaxies are gathered in the Table 4, which lists the TRGB distance moduli from the literature. Note that these distances were estimated using different techniques and calibrations. EDD (12) provides the most homogeneous and precise set of data. Most important is that these measurements are available for all five galaxies of our sample. Thus, we decide to use EDD distances for the zero-point calibration. These five galaxies with TRGB distance measurements were not included in our sample for the regression analysis, as they have too small distances, but we use them for zero-point calibration of the final multiparametric TF relation. The best agreement between our multiparametric TF relation and nearby galaxies with known distances is reached when the Hubble constant is qual 73.9 ± 0.6 km s^{-1} Mpc^{-1}. The zero-point for this case is shown in corresponding line of the Tables 4 and 3.

6. Discussion

Our multiparametric TF relation has typical standard deviation of 0.32 mag for giant galaxies. It is significantly less than in previous works on TF relations for flat galaxies. Kudrya et al. (27) estimated the standard deviation $\sigma = 0.58$ mag for $B_{\rm T}$–W_{50} relation for FGC-galaxies. They used indirect estimates of the total B-band magnitude from the other parameters of flat galaxies in the FGC catalog, such as angular diameter, surface brightness index and so on. Karachentsev et al. (20) consider statistical properties of the TF relations for flat edge-on galaxies in the B, I, J, H and K_s bands. The near-IR photometry was taken from the Two Micron All Sky Survey (2MASS; 41). They found the RMS scatter of 0.48 mag in deep I-photometry and 0.61–0.63 mag in near IR for a sample of 436 RFGC galaxies. In framework of study of large scale motions in the local Universe, Kudrya et al. (28) and Kashibadze (25) constructed multiparametric TF relations using 2MASS pho-

PGC	RFGC	EGIS	$(m-M)_0$	
6699	384	EON 027.382 +32.589	28.61 ± 0.01	*
			28.53	(45)
			28.55 ± 0.03	(46)
24930		EON 133.173 +33.421	29.96 ± 0.38	*
			29.86 ± 0.06	(22)
39422	2245	EON 184.374 +37.807	28.17 ± 0.07	*
			28.21 ± 0.11	(37)
			28.19 ± 0.12	(30)
			28.20 ± 0.03	(40)
			28.26 ± 0.24	(21)
			27.88 ± 0.17	(33)
			28.16 ± 0.08	(44)
41618	2315	EON 188.190 +00.115	29.61 ± 0.12	*
			29.61 ± 0.21	(23)
54470	2946	EON 228.973 +56.329	31.19 ± 0.05	*
			31.13 ± 0.10	(37)

* EDD CMD/TRGB 2016/04/27 (12)

Table 4: List of the TRGB distance measurements.

tometry. Kudrya et al. (28) find the dispersion $\sigma_{\rm TF} = 0.42$ mag for a sample of 971 RFGC galaxies with $V_{\rm 3K} < 18000$ km s^{-1}, while Kashibadze (25) obtaines the scatter of 0.52 mag for a sample of 410 nearby edge-on galaxies ($V_{\rm h} \leq 3000$ km s^{-1}) from the 2MASS-selected Flat Galaxy Catalog (2MFGC; 32). The quality of these near-IR TF relations is obviously limited by short exposures of 2MASS survey, which can lead to an underestimation of the galactic disk luminosity. Obviously, that we achieved such an improvement over predecessors due to the use of high-precision photometry and new HI data.

As can be seen from the tables 4 and 3, the final regression expands the standard TF relation by including only the HI colour index and the colour of galaxies. Both indices are associated with the presence and evolution of baryonic matter in galaxies. The HI colour index, $(m_{21} - \{g, r, i\})$, reflects the ratio of hidrogen to the total luminosity of a galaxy, while the total colour, $(g - r)$ or $(g - i)$, depends on stellar populations of a galaxy. In fact, we got the baryonic TF relation, without imposing any restrictions on the type of considered parameters.

Another surprise was the lack of the relative thickness of a galactic disk in the final regression. It is known that the presence of a spheroidal component stabilizes a galactic disk. Therefore, a disk submerged in a halo may have lower values of the vertical velocity dispersion. Zasov et al. (49) show that the minimal relative thickness of a collisionless disk decreases with its relative mass, $z/h \sim \mathfrak{M}_{\rm disk}/\mathfrak{M}_{\rm total}$ (48), where $\mathfrak{M}_{\rm disk}$ and $\mathfrak{M}_{\rm total}$ are masses of the disk component and total mass, respectively. One

can expect that this connection has to be reflected by the TF relation. However, the relative thickness is statistically insignificant in our multiparametric TF relation.

We see several possible explanations. The disk orientation of our galaxies is close to 90 degrees, but not exactly. Even small deviations from the edge-on view affect estimation of the observable vertical scale length of a galaxy. Without visible dust line, it seems impossible to separate the contribution of the radial light distribution into the measured vertical profile in galaxies oriented not exactly edge-on. Variation in orientation of galaxies smears the relation and makes less significant the influence of the relative thickness on the multiparametric TF relation.

The stellar parameters determined for optical SDSS images are affected by dust, especially for objects with small angular sizes (2). Using near-infrared images instead of the optical ones would help mitigate the effects of the dust extinction.

One more factor that may play its role is that our sample consists of only thin ($a/b > 7$) and bulgeless (Sc–Sd) galaxies by design. The sample with a/b ranging from 7 to 12 does not represent all edge-on galaxies with arbitrary disk thickness. The effective dynamic range of the disk thicknesses may be not enough to feel the influence of it on the TF relation.

Note that the relationship between the disk thickness and the spherical-to-disk component mass ratio sets only the lower limit on the spherical halo mass (42). In reality many evolutionary factors, such as minor interactions or sources of the internal dynamical heating, deteriorate the relationship. Thus, low effect of the disk thickness on the TF relation may also reflect small-scale dynamical factors during galactic evolution.

7. Conclusions

1. We constructed a multiparametric TF relation for a sample of 331 edge-on RFGC galaxies. These objects have precise HI linewidth measurements with uncertainty better than 20 $\mathrm{km\,s^{-1}}$ from the All Digital HI Profile Catalog (7) of the EDD database (47). The optical photometry and structural parameters of the galaxies were taken from the SDSS-based EGIS catalog (2).

2. A classical relation between an absolute magnitude and a HI linewidth reveals different trends for the giant and dwarf galaxies. The slow rotating $V_{\mathrm{rot}} < 91$ $\mathrm{km\,s^{-1}}$ dwarfs are underluminous with respect to the extrapolation from the fast rotating galaxies. This fact can be well explained in the framework of baryonic TF paradigm. Dwarf galaxies hold sufficient fraction of baryonic matter in their gas still not converted into stars. Thus, their optical luminosity is lower than expected for the giant galaxies with high star formation efficiency. Using the total mass of baryons instead of the stellar luminosity takes this effect into account and puts the giant and dwarf galaxies on the same relation (31). We show that both slowly and highly rotating galaxies obey the same relation on our multiparametric TF relation made for edge-on galaxies.

3. Our multiparametric relation expands the classical TF law with two terms: the HI color index and optical colors of the galaxies. The HI color index $m_{21} - \{g, r, i\}$ reflects the fraction of HI mass with respect to the optical luminosity. The $(g - i)$ or $(g - r)$ colors reflects properties of stellar populations, such as mean age and metallicity. Any other structural parameters or their combinations have statistically negligible effect for the TF relation. We note that only parameters directly related to the baryonic matter, stellar population and fraction of gas, play significant role in the TF relation.

4. The coefficients of the multiparametric TF relation are almost independent of passbands. This differs from the simple HI-linewidth–absolute magnitude relation where the slope significantly changes with the passband used, what can be seen from Table 1. Thus, taking into account the optical and HI color indexes helps us find a universal relation.

5. The standard deviation of the multiparametric TF relation is 0.32 mag in the r and i bands for the galaxies with $V_{\max} \geq 91$ km s^{-1}. Usage of HI and optical color indexes improves the TF relation for edge-on galaxies by about 10% for giant galaxies.

6. We calibrate zero-point of our multiparametric TF relation using five edge-on galaxies with precise TRGB-distance measurements. It allows us to estimate the Hubble constant of 73.9 ± 0.6 km s^{-1} Mpc^{-1} for our sample of flat galaxies with effective depth of 75 Mpc.

7. The scatter of our TF relation for flat galaxies is comparable with the best modern estimations of the TF relation, where highly inclined galaxies were not used. We find that the flat edge-on galaxies with extended set of available parameters make good tool to study bulk motions of galaxies in the nearby Universe.

Acknowledgements

We thank prof. A.V. Zasov for very relevant conversation.

The work was carried out under support of the Russian Scientific Foundation grant 14–12–00965. We acknowledge the usage of the HyperLeda database[3] (29).

References

[1] K. N. Abazajian, J. K. Adelman-McCarthy, M. A. Agüeros, S. S. Allam, C. Allende Prieto, D. An, K. S. J. Anderson, S. F. Anderson, J. Annis, N. A. Bahcall, et al. The Seventh Data Release of the Sloan Digital Sky Survey. *ApJS*, 182:543–558, June 2009.

[3] `http://leda.univ-lyon1.fr`

[2] D. V. Bizyaev, S. J. Kautsch, A. V. Mosenkov, V. P. Reshetnikov, N. Y. Sotnikova, N. V. Yablokova, R. W. Hillyer. The Catalog of Edge-on Disk Galaxies from SDSS. I. The Catalog and the Structural Parameters of Stellar Disks. *ApJ*, 787:24, May 2014.

[3] M. Boylan-Kolchin, V. Springel, S. D. M. White, A. Jenkins, G. Lemson. Resolving cosmic structure formation with the Millennium-II Simulation. *MNRAS*, 398:1150–1164, September 2009.

[4] I. V. Chilingarian, A. -L. Melchior, I. Y. Zolotukhin. Analytical approximations of K-corrections in optical and near-infrared bands. *MNRAS*, 405:1409–1420, July 2010.

[5] I. V. Chilingarian, I. Y. Zolotukhin. A universal ultraviolet-optical colour-colour-magnitude relation of galaxies. *MNRAS*, 419:1727–1739, January 2012.

[6] H. M. Courtois, R. B. Tully. Update on H I data collection from Green Bank, Parkes and Arecibo telescopes for the Cosmic Flows project. *MNRAS*, 447:1531–1534, February 2015.

[7] H. M. Courtois, R. B. Tully, J. R. Fisher, N. Bonhomme, M. Zavodny, A. Barnes. The Extragalactic Distance Database: All Digital H I Profile Catalog. *AJ*, 138:1938–1956, December 2009.

[8] H. M. Courtois, R. B. Tully, D. I. Makarov, S. Mitronova, B. Koribalski, I. D. Karachentsev, J. R. Fisher. Cosmic Flows: Green Bank Telescope and Parkes H I observations. *MNRAS*, 414:2005–2016, July 2011.

[9] G. de Vaucouleurs, A. de Vaucouleurs, H. G. Corwin, Jr., R. J. Buta, G. Paturel, P. Fouqué. *Third Reference Catalogue of Bright Galaxies. Volume I: Explanations and references. Volume II: Data for galaxies between 0^h and 12^h. Volume III: Data for galaxies between 12^h and 24^h.* 1991.

[10] Q. Guo, S. White, M. Boylan-Kolchin, G. De Lucia, G. Kauffmann, G. Lemson, C. Li, V. Springel, S. Weinmann. From dwarf spheroidals to cD galaxies: simulating the galaxy population in a ΛCDM cosmology. *MNRAS*, 413:101–131, May 2011.

[11] M. P. Haynes, R. Giovanelli, A. M. Martin, K. M. Hess, A. Saintonge, E. A. K. Adams, G. Hallenbeck, G. L. Hoffman, S. Huang, B. R. Kent, R. A. Koopmann, E. Papastergis, S. Stierwalt, T. J. Balonek, D. W. Craig, S. J. U. Higdon, D. A. Kornreich, J. R. Miller, A. A. O'Donoghue, R. P. Olowin, J. L. Rosenberg, K. Spekkens, P. Troischt, E. M. Wilcots. The Arecibo Legacy Fast ALFA Survey: The α.40 H I Source Catalog, Its Characteristics and Their Impact on the Derivation of the H I Mass Function. *AJ*, 142:170, November 2011.

[12] B. A. Jacobs, L. Rizzi, R. B. Tully, E. J. Shaya, D. I. Makarov, L. Makarova. The Extragalactic Distance Database: Color-Magnitude Diagrams. *AJ*, 138:332–337, August 2009.

[13] I. D. Karachentsev. Thin edge-on galaxies as a tool for the investigation of large-scale streaming motions in the universe. *AJ*, 97:1566–1575, June 1989.

[14] I. D. Karachentsev. Flat edge-on galaxies on the Tully-Fischer diagram. *Pisma v Astronomicheskii Zhurnal*, 17:671–683, August 1991.

[15] I. D. Karachentsev, V. E. Karachentseva, Y. N. Kudrya, D. I. Makarov, S. L. Parnovsky. A list of peculiar velocities of RFGC galaxies. *Bulletin of the Special Astrophysics Observatory*, 50:5–38, 2000.

[16] I. D. Karachentsev, V. E. Karachentseva, Y. N. Kudrya, S. L. Parnovskiĭ. The Bulk Motion of FGC Galaxies on Scales of 100 Mpc. *Astronomy Reports*, 44:150–160, March 2000.

[17] I. D. Karachentsev, V. E. Karachentseva, Y. N. Kudrya, S. L. Parnovsky. Largescale Streaming of Flat Galaxies. *Astronomische Nachrichten*, 316:369, September 1995.

[18] I. D. Karachentsev, V. E. Karachentseva, Y. N. Kudrya, M. E. Sharina, S. L. Parnovskij. The revised Flat Galaxy Catalogue. *Bulletin of the Special Astrophysics Observatory*, 47:5, 1999.

[19] I. D. Karachentsev, V. E. Karachentseva, S. L. Parnovskij. Flat galaxy catalogue. *Astronomische Nachrichten*, 314:97–222, May 1993.

[20] I. D. Karachentsev, S. N. Mitronova, V. E. Karachentseva, Y. N. Kudrya, T. H. Jarrett. The 2MASS Tully-Fisher relation for flat edge-on galaxies. *A&A*, 396:431–438, December 2002.

[21] I. D. Karachentsev, M. E. Sharina, A. E. Dolphin, E. K. Grebel, D. Geisler, P. Guhathakurta, P. W. Hodge, V. E. Karachentseva, A. Sarajedini, P. Seitzer. Galaxy flow in the Canes Venatici I cloud. *A&A*, 398:467–477, February 2003.

[22] I. D. Karachentsev, R. B. Tully, L. N. Makarova, D. I. Makarov, L. Rizzi. Peculiar Velocities of Galaxies in the Leo Spur. *ApJ*, 805:144, June 2015.

[23] I. D. Karachentsev, R. B. Tully, P. F. Wu, E. J. Shaya, A. E. Dolphin. Infall of Nearby Galaxies into the Virgo Cluster as Traced with Hubble Space Telescope. *ApJ*, 782:4, February 2014.

[24] V. E. Karachentseva, Y. N. Kudrya, I. D. Karachentsev, D. I. Makarov, O. V. Melnyk. Ultra-flat galaxies selected from RFGC catalog. I. The sample properties. *Astrophysical Bulletin*, 71:1–13, January 2016.

[25] O. G. Kashibadze. Multiparametric infrared Tully-Fisher relation as a tool for mapping cosmic flows. *Astrophysics*, 51:336–348, July 2008.

[26] A. Khoperskov, D. Bizyaev, N. Tiurina, M. Butenko. Numerical modelling of the vertical structure and dark halo parameters in disc galaxies. *Astronomische Nachrichten*, 331:731, July 2010.

[27] Y. N. Kudrya, V. E. Karachentseva, I. D. Karachentsev. Apparent magnitudes and Tully-Fisher's diagram for FGC galaxies. *Astronomy Letters*, 23:633–637, September 1997.

[28] Y. N. Kudrya, V. E. Karachentseva, I. D. Karachentsev, S. N. Mitronova, T. H. Jarrett, W. K. Huchtmeier. The bulk motion of flat edge-on galaxies based on 2MASS photometry. *A&A*, 407:889–898, September 2003.

[29] D. Makarov, P. Prugniel, N. Terekhova, H. Courtois, I. Vauglin. HyperLEDA. III. The catalogue of extragalactic distances. *A&A*, 570:A13, October 2014.

[30] D. I. Makarov, L. N. Makarova, R. I. Uklein. Distances to dwarf galaxies of the Canes Venatici I cloud. *Astrophysical Bulletin*, 68:125–138, April 2013.

[31] S. S. McGaugh, J. M. Schombert, G. D. Bothun, W. J. G. de Blok. The Baryonic Tully-Fisher Relation. *ApJ*, 533:L99–L102, April 2000.

[32] S. N. Mitronova, I. D. Karachentsev, V. E. Karachentseva, T. H. Jarrett, Y. N. Kudrya. The 2MASS-selected Flat Galaxy Catalog. *Bulletin of the Special Astrophysics Observatory*, 57:5–163, 2004.

[33] M. Mouhcine, H. C. Ferguson, R. M. Rich, T. M. Brown, T. E. Smith. Halos of Spiral Galaxies. I. The Tip of the Red Giant Branch as a Distance Indicator. *ApJ*, 633:810–820, November 2005.

[34] S. L. Parnovsky, Y. N. Kudrya, V. E. Karachentseva, I. D. Karachentsev. The Bulk Motion of Flat Galaxies on Scales of 100 Mpc in the Quadrupole and Octupole Approximations. *Astronomy Letters*, 27:765–774, December 2001.

[35] S. L. Parnovsky, A. S. Parnowski. Large-scale collective motion of RFGC galaxies. *Ap&SS*, 325:163–175, February 2010.

[36] S. L. Parnovsky, A. V. Tugay. Bulk Motions of Flat Galaxies on 100-Mpc Scales from New Data. *Astronomy Letters*, 30:357–367, June 2004.

[37] D. J. Radburn-Smith, R. S. de Jong, A. C. Seth, J. Bailin, E. F. Bell, T. M. Brown, J. S. Bullock, S. Courteau, J. J. Dalcanton, H. C. Ferguson, P. Goudfrooij, S. Holfeltz, B. W. Holwerda, C. Purcell, J. Sick, D. Streich, M. Vlajic, D. B. Zucker. The GHOSTS Survey. I. Hubble Space Telescope Advanced Camera for Surveys Data. *ApJS*, 195:18, August 2011.

[38] R. Sánchez-Janssen, J. Méndez-Abreu, J. A. L. Aguerri. Thin discs, thick dwarfs and the effects of stellar feedback. *MNRAS*, 406:L65–L69, July 2010.

[39] D. J. Schlegel, D. P. Finkbeiner, M. Davis. Maps of Dust Infrared Emission for Use in Estimation of Reddening and Cosmic Microwave Background Radiation Foregrounds. *ApJ*, 500:525–553, June 1998.

[40] A. C. Seth, J. J. Dalcanton, R. S. de Jong. A Study of Edge-On Galaxies with the Hubble Space Telescope Advanced Camera for Surveys. I. Initial Results. *AJ*, 129:1331–1349, March 2005.

[41] M. F. Skrutskie, R. M. Cutri, R. Stiening, M. D. Weinberg, S. Schneider, J. M. Carpenter, C. Beichman, R. Capps, T. Chester, J. Elias, J. Huchra, J. Liebert, C. Lonsdale, D. G. Monet, S. Price, P. Seitzer, T. Jarrett, J. D. Kirkpatrick, J. E. Gizis, E. Howard, T. Evans, J. Fowler, L. Fullmer, R. Hurt, R. Light, E. L. Kopan, K. A. Marsh, H. L. McCallon, R. Tam, S. Van Dyk, S. Wheelock. The Two Micron All Sky Survey (2MASS). *AJ*, 131:1163–1183, February 2006.

[42] N. Y. Sotnikova, S. A. Rodionov. Estimating the dark halo mass from the relative thickness of stellar disks. *Astronomy Letters*, 32:649–660, October 2006.

[43] V. Springel, S. D. M. White, A. Jenkins, C. S. Frenk, N. Yoshida, L. Gao, J. Navarro, R. Thacker, D. Croton, J. Helly, J. A. Peacock, S. Cole, P. Thomas, H. Couchman, A. Evrard, J. Colberg, F. Pearce. Simulations of the formation, evolution and clustering of galaxies and quasars. *Nature*, 435:629–636, June 2005.

[44] N. A. Tikhonov, O. A. Galazutdinova. Stellar Disks and Halos of Edge-on Spiral Galaxies: NGC 891, NGC 4144, and NGC 4244. *Astrophysics*, 48:221–236, April 2005.

[45] N. A. Tikhonov, O. A. Galazutdinova. Stellar subsystems of different ages in spiral and irregular galaxies. *Astronomy Letters*, 38:147–156, March 2012.

[46] R. B. Tully, L. Rizzi, A. E. Dolphin, I. D. Karachentsev, V. E. Karachentseva, D. I. Makarov, L. Makarova, S. Sakai, E. J. Shaya. Associations of Dwarf Galaxies. *AJ*, 132:729–748, August 2006.

[47] R. B. Tully, L. Rizzi, E. J. Shaya, H. M. Courtois, D. I. Makarov, B. A. Jacobs. The Extragalactic Distance Database. *AJ*, 138:323–331, August 2009.

[48] A. V. Zasov, D. V. Bizyaev, D. I. Makarov, N. V. Tyurina. Relationship between the Thickness of Stellar Disks and the Relative Mass of a Dark Galactic Halo. *Astronomy Letters*, 28:527–535, August 2002.

[49] A. V. Zasov, D. I. Makarov, E. A. Mikhailova. Thickness of Thin Stellar Disks and the Mass of the Dark Halo. *Soviet Astronomy Letters*, 17:374, April 1991.

Conference *Cosmology on Small Scales 2018*
Michal Křížek and Yurii Dumin (Eds.)
Institute of Mathematics CAS, Prague

CLASSIFICATION OF DISTANCES IN COSMOLOGY

Michal Křížek[1], Attila Mészáros[2]

[1]Institute of Mathematics, Czech Academy of Sciences, Žitná 25,
CZ-115 67 Prague 1, Czech Republic, krizek@math.cas.cz
[2]Astronomical Institute of Charles University, V Holešovičkách 2,
CZ-180 00 Prague 8, Czech Republic, meszaros@cesnet.cz

Abstract: In cosmology many different distances are defined: angular, comoving, Euclidean, Hubble, light-year, luminosity, Minkowski, parallax, proper motion, redshift, ... distance. There is not one single natural distance, since the universe is expanding, curved, and we look back in time. In this survey paper we will concentrate on geometrical interpretations of the above-mentioned distances.
We also show how to calculate the total mass of the Einstein static universe by means of four fundamental constants only.

Keywords: standard cosmological model, cosmological principle, Friedmann equation, cosmological parameters, Einstein static universe

PACS: 04.20-q, 95.35+d, 98.80-k

1. The ambiguity of the notion universe

The aim of this overview paper is to present various distances used in cosmology. We will focus on their mutual relations and geometrical interpretations. We will mostly follow the notation from the well-known Weinberg's book [42] (see also [6], [17], [30]).

Cosmological distances in the remote universe obviously cannot be measured directly due to large scales in space, time, and a relatively small speed of electromagnetic interaction. Therefore, this problem is usually transformed to measurements of angles, luminosities, redshifts, etc.

The term "universe" is used in cosmology with various meanings: true spacetime, true space (i.e. spacetime for a fixed time), and the observable universe, which is seen as a projection on the celestial sphere. These are three different entities. Their mathematical models are also three completely different manifolds (see Fig. 1). Thus altogether we have $6 = 3+3$ meanings of the problematic notion "universe" for which the terminology is not fixed yet. The first three contain real matter, whereas the other three are abstract mathematical idealizations of reality.

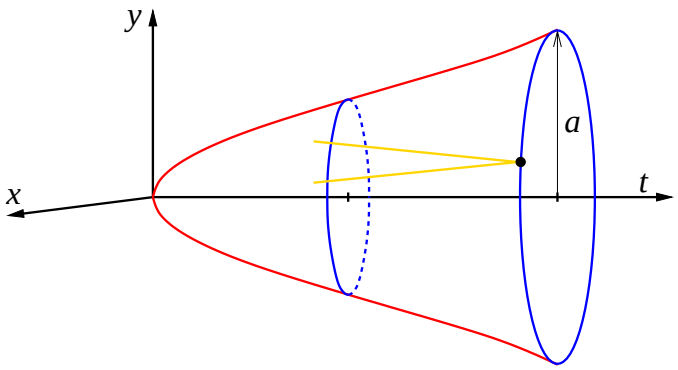

Figure 1: Three different manifolds corresponding to the curvature index $k = 1$ (cf. (3)). For simplicity, the hypersphere $\mathbb{S}^3_{a(t)}$ defined in (4) is reduced to its great blue circle $\mathbb{S}^1_{a(t)}$ for $z = w = 0$ and for a fixed time instant t. This is the model of space (the universe). The model of spacetime can be obtained by rotation of the red graph of the expansion function $a = a(t)$ about the time axis t. The observable universe is marked by the yellow light cone. The space dimensions are reduced by two.

According to the *Einstein cosmological principle* our "universe" is homogeneous and isotropic for large spatial scales and fixed time. The *homogeneity* is expressed by a translational symmetry (i.e., space has at any point the same mass density, temperature, pressure, etc.), while *isotropy* is expressed by rotational symmetry (i.e., there are no preferred directions at any point and an observer is not able to distinguish a given direction from another direction by means of local physical measurements).

2. Maximally symmetric three-dimensional manifolds

In accordance with the cosmological principle, we shall understand by the *universe* a cross-section of spacetime for a fixed time instant t, i.e., the universe will be an isochrone in spacetime for constant t. Sometimes it is called the *space*. It is represented by one of the three maximally symmetric manifolds: the hypersphere

$$\mathbb{S}^3 = \{(x, y, z, w) \in \mathbb{E}^4 \,|\, x^2 + y^2 + z^2 + w^2 = 1\}, \tag{1}$$

the Euclidean space $\mathbb{E}^3$, or the hyperbolic pseudosphere $\mathbb{H}^3$, i.e., those manifolds that have the maximum number of symmetries. According to [42, Chapt. 13], there are no other maximally symmetric manifolds up to scaling. The *curvature index* k of the manifolds $\mathbb{S}^3$, $\mathbb{E}^3$, and $\mathbb{H}^3$ attains the values $k \in \{1, 0, -1\}$, respectively. Sometimes the index k is also called the *normalized curvature*. In [21] we present five different ways to imagine the hypersphere $\mathbb{S}^3$. Its equator $w = 0$ is a two-dimensional sphere $\mathbb{S}^2$ (see Fig. 2).

We are in the center of the observable universe, and the center of the space $\mathbb{S}^3$ lies at the origin $(0, 0, 0, 0)$. Similarly each circle has its center even though it does

not belong to it. Thus, the frequently repeated statement that the universe has no center is false if $k = 1$.

Also the often used expression $\mathbb{H}^3 = \{(x, y, z, w) \in \mathbb{E}^4 \,|\, x^2 + y^2 + z^2 - w^2 = -1\}$ with the Minkowski metric is confusing, since w is not equivalent with the other three variables x, y, z. Moreover, the corresponding Minkowski distance does not satisfy the triangle inequality, which is a fundamental property of any metric space for a fixed time. Therefore, the Minkowski metric is often called the *Minkowski pseudometric*. Let us emphasize that w is a space coordinate and not time (cf. [40, p. 95]). The manifold $\mathbb{H}^3$ cannot be isometrically imbedded to $\mathbb{E}^4$ like $\mathbb{S}^3$, see [20, p. 279] for details. Concerning the hyperbolic plane $\mathbb{H}^2$, let us point out that no arbitrarily small open neighborhood of a given point of $\mathbb{H}^2$ can be isometrically imbedded in $\mathbb{E}^3$. However, it can be isometrically imbedded in $\mathbb{E}^6$, see [1] and [2]. The discovery and development of non-Euclidean geometries are discussed in the survey paper [4].

Note that the unit hypersphere $\mathbb{S}^3$ can be described by the following *hyperspherical coordinates*

$$\begin{aligned} x &= \sin\chi \sin\theta \cos\phi, \\ y &= \sin\chi \sin\theta \sin\phi, \\ z &= \sin\chi \cos\theta, \\ w &= \cos\chi, \end{aligned}$$

where $\chi, \theta \in [0, \pi]$ and $\phi \in [0, 2\pi)$ are called the *comoving coordinates*. We observe that these coordinates are a natural generalization of the standard spherical coordinates for the unit sphere $\mathbb{S}^2$ and $\chi = \frac{\pi}{2}$. In the Appendix we show how to derive the metric (2) corresponding to $\mathbb{S}^3$.

Let us emphasize that a given metric need not define the corresponding manifold uniquely. For instance the manifolds $\mathbb{E}^3$ and $\mathbb{E}^2 \times \mathbb{S}^1$ can be both equipped with the Euclidean metric, but their topology is different.

Let us present an important argument that favors $\mathbb{S}^3$ as a model of our universe for a fixed time. The manifolds $\mathbb{E}^3$ and $\mathbb{H}^3$ have infinite volume. However, the actual space could not first be finite (i.e. bounded) after its origin and then change to infinite (unbounded). Moreover, one can hardly imagine that the infinite universe would have everywhere on large scales the same mass density, temperature, pressure[1], and so on, at a given time instant $t > 0$ after the Big Bang as required by the Einstein cosmological principle. In this case, information would have to be transmitted at infinite speed. The popular theory of inflation [16] cannot explain such a homogeneity and isotropy of an infinite universe.

If gravity propagates at the speed of light, our further development is influenced by the distribution of the mass in the yellow conical manifold of Fig. 1. On the other hand, for an infinite speed of gravity (assumed by Newton's theory) we would be influenced by the larger blue manifold of Fig. 1. This contradicts to causality.

[1]Furthermore, these quantities should attain arbitrarily large values at all points of the infinite universe just after the Big Bang.

Albert Einstein derived that the gravitational interaction causes a positive curvature inside mass bodies and that the universe can be modeled by a three-dimensional hypersphere $\mathbb{S}^3$ with unchanging radius, see [10, p. 152]. In [19], it is also shown why the uniform distribution of matter yields a positive curvature. Namely, the interior Schwarzschild metric is the same as the metric of $\mathbb{S}^3$ (see Appendix) up to a fixed positive constant.

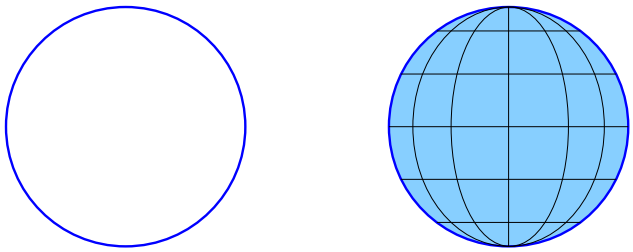

Figure 2: The unit circle on the left is the sphere $\mathbb{S}^1 = \{(x, y) \in \mathbb{E}^2 \,|\, x^2 + y^2 = 1\}$. The surface of the unit ball is the sphere $\mathbb{S}^2 = \{(x, y, z) \in \mathbb{E}^3 \,|\, x^2 + y^2 + z^2 = 1\}$.

3. Spacetime metric

In cosmology, the (pseudo)metric of the expanding homogeneous and isotropic universe is written by means of infinitesimally small quantities as follows (see e.g. [24], [30], [37], [42])

$$\mathrm{d}s^2 = c^2\mathrm{d}t^2 - a(t)^2\big(\mathrm{d}\chi^2 + f^2(\chi)(\mathrm{d}\theta^2 + \sin^2\theta\,\mathrm{d}\phi^2)\big), \tag{2}$$

where $\theta \in [0, \pi]$, $\phi \in [0, 2\pi)$, $\chi \in [0, \pi]$ for $k = 1$ and $\chi \in [0, \infty)$ otherwise, χ is a dimensionless *comoving distance*[2], $a = a(t)$ is a positive time variable function which is called the *expansion function* (sometimes it is called the *scaling parameter*), and f depends on the curvature index k as follows

$$f(\chi) = \begin{cases} \sin\chi & \text{if } k = 1, \\ \chi & \text{if } k = 0, \\ \sinh\chi & \text{if } k = -1. \end{cases} \tag{3}$$

This metric is called the *Robertson–Walker metric*. It was first introduced in papers [37] and [41]. Sometimes it is also called the *Friedmann–Lemaître–Robertson–Walker metric* or just shortly the *FLRW-metric*. Note that Willem de Sitter [8] already in 1917 (see also [9]) introduced a metric which is very similar to (2).

The case $k = 1$ corresponds to the expanding three-dimensional hypersphere given by

$$\mathbb{S}^3_{a(t)} = \{(x, y, z, w) \in \mathbb{E}^4 \,|\, x^2 + y^2 + z^2 + w^2 = a^2(t)\}, \tag{4}$$

[2]When $k = 1$ then the comoving distance χ plays the same role as the angle θ in Fig. 6.

where the function $a = a(t)$ stands for the variable radius. The hypersphere (4) for a fixed time t has at any point and any direction the same curvature $1/a(t)$, i.e., the inverse of the radius of the osculation circle. Similarly $\mathbb{E}^3$ has at any point and any direction zero curvature. This enables us to model the universe as having a high homogeneity and isotropy on large scales. In fact, the cosmological principle is the assumption that the spacetime manifold of the universe is described by metric (2), where $f(\chi)$ satisfies one of the three possibilities given in (3), see [42, Chapt. 14.2].

Recall that the expansion function $a(t) \equiv$ const. in the *Einstein static model* [10]. In 1917, Willem de Sitter found a very special solution to Einstein's equations [7], which describes an isotropic expansion of the universe with zero mass density and positive cosmological constant. In the de Sitter model, the expansion function takes the form $a(t) = \alpha \cosh(ct/\alpha)$ for a suitable constant $\alpha > 0$. In the Einstein–de Sitter parabolic model, the expansion function is defined by $a(t) = \beta t^{2/3}$, where $\beta > 0$ is a constant (see Fig. 3). There are many other models with different expansion functions, e.g., the anti-de Sitter model with a negative cosmological constant, the Friedmann model (cf. (7) and [12]), the Minkowski model [30], the Tolman model of an oscillating universe when time has no beginning and no end [39].

Remark 1. The comoving distance is independent of time and sometimes (see e.g. [32]) it is also defined as

$$d_{\mathrm{C}} = a(t_0)\chi,$$

where t_0 is the *age of the universe* (the subscript 0 will correspond to the present time). This is the distance between an object and the observer which sits at the origin of the considered coordinate system, e.g., at the North Pole in the case $k = 1$. Moreover, we note that for $k = 0$ the above variable d_{C} is the usual *Euclidean distance*. Only in this case the space manifold for a fixed time is not curved.

Remark 2. Kurt Gödel in [14] worked on a theory of a rotating universe $\mathbb{S}^3$. For any odd dimension $n = 1, 3, 5, \ldots$ the sphere $\mathbb{S}^n$ may rotate around its center such that all points have the same speed $|v|$, where $|\cdot|$ stands for the Euclidean norm in $\mathbb{E}^4$. The reason is that $\mathbb{S}^n$ "with hairs can be combed" if n is odd. It is not a rotation around an axis as e.g. for $n = 2$. For $n = 3$ the corresponding centrifugal force could then contribute to the expansion of the universe (as in case of a rotating circle for $n = 1$). Gödel also investigated a homogeneous anisotropic universe which everywhere looks like an anisotropic crystal lattice, where atoms are replaced by galaxies.

4. Expansion function versus redshift

The *redshift* z of an object resulting from its radial motions is defined by[3]

$$z := \frac{\lambda_1}{\lambda_0} - 1 = \frac{\nu_0}{\nu_1} - 1,$$

[3]The coordinate z in (4) has a different meaning. However, no ambiguity can arise.

where λ_1 and ν_1 are the observed wavelength and frequency, λ_0 and ν_0 are the emitted, and $\lambda_i\nu_i = c$ for $i = 0, 1$. If $z \gg 0$ then z is referred as the *redshift distance*. Due to local movements in a neighborhood of our Galaxy it may happen that $z \in (-1, 0)$ when an object is approaching to us. In this case z is called the *blueshift*. However, for distant objects we always have $z > 0$, since the universe is expanding. The redshift of Earth's observer is $z = 0$. Hence, altogether we find that

$$z \in (-1, \infty).$$

According to the *Einstein cosmological principle* from Section 1, our universe is homogeneous and isotropic on large scales. However, let us emphasize that the observable universe is supposed to be homogeneous only for $z =$const., since it has different densities for different z. The corresponding light cone (see Fig. 1) is nonlinearly deformed for $z \to \infty$.

Consider the light cone from Fig. 1. The observer sits at its vertex. The events inside this cone are called *time-like*, while those outside are called *space-like*. The "distance" between two consecutive events on the light cone is characterized by the relation (2) for $\mathrm{d}s = 0$. Such events are called *light-like* and the connecting geodesic line is said to be the *world-line*. Since ϕ and θ are fixed, we have $\mathrm{d}\phi = 0$ and $\mathrm{d}\theta = 0$, and thus the relation (2) reduces to the form

$$\mathrm{d}s^2 = 0 = c^2\mathrm{d}t^2 - a(t)^2\mathrm{d}\chi^2$$

for any curvature index $k \in \{-1, 0, 1\}$. Therefore,

$$c\,\mathrm{d}t = \pm a(t)\,\mathrm{d}\chi$$

which implies that for the dimensionless *conformal time* η we have

$$\mathrm{d}\eta := \frac{c\,\mathrm{d}t}{a(t)} = -\mathrm{d}\chi,$$

since the dimensionless comoving distance χ decreases while the time t increases. Denote by t_1 (or η_1) the time instant when a photon (signal) was emitted from $\chi = \chi_1$ and t_0 (or η_0) when it was received at $\chi_0 = 0$, i.e. $0 < t_1 < t_0$. For the corresponding values of the conformal time we have $0 < \eta_1 < \eta_0$. Then by integrating the above relation, we find that

$$\eta_0 - \eta_1 = \int_{\eta_1}^{\eta_0} \mathrm{d}\eta = \int_{t_1}^{t_0} \frac{c\,\mathrm{d}t}{a(t)} = -[\chi]_{\chi_1}^{\chi_0} = \chi_1, \tag{5}$$

since the χ_0 coordinate of the observer was taken without loss of generality to be zero. The comoving distance χ_1 is thus equal to the difference $\eta_0 - \eta_1$ of conformal times. The maximum possible value of the χ coordinate is thus equal to η_0 which is a finite number. On the other hand, the corresponding redshift tends to infinity.

If another signal was sent from $\chi = \chi_1$ at the conformal time $\eta_1 + \delta\eta_1$ for sufficiently small $\delta\eta_1 > 0$ and received in $\chi = \chi_0 = 0$ at $\eta_0 + \delta\eta_0$, then similarly to (5) we obtain[4]

$$(\eta_0 + \delta\eta_0) - (\eta_1 + \delta\eta_1) = \int_{\eta_1+\delta\eta_1}^{\eta_0+\delta\eta_0} \mathrm{d}\eta = \chi_1.$$

Hence, for the physical time we get

$$\delta\eta_1 = \frac{c\delta t_1}{a(t_1)} = \frac{c\delta t_0}{a(t_0)} = \delta\eta_0,$$

where $\delta t_i = \delta\eta_i a(t_i)/c$ for $i = 0, 1$, and thus (cf. (11))

$$\frac{a(t_1)}{a(t_0)} = \frac{\delta t_1}{\delta t_0}.$$

In particular, for a periodic process, where $\lambda_1 = c\delta t_1$ and $\lambda_0 = c\delta t_0$ are the corresponding wave lengths, we have

$$\frac{a(t_0)}{a(t_1)} = \frac{\lambda_0}{\lambda_1} = z + 1.$$

A special case of formula (5), when $a = a(t)$ satisfies the Friedmann equation, will be given in (28) below.

5. Hubble parameter and the Friedmann equation

For a given smooth positive expansion function $a = a(t)$ define the *Hubble parameter* by

$$H(t) = \frac{\dot{a}(t)}{a(t)}, \tag{6}$$

where $t > 0$ is time and the dot denotes the time derivative. The Hubble parameter can be thus expressed as the time derivative of the natural logarithm in the following way

$$H(t) = \frac{\mathrm{d}\big(\ln\frac{a(t)}{a_0}\big)}{\mathrm{d}t},$$

where $a_0 > 0$ is an arbitrary length constant and thus the argument $\frac{a(t)}{a_0}$ is dimensionless.

From now on we shall mainly suppose that $a = a(t)$ satisfies the *Friedmann ordinary differential equation* of the first order (see [12], [13], [42])

$$\dot{a}^2 = \frac{8\pi G\rho a^2}{3} + \frac{\Lambda c^2 a^2}{3} - kc^2 \tag{7}$$

[4]We should write more precisely $\cong$ instead of the last equality.

for $t>\tau$, where $G = 6.674\cdot10^{-11}\,\mathrm{m^3kg^{-1}s^{-2}}$ is the gravitational constant, $\rho=\rho(t) > 0$ is the mean mass density, $\Lambda \approx 10^{-52}\ \mathrm{m^{-2}}$ is the cosmological constant, $c = 299\,792\,458\,\mathrm{m/s}$ is the speed of light in vacuum, and the time

$$\tau \approx 380\,000\ \mathrm{yr} \tag{8}$$

corresponds to the decoupling of the cosmic microwave background (CMB), see [11]. The associated space behaves as an opaque plasmatic wall.[5] We cannot look deeper in time using electomagnetic waves.

By (7) Alexander Friedmann described the dynamical behavior of the universe as an alternative to Einstein's static universe[6] [10]. In 1924, he published another paper [13], where the negative curvature index $k = -1$ is considered. However, equation (7) was derived only for a negative density of mass (see [13, p. 2006]) and it is not clear how to satisfy such a paradoxical assumption. Note that the case $k = 0$ was not considered by Friedmann. From now on, we shall assume that the expansion function $a = a(t)$ satisfying (7) for $t > \tau$ fairly well approximates the expansion of the whole universe (for drawbacks of this questionable assumption see [18], [22], [23]).

Now assume that $\dot a \neq 0$ and divide equation (7) by $\dot a^2$. Then we get

$$\Omega_{\mathrm{M}}(t) + \Omega_\Lambda(t) + \Omega_k(t) = 1 \quad \text{for all } t > \tau, \tag{9}$$

where

$$\Omega_{\mathrm{M}}(t) = \frac{8\pi G\rho(t)}{3H^2(t)} > 0, \quad \Omega_\Lambda(t) = \frac{\Lambda c^2}{3H^2(t)}, \quad \text{and} \quad \Omega_k(t) = -\frac{kc^2}{a^2(t)H^2(t)}, \tag{10}$$

are cosmological parameters called the *density of dark and baryonic matter, density of dark energy,* and the *curvature parameter*, respectively. In the literature on cosmology, the division of (7) by the square $\dot a^2 \geq 0$ is usually done without any preliminary warning that we may possibly divide by zero which may lead to various paradoxes. For instance, we see that $\Omega_{\mathrm{M}}(t) \to \infty$ and $\Omega_\Lambda(t) \to \infty$ when $\dot a(t) \to 0$ (see Section 8).

6. Distances in time

In this section, we derive a relation between the redshift z and the so-called look-back time (see (19) below), i.e., how much time has passed before the photons from the observed object arrived at us. We shall follow the idea of Carroll et al. [3] in more detail.

[5] For instance, if $k = 1$ then the plasmatic wall is described by the manifold $\mathbb{S}^3_{a(\tau)}$. From the Earth we observe only its two-dimensional cross section. Astrophysical aspects of this phenomenon are beyond this article. We only note that John N. Mather and George F. Smooth have been awarded by the Nobel Prize in Physics 2006 for their discovery of the black-body form and anisotropy of the CMB.

[6] Einstein did not ask the question whether stars could shine infinitely long time. The constant solution of Einstein's equations (cf. (39)) is thus unphysical.

For $z \geq 0$ we introduce an auxiliary function

$$X(t) := \frac{a(t)}{a(t_0)} = \frac{1}{z+1}, \tag{11}$$

where t_0 is the age of the universe. By the law of conservation of mass we find for zero pressure that

$$\boxed{\rho(t)a^3(t) = \rho(t_0)a^3(t_0)} \tag{12}$$

is a time independent constant for nonrelativistic matter[7] in matter dominated universe with $z \lesssim 1000$. Thus we have

$$\frac{\rho(t)a^2(t)}{a^2(t_0)} = \frac{\rho(t)a^3(t)}{a^2(t_0)a(t)} = \frac{\rho(t_0)a^3(t_0)}{a^2(t_0)a(t)} = \frac{\rho(t_0)a(t_0)}{a(t)} = \frac{\rho(t_0)}{X(t)}.$$

From this and the Friedmann equation (7) divided by $a^2(t_0)$, we get

$$\dot{X}^2(t) = \frac{8\pi G\rho a^2}{3a^2(t_0)} + \frac{\Lambda c^2 X^2(t)}{3} - \frac{kc^2}{a^2(t_0)} = \frac{8\pi G\rho(t_0)}{3X(t)} + \frac{\Lambda c^2 X^2(t)}{3} - \frac{kc^2}{a^2(t_0)}.$$

Dividing this equation by the *Hubble constant*

$$H_0 = H(t_0) = \frac{\dot{a}(t)}{a(t)}\Big|_{t=t_0} > 0,$$

we obtain

$$\frac{1}{H_0^2}\dot{X}^2(t) = \frac{\Omega_{\rm M}}{X(t)} + \Omega_\Lambda X^2(t) + \Omega_k, \tag{13}$$

where for brevity

$$\Omega_{\rm M} = \Omega_{\rm M}(t_0), \quad \Omega_\Lambda = \Omega_\Lambda(t_0), \quad \text{and} \quad \Omega_k = \Omega_k(t_0) \tag{14}$$

denote the present values of the cosmological parameters (10). The left-hand side of (13) is nonnegative and thus

$$\frac{1}{H_0}\dot{X}(t) = \pm\sqrt{\frac{\Omega_{\rm M}}{X(t)} + \Omega_\Lambda X^2(t) + \Omega_k}. \tag{15}$$

Since by (11)

$$\dot{X}(t) = \frac{\rm d}{{\rm d}t}\Big(\frac{1}{z+1}\Big) = -\frac{1}{(z+1)^2}\frac{{\rm d}z}{{\rm d}t}$$

[7] According to [43, Chapt. 2], for ultrarelativistic matter we have $\rho(t)a^4(t) \equiv$ const. for $t \in (0, \tau)$ which corresponds to $z \gtrsim 1000$ in radiation dominated universe. The use of (7) for this case has to be done with a special care.

and since the derivative $\mathrm{d}z/\mathrm{d}t$ is negative, we find from (15) that

$$\frac{1}{H_0}\dot{X}(t) = -\frac{1}{H_0(z+1)^2}\frac{\mathrm{d}z}{\mathrm{d}t} = \sqrt{\Omega_{\mathrm{M}}(z+1) + \frac{\Omega_\Lambda}{(z+1)^2} + \Omega_k} \tag{16}$$

and thus,

$$\frac{\mathrm{d}z}{H_0(z+1)\sqrt{\Omega_{\mathrm{M}}(z+1)^3 + \Omega_k(z+1)^2 + \Omega_\Lambda}} = -\mathrm{d}t. \tag{17}$$

By (9) we can exclude Ω_k from the denominator using the identity

$$\Omega_{\mathrm{M}}(z+1)^3 + (1-\Omega_{\mathrm{M}}-\Omega_\Lambda)(z+1)^2 + \Omega_\Lambda = (\Omega_{\mathrm{M}}z+1)(z+1)^2 - \Omega_\Lambda z(z+2). \tag{18}$$

Now by integration of (17) we get the relation between the redshift z and the *look-back time* t,

$$t_0 - t = \frac{1}{H_0}\int_0^z \frac{\mathrm{d}\overline{z}}{(\overline{z}+1)\sqrt{(\Omega_{\mathrm{M}}\overline{z}+1)(\overline{z}+1)^2 - \Omega_\Lambda\overline{z}(\overline{z}+2)}}. \tag{19}$$

Numerical relations between the redshift and the corresponding look-back time are given in [32] for $k = 0$.

Remark 3. If

$$\Omega_{\mathrm{M}} \geq 0 \quad \text{and} \quad \Omega_\Lambda \leq 1, \tag{20}$$

then the integral in (19) exists and is finite. These additional conditions are essential, because the expression under the square root in (19)

$$(\Omega_{\mathrm{M}}\overline{z}+1)(\overline{z}+1)^2 - \Omega_\Lambda\overline{z}(\overline{z}+2) \geq (\overline{z}+1)^2 - \overline{z}(\overline{z}+2) = 1$$

is positive (cf. Remark 15).

Remark 4. According to [3, p. 509] and also [35, Sect. 4.3], the formula (19) for $z \to \infty$ gives the age of the universe only by means of the present values of the cosmological parameters Ω_{M}, Ω_Λ, and H_0. However, this need not be true, since (19) was derived under the assumption (12) which is not valid for very large z (see the footnote 7).

Remark 5. The measured value of the Hubble constant is

$$H_0 \approx 70 \text{ km}\,\text{s}^{-1}\text{Mpc}^{-1} \approx 2.27 \cdot 10^{-18} \text{ s}^{-1},$$

where 1 pc $= 3.086 \cdot 10^{16}$ m, $\Omega_{\mathrm{M}} \approx 0.3$ and $\Omega_\Lambda \approx 0.7$. According to [33],

$$t_0 = 13.82 \text{ Gyr},$$

i.e., the age of the universe was derived up to four significant digits by formula (19). Nevertheless, from such a simple calculation we should not make any categorical conclusions about the real age of the universe as it is often done. The Friedmann

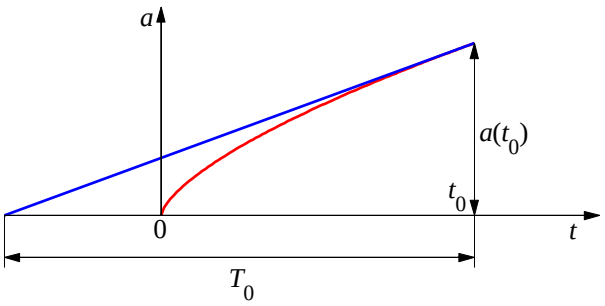

Figure 3: If the expansion function $a = a(t)$ were to be concave, then its graph would be below the tangent line through the point $(t_0, a(t_0))$. Thus for $\dot{a}(t_0) > 0$ by (22) the age of the universe t_0 would not exceed the Hubble age $T_0 = 13.97$ billion years.

equation was derived from Einstein's equations by excessive extrapolations to cosmological scales. Moreover, the present state of our universe depends on its history, whereas the Friedmann equation (7) is reversible, i.e., its solution for $t > t_0$ depends only on the value of the expansion function at the present time t_0 and not on the history. Other models that are not based on the Friedmann equation may yield a different age of our universe, e.g. an infinite age for $a(t) = C_1 + C_2 \mathrm{e}^{C_3 t}$ and some constants C_i, see [20, p. 305].

Remark 6. The *Hubble time*, sometimes called the *Hubble age* (see Fig. 3), is defined by the relation

$$T_0 := \frac{1}{H_0} \approx 13.97 \text{ Gyr} \approx 4.41 \cdot 10^{17} \text{ s},$$

where 1 yr = 31 558 149.54 s and the measured value of H_0 is stated in Remark 5. The *Hubble distance* is then given by

$$d_{\mathrm{H}} := cT_0 = 1.32 \cdot 10^{26} \text{ m}. \tag{21}$$

If the expansion function $a = a(t)$ in its definition domain were to be concave everywhere (which probably does not correspond to reality) and $\dot{a}(t_0) > 0$, then by (6) the following would hold for the truth age t_0 of the universe (see Fig. 3):

$$t_0 \le T_0 = \frac{a(t_0)}{\dot{a}(t_0)} = \frac{1}{H(t_0)} \approx 13.97 \text{ Gyr}. \tag{22}$$

Remark 7. If $0 \le z \ll 1$ then by (19)

$$z = \int_0^z \mathrm{d}\overline{z} = H_0(t_0 - t),$$

i.e., for a small z the look-back time t is independent of Ω_{M} and Ω_Λ. Multiplying this equation by c and using the well-known *Hubble law*

$$v = H_0 d,$$

where v the recession speed of galaxies at distance d, we get

$$v = cz$$

and thus the distance can be calculated from the measured redshift $z \ll 1$ as follows (cf. [36])

$$d = \frac{cz}{H_0}.$$

This relation is a very good approximation for $z \lesssim 0.1$, i.e., for distances not greater than 400 Mpc.

Remark 8. If $\Omega_k = \Omega_\Lambda = 0$ then by (9) and (19)

$$\int_0^z \frac{\mathrm{d}\overline{z}}{(\overline{z}+1)^{5/2}} = \Big[\frac{-2}{3(\overline{z}+1)^{3/2}}\Big]_0^z = \frac{2}{3}\Big(1 - \frac{1}{(z+1)^{3/2}}\Big) = H_0(t_0 - t).$$

From this and $z \to \infty$ we get $H_0 = 2/(3t_0)$, i.e.,

$$H_0(t_0 - t) = \frac{2}{3} - \frac{2t}{3t_0}.$$

For instance, if $z = 8$ then $(z+1)^{3/2} = 27$ and the corresponding age of the universe was $t = \frac{1}{27}t_0$. In fact, this represents an upper estimate of the age $\overline{t}$ for nonzero cosmological parameters Ω_k and Ω_Λ. To see this, assume that (20) is valid. Then

$$(\Omega_{\mathrm{M}}\overline{z}+1)(\overline{z}+1)^2 - \Omega_\Lambda\overline{z}(\overline{z}+2) \le (\overline{z}+1)^3,$$

and thus by (19)

$$t_0 - \overline{t} := \frac{1}{H_0}\int_0^z \frac{\mathrm{d}\overline{z}}{(\overline{z}+1)\sqrt{(\Omega_{\mathrm{M}}\overline{z}+1)(\overline{z}+1)^2 - \Omega_\Lambda\overline{z}(\overline{z}+2)}} \ge \frac{1}{H_0}\int_0^z \frac{\mathrm{d}\overline{z}}{(\overline{z}+1)^{5/2}} = t_0 - t,$$

that is $\overline{t} \le t = \frac{1}{27}t_0$.

Remark 9. If $\Omega_k = 0$ then the integral appearing in (19) can be calculated analytically (see [26]) by means or elliptic integrals (cf. also [15]). However, testing whether $\Omega_{\mathrm{M}} + \Omega_\Lambda$ is exactly equal to 1 might be a very difficult task. The main reason is that an arbitrarily small neighborhood of 1 contains infinitely many real numbers. For instance, if the sum were to be

$$\Omega_{\mathrm{M}}(t_0) + \Omega_\Lambda(t_0) = 1.000000000000000001,$$

we would still have a bounded universe that can be described by the hypersphere (4) with an incredibly large radius. Such a space is locally almost Euclidean, but bounded. There is, of course, a very big difference between a bounded and unbounded space. Moreover, the hypersphere $\mathbb{S}^3_a$ has entirely different topology than the flat space $\mathbb{E}^3$ which is promulgated by cosmologists at present. The integral appearing in (19) for $\Omega_k \neq 0$ is calculated in [27].

Remark 10. Using (6) and (11), we get

$$H(t) = \frac{a(t_0)}{a(t)} \cdot \frac{\dot{a}(t)}{a(t_0)} = (z+1)\dot{X}(t).$$

From this, (16), and (18) we can express the behavior of the Hubble parameter under the assumption (20) by means of the redshift z as follows

$$\mathcal{H}(z) = (z+1)H_0\sqrt{\Omega_{\mathrm{M}}(z+1) + \frac{\Omega_\Lambda}{(z+1)^2} + \Omega_k} = H_0\sqrt{(\Omega_{\mathrm{M}}z+1)(z+1)^2 - \Omega_\Lambda z(z+2)},$$

where $\mathcal{H}(z) = H(t)$ and $z = a(t_0)/a(t) - 1$ by (11). The inverse relation between z and t can be derived from (19).

Remark 11. Consider the linear equation of the second order

$$\ddot{a} = -\frac{4\pi G}{3}\Big(\rho + \frac{3p}{c^2}\Big)a + \frac{\Lambda c^2}{3}a \tag{23}$$

which is a direct consequence of the Einstein equations (see [21, p. 170]). For $\dot{a} \neq 0$ define the dimensionless *deceleration parameter* by

$$q = q(t) := -\frac{\ddot{a}a}{(\dot{a})^2}.$$

In particular, if the pressure $p \equiv 0$, then q can be expressed by means of the cosmological parameters (10) as follows

$$q(t) = \frac{4\pi G\rho}{3H^2} - \frac{\Lambda c^2}{3H^2} = \frac{1}{2}\Omega_{\mathrm{M}}(t) - \Omega_\Lambda(t)$$

due to (23). For $\Omega_{\mathrm{M}} \approx 0.3$ and $\Omega_\Lambda \approx 0.7$ the present value of the deceleration parameter $q(t_0) \approx -0.55$ is negative, and thus the expansion of the universe is accelerating.

Remark 12. The standard cosmological model assumes that the time flows completely uniformly from the Big Bang on (see Fig. 1). Therefore, we often hear the question: *What was before the Big Bang?*

However, it is important to realize that in the observable universe we actually look in any direction into the vast spacetime singularity. The more distant the objects that are observed, the more it seems to us that time passes more slowly. If there were a huge clock placed at $z = 1$ from the Earth, then we would see that it goes twice as slow. The largest currently observed distance corresponds to the CMB with redshift $z = 1089$ which appeared 380 000 years after[8] the Big Bang. In this case,

[8]At that time the universe was 1090 times smaller and the radius of the corresponding CMB sphere was about 10^{24} m. The most typical diameter of fluctuations in the CMB is about one angular degree which is about 10^{21} m in diameter, i.e. greater than our Galaxy. Note that this is too large an object for the well-known method of baryonic acoustic oscillations, cf. [11].

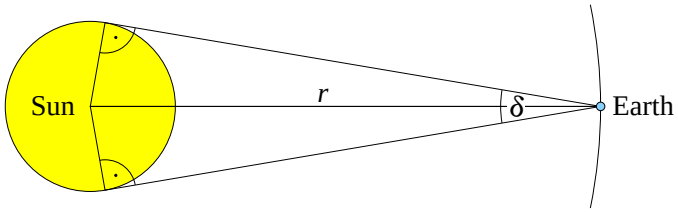

Figure 4: If D is the diameter of the Sun, then its angular distance observed from the Earth is equal to $d_{\mathrm{A}} = D/\delta = r$, where $D = 2r\sin(\delta/2) \approx r\delta$.

during one earthly hour we would observe that the CMB clock had moved only about $3.3 = \frac{3600}{1090}$ seconds. If we would ever see objects more distant than $z = 1089$ (using e.g. detectors of relic neutrinos), we would find that time there passes even more slowly, and so on.[9] Thus the Big Bang singularity deforms not only space but also time. This is a similar phenomenon like time dilatation in a gravitational potential hole, since photons reduce their frequency.

Remark 13. In applying the standard cosmological model various "delicate" limits are performed: $a \to 0$, $a \to \infty$, $t \to 0$, $t \to \infty$, $z \to \infty, \ldots$ (see, for instance, Remark 4 and [30], [42]). At present it is believed that $a(t) \to \infty$ for $t \to \infty$. By (9) and (10) for $k \leq 0$ it follows that $1 > \Omega_\Lambda(t)$, and thus $\frac{1}{3}\Lambda c^2 < H^2(t)$ for arbitrary time. From this and (6) we observe that also the time derivative of the expansion function grows beyond all bounds if Λ is a positive constant. Hence, the derivative $\dot{a}(t) \to \infty$ for $t \to \infty$ in an infinite universe (Euclidean or hyperbolic).

7. Distances in space

By [42] the *angular distance* (sometimes called the *angular-size distance*) is in the Euclidean space defined by the relation

$$d_{\mathrm{A}} = \frac{D}{\delta}, \tag{24}$$

where D is a known (or assumed) proper size of an object and $\delta \in (0, 2\pi)$ is its apparent angular size (see e.g. Fig. 4). Since δ is usually very small, we have $\tan\delta \approx \sin\delta \approx \delta$ in radians.

Remark 14. Let an observer be located at the North Pole of the sphere $\mathbb{S}^2$ in Fig. 2. The arcs of the parallel $\pm 60°$ between the meridians $0°$ and $30°$ are obviously viewed under the same angle. A similar nonuniqueness may cause some troubles when using the angular distance (24) in $\mathbb{S}^3$. On the other hand, a very long and distant segment in $\mathbb{H}^3$ can be viewed under a very small angle. Since the real curvature index k is not known up to now, one has to be careful when using the angular distance in cosmology for large z.

[9] To avoid this drawback, a conformal time is usually applied (see (27) below).

The *proper motion distance* (sometimes called only the *proper distance* or the *comoving transverse distance*) is defined by the relation (cf. Remark 1)

$$d_{\mathrm{M}} = a(t_0) f(\chi), \tag{25}$$

where f is defined by (3). Hence, d_{M} is always bounded for $z \to \infty$, since the maximum possible coordinate χ is bounded (see Section 4). When $k = 1$ the formula (25) should be used by Remark 14 only for $\chi \leq \pi/2$. For $\pi/2 \leq \chi \leq \pi$ and $k = 1$ the proper motion distance d_{M} is maximal for $\chi = \pi/2$ and $d_{\mathrm{M}} = 0$ for $\chi = \pi$, i.e., the proper motion distance does not satisfy the standard mathematical requirements attributed to the distance, see [43].

Let L be the bolometric luminosity (i.e. total — integrated over all frequencies) of an object. It is measured in Watts. Then the *luminosity distance* d_{L} is related with the flux ℓ measured in $\mathrm{W/m^2}$ by

$$\ell = \frac{L}{4\pi d_{\mathrm{L}}^2}, \quad \text{i.e.} \quad d_{\mathrm{L}} = \sqrt{\frac{L}{4\pi \ell}}.$$

The luminosity distance in Mpc can be established from the observed apparent magnitude μ and the absolute magnitude μ_{abs} of an object by the formula

$$\mu - \mu_{\mathrm{abs}} = 25 + 5 \log_{10} d_{\mathrm{L}}.$$

This is a key formula in cosmology [3], since one can use the observed flux to establish d_{L}. The main idea is based on the known density of light flux, the distance and flux of some reference galaxy, and Pogson's equation (for details see [20, p. 110] and [42]).

According to [29, Eq. (6)] and [28, Eqs. (1)–(3)] the luminosity distance is given by formula

$$d_{\mathrm{L}} = a(t_0) f(\chi)(1 + z).$$

Hence, the formula for the flux ℓ has to be modified as follows (see [42]):

$$\ell = \frac{L}{4\pi a^2(t_0) f^2(\chi)(z+1)^2}.$$

Since photons loose their energy during the expansion of the universe, the factor $(z + 1)$ appears in the denominator. Another factor $(z + 1)$ is due to the fact that 1 second lasted longer when a photon was emitted than when it was received. According to [42, p. 485],

$$d_{\mathrm{L}}(z) = (z + 1) d_{\mathrm{M}}. \tag{26}$$

Now we will derive the dependence of the proper motion and luminosity distances, respectively, on the redshift z. To this end, we will again consider the conformal time η given by[10]

$$\mathrm{d}\eta = \frac{c\,\mathrm{d}t}{a(t)} \tag{27}$$

[10]For $a(t) \equiv \text{const.}$ we see that η is linearly proportional to t.

instead of the usual time t. Then from (17) and (11) we find that

$$\frac{\mathrm{d}z}{a(t_0)H_0(z+1)\sqrt{\Omega_{\mathrm{M}}(z+1)^3+\Omega_k(z+1)^2+\Omega_\Lambda}} = -\frac{a(t)\mathrm{d}\eta}{c\,a(t_0)} = -\frac{\mathrm{d}\eta}{c(z+1)}.$$

Multiplying the both sides by $z+1$, we get by (18) and integration as in (19) that

$$\chi = \eta_0 - \eta = \frac{c}{a(t_0)H_0}\int_0^z \frac{\mathrm{d}\overline{z}}{\sqrt{(\Omega_{\mathrm{M}}\overline{z}+1)(\overline{z}+1)^2-\Omega_\Lambda\overline{z}(\overline{z}+2)}}. \tag{28}$$

This a dimensionless number that represents the distance in the comoving coordinates (cf. (5) for a general case). The largest possible distance in χ is thus $\chi_{\mathrm{horizon}} = \eta_0$ (see Section 4). Therefore, the observable universe is bounded.

Remark 15. If $\overline{z} = 3$, $\Omega_{\mathrm{M}} = 0.01$, and $\Omega_\Lambda = 1.1$, then in (28) we would have to take the square root of a negative number, since

$$(\Omega_{\mathrm{M}}\overline{z}+1)(\overline{z}+1)^2-\Omega_\Lambda\overline{z}(\overline{z}+2) = 1.03\cdot 4^2 - 1.1\cdot 3\cdot 5 = -0.02,$$

which would yield complex values (see also [21, p. 172]). In spite of that the standard Ned Wright's Calculator (see `http://www.astro.ucla.edu/~wright/CosmoCalc.html`) gives a quite acceptable value $d_{\mathrm{L}} = 164.1$ Gly (which is sometimes also called the *light-year distance*).

From now on we shall assume that conditions (20) hold. These conditions are only sufficient (not necessary) for the existence of the integral in (28).

Remark 16. Let $k = 0$. Then by (3), (25), (26), and (28) we get

$$d_{\mathrm{L}}(z) = (z+1)a(t_0)\chi = \frac{(z+1)c}{H_0}\int_0^z \frac{\mathrm{d}\overline{z}}{\sqrt{(\Omega_{\mathrm{M}}\overline{z}+1)(\overline{z}+1)^2-\Omega_\Lambda\overline{z}(\overline{z}+2)}}.$$

Remark 17. By (14) and (10) we see that

$$\Omega_k = -\frac{kc^2}{H_0^2 a^2(t_0)}.$$

Hence, by (3), (25), (26), and (28) we get for $k = 1$ that

$$d_{\mathrm{M}}(z) = a(t_0)\sin\chi = \frac{c}{H_0\sqrt{|\Omega_k|}}\sin\left(\sqrt{|\Omega_k|}\int_0^z \frac{\mathrm{d}\overline{z}}{\sqrt{(\Omega_{\mathrm{M}}\overline{z}+1)(\overline{z}+1)^2-\Omega_\Lambda\overline{z}(\overline{z}+2)}}\right).$$

Similarly for $k = -1$ we find that

$$d_{\mathrm{M}}(z) = a(t_0)\sinh\chi = \frac{c}{H_0\sqrt{\Omega_k}}\sinh\left(\sqrt{\Omega_k}\int_0^z \frac{\mathrm{d}\overline{z}}{\sqrt{(\Omega_{\mathrm{M}}\overline{z}+1)(\overline{z}+1)^2-\Omega_\Lambda\overline{z}(\overline{z}+2)}}\right).$$

These formulae derived in [3] were also used by the Nobel Prize Winner S. Perlmutter et al. in [31, p. 566]. Note that the observed flux essentially depends on the used measuring instruments.

Remark 18. By [42, p. 485] the *angular distance* for any $k \in \{-1, 0, 1\}$ is defined as follows (for $k = 0$ it coincides[11] with (24))

$$d_{\mathrm{A}}(z) = \frac{d_{\mathrm{M}}(z)}{z+1},$$

where the proper motion distance d_{M} is given by (25). Hence, by (26),

$$\frac{1}{z+1} d_{\mathrm{L}}(z) = d_{\mathrm{M}}(z) = (z+1) d_{\mathrm{A}}(z). \tag{29}$$

From (25) we see that $d_{\mathrm{L}}(z)$ is unbounded for $z \to \infty$, $d_{\mathrm{M}}(z)$ remains bounded for $z \to \infty$, and $d_{\mathrm{A}}(z)$ converges to zero for $z \to \infty$. Here one has to realize that the light of distant objects with redshift $z > 0$ propagates into a larger volume than if the universe were not to expand. This gives the factor $(z+1)^{-1}$ on the left-hand side of (29).

Moreover, we must consistently distinguish between "at that time" and "actual dimensions", i.e. the size of the universe when observed photons left a distant object and the universe was much smaller, and "today's" dimensions when "ancient" photons arrived at our ground-based telescopes. Roughly speaking, the younger the objects which are observed, the larger the magnification appears. Therefore, by angular measurements we paradoxically see a very distant object as being larger. We call this phenomenon the *time lens*. The magnification is given by the factor

$$(z+1),$$

which appears on the right-hand side of (29). In [20, p. 314], the functioning of the time lens is illustrated by three real-world examples.

From (29) and Remark 7 we also see that

$$d_{\mathrm{L}}(z) \approx d_{\mathrm{M}}(z) \approx d_{\mathrm{A}}(z) \approx \frac{cz}{H_0} \approx c(t_0 - t)$$

when z is small, i.e. $0 \leq z \ll 1$. The error is only a few percent for $z \lesssim 0.1$.

Remark 19. By (10) and (6) we see that

$$\Omega_k(t) = -\frac{kc^2}{a^2(t)H^2(t)} = -\frac{kc^2}{(\dot{a}(t))^2}.$$

Hence, if $\dot{a}$ is decreasing with time, then $|\Omega_k(t)|$ is increasing. This shows that the name *curvature parameter* for $\Omega_k(t)$ was not appropriately chosen (see [33]).

[11] For $k = 0$ and very short distances one may also define the standard parallax distance by means of a parallactic angle (see e.g. [42, pp. 420, 485]).

8. Solution of the Friedmann equation

Throughout this section we shall suppose that[12]

$$\Lambda > 0.$$

The time instant τ will again correspond to the decoupling of the cosmic microwave background (8). Then the expansion fuction $a = a(t)$ satisfies the following condition

$$\dot{a}(\tau) > 0, \tag{30}$$

since the universe was expanding.

Setting

$$A = \frac{\Lambda c^2}{3} \quad \text{and} \quad B = -kc^2,$$

the Friedmann equation (7) can be written as the following simple autonomous ordinary differential equation with constant coefficients

$$\dot{a}^2 = Aa^2 + B + \frac{C}{a} \quad \text{for } t \geq \tau, \tag{31}$$

where

$$C = \frac{8\pi G\rho a^3}{3} > 0 \tag{32}$$

is a constant due to (12). The required zero pressure fits to astronomical observations for $t \geq \tau$. For the existence and uniqueness of the solution of (31) we refer to [5, Chapt. 1] and [34, vol. II].

We can easily find that the physical dimensions of A, B, and C are s^{-2}, $\mathrm{m}^2\mathrm{s}^{-2}$, and $\mathrm{m}^3\mathrm{s}^{-2}$, respectively. Since the expansion function $a = a(t) > 0$ is continuous, its time derivative $\dot{a} = \dot{a}(t)$ is by (31) also a continuous function.

If $a > 0$ is sufficiently small, then C/a is much larger than the terms Aa^2 and B on the right-hand side of (31). Hence, $\dot{a}^2 a \approx C$ and the corresponding density parameter $\Omega_{\mathrm{M}} \simeq 1$ also dominates the other parameters from (10). In this case the expansion function behavies as $t^{2/3}$ up to some multiplicative positive constant (like in the Einstein–de Sitter parabolic model).

The right-hand side of (31)

$$F(a) = Aa^2 + B + \frac{C}{a}, \quad a \in (0, \infty), \tag{33}$$

is a strictly convex function, since its second derivative $F''(a) = 2A + 2C/a^3$ is positive for $a > 0$. From the equation

$$F'(a) = 2Aa - \frac{C}{a^2} = 0 \tag{34}$$

[12]The case $\Lambda \leq 0$ can be investigated similarly, see e.g. [39]. The inequality $\Lambda < 0$ leads to an oscillating universe, while for $\Lambda = 0$ the behavior of the expansion function depends on the so-called critical density [20, p. 285].

we find that F attains its unique minimum at the point

$$a_{\min} = \sqrt[3]{\frac{C}{2A}} = \sqrt[3]{\frac{3C}{2\Lambda c^2}} > 0. \tag{35}$$

First assume that the curvature index $k \leq 0$. Then we see that the right-hand side of (31) is positive, and therefore $\dot{a}$ does not change its sign and by (30) the expansion function $a = a(t)$ is increasing on $[\tau, \infty)$. The global solution exists due to the following linear upper bound of

$$\dot{a} = \sqrt{Aa^2 + B + C/a} \leq 2\sqrt{A}a$$

for sufficiently large a. Note that the upper bound function $b(t) = \exp(2\sqrt{A}t)$ for $a = a(t)$ is the solution of the equation $\dot{b} = 2\sqrt{A}b$.

The solutions $a = a(t)$ for various initial conditions $a(\tau) > 0$ do not intersect and they also do not bifurcate[13], since the right-hand side of the equation $\dot{a} = \sqrt{F(a)}$ is a Lipschitz continuous[14] function over the interval $[a(\tau), \infty)$. This guaratees that the solution $a = a(t)$ exists and is unique over the whole interval $[\tau, \infty)$, see [5, Chapt. 1] and [34, vol. II].

Second assume that $k = 1$ and consider the following three cases:

1. Let $F(a_{\min}) > 0$. Then by (30) and (31) we have $\dot{a}(t) \geq \sqrt{F(a_{\min})} > 0$ for all $t \geq \tau$, where τ is given by (8). Therefore, the expansion function is again increasing over the whole interval $[\tau, \infty)$ due to the following linear upper bound $\dot{a} \leq 2\sqrt{A}a$ for sufficiently large a.

2. Let $F(a_{\min}) = 0$. Then $F(a) > 0$ for all $a \neq a_{\min}$ and by (31) the second derivative is[15]

$$\ddot{a} = \pm\frac{2Aa - \frac{C}{a^2}}{2\sqrt{Aa^2 + B + \frac{C}{a}}}\dot{a} = \pm\Big(Aa - \frac{C}{2a^2}\Big). \tag{36}$$

We see that its value for $a = a_{\min}$ is

$$Aa_{\min} - \frac{C}{2a_{\min}^2} = 2^{-1/3}A^{2/3}C^{1/3} - 2^{-1/3}A^{2/3}C^{1/3} = 0. \tag{37}$$

If $a(\tau) > a_{\min}$ then

$$\ddot{a}(t) > Aa_{\min} - \frac{C}{2a_{\min}^2} = 0$$

[13]The equation $\dot{a} = \sqrt{a}$ with the initial condition $a(0) = 0$ has two solutions $a(t) = \frac{1}{4}t^2$ and $a \equiv 0$, since the right-hand side $\sqrt{a}$ is not Lipschitz continuous. The fact that $\dot{a}$ has a different physical dimension than $\sqrt{a}$ can be easily avoided by a suitable constant.

[14]The function $b(t) = \tan t$ for $t \in [0, \pi/2)$ solves the Riccati equation $\dot{b} = b^2 + 1$, whose right-hand side is not Lipschitz continuous. This expample shows that the existence of the global solution over $[0, \infty)$ need not be guaranteed for right-hand sides that are not Lipschitz continuous.

[15]Comparing this equation with (23), we observe that the sign + should only be considered.

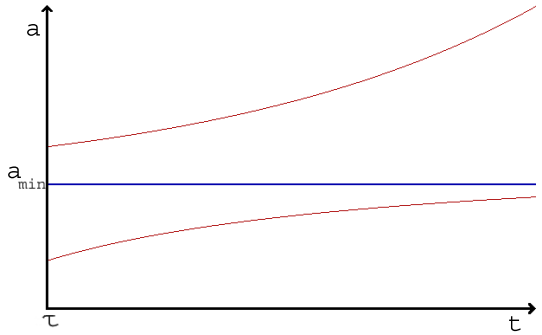

Figure 5: Solutions $a = a(t)$ of the Friedmann equation (31) for the case $F(a_{\min}) = 0$. If (30) holds, then all solutions are increasing. For $0 < a(\tau) < a_{\min}$ the corresponding solution is strictly concave and for $a(\tau) > a_{\min}$ it is strictly convex. The asymptotic function $a(t) \equiv a_{\min}$ does not satisfy (30).

and $a = a(t)$ is strictly convex and increasing over the interval $[\tau, \infty)$ due to (31), see Fig. 5.

If $a(\tau) = a_{\min}$ then $a = a(t)$ is a constant function everywhere due to (31), (36), and (37) which contradicts (30). Hence, this case cannot happen. It corresponds to the Einstein static universe, which will be treated more detailly in Theorem 1.

If the initial condition satisfies the inequalities $0 < a(\tau) < a_{\min}$, then

$$\ddot{a}(t) = Aa(t) - \frac{C}{2a^2(t)} < Aa_{\min} - \frac{C}{2a_{\min}^2} = 0$$

and $a = a(t)$ is strictly concave and increasing for all $t \in [\tau, \infty)$. The sharp inequality in the above relation follows from the uniqueness, since no solution can cross the line $a(t) \equiv a_{\min}$.

3. Finally, let $F(a_{\min}) < 0$. Then there exist two roots $a_1 < a_2$ such that $F(a_1) = F(a_2) = 0$ and F is negative on the interval (a_1, a_2). However, the left-hand side of (31) is nonnegative everywhere. Hence, the case $a_1 < a(t) < a_2$ for $t \geq \tau$ cannot happen.

If $a(\tau) = a_1$ or $a(\tau) = a_2$, then by (31) we have $\dot{a}(\tau) = 0$ which contradicts (30), i.e., these cases can be excluded, too.

If the initial condition satisfies $a(\tau) > a_2$, then $F(a) > 0$ for all $a > a_2$ and by (30) the expansion function is again increasing.

We will not investigate the case $a_1 \leq 0$, since the radius of $\mathbb{S}^3_a$ is positive. So let the initial condition $a(\tau)$ satisfy the inequalities $0 < a(\tau) < a_1$. Then F is positive on the interval $(0, a_1)$. Set

$$K := Aa_1 - \frac{C}{2a_1^2}.$$

Since $0 < a_1 < a_{\min}$, we obtain by (36) and (37) that

$$\ddot{a}(t) = Aa(t) - \frac{C}{2a^2(t)} \leq K < Aa_{\min} - \frac{C}{2a_{\min}^2} = 0$$

for all $t > \tau$ such that $a(t) > 0$, i.e.

$$\ddot{a}(t) \leq K < 0$$

which means that $a = a(t)$ is strictly concave. By integration we find that

$$\dot{a}(t) - \dot{a}(\tau) = \int_{\tau}^{t} \ddot{a}(\sigma)\,\mathrm{d}\sigma \leq K(t-\tau) < 0.$$

Consequently, $Kt \to -\infty$ as $t \to \infty$ and since $\dot{a}(\tau)$ and $K\tau$ are fixed numbers, there exists exactly one time instant $t_2 > \tau$ such that

$$\dot{a}(t_2) = 0 = F(a_1).$$

Then the cosmological density parameters are not well defined due to the division by zero in (10). This case corresponds to universe of finite duration. The unique solution of (31) is given by the equation $\dot{a} = \sqrt{F(a)}$ on the interval $[\tau, t_2]$ and by the equation $\dot{a} = -\sqrt{F(a)}$ after the point t_2 until $a = a(t)$ reaches the zero value.

• • •

Instead of (30) we shall now assume that $\dot{a} \equiv 0$ and moreover, let $k = 1$. This special case corresponds to the *Einstein static universe*. By (33) and (35) we have

$$0 = F(a_{\min}) = Aa_{\min}^2 - c^2 + \frac{C}{a_{\min}} = A\sqrt[3]{\frac{C^2}{4A^2}} - c^2 + C\sqrt[3]{\frac{2A}{C}} = \sqrt[3]{\frac{AC^2}{4}} - c^2 + 2\sqrt[3]{\frac{AC^2}{4}}.$$

Hence,

$$C = c^3\sqrt{\frac{4}{27A}} = \frac{2c^2}{3\sqrt{\Lambda}}. \tag{38}$$

Substituting (38) into (35), we get the formula for the radius of the Einstein static universe, namely

$$a = \frac{1}{\sqrt{\Lambda}}. \tag{39}$$

Theorem 1. *The total mass of the Einstein static universe M and its mean density ρ can be expressed by the following fundamental constants π, c, G, and Λ,*

$$M = \frac{\pi c^2}{2G\sqrt{\Lambda}}, \qquad \rho = \frac{\Lambda c^2}{4\pi G}.$$

P r o o f. Applying the hyperspherical coordinates (see Section 2), the unit hypersphere $\mathbb{S}^3$ can be divided into elementary spherical shells with areas $4\pi\sin^2\chi$ and thickness $\mathrm{d}\chi$. For its volume we thus get

$$\mathrm{Vol}(\mathbb{S}^3) = 4\pi\int_0^{\pi}\sin^2\chi\,\mathrm{d}\chi = 2\pi[\chi - \tfrac{1}{2}\sin(2\chi)]_0^{\pi} = 2\pi^2.$$

Hence, the volume of the hypersphere $\mathbb{S}^3_a$ with radius a is (see [10, p. 152])

$$V = 2\pi^2 a^3.$$

From this, (38), and (32) we obtain

$$\frac{2c^2}{\sqrt{\Lambda}} = 3C = 8\pi G\rho a^3 = \frac{4G\rho V}{\pi} = \frac{4GM}{\pi},$$

which yields the proposed relation for M. From this and (39) we get the formula for the density ρ. (This formula can also be obtained from (23) for $\ddot{a} \equiv 0$ and $p \equiv 0$.) □

Remark 20. The mass of our Galaxy is about 10^{42} kg. For comparison let us evaluate the mass of the Einstein static universe by Theorem 1 for $\Lambda \approx 10^{-52}\,\mathrm{m}^{-2}$,

$$\boxed{M = \frac{\pi c^2}{2G\sqrt{\Lambda}} \approx 2.12 \cdot 10^{53}\,\mathrm{kg}.} \tag{40}$$

Hence, the Einstein static universe is tuned very finely. However, the resulting stationary solution $a = \Lambda^{-1/2} \approx 10^{26}\,\mathrm{m}$ of equation (7) is not stable, i.e., any small deviation from the constant $a = a(t) = \Lambda^{-1/2}$ will cause either a gravitational collapse, or expansion (see [30, p. 746] or [39, p. 405]). We also see that the constant C in (38) is independent of the total mass of the universe, while in the general case treated in (32) the constant C depends on the total mass. Furthermore, we observe that the density parameter $\Omega_{\mathrm{M}}(t)$ defined in (10) is infinity even though nothing dramatic happens. The mean density of baryonic matter is of course finite, namely

$$\rho = \frac{M}{V} = \frac{\Lambda c^2}{4\pi G} \approx 10^{-26}\,\mathrm{kg/m}^3. \tag{41}$$

Interestingly, this density and the mass given in (40) are quite realistic numbers.

Remark 21. The numbers appearing in the Friedmann equation (7) are very different in size in the SI units, e.g., $\Lambda \approx 10^{-52}$ m^{-2}, $\rho(t_0) \approx 10^{-27}$ kg/m^3, $G = 6.674 \cdot 10^{-11}$ m^{3}kg^{-1}s^{-2}, $c = 3 \cdot 10^8$ m/s, and $a(t_0) \approx 10^{26}$ m. This, of course, produces various numerical troubles in finite arithmetic precision. Therefore, for clarity, it is convenient to introduce a new cosmological length unit

$$1\ \mathrm{j} = 10^{26}\ \mathrm{m}.$$

Then $a(t_0) \approx 1$ j and $\Lambda \approx 1\ \mathrm{j}^{-2}$. Setting $c = 1$, the time unit can be identified with the length unit 1 j. In this case the Hubble distance is (see (21) and Fig. 3)

$$d_{\mathrm{H}} = cT_0 = 1.32\ \mathrm{j}.$$

Remark 22. Now let us calculate the inflection point of the expansion function $a = a(t)$, i.e., when the strictly concave expansion function (see e.g. Fig. 3) changes into the strictly convex function. From (31) we find that

$$\ddot{a} = \frac{2Aa - \frac{C}{a^2}}{2\sqrt{Aa^2 + B + \frac{C}{a}}} = 0.$$

Hence, $\frac{2}{3}\Lambda c^2 a^3 = 2Aa^3 = C$ and thus for the inflection point we obtain[16] surprisingly the same relation as (35), i.e. the radius of the Einstein static universe (see (38) and (39)), namely

$$a = \sqrt[3]{\frac{3C}{2\Lambda c^2}}$$

which is independent of the curvature index k. From this and (32) we get $2\Lambda c^2 = 8\pi G\rho$ which for $\Lambda \approx 10^{-52}\,\mathrm{m}^{-2}$ yields the corresponding density.

$$\rho = \frac{\Lambda c^2}{4\pi G} \approx 10^{-26}\,\mathrm{kg/m}^3.$$

Interestingly, its value is again the same as that in (41). Since the measured mean density in our neighborhood is smaller, the expansion function seems to already be strictly convex at present. This fact was predicted already in 1931 by Georges Lemaître [25, p. 422] (see also [30, Box 27.5], [38], [39, p. 411]).

Remark 23. If $\Lambda = 0$ and $k = 1$, then from (31) we get $\dot{a}^2a^2 = c^2(\alpha a - a^2)$, where $\alpha = C/c^2$ is a positive constant. Using the conformal time η defined by (27), we find that $\dot{a} = \frac{c}{a}a'$, where $a' = \mathrm{d}a/\mathrm{d}\eta$. Therefore, $(a')^2 = \alpha a - a^2$. Employing the substitution $x = \frac{2a}{\alpha} - 1$, we obtain

$$\int \frac{\mathrm{d}a}{\sqrt{\alpha a - a^2}} = \int \frac{2}{\alpha}\frac{\mathrm{d}a}{\sqrt{1 - \left(\frac{2a}{\alpha} - 1\right)^2}} = \int \frac{\mathrm{d}x}{\sqrt{1 - x^2}} = \arcsin\Big(\frac{2a}{\alpha} - 1\Big).$$

Hence, $\eta - \eta_0 = \arcsin\big(\frac{2a}{\alpha} - 1\big)$ and $\sin(\eta - \eta_0) = \frac{2a}{\alpha} - 1$, which implies that $-\sin\eta_0 = -1$ and $\eta_0 = \pi/2$. Thus, $a(\eta) = \frac{\alpha}{2}(1 - \cos\eta)$ for $\eta \in [0, 2\pi]$ which leads to an oscillating universe, see also [39, p. 412].

9. Appendix

Here we briefly describe how to calculate the metric of the unit hypersphere $\mathbb{S}^3$ defined by (1). This is a three-dimensional hypersurface in the four-dimensional Euclidean space $\mathbb{E}^4$. It can be described by hyperspherical coordinates $\chi, \theta \in [0, \pi]$

[16] Note that from (23) one can derive the same formula if and only if the pressure $p = 0$.

and $\phi \in [0, 2\pi)$, see Section 2. Hence, [34, p. 253, vol. I], the components of local coordinate vectors are

$$\begin{aligned} p_1 &= \frac{\partial}{\partial \chi} p(\chi, \theta, \phi) = (\cos\chi \sin\theta \cos\phi, \cos\chi \sin\theta \sin\phi, \cos\chi \cos\theta, -\sin\chi), \\ p_2 &= \frac{\partial}{\partial \phi} p(\chi, \theta, \phi) = (\sin\chi \cos\theta \cos\phi, \sin\chi \cos\theta \sin\phi, -\sin\chi \sin\theta, 0), \\ p_3 &= \frac{\partial}{\partial \phi} p(\chi, \theta, \phi) = (-\sin\chi \sin\theta \sin\phi, \sin\chi \sin\theta \cos\phi, 0, 0), \end{aligned} \tag{42}$$

where the vector $\vec{p}$ with components p_1, p_2, p_3 (cf. Fig. 6) lies in the hyperplane tangent at the point $(x, y, z, w) \in \mathbb{S}^3$.

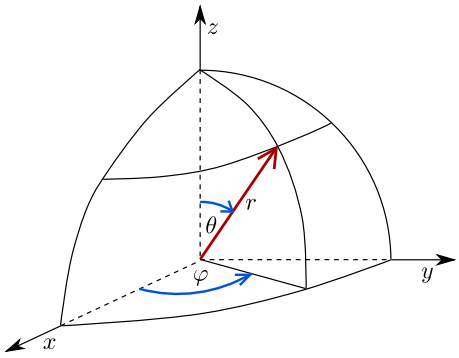

Figure 6: The point (x, y, z) in the standard spherical coordinates (r, φ, θ)

The covariant coordinates of the symmetric metric tensor corresponding to the unit hypersphere $\mathbb{S}^3$ are given by relations

$$\tilde{g}_{ij} = p_i \cdot p_j \quad \text{for} \quad i, j = 1, 2, 3,$$

where $\cdot$ denotes the scalar product. Hence from (42), it follows that

$$\begin{aligned} \tilde{g}_{11} &= \cos^2\chi \sin^2\theta \cos^2\phi + \cos^2\chi \sin^2\theta \sin^2\phi + \cos^2\chi \cos^2\theta + \sin^2\chi = 1, \\ \tilde{g}_{22} &= \sin^2\chi \cos^2\theta \cos^2\phi + \sin^2\chi \cos^2\theta \sin^2\phi + \sin^2\chi \sin^2\theta = \sin^2\chi, \\ \tilde{g}_{33} &= \sin^2\chi \sin^2\theta \sin^2\phi + \sin^2\chi \sin^2\theta \cos^2\phi = \sin^2\chi \sin^2\theta, \end{aligned}$$

and the other entries vanish, because by inspection we can derive that

$$p_1 \cdot p_2 = p_1 \cdot p_3 = p_2 \cdot p_3 = 0.$$

The metric tensor corresponding to the unit hypersphere $\mathbb{S}^3$ is therefore given by the diagonal matrix

$$\tilde{g}_{ij} = \begin{pmatrix} 1 & 0 & 0 \\ 0 & \sin^2\chi & 0 \\ 0 & 0 & \sin^2\chi \sin^2\theta \end{pmatrix}, \quad i, j = 1, 2, 3.$$

The length element of $\mathbb{S}^3$ is thus given by (cf. (2))

$$\mathrm{d}\ell^2 = \mathrm{d}\chi^2 + (\mathrm{d}\theta^2 + \sin^2\theta\,\mathrm{d}\phi^2)\sin^2\chi.$$

For $k = 0$ and $k = -1$ the function $\sin^2\chi$ has to be replaced by χ^2 and $\sinh^2\chi$, respectively (see (3) and [42, Chapt. 13]).

Acknowledgment. The authors are indebted to J. Brandts, Y. Dumin, and L. Somer for valuable suggestions. The paper was supported by RVO 67985840 of the Czech Republic.

References

[1] Blanuša, D.: Über die Einbettung hyperbolischer Räume in euklidische Räume. Monatsh. Math. **59** (1955), 217–229.

[2] Brander, D.: Isometric embeddings between space forms. Master Thesis, Univ. of Pennsylvania, 2003, 1–48.

[3] Carrroll, S. M., Press, H. W., Turner, E. L.: The cosmological constant. Annu. Rev. Astron. Astrophys. **30** (1992), 499–542.

[4] Cannon, J. W., Floyd, W. J., Kenyon, R., Parry, W. R., Hyperbolic geometry. In: Flavors of Geometry, Math. Sci. Res. Inst. Publ. **31**, Cambridge Univ. Press, 1997, 59–115.

[5] Coddington, E. A., Levinson, N., Theory of ordinary differential equations. McGraw-Hill Book Company, New York, 1955.

[6] Davis, T. M., Lineweaver, C. H.: Expanding confusion: common misconceptions of cosmological horizons and the superluminal expansion of the universe. Publ. Astron. Soc. Australia **21** (2004), 97–109.

[7] De Sitter, W.: On the relativity of inertia. Remarks concerning Einstein latest hypothesis. Proc. Kon. Ned. Acad. Wet. **19** (1917), 1217–1225.

[8] De Sitter, W.: On Einstein's theory of gravitation, and its astronomical consequences. Third paper, Monthly Notices Roy. Astron. Soc. **78** (1917), 3–28.

[9] De Sitter, W.: On the curvature of space. Proc. Kon. Ned. Acad. Wet. **20** (1918), 229–243.

[10] Einstein, A.: Kosmologische Betrachtungen zur allgemeinen Relativitätstheorie. Königlich-Preuss. Akad. Wiss. Berlin (1917), 142–152.

[11] Eisenstein, D. J., Bennett, C. L.: Cosmic sound waves rule. Physics Today **61** (2008), 44–50.

[12] Friedman, A.: Über die Krümmung des Raumes. Z. Phys. **10** (1922), 377–386. English translation: On the curvature of space. General Relativity and Gravitation **31** (1999), 1991–2000.

[13] Friedmann, A.: Über die Möglichkeit einer Welt mit konstanter negativer Krümmung des Raumes. Z. Phys. **21** (1924), 326–332. English translation: General Relativity and Gravitation **31** (1999), 2001–2008.

[14] Gödel, K.: An example of a new type of cosmological solutions of Einstein's field equations of gravitation. Rev. Mod. Phys. **21** (1949), 447–450.

[15] Gradštejn, I. S., Ryžik, I. M.: *Tablicy intěgralov, summ, rjadov i proizveděnij*. Nauka, Moscow, 1971.

[16] Guth, A. H.: *The inflationary universe*. Massachusetts Perseus Books, 1997.

[17] Hogg, D. W.: Distance measures in cosmology. ArXiv: astro-ph/9905116v4, 2000, 1–16.

[18] Křížek, M.: Ten arguments againts the proclaimed amount of dark matter. Grav. Cosmol. 24 (2018), 16 pp.

[19] Křížek, M., Křížek, F.: Quantitative properties of the Schwarzschild metric. Publ. Astron. Soc. Bulg. (2018), 1–10.

[20] Křížek, M., Křížek, F., Somer, L.: *Antigravity — Its Origin and Manifestations*. Lambert Acad. Publ., Saarbrücken, 2015.

[21] Křížek, M., Mészáros, A.: On the Friedmann equation for the three-dimensional hypersphere. Proc. Conf. Cosmology on Small Scales 2016, (eds. M. Křížek, Y. V. Dumin), Inst. of Math., Prague, 2016, 159–178.

[22] Křížek, M., Somer, L.: Excessive extrapolations in cosmology. Grav. Cosmol. **22** (2016), 270–280.

[23] Kroupa, P.: Galaxies as simple dynamical systems: observational data disfavor dark matter and stochastic star formation. Can. J. Phys. **93** (2015), 169–202.

[24] Landau, L. D., Lifshitz, E. M.: *The classical theory of fields* (4th revised edition). Pergamon Press Ltd, 1975.

[25] Lemaître, G. E.: L'expansion de l'espace. Rev. Quest. Sci. **17** (1931), 391–440.

[26] Mészáros, A., Řípa, J.: A curious relation between the flat cosmological model and the elliptic integral of first kind. Astron. Astrophys. **556** (2013), A13.

[27] Mészáros, A., Řípa, J.: On the relation between the non-flat cosmological models and the elliptic integral of first kind. Astron. Astrophys. **573** (2015), A54.

[28] Mészáros, A., Řípa, J., Ryde, F.: Cosmological effects on the observed flux and fluence distributions of gamma-ray bursts: Are the most distant bursts in general the faintest ones? Astron. Astrophys. **529** (2011), A55, 9 pp.

[29] Mészáros, P., Mészáros, A.: The brightness distribution of bursting sources in relativistic cosmologies. Astrophys. J. **449** (1995), 9–16.

[30] Misner, C. W., Thorne, K. S., Wheeler, J. A.: *Gravitation*, 20th edition. W. H. Freeman, New York, 1997.

[31] Perlmutter, S. et al.: Measurements of the cosmological parameters Ω and Λ from the first seven supernovae at $z \geq 0.35$. Astrophys. J. **483** (1997), 565–581.

[32] Pilipenko, S. V.: Paper-and-pencil cosmological calculator. Preprint, arXiv: 1303.5961v1, 2013, 1–4.

[33] Planck Collaboration: Planck 2013 results, XVI. Cosmological parameters. Astron. Astrophys. **571** (2014), A16, 66 pp.

[34] Rektorys, K.: Survey of applicable mathematics, vol. I and II. Kluwer Acad. Publ., Dordrecht, 1994.

[35] Riess, A. G. et al.: Observational evidence from supernovae for an accelerating universe and a cosmological constant. Astron. J. **116** (1998), 1009–1038.

[36] Riess, A. G. et al.: Milky Way Cepheid standards for measuring cosmic distances and application to Gaia DR2: Implications for the Hubble constant. Astrophys. J. **861** (2018), 126.

[37] Robertson, H. P.: On the foundation of relativistic cosmology. Proc. Nat. Acad. Sci. **15** (1929), 822–829.

[38] Tinsley, B.: Accelerating Universe revisited. Nature **273** (1978), 208–211.

[39] Tolman, R. C.: *Relativity, thermodynamics, and cosmology.* Clarendon Press, Oxford, 1934; Dover, New York, 1987.

[40] Wald, R. M.: *General relativity.* Univ. of Chicago Press, 1982.

[41] Walker, A. G.: On Milne's theory of world-structure. Proc. London Math. Soc. **42** (1936), 90–127.

[42] Weinberg, S.: *Gravitation and cosmology: Principles and applications of the general theory of relativity.* John Wiley, New York, London, 1972.

[43] Zeldovich, Y. B., Novikov, I. D.: *Relativistic astrophysics, vol. 2: The structure and evolution of the Universe.* Univ. of Chicago Press, 1983.

Conference *Cosmology on Small Scales 2018*
Michal Křížek and Yurii Dumin (Eds.)
Institute of Mathematics CAS, Prague

FOLLOWING THE EVOLUTION OF STARS, GLOBULAR CLUSTERS AND SPIRAL GALAXIES

Pavel Kroupa[1], Jana Žďárská[2]

[1] Rheinische Friedrich-Wilhelms-Universitt Bonn, D-53121 Bonn, Germany
[2]Cosmological Section of the Czech Astronomical Society, Prague, Czech Republic

The following interview has been translated into the Czech language and extended in the reference [2].

Jana Žďárská: You deal with many scientific questions, for example, dynamical properties of stellar systems (IMF, multiplicity), evolution of young multiple stellar systems in birth aggregates, star formation, dynamical evolution of open and globular clusters, spatial and kinematical distribution of stars, origin of field stars, structure and mass of the Galaxy, galactic dynamics, formation and evolution of dwarf satellite galaxies, dark matter content of galaxies. Could you kindly tell us which of these scientific topics is the most interesting for you?

Pavel Kroupa: The greatest question I am perhaps mostly interested in now is to understand how galaxies evolve. Given al the observations and calculations performed to date, dark matter does not exist. This can be written with the greatest of certainty. The vast number of galaxies are, like our Milky Way, star-forming disk galaxies. These need to constantly be supplied by gas, as otherwise they would stop forming stars. Where does this gas come from? And, why are all galaxies of a similar mass so incredibly similar to each other? These questions are touching on our deepest level of understanding of space-time-matter physics, and I have been developing some rather exciting ideas on how to possibly advance our understanding.

J.Ž.: Two years ago you participated at the conference Cosmology on Small Scales 2016: Local Hubble Expansion and Selected Controversies in Cosmology held in Prague. What is your opinion on this issue?

P.K.: I do not have an opinion concerning any of the questions, but the observational data show that there is something very wrong in our current understanding. The counts of galaxies with distance tell us that we are situated in a huge under density which has a radius of about 1 200 million light years. This is completely in contradiction with any cosmological model, and is also largely ignored by the community. But such a huge under density must have a big effect on local expansion and also implies that our understanding of cosmology is currently not correct.

J.Ž: There exist about 150 globular clusters in the Milky Way. They are very old systems and contain hundreds of thousands or up to millions of stars. Do you know how globular clusters looked like ten billion years ago?

P.K.: Most of the globular clusters would have been already about 2 billion years old. They would have been 10 to 100 times brighter than today, because they would have contained many more stars, and they would have been bluer, because the stars would have been about 10 Gyr younger than in today's globular clusters. Also, they would have had similar extensions as today. There would have also been many more such clusters. They may have been more distant, because as our Galaxy became more massive over time, it pulled in its globular clusters. In my research group we are calculating how such clusters evolve, and Dr. Long Wang from China for example, has just joined us as a new Alexander von Humboldt Fellow. He performed the first ever physically fully realistic calculation of a globular cluster with a million stars over a full Hubble time using supercomputers.

Globular cluster M13 in the constellation Hercules

J.Ž.: What is the main reason of their long-term stability?

P.K.: They are stable over many billions of years, because they were born with more than a million stars and the gravitational pull from all the stars on each other is strong. As the clusters age, they loose their stars, one by one, and so the globular clusters we see today must have been born a few to maybe 10 to 100 times more massive than their present day masses.

J.Ž.: How are the stars moving inside the globular cluster and what is the distribution of their velocities?

P.K.: Stars move on smooth but chaotic orbits within the globular clusters. A typical star spends most of its time in the outer regions of the cluster, perhaps 10 light years away from the centre. It then falls though the cluster racing quite rapidly though its inner region to move out again. A typical star moves with about 10 km/s, and the velocity may vary from a few times this amount to nearly zero km/s. At any time, taking all the stars together, the velocities range from near zero to about a few times 10 km/s. About 10 billion years ago all velocity would have been a few times larger, because the clusters were more massive then.

J.Ž.: Do you believe that there are medium-sized black holes inside globular clusters?

P.K.: A scientist should only work with hypotheses rather than have beliefs. So the hypothesis that many globular clusters have massive black holes in them has not been disproven conclusively, and some massive globular clusters could have, near their centres, black holes as massive as a hundred thousand Suns. But there is no theory available today which clearly predicts such black holes to be there. In my research group we are working on this problem, which is directly related to how super-massive black holes form in the centres of galaxies.

J.Ž.: Why do some spiral galaxies have such a perfectly symmetric shape? What is the main reason of this phenomenon?

P.K.: Spiral galaxies, when they are not disturbed, are nearly perfectly round disks. They are, basically, huge accretion disks with radii of up to about 100 thousand light years. Gas falls onto the galaxies at a well defined rate all the time (we neither yet know where this gas comes from nor do we understand why the infall is so well regulated) and, because gas is dissipative, it settles into a rotating disk. In the disk the gas density is higher, and in some places, where it is very high but still much lower than the best vacuum on Earth, the gas clouds fall together because of their self-gravity and stars form. Thus the galaxy evolves by having an increasing number of stars in it, and because it is rotating, it appears round when viewed from the top or bottom, while it is a thin disk when viewed from the side. Such a galaxy remains quite smooth with a huge stellar and gas disk. When it is slightly perturbed, for example, when another galaxy flies past it, even at a large distance, the gravitational pull of the other galaxy changes the forces within the galaxy, and this develops symmetrical spiral patterns. The galaxy reacts to this by becoming a spiral galaxy. This is similar to the Moon tides on the Earth which are also on both sides of the Earth. The spiral pattern in a galaxy is long-lived on human standards. It lasts maybe ten rotation periods, that is, maybe a billion years or more, because once the spiral pattern is there, it might be able to keep itself going through resonances. Additional instabilities may develop. For example, the inner region can form a bar

Some spiral galaxies show a perfectly point-symmetric shape.

in which stars and gas move on more radial orbits. But because disk galaxies are rotating and self-gravitating, they are generally (when not perturbed) symmetrical about their centre.

J.Ž.: What, in your opinion, is the composition of the halo of the Milky Way?

P.K.: The halo of the Milky Way is made up of ancient stars. These stars are as old as the globular clusters, and probably come from them, because the globular clusters loose their stars over time. Many of the halo stars were also formed in much less massive clusters at the same time as the massive present-day globular clusters, which have already lost all their stars long ago. The halo of our Galaxy is the oldest structure. It formed before the Galaxy existed as a spiral galaxy. At that time this birth of our porto-galaxy was extremely violent, with incredibly massive gas clouds falling together into the proto-galaxy and vigorously forming stars in huge star bursts which later became our globular clusters. The gas has today gone a long time ago, probably used up in making the halo stars and the globular clusters, possibly also being driven out of the young Galaxy or fallen into it to make the spiral Galaxy. The halo of the Galaxy is thus mostly without gas. The gas present in it comes from the stellar winds and by falling onto the Galaxy from the outside. That gas is falling onto the Galaxy and this sustains its on-going star formation. If no new gas were falling onto the Galaxy, then it would have consumed its gas many billions of years ago.

J.Ž.: Can you please explain us the notion of gravothermal catastrophe?

P.K.: The gravothermal catastrophe or instability is an interesting phenomenon in self-gravitating stellar-dynamical systems. In a star cluster with sufficiently many stars to live for a sufficiently long time, the following happens: the stars constantly meet each other and pull at each other gravitationally. Even though these pulls are very weak, they cause the stars to slightly change their orbits in the cluster. A star which, for example, is on a circular orbit, will with time change its velocity and begin to move on an eccentric non-circular orbit. As it then falls towards the inner region of the cluster, it becomes faster, passing more stars in a shorter time, and thus allowing it to change the speeds of the other stars. Over time this develops such that some stars end up falling towards the inner most regions, while other stars move out into the outer regions. This is a consequence of energy conservation. The stars falling towards the inner region have the smallest amount of energy, and the stars moving outwards compensate by having the largest energies. The stars form a thermodynamic system in which the fastest stars (the ones in the inner regions) shed some of their energy to the other, slower stars, which absorb this energy and move out of the inner regions. Since a star gets faster the deeper it falls into a gravitational potential, this process has no end. A group of stars can keep on falling inwards, generating ever more negative (binding) energy and a very dense central region in the cluster, while the rest of the cluster expands. This is called the gravothermal instability. It comes about because a self-gravitating system of stars has a negative heat capacity, that is, taking energy out of it makes it hotter. This can be visualized by looking at a satellite of the Earth. If we slow down the satellite, the satellite falls towards the Earth, becoming faster. The more we slow it down, the faster it falls. The same process happens in a cluster of stars. A star, which is slowed down by a gravitational encounter with another star, speeds up as it falls towards the cluster centre. By the principle of energy equipartition, this sped-up star can again share its kinetic energy with other stars, thus becoming even slower, and therefore, speeding up again as it falls towards the centre.

J.Ž.: You are dealing mainly with Newton's theory. Do you think that this theory of gravity sufficiently accurately describes the behavior of spherical clusters and that there is no need to assume the hypothetical nonbaryonic dark matter?

P.K.: When addressing this particular question one needs to understand that Newton derived his universal law of gravitation using data limited to the physical parameters of the Solar System, out to Uranus only. This was published around 1686 while Neptune was discovered about 100 years later. Einstein used this same law as a necessary and required classical limit of his re-interpretation of gravitation in 1916 as a geometrical space-time distortion, because observational data which constrain the law of gravitation were still limited to the Solar System. Galaxies, let alone the dynamics of the Universe, had not been understood in the days of Einstein. Astronomers and physicists extrapolate the empirical laws of gravitation by many orders of magnitude to the scales of star clusters and galaxies. Every

school child knows that such extrapolations almost certainly never work. But, on the scales of the normal globular star-clusters, which corresponds to an extrapolation by more than 4 orders of magnitude in spatial scale, the universal law of gravitation as derived by Newton and Einstein largely holds well. That is, the stars are moving, statistically, within the clusters, as is expected that they should be moving. There is no evidence for major departures. Very large departures are seen on the scales of galaxies, which constitute an extrapolation in spatial scale by roughly eight orders of magnitude. Here the observed speeds of stars are too fast, that is, the observed normal matter in stars and gas cannot provide enough gravitational pull (according to the huge extrapolation of Einstein's or Newton's theories) to hold onto the stars. The average physicist and astronomer interprets this to be due to unseen mass, the "dark matter", which provides extra gravitational pull so that the stars and gas move faster (see [1]). A big problem with this explanation is that this additional "dark" matter is not part of the standard model of particle physics. One needs to speculate that the dark matter is made up of particles which are very exotic and do not interact electromagnetically at all so that they remain entirely invisible. But another, and physically more convincing explanation, is that the "universal law of gravitation" as formulated by Newton and reformulated later by Einstein cannot be extrapolated to this extend.

J.Ž.: Einstein's theory of general relativity is examined on relatively small scales. Do you think it is applicable to galactic scales, or to the whole universe?

P.K.: The theory of General Relativity has been found to be in excellent agreement with all available observational data on small scales (i.e. Solar System and smaller) and in gravitational potentials which are deeper than that of the Solar System, that is in space-the curvatures which are larger than found in the Solar System.

J.Ž.: In 2011, the Nobel Prize for Physics was awarded for the discovery of an accelerated expansion of the universe. Did this discovery surprise you?

P.K.: I am in general against the existence of such prizes in the pure sciences, because they corrupt progress. What I mean here is that many institutions are eager to have staff which obtained such and other prizes, and scientists who obtain such prizes have a special status in these institutions and in society. It would be better if scientists achieve recognition, not through prizes, but by naming of some effect after them (e.g. Einstein's theory of general relativity, or Newton's theory of gravitation). My feeling is that too many scientists therefore try to do scientific work which enhances the chances of getting some major prize. But the true aim of a pure scientist should be only and only to try to understand how nature works, irrespective of achieving prizes. Thus, for example, the reason why the scientific community has gone essentially insane on dark matter and dark energy is probably due to this issue, namely that by working well within some conceived main stream which emerged over time, one may enhance ones own chances of getting rewarded. So one can observe how certain young researchers make steep careers by working closely within the main

stream ideas and harshly rejecting critical work. This is an in general interesting problem for philosophers to study — how did modern science fail in this way — but concerning the question at hand, the reward of the Nobel Prize in 2011 to Perlmutter, Schmidt and Riess for discovering the accelerated expansion of the Universe, I can state that this discovery is important. Why? Well, the main stream interprets the observations to mean that the Universe is expanding faster than thought, based on the above mentioned extrapolation by a huge order of magnitudes. The main stream scientist had become so overwhelmingly convinced that the extrapolation is correct and the only proper way of doing research, that it came as a surprise that the observations showed a failure of the theory. This failure can be fixed by inventing "dark energy". So the average main stream researcher was convinced that Pearlmutter, Schmidt and Riess made a major discovery of new physics (called dark energy). But this may be an entirely wrong physical explanation, because the extrapolation of physical laws, which were constrained only within the Solar System, as described above, is almost certainly wrong. In truth, it is more likely that the observations organized by Perlmutter, Schmidt and Riess are indicating that the extrapolation is wrong, and that the dynamics of the Universe cannot be described by the Einsteinian/Newtonian formulation as is used by the main stream scientist today. In my research group we are following this path of investigation, that is, we want to learn what these type of observations, as well as many other data, are telling us about the physical theory which governs the gravitational dynamic of galaxies and the Universe. We are explicitly following ideas on gravitation and dynamics which go beyond Newton and Einstein.

J.Ž.: Last year the Nobel Prize for Physics was awarded for the detection of gravitational waves. They were generated by two merging black holes of about thirty Sun's masses. Is the origin of such a system realistic at all?

P.K.: The formation of a binary system composed of two black holes with masses near 30 $M_\odot$ is reasonably well understood today. In my research group, Dr. Sambaran Banerjee, a brilliant researcher from India, is one of the world-wide leaders on this problem. He is calculating how globular star clusters, the stars within which have low-metallicities, evolve over many billions of years. Early-on and within the first 50 million years, the many massive stars die, many leaving black holes. These sink to the centre of the cluster through the above described process of energy equipartition which leads to the gravothermal instability. In the core of the globular cluster, the black holes form binary systems. These binary systems loose energy (thereby becoming more bound) by ejecting stars and other black holes out of the cluster and they can become very compact. Typically, they too are expelled from the cluster after some time, leaving a very tight black hole binary system. Such systems radiate gravitational waves until they merge. They merge in their cluster, or they may merge far away from it. Dr. Banerjee has made many calculations which show that what has been observed is very natural and quite common. In fact, in 2010 we were one of the first to make proper predictions for the type of gravitational events now

observed. It may also be possible to make such a binary black hole system only from two massive stars which were born in a binary system. The stars need to be very massive, maybe 100 times as massive as the Sun, and the evolution of this stellar binary needs to be extremely fine-tuned in order for the final black hole binary to survive the huge mass loss from the binary system as the two massive stars evolve and to in the end be so tight as to emit gravitational waves for it to merge to make observed signal. Both lines of research, via the dynamics in star clusters and via stellar evolution, are important and very interesting current hot research topics.

References

[1] Kroupa, P.: The dark matter crisis: Falsification of the current standard model od cosmology. Publ. Astron. Soc. Austral. 29 (2012), 395–433.

[2] Kroupa, P., Žďárská J.: Po stopách evoluce hvězd, kulových hvězdokup a spirálních galaxií. Čs. čas. fyz. 67 (2017), 362–369.

Conference *Cosmology on Small Scales 2018*
Michal Křížek and Yurii Dumin (Eds.)
Institute of Mathematics CAS, Prague

PRIMORDIAL COSMIC TURBULENCE: GENERATION AND IMPLICATIONS

Itzhak Goldman[1,2]

[1] Department of Physics, Afeka Engineering College
Tel Aviv, Israel
goldman@afeka.ac.il
[2] Department of Astrophysics, Tel Aviv University
Tel Aviv, Israel

Abstract: It is shown that density fluctuations that originate in the phase transition leading to inflation, can give rise to velocity turbulence. Turbulence can be generated, by this mechanism, in the radiation dominated era with the largest scales generated just before recombination. We find that the turbulence survives the viscous dissipation due to Thomson scattering. In the post-decoupling era the turbulent velocity becomes supersonic, and will generate shocks and thus could be an important contributor to early structure formation for baryon masses of $\sim 7 \times 10^8\ M_\odot$. This turbulence can amplify seed magnetic fields and also contribute to the cosmic gravitational waves background.

Keywords: cosmology, turbulence, structure formation, magnetic fields

PACS: 98.80.-k, 98.80.Bp, 47.27.Gs, 47.70.Mc, 47.75.+f

1. Introduction

Cosmic turbulence has been suggested some 70 years ago as a mechanism to generate the large scale structure [1], [2]. Many papers [3]–[15] followed various aspects in the coming decades. The idea was that turbulence generated prior to recombination would become supersonic past recombination, and the following shocks will be the seeds of structure formation.

The origin of the turbulence was not specified and usually was assumed to be part of the cosmological initial conditions. This was a main difficulty for the above approach. Another serious problem was that it predicted too much structure on the largest scales, comparable to the Horizon size.

Inflation (see review by [16]) suggested a solution for the first problem since the phase transition causing inflation would on one had produce the observable density fluctuations and on the other hand turbulence. However, inflation will erase any turbulence that was created, see e.g. [17].

In addition, the authors of [17] demonstrated that the density fluctuations that were created by the inflation, can generate longitudinal turbulence in the radiation dominated era. Recently [18], suggested that a QCD phase transition in the early radiation dominated era could induce a Kelvin Helmholtz instability (KHI) that will generate turbulence. These authors also noted that such turbulence will significantly contribute to the cosmological background of gravitational waves. It will also lead to amplification of cosmic seed magnetic fields.

In the present work we critically follow the mechanism suggested by [17]. The present day cosmological parameters are implemented, and the question of the turbulence decay prior to decoupling is *quantitatively examined*.

2. Coupled velocity and density fluctuations

We use the FRW cosmological metric with a flat spatial part, in accordance with the latest cosmological parameters that indicate $\Omega = 1$,

$$ds^2 = c^2dt^2 - a^2(t)\big((dx^1)^2 + (dx^2)^2 + (dx^3)^2\big). \tag{1}$$

We consider the coupled equations describing density and velocity fluctuations. Given the small value of the density fluctuations they are treated in the linear approximation. As for the velocity fluctuations, we include the nonlinear velocity interaction terms, thus allowing for turbulence. These terms are important, regardless of the amplitude of the velocity fluctuations, as long as the eddy interaction timescale is shorter than the timescales of viscous dissipation and of cosmic expansion. Qualitatively, density fluctuations can generate longitudinal velocity fluctuations which in turn, through the nonlinear terms, can generate longitudinal turbulence.

Following Weinberg [22], we consider small perturbations in the metric, the energy density, the pressure, and the four-velocity. The dissipative terms proportional to the heat conduction and to bulk viscosity are neglected and only terms proportional to the shear viscosity are retained. The unperturbed energy density and pressure are denoted by ρ and p, respectively. The corresponding perturbations are ρ_1 and p_1, respectively. The metric is given as

$$g_{\mu\nu} = g^0_{\mu\nu} + h_{\mu\nu}, \tag{2}$$

where $g^0_{\mu\nu}$ is the unperturbed metric of equation (1) and $h_{\mu\nu}$ is the metric perturbation. The perturbation in the velocity is denoted by u^i. It can be shown [21] that it is possible to apply coordinate transformations that do not change the unperturbed quantities but yield $h_{0\alpha} = 0$. In the perturbation equations we retain only linear terms except for the velocity equation in which we retain, as explained above, the nonlinear term in the velocities that can give rise to turbulence. The resulting equations are

$$\frac{\partial \rho_1}{\partial t} + 3\frac{\dot{a}}{a}(\rho_1 + p_1) = -(\rho + p)\left(\frac{\partial}{\partial t}\left(\frac{h^*}{2a^2}\right)\frac{\partial u^j}{\partial x^j}\right), \tag{3}$$

$$\frac{\partial^2 h^*}{\partial t^2} - 2\frac{\dot{a}}{a}\frac{\partial h^*}{\partial t} + 2\left(\left(\frac{\dot{a}}{a}\right)^2 - \frac{\ddot{a}}{a}\right)h^* = -8\pi\frac{G}{c^2}(\rho_1 + 3p_1)a^2, \tag{4}$$

$$\begin{aligned}\frac{\partial u^i}{\partial t} + u^j\frac{\partial u^i}{\partial x^j} =& -c^2 a^{-2}(\rho+p)^{-1}\frac{\partial p_1}{\partial x^i} - \frac{\partial \ln[(\rho+p)a^5]}{\partial t}u^i \\ &- 16\pi\frac{G}{c^4}\nu(\rho+p)u^i + \nu a^{-2}\left[\frac{\partial^2 u^i}{\partial x^j\partial x^j} + \frac{1}{3}\frac{\partial^2 u^j}{\partial x^i\partial x^j} + \frac{4}{3}\frac{\partial^2}{\partial t\partial x^i}\left(\frac{h^*}{2a^2}\right)\right],\end{aligned} \tag{5}$$

where $h^* = a^2 h^k_k$ and ν is the microscopic kinematic viscosity, which is due to Thomson scattering of photons on electrons.

The two last terms multiplying the viscosity in equation (5), can be shown to be of order $(l/l_H)^2$ compared to the first viscosity term. As will be shown in the following the above factor is much smaller than 1.

For adiabatic perturbations we have

$$p_1 = \left(\frac{v_s}{c}\right)^2 \rho_1 \tag{6}$$

with the sound velocity v_s given by

$$v_s^2 = \frac{c^2}{3}\frac{\rho_\gamma}{\rho_\gamma + \frac{3}{4}\rho_b}. \tag{7}$$

Applying the conservation equation for the unperturbed energy-momentum tensor, it is possible to eliminate h^* from the above equations leading to

$$\frac{\partial^2\delta}{\partial t^2} + 2\frac{\dot{a}}{a}\frac{\partial\delta}{\partial t} = 4\pi\frac{G}{c^2}(\rho+p)\left(1+3\frac{v_s^2}{c^2}\right)\delta - \left(\frac{\partial}{\partial t} + 2\frac{\dot{a}}{a}\right)\frac{\partial u^j}{\partial x^j}, \tag{8}$$

$$\begin{aligned}\frac{\partial u^i}{\partial t} + u^j\frac{\partial u^i}{\partial x^j} =& -a^{-2}v_s^2\frac{\partial\delta}{\partial x^i} - \frac{\partial\ln[(\rho+p)a^5]}{\partial t}u^i \\ &- 16\pi\frac{G}{c^4}\nu(\rho+p)u^i + \nu a^{-2}\left[\frac{\partial^2 u^i}{\partial x^j\partial x^j} - \frac{\partial^2 u^j}{\partial x^i\partial x^j} - \frac{4}{3}\frac{\partial^2\delta}{\partial t\partial x^i}\right].\end{aligned} \tag{9}$$

where

$$\delta = \frac{\rho_1}{\rho+p}.$$

In terms of the physical velocity $v^i = a(t)u^i$ the equations are

$$\frac{\partial^2\delta}{\partial t^2} + 2\frac{\dot{a}}{a}\frac{\partial\delta}{\partial t} = 4\pi\frac{G}{c^2}(\rho+p)\left(1+3\frac{v_s^2}{c^2}\right)\delta - a^{-1}\left(\frac{\partial}{\partial t} + \frac{\dot{a}}{a}\right)\frac{\partial v^j}{\partial x^j}, \tag{10}$$

$$\begin{aligned}\frac{\partial v^i}{\partial t} + a^{-1}v^j\frac{\partial v^i}{\partial x^j} =& -a^{-1}v_s^2\frac{\partial\delta}{\partial x^i} - \frac{\partial\ln[(\rho+p)a^4]}{\partial t}v^i \\ &- 16\pi\frac{G}{c^4}\nu(\rho+p)v^i + \nu a^{-2}\left[\frac{\partial^2 v^i}{\partial x^j\partial x^j} - \frac{\partial^2 v^j}{\partial x^i\partial x^j} - \frac{4}{3}a(t)\frac{\partial^2\delta}{\partial t\partial x^i}\right].\end{aligned} \tag{11}$$

In the general case, the nonlinear term in the velocities couples and mixes longitudinal and vortical velocities. However, in the present case, the density fluctuations excite purely longitudinal velocity fluctuations. For longitudinal velocity fluctuations, the nonlinear term in equation (11) that generates the turbulence can be shown to have a zero curl. Thus, also the generated turbulence will be purely longitudinal. Only if some seed of vortical velocity fluctuations is present, could it be amplified by the nonlinear interactions with the longitudinal turbulence, so that a component of vortical turbulence could be generated also. In what follows, the term turbulence will be meant to denote the above longitudinal turbulence.

3. Turbulence in the radiation dominated era

Our plan is to use the equations in the previous section to answer the following questions:

- Is there an epoch which allows the buildup of velocity turbulence from the density fluctuations?
- What are the scale and rms value of the turbulent velocity?
- Would the turbulence survive past recombination?
- What are the scale and value of the turbulent magnetic field generated by the velocity turbulence?

In order to obtain a detailed and quantitative answer, the equations should be solved numerically. However, one can gain quite a considerable insight from an analytic study based on the *timescales of the competing physical processes*.

The cosmic fluid considered for the turbulence consists of all particles that are coupled and in thermal equilibrium. The uncoupled components obey separate conservation equations, and although decoupled, their energy density contributes to the cosmological expansion. For redshifts $10^{10} \geq z \geq z_d$, the fluid consists of photons and baryonic matter while for $z < z_d$, it consists of baryonic matter only. Neutrinos that were part of the coupled fluid in the early universe, decoupled at $z \leq 10^{10}$.

We employ the 2018 Planck Collaboration cosmological parameters [19]:

$$\Omega = 1,\ \Omega_m = 0.316,\ \Omega_b = 0.049,\ \Omega_r = 9.3 \times 10^{-5},\ \Omega_\gamma = 5.44 \times 10^{-5}, \qquad (12)$$
$$N_\nu = 3,\ z_d = 1090,\ z_{eq} = 3411,\ H_0 = 67.4 \text{ km s}^{-1}\text{Mpc}^{-1}.$$

The timescale of the cosmological expansion is $H^{-1}(z)$, with $H(z)$ the Hubble parameter at redshift z.

$$H(z) = H_0 \left(\Omega_m (1+z)^3 + \Omega_r (1+z)^4\right)^{1/2}. \qquad (13)$$

From equation (11) it follows that the timescale for buildup of the turbulence on scale l , τ_b us given by

$$\tau_b^{-1} = \frac{1}{v}\frac{\partial v}{\partial t} \sim \frac{v_s^2 \delta}{l v(l)}, \qquad (14)$$

where l is the physical size of the scale generated and $v(l)$ is the amplitude of the generated velocity; both values are considered at the time of generation corresponding to the redshift z. The dimensionless density perturbation is also the value on the scale l.

Requiring that $\tau_b^{-1} > H$ yields

$$v(l) < v_s^2 \delta H^{-1}. \tag{15}$$

The timescale characterizing the non-linear eddy interaction scale l is $\tau_{eddy} = \frac{l}{v}$, where here too $v = v(l)$ the turbulent velocity on scale l. It is required that this timescale too is shorter than the Hubble time

$$\frac{v}{l} > H. \tag{16}$$

The relevant scales must be smaller than the horizon

$$l < l_H = cH^{-1}(z). \tag{17}$$

Assuming that the turbulence reached a quasi- steady state implies that the buildup and the eddy interaction timescales are comparable. This is to be expected, since the largest scales generated at a given time do not receive energy cascaded from even larger scales. As the buildup of the velocity continues, τ_b increases while the eddy timescale decreases. The buildup saturates when the two timescales become equal.

Therefore, one gets

$$v \sim v_s \delta^{1/2}. \tag{18}$$

Note that the kinetic energy density associated with the turbulence is roughly in equipartition with the thermal energy density associated with the density perturbations.

From equations (16) and (18)

$$\frac{l}{l_H} = \alpha \frac{v_s}{c} \delta^{1/2}, \quad 0 < \alpha < 1. \tag{19}$$

The sound velocity for $10^{10} \geq z \geq z_d$ is

$$v_s = c\sqrt{\frac{1}{3}\frac{\rho_\gamma}{\rho_\gamma + \rho_b}} = \frac{c}{\sqrt{3}}\left(1 + 1.68\frac{\rho_b}{\rho_r}\right)^{-1/2} = \frac{c}{\sqrt{3}}\left(1 + \frac{885}{1+z}\right)^{-1/2}. \tag{20}$$

The dominant viscosity for $z > z_d$, is the radiative viscosity resulting from scattering of photons by electrons, given by [21], [22]

$$\nu = \frac{4}{15} l_0 c \frac{\rho_\gamma}{\rho_b + \frac{4}{3}\rho_\gamma}, \tag{21}$$

where l_0 is the effective Thomson mean free path. It equals $l_T(1-(1+l/l_T)\mathrm{e}^{-l/l_T}$ where l_T is the mean free path for very large values of l. In the limit of very small l/l_T, the effective mean free path is reduced by a factor of $(l/l_T)^2$. This reflects the reduction of the probability for scattering when the size is smaller than the l_T,

$$l_T = (\sigma_T n_e)^{-1} \tag{22}$$

and $\sigma_T = 6.65 \times 10^{-25}$ cm^2 is the Thomson electron scattering crossection. The electron number density n_e is taken to be

$$n_e = \frac{\rho_b}{m_p}(X + 0.5Y) \sim 0.88\frac{\rho_b}{m_p},$$

where X and Y denote the cosmological abundances of hydrogen and helium, respectively, m_p is the mass of the proton, and ρ_b is the density of baryonic matter. It is assumed that matter is fully ionized which is valid for cosmic times earlier than the decoupling time t_d. From the above equations and using the cosmological parameters of equation (12), the Thomson length relative to the horizon scale can be written as

$$\frac{l_T}{l_H} = 502.3(1+z)^{-3}\sqrt{0.316(1+z)^3 + 0.0000926(1+z)^4}. \tag{23}$$

In Figure 1 are shown l_T/l_H and l/l_H for $\alpha = 0.01$, as functions of the redshift z. In Figure 2 are shown the dimensionless radiative viscosity $\frac{\nu}{l_h c}$ and the dimensionless turbulent viscosity $l_v/l_h c$ as functions of the redshift. For $z_d < z < 6500$ the turbulent viscosity becomes larger than the radiative viscosity. When the redshift is close to z_d it is larger by a factor of ~ 15.

For smaller scales (smaller eddies) the factor will increase as $\propto l^{-2/3}$ for a Kolmogorov turbulent power spectrum. Therefore we conclude that the largest turbulent scale is created just before recombination. Smaller scales can be created at larger redshifts. The turbulence largest scale is $\sim 3 \times 10^{-5} l_H$ at decoupling. Translated to present day scale it corresponds to $\sim 250\,$kpc, and to a baryon mass of $\sim 7 \times 10^8 M_\odot$. The turbulent velocity is $\sim 400\,\mathrm{km\,s^{-1}}$.

4. Discussion

We performed an analysis on the feasibility of primordial turbulence generation in the predecoupling era and of its survival past decoupling. We obtained that density fluctuation can generate turbulence. The (present epoch) scale of the turbulence is $\sim 250\,$kpc corresponding to a baryonic mass $\sim 7 \times 10^8 M_\odot$. The turbulent velocity is $\sim 400\,\mathrm{km\,s^{-1}}$. The turbulence scale is $\sim 3 \times 10^{-5}$ the horizon size, two orders of magnitude smaller than the BAO scale. On this scale the Thomson scattering viscosity is well bellow the turbulent viscosity so the turbulence could survive past recombination.

When this occurs, the turbulent velocity turns supersonic — generating shocks that enhance the density fluctuations on these scales and could serve as *very early* seeds for structure formation.

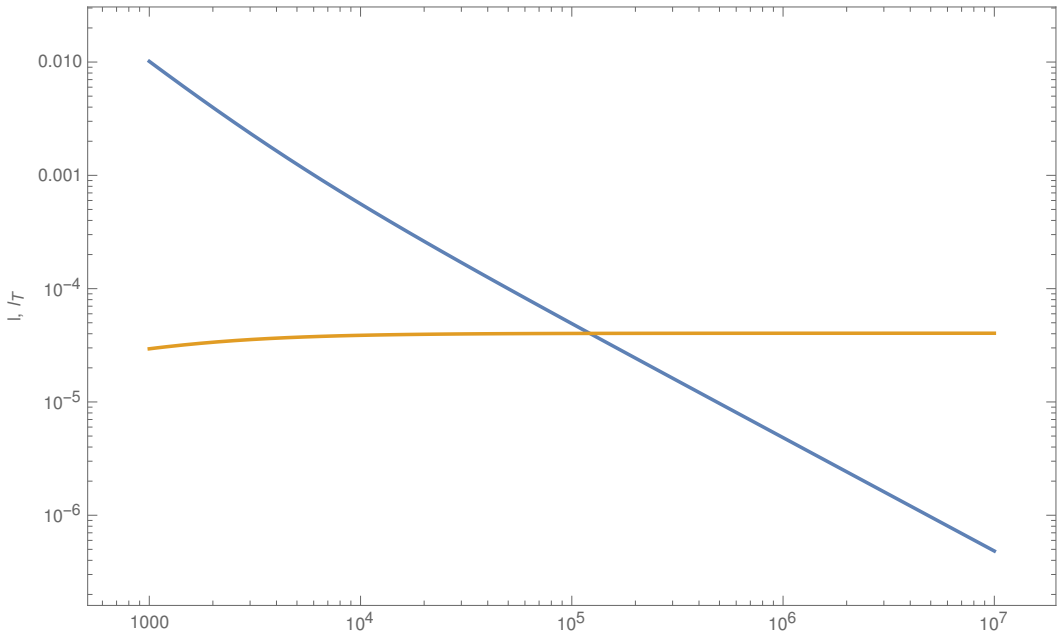

Figure 1: Thomson length (blue diagonal line) and the turbulent length (orange flat line) in units of l_H as functions of the redshift.

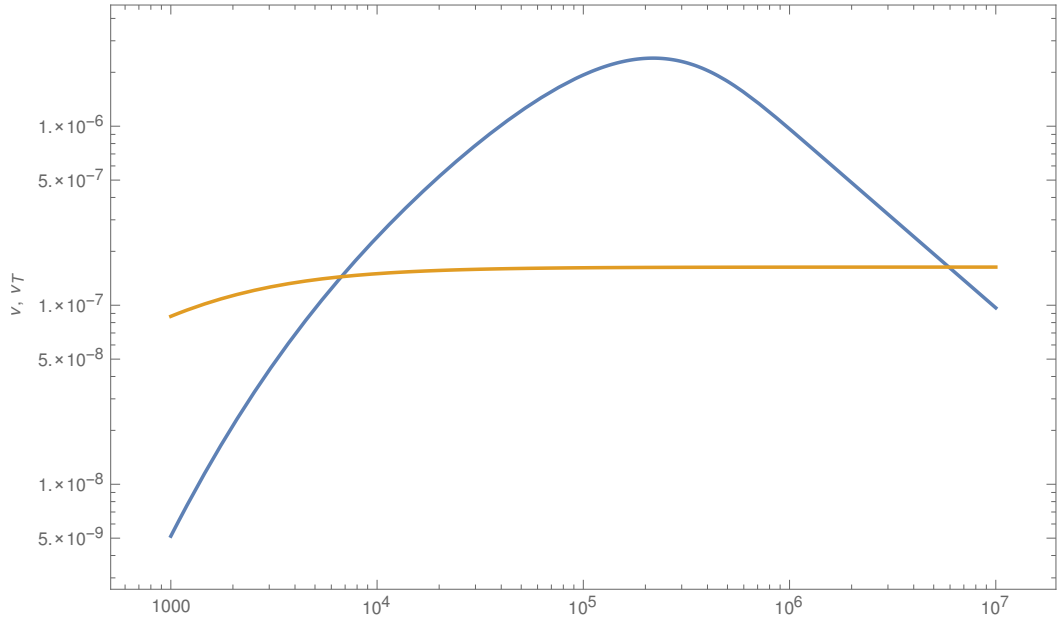

Figure 2: Thomson viscosity (blue concave line) and turbulent viscosity (orange flat line) normalized to $l_H c$, as function of redshift.

The source for the turbulence is non-solenoidal and therefore it appears that the generated turbulence will not include any vorticity. However, in a numerical simulation [20], the authors did obtain a turbulent vorticity even tough the source of the turbulence was not solenoidal. It should be also noted that any small vorticity present, will be amplified by the non-linear eddy interactions and will reach equilibrium with the non-vortical component.

The turbulence will amplify any seed magnetic field to equilibrium levels of $\sim 5\,\mathrm{mG}$. This magnetic field would be further amplified past recombination. The turbulence would also contribute to the gravitational waves cosmic background.

The present study was based on study of timescales and thus is largely qualitative, presenting orders of magnitude estimates. We intend to continue this research by constructing a semi-analytic model for turbulence that will allow to obtain a detailed power spectrum of the turbulence.

Acknowledgements

This work has been supported by the Afeka College Research Fund.

References

[1] von Weizsäcker, C. F. 1951. The Evolution of Galaxies and Stars. The Astrophysical Journal 114, 165.

[2] Gamow, G. 1952. The role of Turbulence in the Evolution of the Universe. Physical Review 86, 251–251.

[3] Ozernoi, L. M., Chernin, A. D. 1968. The Fragmentation of Matter in a Turbulent Metagalactic Medium. I. Soviet Astronomy 11, 907.

[4] Ozernoi, L. M., Chernin, A. D. 1969. The "Photon Eddy" Hypothesis and the Formation of Protogalaxies. II. Soviet Astronomy 12, 901.

[5] Ozernoj, L. M., Chibisov, G. V. 1971. Galactic parameters as a consequence of cosmological turbulence. Astrophysical Letters 7, 201–204.

[6] Tomita, K., Nariai, H., Satō, H., Matsuda, T., Takeda, H. 1970. On the Dissipation of Primordial Turbulence in the Expanding Universe. Progress of Theoretical Physics 43, 1511–1525.

[7] Ozernoi, L. M., Chibisov, G. V. 1971. Dynamical Parameters of Galaxies as a Consequence of Cosmological Turbulence. Soviet Astronomy 14, 615.

[8] Kurskov, A. A., Ozernoi, L. M. 1974. Evolution of cosmological turbulence. II. Dissipation of subsonic motions and alternative modes of post-recombination evolution. Soviet Astronomy 18, 300–306.

[9] Kurskov, A. A., Ozernoi, L. M. 1974. Evolution of cosmological turbulence. I. Intertial redistribution of vortex spectrum. Soviet Astronomy 18, 157.

[10] Tanabe, K., Nariai, H., Matsuda, T., Takeda, H. 1975. On the Acoustic Decay of Primordial Cosmic Turbulence. Progress of Theoretical Physics 54, 719–729.

[11] Kurskov, A. A., Ozernoi, L. M. 1975. Evolution of cosmological turbulence. III - Spectrum of density inhomogeneities produced by turbulence. Soviet Astronomy 18, 700–707.

[12] Kurskov, A. A., Ozernoi, L. M. 1976. Evolution of cosmological turbulence. IV - Gravitational growth of inhomogeneities with isolation of galaxies and galaxy systems. Soviet Astronomy 19, 569–576.

[13] Anile, A. M., Danese, L., de Zotti, G., Motta, S. 1976. Cosmological turbulence reexamined. The Astrophysical Journal 205, L59–L63.

[14] Nariai, H., Tanabe, K. 1978. On a Closure Hypothesis in the Theory of Cosmic Turbulence. Progress of Theoretical Physics 60, 1583–1585.

[15] Kurskov, A. A., Ozernoi, L. M. 1978. Angular fluctuations of RELICT radiation produced by cosmological turbulence. Astrophysics and Space Science 56, 67–80.

[16] Narlikar, J. V., Padmanabhan, T. 1991. Inflation for astronomers. Annual Review of Astronomy and Astrophysics 29, 325–362.

[17] Goldman, I., Canuto, V. M. 1993. Cosmic turbulence revisited. The Astrophysical Journal 409, 495–503.

[18] Mourão Roque, V. R. C., Lugones, G. 2018. Assessing the role of the Kelvin-Helmholtz instability at the QCD cosmological transition. Journal of Cosmology and Astro-Particle Physics 3, 051.

[19] Planck Collaboration (178 co-authors) 2018. Planck 2018 results. VI. Cosmological parameters. E-prints arXiv:1807.06209.

[20] Batchelor, G. K., Canuto, V. M., Chasnov, J. R. 1992. Homogeneous buoyancy-generated turbulence. Journal of Fluid Mechanics 235, 349–378.

[21] Weinberg, S. 1972. Gravitation and Cosmology: Principles and Applications of the General Theory of Relativity. J. Wiley & Sons, New York.

[22] Weinberg, S. 1971. Entropy Generation and the Survival of Protogalaxies in an Expanding Universe. The Astrophysical Journal 168, 175.

Conference *Cosmology on Small Scales 2018*
Michal Křížek and Yurii Dumin (Eds.)
Institute of Mathematics CAS, Prague

COSMOLOGICAL INFLATION FROM THE QUANTUM-MECHANICAL UNCERTAINTY RELATION

Yurii V. Dumin[1,2]

[1]P.K. Sternberg Astronomical Institute of M.V. Lomonosov Moscow State University
Universitetskii prosp., 13, 119234, Moscow, Russia
[2]Space Research Institute of the Russian Academy of Sciences
Profsoyuznaya str. 84/32, 117997, Moscow, Russia
dumin@yahoo.com, dumin@sai.msu.ru

Abstract: The inflationary paradigm is commonly accepted now for the description of the early Universe. However, the most of the corresponding models are derived from the Lagrangians of the scalar fields (inflatons) or the high-order-curvature corrections to the gravitational Lagrangian that are taken quite arbitrarily; so that only the final results are confronted with observations. In contract to this approach, we try to develop a less-model-dependent inflationary scenario, which is based on the quantum-mechanical uncertainty relation in the Mandelstam–Tamm form. As a result, we find that the law of expansion of the Universe should be "quasi-exponential" (proportional to the exponent of the square root of time). Moreover, it can be formally extended up to the present time, thereby giving a universal explanation of the "dark energy" (effective Lambda-term) throughout the entire cosmological evolution.

Keywords: inflationary models, Mandelstam–Tamm uncertainty relation, dark energy, Lambda-term

PACS: 98.80.Cq, 03.65.Ta, 95.36.+x

1. Introduction

The inflationary models, assuming a very sharp (typically, exponential) increase of the scale factor of the Universe $R(t)$, are widely used now to describe evolution of the early Universe (e.g., recent review [1]). Such sharp expansion is commonly assumed to be caused by the "vacuum-like" equation of state of the matter, $p = -\rho$ dominating at that time (which is formally equivalent to the Λ-term in Einstein equations). The main advantage of such scenarios is their ability to resolve the problem of homogeneity of the early Universe, the absence of singularity, etc.

In the very first models, suggested in the early 1980's, emergence of the effective Λ-term was attributed to the potential energy of a scalar field (such as a Higgs field

in the electroweak theory of elementary particles) in the overcooled metastabe state formed after its symmetry-breaking phase transition (e.g., review [2]). Unfortunately, these first models—which were closely related to the well-established elementary-particle physics—did not get support from a more careful analysis. As a result, a subsequent development of the inflationary theory, up to the present time, was based on the empirical inflaton potentials, which are postulated quite arbitrarily; so that only the final predictions are confronted with observations.

Yet another approach to the construction of inflationary models, which also started in the early 1980's [3], was based on taking into account the higher-order terms of curvature in the Lagrangian of gravitational field. Such higher-order terms naturally appeared as quantum corrections to the expectation values of energy–momentum tensor $\langle T_{\mu\nu} \rangle$ of matter fields in a curved space–time. However, the exact numerical coefficients remain unknown, because we do not have the definitive elementary-particle theory. In the recent time, the corresponding high-order contributions are usually parameterized by the empirical $f(R)$ function, which is estimated *a posteriori*, by confronting the theoretical predictions with observations.

A natural question arises: Is it possible to formulate the inflationary model from a more general point of view, irrelevant to the particular kind of the underlying field theory, which still remains unknown to us, or any *a priori* assumptions about the function $f(R)$?

From our point of view, a reasonable starting point to do so can be the quantum-mechanical uncertainty relation between the time and energy. As is known, the inequality

$$\Delta E \, \Delta t \geq \frac{1}{2} \, \hbar \, , \tag{1}$$

was proposed in the late 1920's in the context of quantum measurements. However, as was shown later by Mandelstam and Tamm [4], Eq. (1) can be treated also in a much wider context: namely, it gives an estimate of the variation of energy of the quantum system in the course of its long-term evolution. So, such inequalities are widely used now in the problems of quantum information processing, quantum communication, etc. [5][1]. Regarding the astrophysics, an important recent result is the employment of Mandelstam–Tamm relation to the description of neutrino oscillations [6]. The aim of our subsequent consideration will be to show that the same idea can be useful also in studying the cosmological evolution.

2. Theoretical model

To describe a space–time geometry, we shall use the standard Robertson–Walker metric:

$$ds^2 = c^2 dt^2 - R^2(t) \Big[\frac{dr^2}{1 - kr^2} + r^2 (d\theta^2 + \sin^2\theta \, d\varphi^2) \Big] \, , \tag{2}$$

[1]Let us mention that the numerical coefficient in the right-hand side of Eq. (1) may be somewhat different depending on the particular context (for example, $\pi/2$ instead of $1/2$). So, the subsequent formulas will be valid up to numerical factors on the order of unity.

where c is the speed of light, R is the scale factor of the Universe; r, θ, and φ are the dimensionless coordinates; $k = 1$, 0, and –1 for the closed, flat, and open three-dimensional space.

Then, the General Relativity equations are reduced to the Friedmann equation [7]:

$$H^2 \equiv \left(\frac{\dot{R}}{R}\right)^2 = \frac{8\pi G}{3c^2}\,\rho \,-\, kc^2\frac{1}{R^2} \,+\, \frac{c^2}{3}\,\Lambda\,, \tag{3}$$

where H is the Hubble parameter, G is the gravitational constant, ρ is the energy density of ordinary (luminous and dark) matter, and dot denotes differentiation with respect to time.

Since Λ-term is associated with the vacuum energy density $\rho_{\rm v}$ as

$$\Lambda = \frac{8\pi G\rho_{\rm v}}{c^4}\,, \tag{4}$$

it is reasonable to consider the vacuum energy in the Planck volume[2]

$$\Delta E = \rho_{\rm v} l_{\rm P}^3 \tag{5}$$

(where $l_{\rm P} = \sqrt{G\hbar/c^3}$ is the Planck length) and then to estimate the relevant energy density $\rho_{\rm v}$ from the Mandelstam–Tamm relation (1) with the equality sign, assuming that $\Delta t \equiv t$ is the total period of the cosmological evolution (i.e., the age of the Universe by the corresponding instant of time). Consequently, we get the effective Λ-term, varying with time:

$$\Lambda(t) = \frac{4\pi}{c\,l_{\rm P}}\,\frac{1}{t}\,. \tag{6}$$

At last, substitution of this expression into Eq. (3) results in the basic equation of our cosmological model:

$$H^2 \equiv \left(\frac{\dot{R}}{R}\right)^2 = \frac{8\pi G}{3c^2}\,\rho \,-\, kc^2\frac{1}{R^2} \,+\, \frac{4\pi}{3\tau}\,\frac{1}{t}\,, \tag{7}$$

where $\tau = l_{\rm P}/c = \sqrt{G\hbar/c^5}$ is the Planck time.

To study the main properties of this equation, let us consider the case when the Universe is spatially flat ($k = 0$), and the energy density of matter can be ignored ($\rho \approx 0$). Then, formula (7) is reduced to

$$H^2 \equiv \left(\frac{\dot{R}}{R}\right)^2 = \frac{4\pi}{3\tau}\,\frac{1}{t}\,. \tag{8}$$

This can be trivially integrated and gives

$$\tilde{R}(t) = \tilde{R}^* \exp\left[\sqrt{\frac{16\pi}{3}}\,\sqrt{\frac{t}{\tau}}\,\right], \tag{9}$$

[2]It is a quite subtle point why we estimate ΔE just in the Planck volume. This issue will be discussed in more detail in the very end of the paper.

where the integration constant was defined as $\tilde{R}^* = \tilde{R}(0)$, and we consider only the solution increasing with time. (The tilde is used here to identify the simplest approximation.)

By using the perturbation theory, it is not difficult to get a refined solution of Eq. (7), when small contribution from the ordinary matter is taken into account. In such a case, we need to employ the additional equation for temporal evolution of the energy density:

$$\dot{\rho} = -3\,\frac{\dot{R}}{R}\,(\rho + p)\,. \tag{10}$$

Taking the equation of state of the matter in the usual form, $p = w\rho$ (where $w = 0$ for dust and 1/3 for radiation), and assuming that there is only one matter component, Eq. (10) can be easily integrated:

$$\rho = \rho_0 \Big(\frac{R}{R_0}\Big)^{-3(1+w)}. \tag{11}$$

Next, we can seek a refined solution in the form

$$R(t) = \tilde{R}(t)\,[1 + \alpha(t)]\,, \tag{12}$$

assuming that $|\alpha(t)| \ll 1$ and $\rho/\rho_{\rm v} \ll 1$. Substituting formulas (11) and (12) into the basic equation (7) and collecting the lowest-order terms of the small quantities, we get a differential equation for $\alpha(t)$, whose solution results in

$$\alpha(\xi) = -\frac{G\,\rho_0\,\tau^2}{144\,\pi\,(1+w)^3\,c^2}\Big(\frac{R_0}{R^*}\Big)^{3(1+w)}(\xi^2 + 2\xi + 2)\,e^{-\xi}\,, \tag{13}$$

where

$$\xi = 4\sqrt{3\pi}\,(1+w)\sqrt{t/\tau}\,. \tag{14}$$

However, as evidently seen from the above formulas, this first-order correction is noticeable only at the Planckian scales. So, the simplest solution (9) is a very good approximation for the most part of the cosmological evolution.

3. Discussion and conclusions

(a) The main advantage of the proposed model is that it provides a unified explanation for the existence of the effective Λ-term (or the so-called "dark energy") throughout the entire evolution of the Universe. Really, according to the modern paradigm, the Λ-term is of crucial importance both in the very early Universe and nowadays [8]. However, its magnitudes in these periods are absolutely different. So, it is unclear if this is the same entity or just an accidental coincidence of two different physical phenomena? The proposed cosmological model, where the effective Λ-term decays inversely proportional to time (see Eq. (6)) naturally resolves this puzzle. The

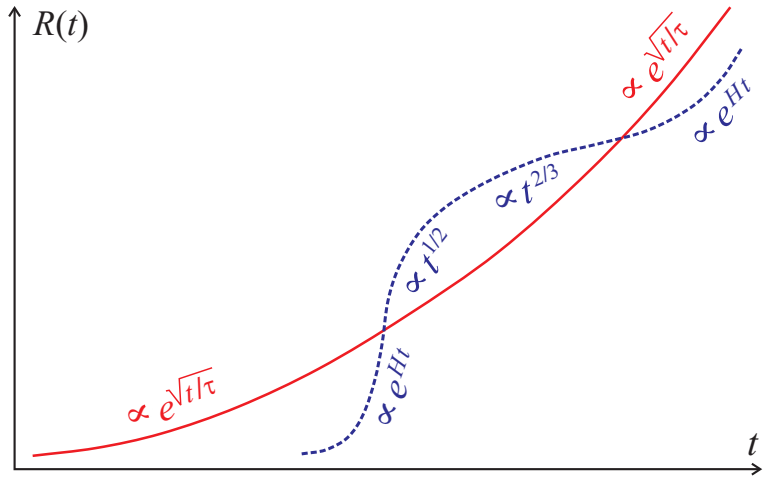

Figure 1: Temporal variation of the scale factor $R(t)$ in the "standard" cosmology (dashed blue curve) and in the proposed model, based on the quantum-mechanical uncertainty relation (solid red curve).

corresponding temporal evolution of the scale factor is given by the universal "quasi-exponential" law (9) instead of being composed of a few very different (exponential and power-like) dependencies in the standard cosmological model; see Fig. 1.

(b) Yet another cosmological puzzle, revealed in the last years, is a systematic discrepancy between the values of Hubble parameter at the present time H_0 derived by different methods [9], [10]: the values obtained from the "standard candles" in the local Universe ($\approx 73\ \mathrm{km\,s^{-1}\,Mpc^{-1}}$) turn out to be appreciably greater than the ones derived from the global-scale analysis of the cosmic microwave background spectrum ($\approx 67\ \mathrm{km\,s^{-1}\,Mpc^{-1}}$). The most popular way to remove this tension is to correct the expansion history of the Universe, which has been done in the recent works by the empirical modifications of the equation of state of the dark energy [11], [12], [13], [14]. From this point of view, the substantially modified law of cosmological expansion in our model (9) offers an additional opportunity to do so. Of course, a detailed quantitative analysis is still to be done to check this hypothesis.

(c) The most drastic deviation of our model from the predictions of "standard" cosmology is the age of the Universe. Really, according to Eq. (8),

$$T = \frac{4\pi}{3}\,\frac{1}{\tau H_0}\,\frac{1}{H_0}\,, \tag{15}$$

where T is the age of the Universe, and H_0 is the modern value of the Hubble parameter. Since in the standard cosmological model (whose values will be marked by asterisks) $T^* \approx 1/H_0$, the above relation predicts that $T \approx (T^*/\tau)\,T^*$. Substituting $T^* \approx 4{\cdot}10^{17}\,\mathrm{s}$ and $\tau = 5{\cdot}10^{-44}\,\mathrm{s}$, we see that this age increases by a huge quantity $(T^*/\tau) \approx 10^{61}$. In a sense, the Universe becomes "quasi-perpetual". However, such

anomalous lifetime should not be a fatal failure of the model: for example, the most of problematic issues in the large-structure formation are caused by the insufficient rather than excessive lifetimes. Of course, a lot of calculations should be performed to check carefully if the processes of nucleosynthesis, cosmological structure formation, etc. can reasonably proceed in the case of expansion by law (9).

(d) From the purely theoretical point of view, a crucial issue is why we took just the Planck volume to estimate ΔE in formula (5)? A more traditional way would be to calculate the fluctuation of energy within the volume of cosmological horizon, $\approx(ct)^3$. Then, the quantum uncertainty relation will lead to $\rho_{\rm v} \sim \hbar/(c^3t^4)$ and, according to Eq. (4), $\Lambda \sim G\hbar/(c^7t^4) = l_{\rm P}^2/(ct)^4$. This is evidently much less than our previous expression (6) and does not result in any inflation at all. However, taking the cosmological horizon to estimate the characteristic volume—although intuitively appealing—looks hardly compatible with a self-consistent treatment of the Mandelstam–Tamm relation (1): Really, the cosmological horizon expands with time and covers a continuously increasing amount of matter, while the uncertainty relation should be applied to a fixed quantum system. So, our choice of the Planck volume as the decisive parameter looks more reasonable.

In summary, let us emphasize that we do not have now a rigorous mathematical prescription how to apply the Mandelstam–Tamm uncertainty relation in the quantum field theory. However, the above analysis, based on the Planck volume as the fundamental parameter, seems to be quite self-consistent and, from our point of view, deserves a further investigation of the corresponding observable consequences.

Acknowledgements

I am grateful to J.-P. Uzan, C. Wetterich, C. Kiefer and members of his group, as well as to the referee for valuable discussions and critical comments. I am also grateful to the WE-Heraeus-Stiftung for the financial support.

References

[1] Ellis, J. and Wands, D.: Inflation. In: Particle Data Group: *Review of Particle Physics.* Chin. Phys. C **40** (2016), 100001, p. 367.

[2] Linde, A.D.: The inflationary Universe. Rep. Prog. Phys. **47** (1984), 925.

[3] Starobinsky, A.A.: A new type of isotropic cosmological models without singularity. Phys. Lett. **91B** (1980), 99.

[4] Mandelstam, L.I. and Tamm, I.E.: The energy–time uncertainty relation in nonrelativistic quantum mechanics. Izv. Akad. Nauk SSSR (Ser. Fiz.) **9** (1945), 122 (in Russian).

[5] Deffner, S. and Campbell, S.: Quantum speed limits: from Heisenberg's uncertainty principle to optimal quantum control. J. Phys. A: Math. Theor. **50** (2017), 453001.

[6] Blasone M., Jizba P., and Smaldone L.: Energy–time uncertainty principle and neutrino oscillations in quantum field theory. In: *Hundred Years of Gauge Theory, 678. WE-Heraeus-Seminar*, p. 53. Wilhelm und Else Heraeus-Stiftung, 2018.

[7] Olive, K.A. and Peacock, J.A.: Big-bang cosmology. In: Particle Data Group: *Review of Particle Physics.* Chin. Phys. C **40** (2016), 100001, p. 355.

[8] Mortonson, M.J., Weinberg, D.H., and White, M.: Dark energy. In: Particle Data Group: *Review of Particle Physics.* Chin. Phys. C **40** (2016), 100001, p. 402.

[9] Ryden, B.: A constant conflict. Nature Phys. **13** (2017), 314.

[10] Freedman, W.L.: Cosmology at a crossroads. Nature Astron. **1** (2017), 0121.

[11] Huang, Q.-G. and Wang, K.: How the dark energy can reconcile Planck with local determination of the Hubble constant. Eur. Phys. J. C **76** (2016), 506.

[12] Liu, Z.-E., Yu, H.-R., Zhang, T.-J., and Tang, Y.-K.: Direct reconstruction of dynamical dark energy from observational Hubble parameter data. Phys. Dark Univ. **14** (2016), 21.

[13] Di Valentino, E.: Crack in the cosmological paradigm. Nature Astron. **1** (2017), 569.

[14] Zhao, G.-B., Raveri, M., Pogosian, L., et al.: Dynamical dark energy in light of the latest observations. Nature Astron. **1** (2017), 627.

Conference *Cosmology on Small Scales 2018*
Michal Křížek and Yurii Dumin (Eds.)
Institute of Mathematics CAS, Prague

EFFECTS OF INTER-UNIVERSAL ENTANGLEMENT ON THE STATE OF THE EARLY UNIVERSE

Salvador J. Robles-Pérez[1,2]

[1] Estación Ecológica de Biocosmología Pedro de Alvarado, 14, 06411 Medellín, Spain
[2] Departamento de matemáticas, IES Miguel Delibes, Miguel Hernández 2, 28991 Torrejón de la Calzada, Spain
salvador.robles@educa.madrid.org

Abstract: The creation of universes in entangled pairs with opposite values of the momenta conjugated to the configuration variables of the minisuperspace would be favoured in quantum cosmology by the conservation of the total momentum, in a parallel way as particles are created in pairs with opposite momenta in a quantum field theory. Then, the matter fields that propagate in the two universes may become entangled too, the result of which is the appearance of a quasi thermal state that would produce a specific and distinguishable pattern in the spectrum of fluctuations of the matter fields in the early universe.

Keywords: multiverse, entanglement, early universe
PACS: 98.80.Bp, 03.65.Ud

1. Introduction

The non local effect of quantum entanglement is probably the distinguishing feature of quantum mechanics [20] and certainly the one that most departures from the intuition of classical mechanics. In classical mechanics the closer the systems are the stronger are the effects of any interaction between them. This is not necessarily the case in quantum mechanics. Quantum correlations may have a direct effect in the quantum state of one of the interacting systems irrespective of the distance it is separated from the other.

For instance, let us consider the typical example of quantum entanglement consisted in the generation of particles with spin $\frac{1}{2}$. Let $|+\rangle$ and $|-\rangle$ be the corresponding quantum states of the positive and negative spin, respectively, along the z axis. Because the conservation of the spin the particles must be created in pairs in a composite entangled state given by

$$|\psi\rangle = \frac{1}{\sqrt{2}}\left(|+\rangle_1|-\rangle_2 \pm |-\rangle_1|+\rangle_2\right). \tag{1}$$

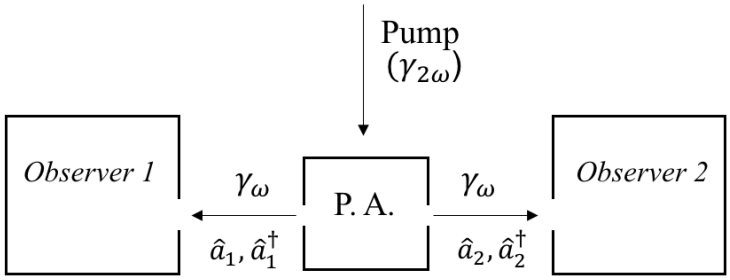

Figure 1: Parametric amplifier

If we perform a measurement over one of the particles in the $\{|+\rangle, |-\rangle\}$ basis, whatever is the result that we obtain, we know at the same time the state of the other particle, regardless of the distance between them. This is essentially the non-local effect of the quantum entanglement.

Another example of quantum entanglement, probably less known but more interesting for the kind of things we are dealing with in this presentation, is the parametric amplifier of quantum optics (see, for instance, Refs. [21], [24]). The parametric amplifier is a non-linear device that splits a photon of frequency 2ω supplied by a pump into two photons each with frequency ω (see, Fig. 1). The Hamiltonian of interaction between the classical pump and the two modes $\hat{a}_1$, $\hat{a}_1^\dagger$ and $\hat{a}_2$, $\hat{a}_2^\dagger$ is [24]

$$H_I = i\hbar\chi \left(\hat{a}_1^\dagger \hat{a}_2^\dagger e^{-2i\omega t} - \hat{a}_1 \hat{a}_2 e^{2i\omega t}\right), \tag{2}$$

where χ is a constant related to the properties of the non-linear optical medium. The solutions to the Heisenberg equations in the interaction picture are

$$\hat{a}_1(t) = \hat{a}_1 \cosh\chi t + \hat{a}_2^\dagger \sinh\chi t \tag{3}$$
$$\hat{a}_2(t) = \hat{a}_2 \cosh\chi t + \hat{a}_1^\dagger \sinh\chi t, \tag{4}$$

and the initial two mode vacuum state of the field evolves into a linear combination of perfectly correlated number states [24]

$$|\Psi(t)\rangle = e^{\chi t\left(\hat{a}_1^\dagger \hat{a}_2^\dagger - \hat{a}_1 \hat{a}_2\right)} |0_1\rangle|0_2\rangle = \frac{1}{\cosh\chi t} \sum_n (\tanh\chi t)^n \, |n_1\rangle|n_2\rangle. \tag{5}$$

Now, the state of the mode 1(2) is given by the reduced density matrix $\rho_{1(2)}$ that is obtained by tracing out from the composite state (5) the degrees of freedom of the partner mode 2(1). It turns out to be [24]

$$\rho_{1(2)} = \mathrm{Tr}_{2(1)}\{|\Psi(t)\rangle\langle\Psi(t)|\} = \frac{1}{Z} \sum_n e^{-\frac{1}{T}(n+\frac{1}{2})} |n_{1(2)}\rangle\langle n_{1(2)}|, \tag{6}$$

where, $Z = \frac{1}{2}\sinh 2\chi t$, and $T^{-1}(t) = \ln\tanh^{-2}\chi t$. The state (6) is a quasi thermal state with a very specific pattern of its thermodynamical properties. If no entanglement were present the modes would remain in their vacuum states and the observers

in the boxes (see, Fig. 1) would measure no particle at all in their photo-counters. The interesting thing is then that even if the observers are isolated from each other, if they recognise the pattern (6) in the state of their corresponding modes they can infer with high probability of success the existence of the partner modes and the entanglement between them.

The example of the parametric amplifier is specially interesting in the case of cosmology because an expanding spacetime may act as a classical pump for the modes of the matter fields that propagate along distant regions of the spacetime. Then, analogously to the case of the parametric amplifier, the state of the field in two classically disconnected regions may become represented by a quasi thermal state with a specific pattern of the thermodynamical properties that would depend on the rate of entanglement between the modes of the field in the two regions. The remarkable thing is then that even if the observer may have no direct access to a very distant region of the spacetime, if he or she finds the field in a quasi thermal state with a pattern that follows that of the entangled case, then, he/she can infer the existence of the distant region and the entanglement of the corresponding modes just from the state of the field in the own region!

This is then directly applicable to the case of a multiverse, where by the multiverse one can generally understand the consideration of many different copies of a single piece of the spacetime, each one with their own properties. In principle, all the copies except the one in which we live should be disregarded as being physically inaccessible, and thus, redundant or irrelevant. The most one could do is to take statistical measures of all the universes of the multiverse and formulate statistical predictions. This is what we can call the statistical paradigm of the multiverse (see, for instance, Refs. [3], [4], [23]) and it was the only paradigm of the multiverse taken into account until recent years. However, the power of predictability of the statistical paradigm of the multiverse is quite reduced because in order to make predictions one must assume a principle of mediocrity [23], i.e. one has to assume that our universe is one of the most probable universes of the multiverse. Making some sense because it generalises the Copernican principle, the assumption of the mediocrity principle is controversial because we could well be a very strange phenomena of nature violating no physical law. Furthermore, because the statistical paradigm of the multiverse predicts everything within it, then, no concrete prediction can be done actually for a single universe (i.e. everything is possible in the multiverse).

A different paradigm of the multiverse has been developed in the last decade. It can be called the interacting multiverse [1], [7], [8], [18], [19], where entanglement and other non local interactions can be present between the states of the corresponding spacetimes and the fields of the classically disconnected regions. The universes still conserve their classical meaning because they are isolated from a classical point of view, i.e. light signals cannot joint events of two different universes and therefore no causal relation may exist between their events, at least in the classical (local) sense. Even though, quantum correlations and other non local interactions may still be present, which would be ultimately rooted in the choice of boundary conditions at

the origin of the universe or in a residual effect from the underlying theory, whether this can be one of the string theories or the quantum theory of gravity. These non local effects are expected to be large in the earliest stage of the universe and they could propagate and imprint some effect in the observable properties of a large universe like ours. In that case, the multiverse, and the underlying theories, would become a testable proposal as any other theory in cosmology.

2. Quantum cosmology and the state of the early universe

Quantum cosmology is the application of the quantum theory to the universe as a whole, i.e. to the spacetime and the matter fields that propagate therein, all together. In the canonical picture the state of the universe is given by a wave function that depends on all the degrees of freedom of the spacetime and the matter fields, and it is the solution of the quantum version of the Hamiltonian constraint,

$$\hat{H}\Psi = 0, \tag{7}$$

where $\hat{H}$ is the operator form of the Hamiltonian that corresponds to the Einstein-Hilbert action of the spacetime plus the action of the matter fields. However, for most of the evolution of the universe this can be described by a slow changing background spacetime and small energy fields propagating therein. In that case, the Hamiltonian constraint (7) can be re-written as

$$\left(\hat{H}_{bg} + \hat{H}_m\right)\Psi = 0, \tag{8}$$

where $\hat{H}_{bg}$ is the Hamiltonian of the background spacetime and $\hat{H}_m$ is the Hamiltonian of the rapid varying fields. The wave function $\Psi(q_{bg}, q_m)$ depends then on the degrees of freedom of the background spacetime, q_{bg}, and on the matter degrees of freedom, q_m. In the semiclassical regime, it can be written as a WKB solution of the form [6]

$$\Psi = C(q_{bg})e^{\pm i/\hbar S_0(q_{bg})}\chi(q_{bg}, q_m), \tag{9}$$

where $C(q_{bg})$ is a slow varying function of the background variables, $S_0(q_{bg})$ is the action of the background spacetime, and $\chi(q_{bg}, q_m)$ is the wave function of the fields that propagate in the background spacetime. Inserting the semiclassical wave function (9) into the Hamiltonian constraint (8) and solving it order by order in $\hbar$, one obtains: at zero order in $\hbar$, the classical equations of the background spacetime; and at first order in $\hbar$, the quantum equations of the fields that propagate therein. Thus, the wave function Ψ and the Hamiltonian constraint (8) contain all the physical information about the classical spacetime and the quantum matter fields. In that sense, the wave function Ψ represents the state of the whole universe.

For the shake of concreteness, let us consider a homogeneous and isotropic spacetime with a scalar field φ propagating therein. Then, the wave function Ψ can be written as the product of two wave functions [9], [16]

$$\Psi(a, \varphi_0; x_n) = \Psi_0(a, \varphi_0)\chi(a, \varphi_0; x_n). \tag{10}$$

The wave function Ψ_0 represents the state of the homogeneous and isotropic background, which is entirely described by the dynamics of the scale factor a and the homogeneous mode of the scalar field φ_0. It is the solution of the Wheeler-DeWitt equation [6], [9]

$$\hat{H}_{bg}\Psi_0 = \frac{1}{2a}\left(\hbar^2\frac{\partial^2}{\partial a^2} + \frac{\hbar^2}{a}\frac{\partial}{\partial a} - \frac{\hbar^2}{a^2}\frac{\partial^2}{\partial\varphi_0^2} + 2a^4V(\varphi_0) - a^2\right)\Psi_0 = 0, \tag{11}$$

where $V(\varphi_0)$ is the potential of the scalar field. All the information about the inhomogeneous modes of the scalar field, x_n, which are here treated as small perturbations, is encoded in the wave function $\chi(a, \varphi_0; x_n)$ in (10). It is now easy to show that the wave function Ψ contains: at zero order in $\hbar$, the dynamical information of the classical background spacetime and, at first order in $\hbar$, the quantum information of the inhomogeneous modes x_n that propagate along the background spacetime. Let us first notice that in the semiclassical regime Ψ_0 can be written as

$$\Psi_0(a, \varphi_0) = C(a, \varphi_0)e^{-\frac{i}{\hbar}S(a,\varphi_0)}. \tag{12}$$

In that case, the Wheeler-DeWitt equation (11) is satisfied at zero order in $\hbar$ if $S(a, \varphi_0)$ is a function that satisfies the Hamilton-Jacobi equation [9]

$$-\left(\frac{\partial S}{\partial a}\right)^2 + \frac{1}{a^2}\left(\frac{\partial S}{\partial\varphi_0}\right)^2 + 2a^4V(\varphi_0) - a^2 = 0. \tag{13}$$

Now, choosing as the time variable the WKB parameter t defined by [9]

$$\frac{\partial}{\partial t} \equiv \frac{1}{a}\frac{\partial S}{\partial a}\frac{\partial}{\partial a} - \frac{1}{a^3}\frac{\partial S}{\partial\varphi_0}\frac{\partial}{\partial\varphi_0}, \tag{14}$$

the equation (13) transforms into

$$\dot{a}^2 + 1 - a^2\left(\dot{\varphi}_0^2 + 2V(\varphi_0)\right) = 0, \tag{15}$$

which is the Friedmann equation of the background spacetime. The dynamical equations of $a(t)$ and $\varphi_0(t)$, given by

$$\dot{a} = \frac{1}{a}\left(\frac{\partial S}{\partial a}\right) \ , \ \dot{\varphi_0} = -\frac{1}{a^3}\left(\frac{\partial S}{\partial\varphi_0}\right), \tag{16}$$

can be directly obtained from (14). Thus, the classical equations of the background spacetime are obtained from the $\hbar^0$ order of the Wheeler-DeWitt equation. On the other hand, inserting the wave function (10) into the total Hamiltonian, $H = H_{bg} + H_m$, where H_m is the Hamiltonian of the perturbation modes, it is obtained at first order in $\hbar$ of H_{bg},

$$i\hbar\left(\frac{1}{a}\frac{\partial S}{\partial a}\frac{\partial}{\partial a} - \frac{1}{a^3}\frac{\partial S}{\partial\varphi_0}\frac{\partial}{\partial\varphi_0}\right)\chi = H_m\chi, \tag{17}$$

which is exactly the Schrödinger equation for the inhomogeneous modes of the scalar field if one considers the time variable defined in (14) for the background spacetime. Therefore, the wave function Ψ in (10) and the Hamiltonian constraint (8) contain all the physical information of a single universe. They contain the classical information of the background spacetime and the quantum information of the matter fields that propagate therein.

3. Creation of universes in entangled pairs

The symmetries of the Friedmann equation with respect to a time reversal change, $t \to -t$, in the definition of the time variable (14), and the associated symmetry in the Wheeler-DeWitt equation (11) with respect to a change in the sign of the function $S(a, \varphi_0)$, makes that the general solution of the Wheeler-DeWitt equation should be written as

$$\Psi = \sum \Psi^- + \Psi^+ = \sum C_- e^{-\frac{i}{\hbar}S_0}\chi_- + C_+ e^{\frac{i}{\hbar}S_0}\chi_+, \tag{18}$$

where, $C_+^* = C_-$ and $\chi_+^* = \chi_-$, and the sum extends to all the possible configurations for the semiclassical regime of the spacetime and the matter fields. In (18), Ψ^- and Ψ^+ are customary referred as the expanding and the contracting branches of the universe, respectively, because in terms of the time parameter t defined in (14) and taking into account the correspondence principle between the classical momentum p_a^c and the quantum momentum, $\hat{p}_a = -i\hbar\partial_a$, in the classical limit ($\hbar \to 0$),

$$-a\dot{a} \equiv p_a^c \sim \langle \Psi^\pm | \hat{p}_a | \Psi^\pm \rangle = \pm \frac{\partial S}{\partial a}, \tag{19}$$

one obtains

$$\dot{a} = \mp \frac{1}{a}\frac{\partial S}{\partial a}, \tag{20}$$

where the $-$ sign corresponds to Ψ^+ and the $+$ sign to Ψ^-. Then, one should assume that Ψ^+ represents a contracting universe and Ψ^- an expanding one. However, the problem with that interpretation is that the time variable t defined in (14) cannot be the physical time in the two branches if for the physical time we mean the time variable measured by a real clock, which is eventually made of matter. The real time is that given in the Schrödinger equation, which is the one that ultimately drives the behaviour of matter. If one follows the development of the preceding section with the time defined in (14) for the wave functions Ψ^+ and Ψ^- one obtains

$$\mp i\hbar \left(\frac{1}{a}\frac{\partial S}{\partial a}\frac{\partial}{\partial a} - \frac{1}{a^3}\frac{\partial S}{\partial \varphi_0}\frac{\partial}{\partial \varphi_0} \right) \chi_\pm = H_m \chi_\pm, \tag{21}$$

where the $-$ sign corresponds again to Ψ^+ and the $+$ sign to Ψ^-. Equation (21) is the Schrödinger equation for the fields χ_+ and χ_- only if one assumes that the physical time variables in each branch, t_+ and t_-, respectively, are defined as

$$t_- = t = -t_+. \tag{22}$$

In that case, each addend in (18) corresponds, in terms of their physical time variables, to a pair of both expanding universes that however carry associated opposite values of their momenta conjugated to the configuration variables a and φ_0. Then, the creation of universes in pairs, as represented in (18), entails the conservation of the total momentum conjugated to the configuration variables. Let us notice that the conservation of the energy is guaranteed even in the case of the creation of a single universe because the gravitational energy is negative and equals the energy of the scalar field. However, the conservation of the generalised momentum $\vec{p} = (p_a, p_{\varphi_0})$ is only preserved by the creation of universes in pairs with opposite values of their momenta, as it happens in the creation of particles in a quantum field theory.

In fact, the resemblance between the expansion (18) and the one made in a quantum field theory is not a coincidence [18], [22]. The configuration space $\{a, \varphi_0\}$, called the minisuperspace in quantum cosmology [6], can be formally taken as a spacetime with a given geometry and metric element given by [16], [18]

$$d\sigma^2 = -ada^2 + a^3 d\varphi_0^2. \tag{23}$$

From (23) one can see that the scale factor formally plays the role of the time like variable of the minisuperspace and the matter field(s) the role of the space like variable(s). The wave function $\Psi(a, \varphi_0)$ can then be seen as a scalar field that *propagates* in the minisuperspace spanned by the variables $\{a, \varphi_0\}$, and thus, a formal parallelism can also be taken between the creation of universes in the minisuperspace and the creation of particles in a curved spacetime. The expansion (18) can be generalised to

$$\Psi(a, \varphi_0) = \int d\mu \left(\Psi_\mu^+ \chi_\mu^+ b_\mu + \Psi_\mu^- \chi_\mu^- b_\mu^* \right), \tag{24}$$

where μ is the set of parameters that determine the transformation (24), $d\mu$ is the corresponding measure, and b_μ and b_μ^* are two constants that can be promoted to the creation and the annihilation operators of universes [16], [14]. The universes must then be created in pairs with opposite values of their momenta to satisfy the conservation of the total momentum in the minisuperspace, as particles are created in pairs with opposite values of their momenta in a quantum field theory.

For instance, let us consider the inflationary stage of the universe, where the potential of the scalar field can be considered approximately constant, $H_0^2 = 2V(\varphi_0)$, with $V(\varphi_0)$ evaluated at some initial value $\varphi_0(t_0)$. Then, the wave function $\Psi(a, \varphi_0)$ can be expanded in Fourier modes as

$$\Psi(a, \varphi_0) = \int \frac{dK}{\sqrt{2\pi}} \left(e^{(i/\hbar)\, K\varphi_0}\, \Psi_K^+\, \chi_K^+\, \hat{b}_K + e^{-(i/\hbar)K\varphi_0}\, \Psi_K^-\, \chi_K^-\, \hat{b}_K^\dagger \right), \tag{25}$$

where the amplitudes $\Psi_K^\pm(a)$ satisfy

$$\hbar^2 \frac{\partial^2 \Psi^\pm{}_K}{\partial a^2} + \frac{\hbar^2}{a} \frac{\partial \Psi^\pm{}_K}{\partial a} + \Omega_K^2(a) \Psi_K^\pm(a) = 0, \tag{26}$$

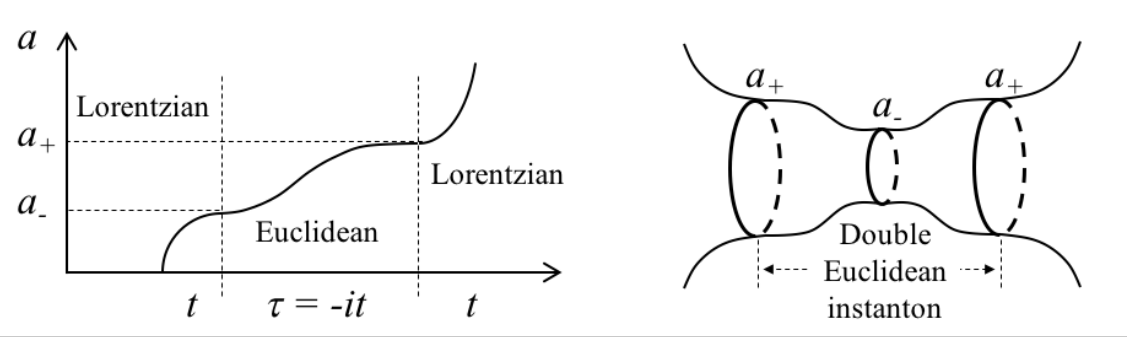

Figure 2: Left: there is a Euclidean region between two Lorentzian regions, where classical solutions of the Friedmann equation can be given. Right: a double Euclidean instanton can be formed by matching two single Euclidean instantons, the analytic continuation of which gives rise to two expanding universes.

with,

$$\Omega_K = \sqrt{H^2 a^4 - a^2 + \frac{K^2}{a^2}} = \frac{H_0}{a}\sqrt{(a^2 - a_+^2)(a^2 - a_-^2)(a^2 + a_0^2)}, \tag{27}$$

being a_+ and a_- the zeros of the function Ω_K, with $a_+ > a_-$ (see, Refs. [2], [19], for the details). The WKB solutions of (26) are given by

$$\Psi_K^{\pm} \propto \frac{1}{\sqrt{a\Omega_K(a)}} e^{\pm \frac{i}{\hbar}\int \Omega_K(a) da}, \tag{28}$$

and the Friedmann equation of each single universes in terms of their physical times reads [see (20) with (22)]

$$\frac{\partial a}{\partial t_\pm} = \frac{1}{a}\Omega_K = \frac{H_0}{a^2}\sqrt{(a^2 - a_+^2)(a^2 - a_-^2)(a^2 + a_0^2)}. \tag{29}$$

There are two Lorentzian regions for which real solutions of the Friedmann equation (29) can be obtained, located at $a < a_-$ and at $a > a_+$, respectively. In between there is a Euclidean region that acts as a quantum barrier, where the Euclidean solutions of the Wick rotated version of (29) are called instantons (see Fig. 2, left). Now, a double Euclidean instanton can be formed by glueing two single instantons at the contact hypersurface a_-, whose analytic continuation gives rise to a pair of universes in the Lorentzian region with opposite values of their momentum (see, Fig. 2, right).

Quantum gravitational corrections should be taken into account as well and they might slightly modify the picture. However, for the case for which the glueing hypersurface a_- is larger enough than the Planck length, the quantum gravitational corrections would be subdominant and the global picture presented here should not be significantly modified.

As explained in Sec. II, the wave functions χ_K^+ and χ_K^- would follow the Schrödinger equation (21) with the time variables t_+ and t_- of their respective spacetime backgrounds, i.e.

$$i\hbar\frac{\partial\chi_\pm}{\partial t_\pm} = H_m\chi_\pm. \tag{30}$$

If we restrict to small linear perturbations the inhomogeneous modes behave like small harmonic oscillators [5], [9]. The quantisation of the modes follows as usual, by expanding them in terms of the solutions of the harmonic oscillator and promoting the constants of the expansion into quantum operators,

$$\hat{x}_n(t) = v_n^*(t)\,\hat{a}_n + v_n(t)\,\hat{b}_{-n}^\dagger, \tag{31}$$

where $v_n(t)$ and $v_n^*(t)$ are two independent solutions of the wave equation

$$\ddot{x}_n + \frac{3\dot{a}}{a}\dot{x}_n + \omega_n^2 x_n = 0, \tag{32}$$

with a time dependent frequency given by [9], [16]

$$\omega_n^2(t) = \frac{n^2-1}{a^2(t)} - m^2, \tag{33}$$

where m is the mass of the scalar field.

In the case that the matter content of the entangled universes is represented by a complex scalar field, then, because $\chi_\pm^* = \chi_\mp$, one would expect that the matter is created in the observer's universes and the antimatter in the partner universe [15], being both separated by the Euclidean barrier of the double instanton. In that case, $\hat{a}_n^\dagger$ and $\hat{a}_n$ in (31) would be the creation and annihilation operators of matter in one of the universes and, $\hat{b}_n^\dagger$ and $\hat{b}_n$, the creation and annihilation operators of matter in the other one[1]. In the case of a real field the particles are their own antiparticles and thus, $\hat{a}_n = \hat{b}_n$, with $[\hat{a}_n, \hat{b}_n^\dagger] = 1$. However, we here retain the different names $\hat{a}_n$ and $\hat{b}_n$ because in the case of the entangled universes they are still commuting operators as they act on the modes of the field in each single universe of the entangled pair.

We need to impose now the boundary conditions that fix the state of the field. For this, we impose that the perturbation modes are in the composite vacuum state of the invariant representation of the harmonic oscillator (32). The invariant representation has the great advantage that once the field is in a number state of the invariant representation it remains in the same state along the entire evolution of the field [13]. In particular, once the field is in the vacuum sate of the invariant representation it remains in the same vacuum state along the entire evolution of the field. It is therefore a stable representation of the vacuum state along the entire evolution of

[1] Antimatter from the point of view of an observer in the former universe.

the universes. For the modes $\hat{a}_n$ and $\hat{b}_{-n}$, the invariant representation can be written as [10], [18]

$$\hat{a}_n = \sqrt{\frac{1}{2}}\left(\frac{1}{\sigma}x_n + i(\sigma p_{x_n} - M\dot{\sigma}x_n)\right), \tag{34}$$

$$\hat{b}^{\dagger}_{-n} = \sqrt{\frac{1}{2}}\left(\frac{1}{\sigma}x_n - i(\sigma p_{x_n} - M\dot{\sigma}x_n)\right), \tag{35}$$

where $\sigma = \sigma(t)$ is an auxiliary function that satisfies a non-linear equation (see, Ref. [13] and references therein for the details). In that case, the perturbation modes stay in the vacuum state of the invariant representation

$$|0\rangle = |0_a 0_b\rangle = |0_a\rangle_I |0_b\rangle_{II}, \tag{36}$$

along the entire evolution of the universes. However, an internal observer would measure the particles of the scalar field in the instantaneous diagonal representation of the harmonic oscillator (32), which is the representation that defines the instantaneous vacuum state at the moment of the observation. Then, if $\hat{c}_n$, $\hat{c}^{\dagger}_n$ and $\hat{d}_n$, $\hat{d}^{\dagger}_n$ are the diagonal representations for the universes I and II, respectively, they are related to the invariant representation by the Bogolyubov transformation [16]

$$a_n = \mu(t)\, c_n - \nu^*(t)\, d^{\dagger}_{-n}, \tag{37}$$

$$b_{-n} = \mu(t)\, d_{-n} - \nu^*(t)\, c^{\dagger}_n, \tag{38}$$

where, $\mu \equiv \mu_n$ and $\nu \equiv \nu_n$, are given by [16]

$$\mu(t) = \frac{1}{2}\left(\sigma\sqrt{a^3\omega_n} + \frac{1}{\sigma\sqrt{a^3\omega_n}} - i\dot{\sigma}\sqrt{\frac{a^3}{\omega_n}}\right), \tag{39}$$

$$\nu(t) = \frac{1}{2}\left(\sigma\sqrt{a^3\omega_n} - \frac{1}{\sigma\sqrt{a^3\omega_n}} - i\dot{\sigma}\sqrt{\frac{a^3}{\omega_n}}\right), \tag{40}$$

with, $|\mu|^2 - |\nu|^2 = 1$ for all time.

The state of the perturbation modes in one single universe of the entangled pair would then be given by the state that is obtained by tracing out from the composite state

$$\rho = |0_a 0_b\rangle\langle 0_a 0_b|, \tag{41}$$

the degrees of freedom of the partner universe. Analogously to the example of the parametric amplifier presented in Sec. I, one can show [16] that the state of the field in each single universe of the entangled pair is

$$\rho_c = Tr_d \rho = \prod_n \frac{1}{Z_n} \sum_N e^{-1/T_n (N+1/2)} |N_{c,n}\rangle\langle N_{c,n}|, \tag{42}$$

where, $Z_n^{-1} = 2\sinh 1/2T_n$, and, $T_n^{-1}(t) = \ln\left(1 + |\nu_n(t)|^{-2}\right)$. The inhomogeneous modes of the scalar field in each single universe of the entangled pair turn out to be in a quasi-thermal state whose thermal properties depend on the rate of entanglement between the universes. The consideration of the state (42) as the initial state of the perturbation modes in the computation of the power spectrum of the CMB would imply a different and possibly distinguishable pattern for the final outcome, so it can provide us with a way of testing definitely the proposal of the creation of universes in entangled pairs.

4. Observable effects of entangled fields in the early universe

The observable consequences of the creation of universes in pairs and the subsequent entanglement of the modes of the scalar field that propagate in their spacetimes can be split in two main effects. The first one is the effective modification of the Friedmann equation and, thus, the modification of the evolution of the universes that departures from the inflationary expansion in the very early stage. This pre-inflationary phase of the universe would have observable effects in the power spectrum of the CMB. In particular, it would produce a suppression of the power spectrum of the lowest modes which is currently under investigation [12], [16]. The other effect is the distribution of the modes of the matter field in a quasi thermal state that should produce specific and distinguishable features in the astronomical data.

In general, quantum corrections and other non local interactions [1], [17] are expected to be present in the early stage of the universe and they may induce some observable effect in the properties of a universe like ours. A first attempt has been made in Ref. [12], where it is obtained a suppression of the power spectrum for the lowest modes that could be compatible with the observed data. However, the appearance of an extra peak in that region of the power spectrum invalidates the simplifications made in the model considered there. However, the importance of Ref. [12] is that it establishes the possibility of observing the effects of quantum cosmology, including those derived from the entanglement between newborn universes, in the properties of the CMB.

Another phenomena that would produce a modification of the Friedmann equation is the backreaction of the matter fields. In our case, the backreaction of the entangled fields is given by the energy of the modes [16]

$$\varepsilon = \frac{H_0^4}{8}\left\{1 - \frac{m^2}{H_0^2}\log\frac{b^2}{H_0^2} + \left(1 + \frac{m^2}{H^2}\right)\left(1 - \frac{b^2}{H_0^2}\right)\right\}, \tag{43}$$

where b is the SUSY breaking scale of the subjacent landscape [7], [8], and it is expected to produce the same observable imprints to those found in Refs. [7], [8], [11]. In that case, it would also produce a suppression of the lowest modes of the CMB. However, a suppression of the lowest modes of the CMB can be produced by many different effects and, furthermore, the dispersion of the observational data in that

region of the spectrum is so high that it is not very useful to discriminate between different models. We need therefore a more specific effect to test the creation of the universes in entangled pairs.

The distinguishing feature of our model is that it predicts that the initial state of the field is in the quasi thermal state (42) that is derived from the entanglement with the modes of a partner universe. It produces a pattern for the spectrum of fluctuations, given in terms of the spectrum of fluctuations of the invariant vacuum (disentangled state) by [16]

$$\frac{\delta\phi^{th}_{\mathbf{n}}}{\delta\phi^{I}_{\mathbf{n}}} = \sqrt{\frac{1}{2}\left(1+\frac{x^2}{(1+x^2)(1+m^2/(H^2x^2))}\right)}, \tag{44}$$

that cannot be reproduced by any other known effect, mainly because: i) it is not derived from a vacuum state, and ii) it is not either derived from an exact thermal state because the modes are not thermalised yet in (42), i.e. the temperature T_n is not the same for all modes. In fact, one can see that the large modes ($x \gg 1$) are not affected by the entanglement between the universes. However, the departure from the vacuum state is significant for the horizon modes, $x \sim 1$. That should produce distinguishable effects in the properties of the CMB and, thus, it might help us to discriminate if our universe was created as a twin universe in an entangled pair.

5. Conclusions

There is a formal parallelism between the quantum description of the wave function that represents homogeneous and isotropic universes in quantum cosmology and the quantum description of a scalar field that propagates in a curved spacetime. It allows us to consider the creation of the universes in entangled pairs as the most favoured way in which the universes can be created because, only in that case, the total momentum associated to the configuration variables of the minisuperspace is conserved. The two created universes are usually referred as the expanding branch and the contracting branch. However, they are both expanding universes in terms of the time variable that appears in the Schrödinger equation of each single universe, which is eventually the physical time variable given by actual clocks.

The matter fields that propagate in the pair of newborn universes become entangled too, an entanglement that is decreasing along the evolution of the universes but can still be enough to modify the state of the field in the early universe. In particular, the matter field of each single universe becomes represented by a quasi thermal state that would induce a specific and distinguishable pattern in the observable properties of an evolved universe like ours. That makes the interacting multiverse be a testable proposal as any other in cosmology.

References

[1] A. Alonso-Serrano, C. Bastos, O. Bertolami, and S. Robles-Pérez. Interacting universes and the cosmological constant. *Phys. Lett. B*, 719:200, 2013.

[2] I. Garay, S. Robles-Pérez. Effects of a scalar field on the thermodynamics of interuniversal entanglement. *Int. J. Mod. Phys. D*, 23:1450043, 2014.

[3] J. Garriga, A. Vilenkin. On likely values of the cosmological constant. *Phys. Rev. D*, 61:083502, 2000.

[4] J. Garriga, A. Vilenkin. Many worlds in one. *Phys. Rev. D*, 64:043511, 2001.

[5] J. J. Halliwell, S. W. Hawking. Origin of structure in the universe. *Phys. Rev. D*, 31:1777–1791, 1985.

[6] J. B. Hartle. The quantum mechanics of cosmology. In S. Coleman, J. B. Hartle, T. Piran, and S. Weinberg, editors, *Quantum Cosmology and Baby Universes*, volume 7. World Scientific, London, UK, 1990, 65–156.

[7] R. Holman, L. Mersini-Houghton, T. Takahashi. Cosmological avatars of the landscape. I. Bracketing the supersymmetry breaking scale. *Phys. Rev. D*, 77:063510, 2008.

[8] R. Holman, L. Mersini-Houghton, T. Takahashi. Cosmological avatars of the landscape. II. CMB and LSS signatures. *Phys. Rev. D*, 77:063511, 2008.

[9] C. Kiefer. Continuous measurement of mini-superspace variables by higher multipoles. *Class. Quant. Grav.*, 4:1369–1382, 1987.

[10] H. R. Lewis, W. B. Riesenfeld. An exact quantum theory of the time-dependent harmonic oscillator and of a charged particle in a time-dependent electromagnetic field. *J. Math. Phys.*, 10:1458–1473, 1969.

[11] L. Mersini-Houghton. Predictions of the quantum landscape multiverse. *Class. Quant. Grav.*, 34: 047001, 2017.

[12] J. Morais, M. Bouhmadi-Lopez, M. Kramer, S. Robles-Pérez. Pre-inflation from the multiverse: can it solve the quadrupole problem in the cosmic microwave background? *Eur. Phys. J. C.*, 78:240, 2018.

[13] S. Robles-Pérez. Invariant vacuum. *Phys. Lett. B*, 774:608–615, 2017.

[14] S. Robles-Pérez. Quantum cosmology of a conformal multiverse. *Phys. Rev. D*, 96:063511, 2017.

[15] S. J. Robles-Pérez. Restoration of matter-antimatter symmetry in the multiverse. Preprint arXiv: 1706.06304[gr-qc], 2017.

[16] S. J. Robles-Pérez. Cosmological perturbations in the entangled inflationary universe. *Phys. Rev. D*, 19:066018, 2018.

[17] S. Robles-Pérez, A. Alonso-Serrano, C. Bastos, O. Bertolami. Vacuum decay in an interacting multiverse. *Phys. Lett. B*, 759:328, 2016.

[18] S. Robles-Pérez, P. F. González-Díaz. Quantum state of the multiverse. *Phys. Rev. D*, 81:083529, 2010.

[19] S. Robles-Pérez, P. F. González-Díaz. Quantum entanglement in the multiverse. *JETP*, 118(1):34, 2014.

[20] E. Schrödinger. Discussion of probability relations between separated systems. *Mathematical proceedings of the Cambridge Philosophical Society*, 31:555–563, 1936.

[21] M. O. Scully, M. S. Zubairy. *Quantum optics*. Cambridge University Press, Cambridge, UK, 1997.

[22] A. Strominger. Baby universes. In S. Coleman, J. B. Hartle, T. Piran, and S. Weinberg, editors, *Quantum Cosmology and Baby Universes*, volume 7. World Scientific, London, UK, 1990, 270–346.

[23] A. Vilenkin. Predictions from quantum cosmology. *Phys. Rev. Lett.*, 74:846–849, 1995.

[24] D. F. Walls, G. J. Milburn. *Quantum optics*. Springer-Verlag, Berlin, Germany, 2008.

Conference *Cosmology on Small Scales 2018*
Michal Křížek and Yurii Dumin (Eds.)
Institute of Mathematics CAS, Prague

ANALYTICAL INVESTIGATION OF BLACK HOLE SHADOW

Oleg Tsupko

Space Research Institute of Russian Academy of Sciences
Profsoyuznaya 84/32, Moscow 117997, Russia
tsupko@iki.rssi.ru

Abstract: In this work we present and discuss selected recent results of analytical investigations of black hole shadow. We begin by discussing the definition of the concept of the black hole shadow and its connection with critical value of the photon impact parameter. Then we describe recently developed fully analytical approach for extraction of spin of black hole from the deformation of its shadow. Finally, we present analytical investigation of plasma influence on the shadow size. In particular, we discuss the influence of plasma on the Schwarzschild black hole shadow.

Keywords: black hole shadow, spin, plasma

PACS: 04.20.-q, 98.62.Sb, 98.62.Mw, 98.35.Jk

1. Introduction

It is believed that there are supermassive black holes at the centers of most galaxies. According to theory, an observer should see such a black hole (BH) as a dark spot, known as the 'shadow' of the BH, in the sky against a backdrop of light sources. Investigations of the shadow are now becoming very popular due to the appearance of projects to observe the shadow of a supermassive BH in the center of our Galaxy and at the center of M87. These projects, which are going to use (sub)millimeter VLBI observations with radio telescopes distributed over the Earth, are called as the Event Horizon Telescope (http://eventhorizontelescope.org) and the BlackHoleCam (http://blackholecam.org). Observing the shadow of BH is both very challenging and very difficult task due to many effects involved. Note, for example, that the angular size of the shadow is very small: for the BH at the center of our Galaxy, it is about $53\,\mu$as. Numerous analytical investigations and numerical simulations of the shadow are presented in literature, see selected classical works and interesting recent papers in [1], [3], [10], [11], [12], [13], [14], [15], [18], [19], [20], [21], [25], [26], [29], [32], [33], [34], [38], [39], [41], [44], [46], [49], see also references below.

In this work we present and discuss selected recent results of analytical investigations of BH shadow, see [7], [32], [33], [34], [46], [47] for more details. We begin by discussing the definition of the concept of the BH shadow and its connection with critical

values of the photon impact parameter. Then we describe recently developed fully analytical approach for extraction of spin of BH from the deformation of its shadow. Finally, we present analytical investigation of plasma influence on the shadow size. In particular, we discuss the influence of plasma on the Schwarzschild black hole shadow.

2. Definition of black hole shadow and its relation with critical photon impact parameter

The shadow is defined as the region of the observer's sky that is left dark if there are light sources distributed everywhere but not between the observer and the BH (see, for example, [20] and [32]). For constructing the shadow we have to consider all past-oriented light rays that issue from a chosen observer position. Each of these light rays corresponds to a point on the observer's sky. We assign darkness to a point if the corresponding light ray goes to the horizon of the BH, and brightness otherwise. Observer will see a dark spot (which we call as shadow) in the angular direction where the BH is located. The boundary of the shadow is determined by the initial directions of light rays that asymptotically spiral towards the unstable circular orbit at outermost photon sphere (for spherically symmetric BH), see Fig. 1 for more details. In case of Kerr BH the formation of shadow is more complicated (we have the photon region filled by spherical orbits instead of the photon sphere) but is based on the same ideas, see papers [7], [20], [21], [33].

There is nothing surprising in that we expect to see a dark spot in the sky, where we suggest a BH is situated. The important thing is that due to very strong bending of light rays coming to us, we see something very different from 'real view' of the BH. In case of spherically symmetric BH the difference is only in angular size (see Fig. 2), but in Kerr metric (which is axially symmetric) picture becomes non-symmetrical: shadow of Kerr BH is oblate and deformed.

In the case of the Schwarzschild metric, the angular radius of the shadow is

$$\sin^2 \alpha_{\rm sh} = \frac{27m^2\left(1-\frac{2m}{r_O}\right)}{r_O^2}\,, \tag{1}$$

where r_O is radial coordinate of observer. This formula was derived by Synge [41]. (Synge calculated what he called the 'escape cone' of light which is just the complement in the sky of what we now call the shadow.)

Formula (1) can be written as

$$\sin^2 \alpha_{\rm sh} = \frac{\left(1-\frac{2m}{r_O}\right) b_{\rm cr}^2}{r_O^2}\,, \tag{2}$$

where $b_{\rm cr}$ is the critical value of the impact parameter corresponding to photons on unstable circular orbits filling the photon sphere. In the Schwarzschild metric the radius of the photon sphere equals $3m$ and

$$b_{\rm cr} = 3\sqrt{3}m\,. \tag{3}$$

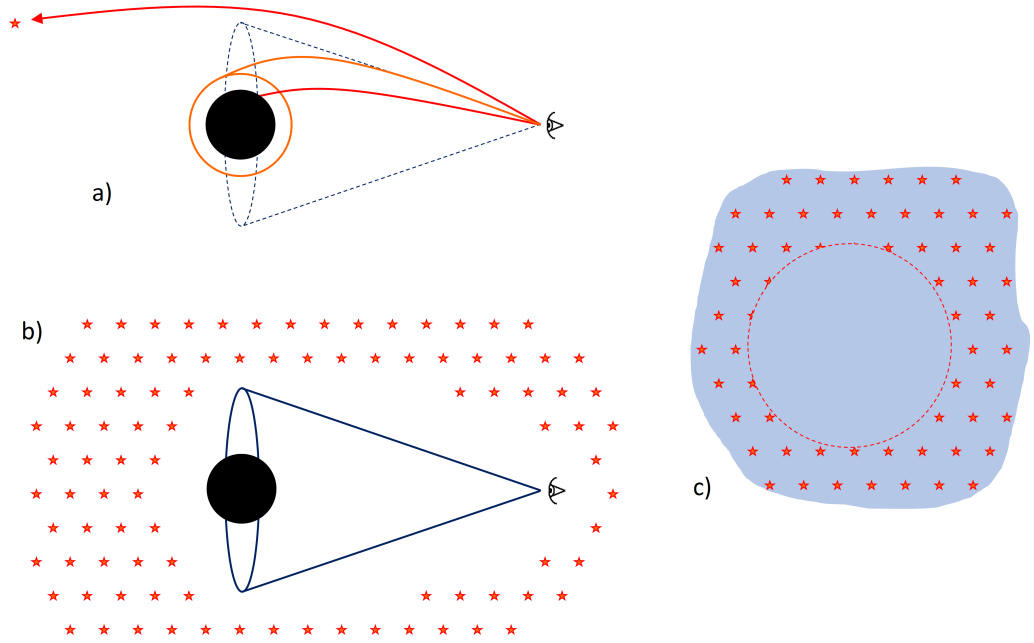

Figure 1: Formation of the BH shadow. The shadow is the black disk an observer sees in the sky if a BH is viewed against a backdrop of light sources that are distributed around the BH but not between the observer and the BH. a) Let us consider light rays sent from an observer with chosen position into the past. These light rays can be divided into two classes: Light rays of the first class go to infinity after being deflected by the BH. Light rays of the second class go towards the horizon of the BH. The boundary between these two classes is determined by the rays that asymptotically spiral towards the outermost photon sphere. b) Now let us consider that there are many light sources distributed everywhere around the BH. We assume that there are no light sources between the observer and the BH (speaking more strictly, there are no light sources in the region filled by the above mentioned light rays of the second class). Initial directions of rays of the second class correspond to darkness on the observers sky. Therefore, the cone which was fulfilled by the rays of the second class will be dark for the observer. c) The observer will see the dark disc in the sky against the backdrop of light sources. Note that the picture is schematic and is drawn as if the stars represent a continuous distribution of light, therefore stars positions are not affected by lensing on this picture.

For large distances the angular size is simplified to

$$\sin^2 \alpha_{\rm sh} \approx \frac{b_{\rm cr}^2}{r_O^2}, \quad r_O \gg m\,. \tag{4}$$

This approach reduces the determination of the angular size of the shadow at large distances to the calculation of the critical value of the impact parameter: knowing the

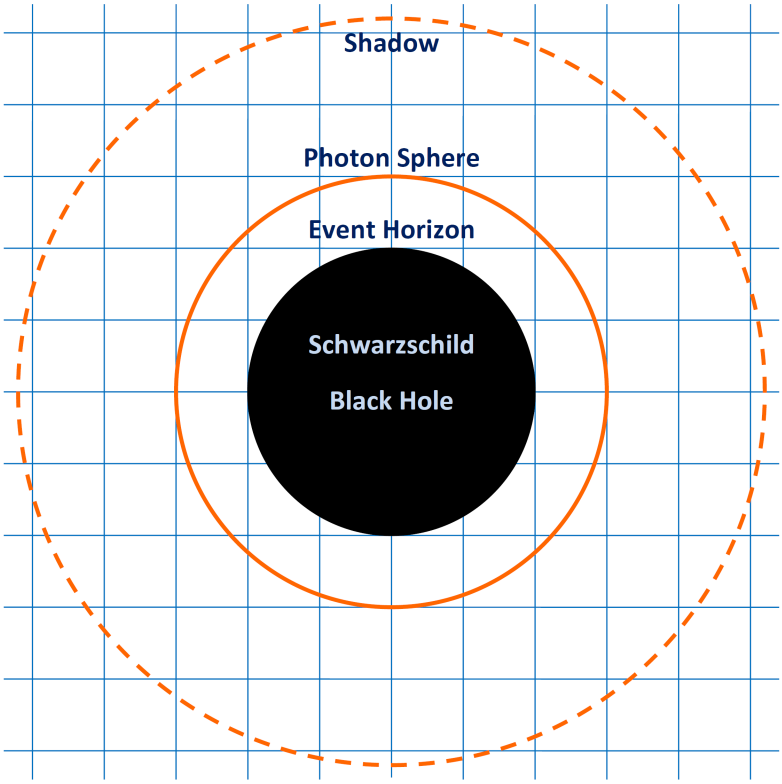

Figure 2: Comparison of shadow size for distant observer with Euclidian sizes of the event horizon and the photon sphere (for Schwarzschild BH).

critical impact parameter, one gets an approximate value for $\alpha_{\rm sh}$ after dividing by r_O. Bardeen [3] has used this approach for the more general case of the Kerr metric. In this case the shadow is not circular; its shape for distant observers is determined by *two* impact parameters. Accordingly, the angular radii of the shadow can be approximately found by dividing these impact parameters by the (Boyer-Lindquist) radius coordinate r_O of the observer.

Described relation between angular size of the shadow and critical impact parameter works only for metrics that are asymptotically flat at infinity. Angular size of the shadow cannot be presented in such way, for example, in the Kottler spacetime which is not asymptotically flat.

Size and shape of the shadow are determined by parameters of the BH and the observer position. By measuring the parameters of the shadow, we can get information about both the BH and its environment through which the light propagates. In next sections, we will describe the analytical ways to do this.

3. Analytical extraction of black hole spin from deformation of black hole shadow

For a non-rotating BH, the shadow is a circular disk at the sky. For the Schwarzschild BH the angular diameter of the shadow was calculated in paper of Synge [41], as a function of the mass of the BH, and of the coordinate distance from the BH. The shape of the shadow of a Kerr BH, for an observer far from BH, was calculated by Bardeen [3]. In the papers of Grenzebach, Perlick and Lämmerzahl [20], [21], the size and the shape of the shadow were calculated for the whole class of Plebański-Demiański spacetimes (which includes the Kerr BH as a special case). Calculations are performed for the observer at an arbitrary position outside of the horizon of the BH.

Deformation of the shadow of Kerr BH depends on BH spin and viewing angle of the observer. The more the spin of the BH, the stronger the deformation of its shadow: for given viewing angle, the deformation will be strongest for extreme Kerr BH. For given spin, the deformation will be strongest for the equatorial observer among all possible angles of view, while for the polar observer the deformation is absent and shadow is circular.

Usually it is supposed that for extraction of spin we need to construct or model the entire curve of the shadow. Extraction of the spin from the shadow deformation was discussed in number of papers [2], [23], [28], [42], [43], [48]. These works imply the use of numerical calculations at some stage, and to the best of our knowledge, there was no fully analytical treatment of the problem. Here we present results of our analytical investigations on the basis of paper [46]. We believe that an explicit analytical dependence of the spin on some parameter characterizing the shadow non-sphericity and observer viewing angle would be very useful as a first step in the development of more complex models. We restrict ourselves to the consideration of distant observer.

To characterize the deformation of the shadow we use oblateness, the ratio of horizontal (Δx) and vertical (Δy) angular diameters of the shadow which are supposed to be measured by an observer ($\Delta x \leq \Delta y$), see Fig. 3a. The oblateness $k = \Delta x/\Delta y$ takes values in the range $\sqrt{3}/2 \leq k \leq 1$. Value 1 corresponds to the Schwarzschild BH (circular shape, no deformation), value $\sqrt{3}/2$ takes place for extreme Kerr BH and the equatorial observer (strongest deformation). For analytical calculation of diameters, we need to know the left and the right horizontal borders of the shadow, x_L and x_R, and the vertical border, y_m. Location of BH and observer is shown in Fig. 3b.

Shape of shadow curve for distant observer is well known from Bardeen's work [3]. Moreover, results of Grenzebach, Perlick and Lämmerzahl [20] allow anyone to calculate the shadow of Kerr BH for any position of the observer, which means arbitrary radial distance from BH and arbitrary inclination of observer. Nevertheless, fully analytical calculation of the horizontal and vertical angular diameters in general case is complicated. Analytical calculation of the shadow means the following: every point

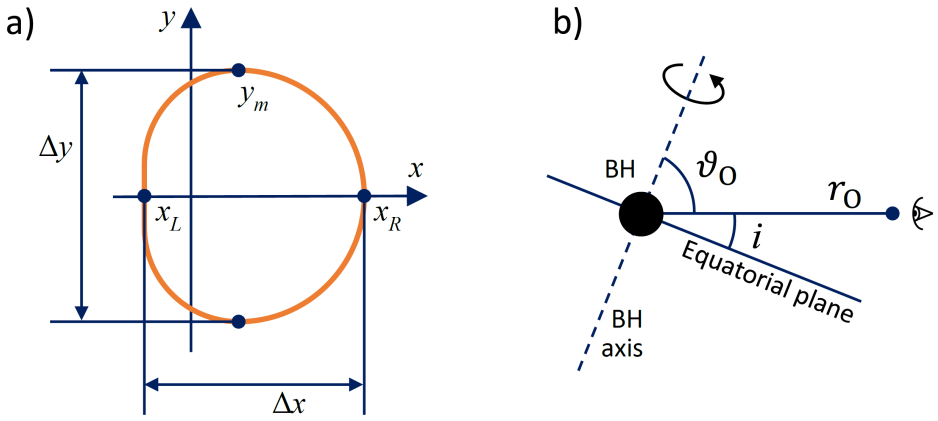

Figure 3: a) Horizontal and vertical angular diameters of the shadow. b) Position of the observer and the BH. We assume that $r_O \gg m$. Angle ϑ_O is the inclination angle of observer, and i is the viewing angle. Main results are obtained for the nearly equatorial observer, which means that $i \ll 1$.

of the curve is evaluated as an analytical function of a special parameter, see details in paper [46]. This parameter is changed in some range, and boundaries of this range are also subject of evaluation. Namely, we need to find zeros of a high-order polynomials. Therefore, in the general case results for diameters cannot be presented in closed analytical form (as explicit functions of spin and inclination). Calculation of the horizontal and vertical angular diameters is addressed in the subsequent paper of Grenzebach, Perlick and Lämmerzahl [21]. The authors consider the equatorial plane of the Kerr BH and explain how to calculate the horizontal and vertical angular diameters of the shadow as a function of the BH mass, spin, and the radial coordinate of the observer. As an example of the situation when results can be written explicitly, the authors have calculated the horizontal and vertical angular diameters of the shadow for extreme Kerr BH.

Let us consider the distant equatorial observer (see Fig. 4). For the Schwarzschild case, the shadow is circular. With increasing of BH spin a, the shadow is shifted to the right. At small a, the left and right borders are shifted almost equally, and the horizontal diameter is not changing. For $a = 0.6m$ the shadow still looks almost circular. Noticeable difference between the shape of the shadow and the circular shape appears only for a BH with spin close to the extreme, see Fig. 4. On basis of these numerical calculations we can formulate the following idea: if you can clearly notice the non-sphericity at the picture of the shadow, this means that you are looking at the shadow of nearly extreme BH and observer is not very far from the equatorial plane. We have used this approximation, and it allowed us to obtain compact formulas which is easy to use.

Let us now consider the nearly extreme Kerr BH $a = (1 - \delta)m$ with $\delta \ll 1$. The

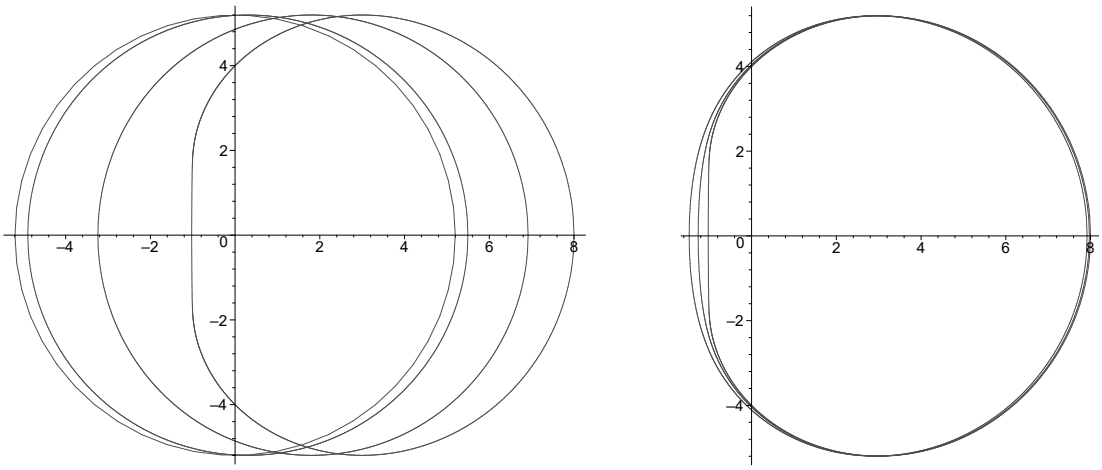

Figure 4: Left: The shadow curves for the distant equatorial observer for (from the leftmost to the rightmost) $a = 0$, $0.1m$, $0.6m$, $0.9999m$, m is the BH mass, $G = c = 1$. Right: The shadow curves for $a = 0.97m$, $0.99m$, $0.9999m$. There is a notable difference in location of left borders, whereas the right borders are approximately at the same place, see (5) and (6).

remarkable thing we have revealed from plotting the shadow for distant equatorial observer is that the displacement of the left border in comparison with the extreme Kerr case is proportional to $\sqrt{\delta}$:

$$x_L|_{a=(1-\delta)m} - x_L|_{a=m} \propto \sqrt{\delta}\,, \tag{5}$$

whereas the right border is shifting proportionally to δ:

$$x_R|_{a=(1-\delta)m} - x_R|_{a=m} \propto \delta\,. \tag{6}$$

This behaviour is clearly visible in the Fig. 4. This property helps us to find explicit dependence of spin on oblateness and viewing angle. To obtain compact formulas, we consider the case of nearly equatorial observer, viewing angle is small: $i \ll 1$.

We have found the following expression of the spin via oblateness and the viewing angle:

$$a = (1-\delta)m\,, \quad \delta = 18\left(k - \frac{\sqrt{3}}{2}\right)^2 - 2k\left(k - \frac{\sqrt{3}}{2}\right) i^2\,. \tag{7}$$

For observer in the equatorial plane ($\vartheta_{\rm O} = \pi/2$, $i = 0$), the BH spin is calculated as

$$a = (1-\delta)m\,, \quad \delta = 18\left(k - \frac{\sqrt{3}}{2}\right)^2\,, \quad k = \frac{\Delta x}{\Delta y}\,. \tag{8}$$

Value of a calculated for the equatorial plane is the lower limit of the spin of the BH at a given oblateness k: if the observer is not located in the equatorial plane, the larger value of the spin is required to obtain the same deformation.

4. Plasma influence on the shadow of spherically symmetric black hole

Influence of a matter on the shadow is usually investigated by numerical calculation, for example, see [17] and [24]. The first attempt of analytical investigation of plasma influence on the shadow size, in the frame of geometrical optics, taking into account effects of general relativity and plasma presence, was performed the paper of Perlick, Tsupko and Bisnovatyi-Kogan [32], see also discussion in [7]. The Synge's formula [41] was generalized to the case of a spherically symmetric and static plasma distribution on a spherically symmetric and static spacetime. Subsequently, the shadow of a Kerr BH under the influence of a plasma have been investigated analytically by Perlick and Tsupko [33]. For discussion other effects of plasma in gravitational lensing see papers [4], [5], [6], [8], [9], [16], [22], [27], [30], [31], [35], [36], [37], [40], [45].

In paper [32], we have considered the simplest non-trivial case: the influence of a non-magnetized pressureless plasma on the size of the shadow of a non-rotating BH was analytically calculated.

Let us consider a spherically symmetric and static metric

$$ds^2 = g_{ik}dx^i dx^k = -A(r)dt^2 + B(r)dr^2 + D(r)(d\vartheta^2 + \sin^2\vartheta\, d\varphi^2)\,, \tag{9}$$

where metric coefficients $A(r)$, $B(r)$ and $D(r)$ are positive, $G = c = 1$. We assume that the spacetime is filled with a static non-magnetized cold inhomogeneous plasma whose electron plasma frequency ω_e is a function of the radius coordinate only,

$$\omega_e^2 = \frac{4\pi e^2}{m_e} N(r)\,. \tag{10}$$

Here ω_e is the electron plasma frequency, $N(r)$ is the electron concentration in plasma, e is the charge of the electron, m_e is the electron mass. The refraction index n of this plasma is

$$n^2 = 1 - \frac{\omega_e^2}{[\omega(r)]^2}\,. \tag{11}$$

The photon frequency measured by a static observer is a function of r, according to the gravitational redshift formula,

$$\omega(r) = \frac{\omega_0}{\sqrt{A(r)}}\,. \tag{12}$$

Here ω_0 is the photon frequency at infinity.

Let us define for convenience a function $h(r)$ which contains all information about spacetime and plasma and is given by

$$h^2(r) = \frac{D(r)}{A(r)}\left(1 - A(r)\frac{\omega_e(r)^2}{\omega_0^2}\right)\,. \tag{13}$$

We have obtained that the angular radius $\alpha_{\rm sh}$ of the shadow is determined by compact formula [32]:

$$\sin^2\alpha_{\rm sh} \;=\; \frac{h^2(r_{\rm ph})}{h^2(r_{\rm O})}\,. \tag{14}$$

Here $r_{\rm O}$ is the observer position, and $r_{\rm ph}$ is the radius of photon sphere (for given space-time and plasma distribution) and can be found from equation

$$0 \,=\, \frac{d}{dr} h^2(r)\,. \tag{15}$$

Using formula (14), it is possible to calculate analytically the angular radius of the BH shadow:

- for any spherically symmetric metric, for example Schwarzschild BH, without approximation of weak field,
- for any position of observer, in particular very close to BH and very far from BH,
- for any spherically symmetric distribution of plasma,
- for any photon frequency.

5. Plasma influence on the shadow of Schwarzschild black hole

For the Schwarzschild spacetime, the angular radius of the shadow (14) specifies to (m is the BH mass)

$$\sin^2\alpha_{\rm sh} = \frac{r_{\rm ph}^2\left(\frac{r_{\rm ph}}{r_{\rm ph}-2m} - \frac{\omega_e^2(r_{\rm ph})}{\omega_0^2}\right)}{r_{\rm O}^2\left(\frac{r_{\rm O}}{r_{\rm O}-2m} - \frac{\omega_e^2(r_{\rm O})}{\omega_0^2}\right)}, \tag{16}$$

where $r_{\rm ph}$ has to be determined from (15) which is simplified to

$$0 = \frac{r\,(r-3m)}{(r-2m)^2} - \frac{\omega_e^2(r)}{\omega_0^2} - r\,\frac{\omega_e(r)\omega_e'(r)}{\omega_0^2}\,. \tag{17}$$

If the plasma frequency is much smaller than the photon frequency, the equations for the photon sphere and for the radius of the shadow can be linearized around the corresponding values for vacuum light rays. As an example, we have considered the Schwarzschild spacetime for the case that the plasma electron density is given by a power law,

$$\frac{\omega_e(r)^2}{\omega_0^2} = \beta_0 \frac{m^k}{r^k}, \tag{18}$$

where $\beta_0 > 0$ and $k \geq 0$ are dimensionless constants. The first-order equation for the radius of the shadow yields [32]

$$\sin^2\alpha_{\rm sh} = \frac{27m^2}{r_{\rm O}^2}\left(1-\frac{2m}{r_{\rm O}}\right)\left(1-\frac{\beta_0}{3^{k+1}}+\left(1-\frac{2m}{r_{\rm O}}\right)\frac{\beta_0 m^k}{r_{\rm O}^k}\right)\,. \tag{19}$$

Presence of homogeneous plasma ($k = 0$) makes the shadow bigger in comparison with vacuum case for any observer in the domain $3m < r_{\rm O} < \infty$. This occurs due to increase of gravitational bending in presence of homogeneous plasma [4], [5], [7].

In case of non-homogeneous plasma with given density distribution both increasing and decreasing effects are possible, depending on the position of the observer. Near the BH, relativistic effects predominate. Gravitational deflection becomes larger in presence of (homogeneous or non-homogeneous) plasma [4], [5], [7], therefore the shadow becomes larger for the observer who is close to the BH. Far from the BH, refraction effects predominate. Refraction on the declining density profile reduces the total deflection angle. Hence, in non-homogeneous case, the shadow becomes smaller if the observer is far enough from the BH. For details see Refs. [7] and [33].

If the observer is far from the BH, $r_{\rm O} \gg m$, formula (19) can be simplified to [7]

$$\text{homogeneous plasma,} \quad k=0: \quad \sin^2\alpha_{\rm sh} = \frac{27m^2}{r_{\rm O}^2}\left(1+\frac{2\beta_0}{3}\right), \tag{20}$$

$$\text{non-homogeneous plasma,} \quad k>0: \quad \sin^2\alpha_{\rm sh} = \frac{27m^2}{r_{\rm O}^2}\left(1-\frac{\beta_0}{3^{k+1}}\right). \tag{21}$$

In presence of plasma around of BH the light deflection becomes chromatic [4], [5], [6], [7]. Therefore in the presence of a plasma the size of the shadow depends on the wavelength at which the observation is made, in contrast to the vacuum case where it is the same for all wavelengths. Very high photon frequencies corresponds to vacuum case. The difference from the vacuum size of the shadow becomes bigger with decrease of the photon frequency ω_0. Dependence of the shadow size on the photon frequency in a homogeneous plasma goes as

$$\text{if} \quad \omega_0^{(1)} < \omega_0^{(2)} < \omega_0^{(3)}, \quad \text{then} \quad \alpha_{\rm sh}(\omega_0^{(1)}) > \alpha_{\rm sh}(\omega_0^{(2)}) > \alpha_{\rm sh}(\omega_0^{(3)}) > \alpha_{\rm sh}^{\rm vacuum}; \tag{22}$$

and in a non-homogeneous plasma for a distant observer we have (for case when the density decreases with increasing radial coordinate)

$$\text{if} \quad \omega_0^{(1)} < \omega_0^{(2)} < \omega_0^{(3)}, \quad \text{then} \quad \alpha_{\rm sh}(\omega_0^{(1)}) < \alpha_{\rm sh}(\omega_0^{(2)}) < \alpha_{\rm sh}(\omega_0^{(3)}) < \alpha_{\rm sh}^{\rm vacuum}. \tag{23}$$

For estimation of the effect, the case of a spherically symmetric accretion of plasma onto the Schwarzschild BH was considered in detail [32]. We have found that for an observer far away from the Schwarzschild BH the plasma makes the shadow smaller. As examples, we have considered Sgr A* and M87. Using this specific accretion model and observed luminosities in these systems, we have estimated the plasma density, and found that the effect of the presence of a plasma on the size of the shadow can be significant only for wavelengths of at least a few centimeters. At such wavelengths the observation of the shadow is made difficult because of scattering. For further details see [32].

6. Conclusions

Our main conclusions are:

(i) angular size of the shadow gives us the information about the BH mass;

(ii) oblateness of the shadow (the ratio of the horizontal and vertical angular diameters) allows us to estimate the BH spin:
   (a) knowing the oblateness by measuring the horizontal and vertical diameters of the shadow, one can easily obtain the lower limit on the BH spin by the formula (8), without need to construct or model the entire curve of the shadow;
   (b) if the viewing angle is known from other observations, one can directly calculate the spin using (7);
   (c) in all situations when the shadow curve is noticeably different from the circular shape, our approximate formulas provide a high accuracy of calculation;

(iii) angular size in different wavelengths can give us the information about plasma environment of BH:
   (a) in the presence of a plasma the size of the shadow depends on the wavelength at which the observation is made, in contrast to the vacuum case where it is the same for all wavelengths;
   (b) the effect of the plasma is significant only in the radio regime;
   (c) for an observer far away from the Schwarzschild BH the non-homogeneous plasma has a decreasing effect on the size of the shadow.

Acknowledgments

The author would like to thank Volker Perlick for the introduction to this topic and many useful discussions. The author brings special thanks to G. S. Bisnovatyi-Kogan for motivation, discussions and permanent support of all scientific initiatives.

References

[1] Abdujabbarov, A. A., Rezzolla, L., Ahmedov, B. J.: A coordinate-independent characterization of a black hole shadow. Mon. Not. R. Astron. Soc. **454** (2015), 2423–2435.

[2] Bambi C., Modesto, L.: Rotating regular black holes. Phys. Lett. B **721** (2013), 329–334.

[3] Bardeen, J. M.: Timelike and null geodesics in the Kerr metric. In: C. DeWitt, B. DeWitt (Eds.), *Black Holes*, pp. 215–239. Gordon and Breach, New York, 1973.

[4] Bisnovatyi-Kogan, G. S., Tsupko, O. Yu.: Gravitational radiospectrometer. Gravitat. Cosmol. **15** (2009), 20–27.

[5] Bisnovatyi-Kogan, G. S., Tsupko, O. Yu.: Gravitational lensing in a non-uniform plasma. Mon. Not. R. Astron. Soc. **404** (2010), 1790–1800.

[6] Bisnovatyi-Kogan, G. S., Tsupko, O. Yu.: Gravitational lensing in plasmic medium. Plasma Phys. Rep. **41** (2015), 562–581.

[7] Bisnovatyi-Kogan, G. S., Tsupko, O. Yu.: Gravitational lensing in presence of plasma: strong lens systems, black hole lensing and shadow. Universe **3** (2017), 57.

[8] Bliokh, P. V., Minakov A. A.: Gravitational lenses. Naukova Dumka, Kiev, 1989 (in Russian).

[9] Broderick, A., Blandford, R.: Covariant magnetoionic theory – I. Ray propagation. Monthly Notice of the Royal Astronomical Society **342** (2003), 1280–1290.

[10] Chandrasekhar, S.: The mathematical theory of black holes. Clarendon Press, Oxford, 1983.

[11] Cunha, P. V. P., Herdeiro, C. A. R., Radu, E., Rúnarsson, H. F.: Shadows of kerr black holes with scalar hair. Phys. Rev. Lett. **115** (2015), 211102.

[12] Cunha, P. V. P., Herdeiro, C. A. R.: Shadows and strong gravitational lensing: a brief review. General Relativity and Gravitation **50** (2018), 42.

[13] Dokuchaev, V. I., Nazarova, N. O.: Gravitational lensing of a star by a rotating black hole. JETP Letters **106** (2017), 637.

[14] Dymnikova, I. G.: Motion of particles and photons in the gravitational field of a rotating body (In memory of Vladimir Afanas'evich Ruban). Sov. Phys. Usp. **29** (1986), 215–237.

[15] Eiroa, E. F., Sendra, C. M.: Shadow cast by rotating braneworld black holes with a cosmological constant. The European Physical Journal C **78** (2018), 91.

[16] Er, X., Mao, S.: Effects of plasma on gravitational lensing. Mon. Not. R. Astron. Soc. **437** (2014), 2180–2186.

[17] Falcke, H., Melia, F., Agol, E.: Viewing the shadow of the black hole at the galactic center. Astrophys. J. **528** (2000), L13.

[18] Frolov, V. P., Zelnikov, A.: Introduction to black hole physics. Oxford University Press, Oxford, 2011.

[19] Goddi, C., Falcke, H., Kramer, M., et al.: BlackHoleCam: Fundamental physics of the galactic center. Int. J. Mod. Phys. D **26** (2017), 1730001.

[20] Grenzebach, A., Perlick, V., Lämmerzahl, C.: Photon regions and shadows of Kerr-Newman-NUT black holes with a cosmological constant. Phys. Rev. D **89** (2014), 124004.

[21] Grenzebach, A., Perlick, V., and Lämmerzahl, C.: Photon regions and shadows of accelerated black holes. Int. J. Mod. Phys. D **24** (2015), 1542024.

[22] Hakimov, A., Atamurotov, F.: Gravitational lensing by a non-Schwarzschild black hole in a plasma. Astrophysics and Space Science **361** (2016), 112.

[23] Hioki, K., Maeda, K.-I.: Measurement of the Kerr spin parameter by observation of a compact object's shadow. Phys. Rev. D **80** (2009), 024042.

[24] James, O., von Tunzelmann, E., Franklin, P., Thorne, K.S.: Gravitational lensing by spinning black holes in astrophysics, and in the movie *Interstellar*. Class. Quantum Grav. **32** (2015), 065001.

[25] Johannsen, T., Broderick, A. E., Plewa, P. M., et al.: Testing general relativity with the shadow size of Sgr A*. Physical Review Letters **116** (2016), 031101.

[26] Konoplya, R., Rezzolla, L., Zhidenko, A.: General parametrization of axisymmetric black holes in metric theories of gravity. Phys. Rev. D **93** (2016), 064015.

[27] Kulsrud, R., Loeb, A.: Dynamics and gravitational interaction of waves in nonuniform media. Physical Review D **45** (1992), 525–531.

[28] Li, Z., Bambi, C.: Measuring the Kerr spin parameter of regular black holes from their shadow. Journal of Cosmology and Astroparticle Physics **01** (2014), 041.

[29] Luminet, J.-P.: Image of a spherical black hole with thin accretion disk. Astron. Astrophys. **75** (1979), 228–235.

[30] Morozova, V. S., Ahmedov, B. J., Tursunov, A. A.: Gravitational lensing by a rotating massive object in a plasma. Astrophys. Space Sci. **2013**, 346, 513–520.

[31] Perlick, V.: Ray Optics, Fermats Principle and Applications to General Relativity. Springer, Heidelberg, Germany, 2000.

[32] Perlick, V., Tsupko, O. Yu., Bisnovatyi-Kogan, G. S.: Influence of a plasma on the shadow of a spherically symmetric black hole. Phys. Rev. D **92** (2015) 104031.

[33] Perlick, V., Tsupko, O. Yu.: Light propagation in a plasma on Kerr spacetime: Separation of the Hamilton-Jacobi equation and calculation of the shadow. Phys. Rev. D **95** (2017), 104003.

[34] Perlick, V., Tsupko, O. Yu., Bisnovatyi-Kogan, G. S.: Black hole shadow in an expanding universe with a cosmological constant. Phys. Rev. D **97** (2018), 104062.

[35] Rogers, A.: Frequency-dependent effects of gravitational lensing within plasma. Mon. Not. R. Astron. Soc. **451** (2015), 17–25.

[36] Rogers, A.: Escape and trapping of low-frequency gravitationally lensed rays by compact objects within plasma. Mon. Not. R. Astron. Soc. **465** (2017), 2151–2159.

[37] Rogers, A.: Gravitational lensing of rays through the levitating atmospheres of compact objects. Universe **3** (2017), 3.

[38] Stuchlík, Z., Hledík, S.: Some properties of the Schwarzschild-de Sitter and Schwarzschild-anti-de Sitter spacetimes. Phys. Rev. D **60** (1999), 044006.

[39] Stuchlík, Z., Charbulák, D., Schee, J.: Light escape cones in local reference frames of Kerrde Sitter black hole spacetimes and related black hole shadows. Eur. Phys. J. C **78** (2018), 180.

[40] Synge, J. L.: Relativity: the general theory. North-Holland Publishing Company, Amsterdam, The Netherlands, 1960.

[41] Synge, J. L.: The escape of photons from gravitationally intense stars. Mon. Not. Roy. Astron. Soc. **131** (1966), 463–466.

[42] Takahashi, R.: Shapes and positions of black hole shadows in accretion disks and spin parameters of black holes. ApJ **611** (2004), 996–1004.

[43] Tsukamoto, N., Li, Z., Bambi, C.: Constraining the spin and the deformation parameters from the black hole shadow. Journal of Cosmology and Astroparticle Physics **06** (2014), 043.

[44] Tsukamoto, N.: Black hole shadow in an asymptotically-flat, stationary, and axisymmetric spacetime: the Kerr-Newman and rotating regular black holes. Phys. Rev. D **97** (2018), 064021.

[45] Tsupko, O. Yu., Bisnovatyi-Kogan, G. S.: Gravitational lensing in plasma: Relativistic images at homogeneous plasma. Phys. Rev. D **87** (2013), 124009.

[46] Tsupko, O. Yu.: Analytical calculation of black hole spin using deformation of the shadow. Phys. Rev. D **95** (2017), 104058.

[47] Tsupko, O. Yu.: Notes on analytical treatment of black hole shadow. International Journal of Modern Physics D **27** (2018), 1844020.

[48] Yang, L., Li, Z.: Shadow of a dressed black hole and determination of spin and viewing angle. International Journal of Modern Physics D **25** (2016), 1650026.

[49] Zakharov, A. F.: Constraints on a charge in the Reissner-Nordström metric for the black hole at the Galactic Center. Phys. Rev. D **90** (2014), 062007.

ALTERNATIVE COSMOLOGICAL THEORIES

Conference *Cosmology on Small Scales 2018*
Michal Křížek and Yurii Dumin (Eds.)
Institute of Mathematics CAS, Prague

NEGLECTED GRAVITATIONAL REDSHIFT IN DETECTIONS OF GRAVITATIONAL WAVES

Michal Křížek[1], Lawrence Somer[2]

[1] Institute of Mathematics, Czech Academy of Sciences, Žitná 25
115 67 Prague 1, Czech Republic
e-mail: krizek@cesnet.cz
[2] Department of Mathematics, Catholic University of America
Washington, D.C. 20064, U.S.A.
e-mail: somer@cua.edu

Abstract: In 2016, the letter [1] about the first detection of gravitational waves was published. They were generated by two merging black holes that had approximately 36 and 29 Sun's masses. However, the authors have not taken into account a large gravitational redshift of this binary system, which is a direct consequence of time dilation in a strong gravitational field. Thus the proposed masses are overestimated. In our paper we also give other arguments for this statement.

Keywords: gravitational redshift, time dilatation, black holes, wavelets

PACS: 4.20-q, 95.30.Sf

1. Introduction

A century ago Albert Einstein [13], [14] predicted the existence of gravitational waves. He assumed only very weak gravitational fields which enabled him to linearize his field equations of general relativity. He considered only small perturbations of Minkowski spacetime and after some further simplifications he got a nonhomogeneous partial differential equation with the d'Alembert operator for plane gravitational waves (see e.g. [6, p. 24]).

Gravitational waves were first detected on September 14, 2015. According to [1], two black holes with masses

$$m_1 = 36^{+5}_{-4} M_\odot \quad \text{and} \quad m_2 = 29^{+4}_{-4} M_\odot, \tag{1}$$

merged and the generated gravitational waves GW150914 were independently intercepted by two LIGO detectors. We show that these masses are not too trustworthy. First of all, we would like to emphasize that our criticism does not concern the

LIGO detectors themselves, which are highly sophisticated and remarkable instruments. It concerns the methodology that was used to process and then interpret the measured data. The used post-Newtonian model, which neglects the infinite gravitational redshift of each single black hole, can only very roughly approximate reality. Therefore, from this heuristic model we cannot make any definite conclusion about the real masses of the considered binary black hole system and derive any reliable error estimates. In our opinion, the post-Newtonian model is not applicable in this case.

In Section 2, we introduce several drawbacks of the used formula for the so-called chirp mass. In Section 3, we show that the masses (1) including also the associated error bars need not correspond to reality, because the gravitational redshift was neglected. Section 4 contains further arguments supporting our hypothesis that the masses (1) are overestimated. We also present some conclusions in Section 5.

2. Emitted versus detected frequencies

The only relation which is given on a single line in [1] reads:

$$\mathcal{M} = \frac{(m_1 m_2)^{3/5}}{(m_1 + m_2)^{1/5}} = \frac{c^3}{G}\Big[\frac{5}{96}\pi^{-8/3} f^{-11/3}\dot{f}\Big]^{3/5}, \tag{2}$$

where $f = f(t)$ and $\dot{f} = \dot{f}(t)$ are the frequency of gravitational waves in time t and its time derivative, m_1 and m_2 are the masses of the components of the binary system for low frequencies, $\mathcal{M}$ is the chirp mass in the detector frame, $G = 6.674 \cdot 10^{-11}\,\mathrm{m^3 kg^{-1} s^{-2}}$ is the gravitational constant, and $c = 299\,792\,458$ m/s is the speed of light in vacuum.

According to [1, p. 3], f is the detected frequency. However, then the formula (2) cannot be true, in general, since f on its right-hand side essentially depends on the total redshift z, whereas the left-hand side of (2) is independent of z. The masses m_1 and m_2 cannot depend on z. Therefore, (2) can be valid only for $z = 0$. Let us emphasize that formula (2) was taken from reference [5]. However, in [5, p. 3516] and [12, p. 2663], the authors rightly consider the emitted frequency f_{em} (or the orbital frequency πf_{em}) in the source frame and not the detected frequency f as in [1]. Therefore, the detected frequency f should be replaced by the emitted frequency

$$f_{\mathrm{em}} = (z + 1)f, \tag{3}$$

where z is the total redshift of gravitational waves.

The masses m_1 and m_2 were estimated by a series of numerical simulations [17] with various input values m_1 and m_2. The numerical methods employed in constructing the templates for the merging black holes can also be found in [9] and [19]. However, no gravitational redshift is mentioned in these references.

Let us look at the equality (2) in more detail. This equality was derived from the relation (3) of the 1995 paper [5] in a manner such that many higher order terms were neglected. In spite of that, the authors of [1] kept the equality sign in (2).

Furthermore, notice that the left-hand side of quality (2) does not depend on time t, while the right-hand side is time dependent. Thus the equality (2) is satisfied if and only if the product $f^{-11/3}\dot{f}$ is a suitable constant C (e.g. $C = 0.00015142\ldots\ \mathrm{s}^{5/3}$ for (1)). This leads to the solution of an ordinary differential equation of the first order

$$\dot{f} = Cf^{11/3} \tag{4}$$

whose general solution is

$$f(t) = \left(\frac{3}{8}\right)^{3/8} \frac{1}{(K - Ct)^{3/8}}, \tag{5}$$

where $K \in (-\infty, \infty)$ is an arbitrary integration constant, see also [12, p. 2663]. By [20, p. 14] the function (5) is the only solution of the differential equation (4) for $t < K/C$. Since this equation is autonomous, we may choose $K = 0$. The relation (5) thus determines how the frequency increases with time.

The authors of [1] had only approximate values of the detected frequency f from the interval 35–250 Hz for approximately 8 orbital periods. Finally note that a numerical computation of the derivatives from smoothed data is an ill-conditioned problem.

3. Neglected gravitational redshift

Unfortunately, in [1] (also in [2], [3], [4], [5], [16]) there is no mention about gravitational redshift of gravitational waves. Let us recall that redshift (or blueshift) of frequency of waves coming to us from the universe has three basic components:

1) a Doppler component caused by the movement of the source or the observer with respect to its neighborhood,

2) a cosmological component caused by the expansion of the universe,

3) a gravitational component caused by the change of frequency of waves in a gravitational field.

According to [1, p. 7], the luminosity distance of the considered binary system is 410^{+160}_{-180} Mpc which is in perfect agreement with the cosmological redshift (see e.g. [21])

$$z = 0.09^{+0.03}_{-0.04}, \tag{6}$$

that is stated by the authors. Thus for the two remaining components of the redshift it remains

$$z \approx 0. \tag{7}$$

Let us note that the gravitational redshift for the surface of a neutron star is $z \approx 0.3$ which is greater than (6), which can be derived from (10) below. For the horizon of a single black hole with mass m with Schwarzschild radius

$$r = \frac{2Gm}{c^2} \tag{8}$$

we even have

$$z = \infty. \tag{9}$$

From this and the relation (7) it follows that the authors of [1] did not consider a large gravitational redshift caused by the binary black hole system.

The gravitational redshift is a direct consequence of Einstein's time dilatation. Time in a gravitational potential hole flows more slowly than outside. A photon has to spend some energy to leave a gravitational field of a mass object. Its frequency is indirectly proportional to the speed of flowing of time. Therefore, the frequency of electromagnetic waves decreases when leaving a large gravitational potential hole of the binary system. A similar phenomenon holds for gravitational waves that carry away energy and thus their frequency will decrease as well.

So let us recall the well-known formula that can be derived from the Schwarzschild solution of Einstein's equations. It expresses the change of frequency of a photon leaving the gravitational field of a single black hole at the distance $R > r$ from its center

$$f = f_{\rm em}\sqrt{1 - \frac{r}{R}}, \tag{10}$$

where r is given by (8), $f_{\rm em}$ is the emitted frequency of a photon and f is the detected frequency by a distant observer. From this and (3) we obtain the limiting relation (9) for $R \to r$.

Setting for instance $R = 2r$ in (10) (cf. [1, p. 3]), we find that $f = 2^{-1/2} f_{\rm em}$. By (3) the corresponding gravitational redshift is

$$z = \sqrt{2} - 1 = 0.414 \tag{11}$$

which is much larger than the value in (6). Similarly, for $R = 3r,\ 4r$, and $5r$, we get $z = 0.225$, 0.155, and 0.118, respectively, which are also larger than (6).

Just before the collision of the two black holes, the spacetime between them exhibited the largest deformations. By the measured data of LIGO detectors it produced gravitational waves with an increasing recorded frequency 35–250 Hz. The distance between both the black holes was only a few Schwarzschild radii [1, p. 3]. From (8)–(11) we may deduce that the gravitational redshift of the emitted gravitational waves will be quite essential and probably larger than that in (6). Unfortunately, the true analytical solution of Einstein's equations for two orbiting bodies is not known. However, a common gravitational potential hole of the two black holes is deeper than that of each of its components (see Fig. 1).

From equality (2) it is obvious that the sought masses of the black holes and also the constant C of (4) depend on the emitted frequency $f_{\rm em} = (z+1)f$. Consequently, a proper determination of the total redshift z is essential. By relation (3) we obtain $\dot{f}_{\rm em} = (z+1)^2 \dot{f}$, where the additional factor $(z+1)$ is due to Einstein's time dilatation. Substituting this and (3) into (2), we get the missing factor

$$(z + 1), \tag{12}$$

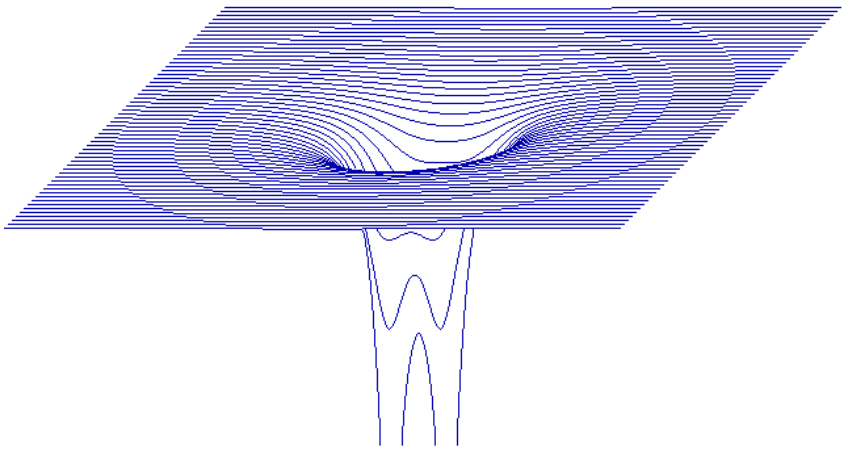

Figure 1: Schematic illustration of the gravitational potential of a binary back hole system. The largest deformation of the spacetime arises close to the central saddle point. According to [1, p. 3] the highest amplitude of the detected signal was reached for the separation $R = \frac{3}{2}r$.

because

$$\left(f^{-11/3}\dot{f}\right)^{3/5} = (z+1)\left(f_{\rm em}^{-11/3}\dot{f}_{\rm em}\right)^{3/5} \tag{13}$$

and because the remaining factors in (2) are constants. In [1] only the cosmological redshift (6) was considered, but the total redshift is larger (cf. e.g. (11)).

Finally, let us note that the Doppler shift may also not be negligible. Unfortunately, we do not know the orientation of the orbital plane of the black holes and its local movement. Therefore, we cannot reliably establish the corresponding Doppler redshift.

4. Other arguments

The mechanism of the origin of the binary black hole system (1) is not known. According to the recent survey paper [11, Fig. 8], all the 17 known X-ray binaries detected in our Galaxy have components with masses less than $10M_\odot$. Masses of all known single stellar mass black holes are in the interval $5M_\odot$ – $20M_\odot$ (cf. e.g. [7], [8], [18]). Hence, from a statistical point of view a system of two much larger black holes such as (1) seems to be quite exceptional, even though some selection effects may be present, since larger masses imply stronger signals. Moreover, its evolution path is unknown. All its parameters should be tuned very finely.

Chen et al. in [10] have also found that the important gravitational redshift of GW150914 was not accounted for. They assume that the black hole binary system was located in close vicinity of a supermassive black hole possessing a large gravitational redshift. Their results indicate that the mass of each component of such a pair of black holes is not greater than $10M_\odot$.

The wavelength $\lambda = c/f$ corresponding to the highest detected frequency $f = 250\,\mathrm{Hz}$ is equal to $\lambda = 1200\,\mathrm{km}$. This is a much larger value than the diameter of the wave zone given by the associated Schwarzschild radii of the black holes. Nevertheless, we observe that the emitted frequency $f_{\mathrm{em}} > f$ would yield a much more reliable size of the wave zone. This also shows that the gravitational redshift was missing.

5. Conclusions

The paper [1] presents an important analysis of signals from LIGO detectors. However, due to the lack of details on the mathematical tools used in this analysis, it can hardly be reproduced. The statement that two black holes with masses (1) have merged seems to be somewhat too strong. The main reason is that the detected frequency f in (2) should be replaced by the emitted frequency f_{em}, i.e., the chirp mass (2) should be divided by the missing factor $(z+1)$ given in (12). From Section 3 we may deduce that the total redshift z could be larger than $\frac{1}{2}$, see (6) and (11). Hence, the masses (1) were overestimated. To see this, suppose for simplicity that $m_1 = m_2$. Then from (2) we observe that the corresponding chirp mass $\mathcal{M} = m_1^{6/5}/(m_1 + m_1)^{1/5} = 2^{-1/5} m_1$ linearly depends on m_1. Hence, the masses m_i are affected by the same redshift correspondingly. In this special case for $z + 1 \geq \frac{3}{2}$ the masses m_i could be at least 33 % smaller.

Acknowledgment. The authors are indebted to Jan Brandts and Filip Křížek for careful reading and valuable suggestions. Michal Křížek was supported by RVO 67985840 of the Czech Republic.

References

[1] Abbott B. P. et al.: *Observation of gravitational wave from a binary black hole merger*. Phys. Rev. Lett. 116 (2016), 061102.

[2] Abbott B. P. et al.: *GW151226: Observation of gravitational waves from a 22-solar-mass binary black hole coalescence*. Phys. Rev. Lett. 116 (2016), 241103.

[3] Abbott B. P. et al.: *GW170104: Observation of a 50-solar-mass binary black hole coalescence at redshift 0.2*. Phys. Rev. Lett. 118 (2017), 221101.

[4] Abbott B. P. et al.: *Multi-messenger observation of a binary neutron star merger*. Astrophys. J. Lett. 848 (2017), L12.

[5] Blanchet L. et al.: *Gravitational-radiation damping of compact binary systems to second post-Newtonian order*. Phys. Rev. Lett. 74 (1995), 3515–3518.

[6] Blanchet L.: *Gravitational radiation from post-Newtonian sources and inspiralling compact binaries*. Living Rev. Relativity 17 (2014), 2, 187 pp.

[7] Broadhurst T., Diego J. M., Smoot G.: *Reinterpreting low frequency LIGO/Virgo events as magnified stellar-mass black holes at cosmological distances*. ArXiv 1802.05273v1, 2018, 1–16.

[8] Casares J.: *Observational evidence for stellar-mass black holes*. In Proc. IAU Sympos. No. 233, Black holes: from stars to galaxies – across the range of masses (V. Karas and G. Matt, eds.), 2006, 1–8.

[9] Centrella J., Baker J. G., Kelly B. J., van Meter J. R.: *Black-hole binaries, gravitational waves, and numerical relativity*. Rev. Mod. Phys. 82 (2010), 3069.

[10] Chen X., Li S., Cao Z.: *Mass-redshift degeneracy for gravitational-wave sources in the vicinity of a supermassive black hole*. ArXiv: 1703.10543v2, 2017, 1–6.

[11] Corral-Santana J. M., Casares J., Muñoz-Darias T., Bauer F. E., Martínez-Pais I. G., Russell, D. M.: *BlackCAT: A catalogue of stellar-mass black holes in X-ray transients*. Astronom. Astrophys. 587 (2016), A61.

[12] Cutler C., Flanagan E. E.: *Gravitational waves from merging compact binaries: How accurately can one extract the binary's parameters from the inspiral waveform?* Phys. Rev. D 49 (1994), 2658–2697.

[13] Einstein A.: *Näherungsweise Integration der Feldgleichungen der Gravitation*. Sitzungsberichte K. Preuss. Akad. Wiss. 1 (1916), 688–696.

[14] Einstein A.: *Über Gravitationswellen*. Sitzungsberichte K. Preuss. Akad. Wiss. 1 (1918), 154–167.

[15] Kim M. H.: *Strange noise in gravitational-wave data sparks debate*. Quanta Magazine (2017), June 30, 6 pp.

[16] Klimenko S. et al.: *Method for detection and reconstruction of gravitational wave transients with networks of advanced detectors*. Phys. Rev. D 93 (2016), 042004.

[17] Mroué A. H. et al.: *Catalog of 174 binary black hole simulations for gravitational wave astronomy*. Phys. Rev. Lett. 111 (2013), 241104.

[18] Narayan R., McClintock J. E.: *Observational evidence for back holes*. ArXiv: 1312.6698v2, 2014, 1–20.

[19] Pfeiffer H. P.: *Numerical simulations of compact object binaries*. Class. Quant. Grav. 29 (2012), 124004.

[20] Rektorys K.: *Survey of applicable mathematics II*. Kluwer Acad. Publ., Dordrecht, 1994.

[21] `https://ned.ipac.caltech.edu/help/cosmology_calc.html`

Conference *Cosmology on Small Scales 2018*
Michal Křížek and Yurii Dumin (Eds.)
Institute of Mathematics CAS, Prague

POSSIBLE COMMON SOLUTION TO THE PROBLEMS OF DARK ENERGY AND DARK MATTER IN THE UNIVERSE

Pavel Voráček

[1] Lund Observatory
Box 43, SE-221 00 Lund, Sweden
postmaster@astro.lu.se (with Subject: Pavel)
[2] RabstejnLab, Institute of Science and Education
P.O.Box 5, CZ-331 62 Manětín, Czech Republic

Abstract: We present here a model for a common explanation of the phenomena of the dark energy and dark matter, which is lying outside the General relativity theory, yet still compatible or, perhaps, even complementary to it. We discuss the principal results of the method of the *Causal dynamical triangulations*, when applied under the assumption of topology S^3 of our world, i.e., assuming the closedness of the Universe. Then it can be concluded that the resulting space-dimensionality three, being equal to what we consider to be the naturally optimal dimensionality of the real space, implies the existence of a certain deviation from this optimal value on the cosmological scale-level (i.e. a deviation from the space-'Euclidicity' there), since a fourth space-dimension is explicitly or implicitly necessary (depending only on what form of the spacetime-metric one has used) in order to allow the Universe to be closed. As a consequence, the bent space (considered to be the component of the curved spacetime), together with the real cosmic stratum there, struggles to arrive to the state with the optimal dimensionality, i.e., it struggles to expand, while the 'pseudo-pressure' is the carrier of the 'dimensionally-elastic' energy, which appears as the *dark energy* (on the global cosmological scale) and the *dark matter* (on the scale-level of cosmic inhomogeneities). The basic rules for their appearance are presented, as well as the pertaining questions are discussed: the feedback of the proposed mechanism, the problem of the entropy and self-organization of the cosmic stratum, and the evolution of the phenomenon.

Keywords: dark energy, dark matter, Causal dynamical triangulations, pseudo-pressure, accelerating expansion, dimensionally-elastic energy, feedback, entropy, self-organization, entropy-course and expansion

PACS: 98.80.-k, 95.35.+d, 95.36.+x

1. Introduction

A plethora of more or less speculative solutions to the problems of the dark energy and dark matter in the Universe were published during recent years. The authors of the proposed solutions, however, do not take into consideration the fact that the expansion of the Universe has a very specific character. It is not generally regarded that the expansion is not a classical physical motion and it has not the conventional dynamics. For the expansion, together with its apparent acceleration ascertained by means of observations of the distant supernovae of type Ia, see [24] and [21], only the common dynamical interpretation is presumed. Yet, other options for explanation of the acceleration exist, which will be presented in a subsequent section.

We start from the assumptions (motivated in [35]) that:

(i) The Universe is more or less marginally closed and Machian, with the trivial topology and the metric of the 3-sphere:

$$\mathrm{d}s^2 = -\mathrm{d}\tau^2 + r^2(\tau)\,[\,\mathrm{d}\psi^2 + \sin^2\psi\,(\,\mathrm{d}\theta^2 + \sin^2\theta\,\mathrm{d}\phi^2\,)\,]. \tag{1}$$

Here τ is the *cosmic time* of the *fundamental cosmological observer* (observing – by definition – the cosmic background radiation being isotropic) and ψ, θ, and ϕ are the angular coordinates on the 3-sphere[1]. Further,

$$\mathrm{d}\tau = \frac{r(\tau)}{r(\tau_0)}\,\mathrm{d}\tau_0\ , \tag{2}$$

where r is the radius of the Universe, τ is a cosmic epoch in general, and τ_0 is the actual cosmic epoch. (Then, $\mathrm{d}\tau_0$ is an element of the York time.)

(ii) For the Universe, the Law of mass-energy conservation is valid, while its *global* (i.e., absolutely total) energy is equal to zero [35].

(iii) The Universe either arose in the *world-start* (big bang) from nothing or it is cyclic (i.e., the *world-end* (big crunch) of the actual cycle becomes the world-start of the subsequent cycle).

(iv) There exists only one form of the Friedmann equation (FE), valid both for the radiation-dominated and mass-dominated Universe:

$$\left(\frac{\mathrm{d}r}{\mathrm{d}\tau}\right)^2 - \frac{Rr_0}{r^2} = -1 \tag{3}$$

where R and r_0 is the radius of the Universe at its maximal expansion and at the actual epoch, respectively. Except for situations where the derivative of

[1] We avoid the notion 'co-moving coordinates', since – as already mentioned – the expansion of the Universe is not a classical physical motion.

equation (3) is taken (when the model parameters, but no observational parameters, are considered), it is possible to put $r_0 = r$; then the equation, according to the currently established opinion considered to be the FE valid only for the matter-dominated (closed) Universe, is obtained:

$$\left(\frac{\mathrm{d}r}{\mathrm{d}\tau}\right)^2 - \frac{R}{r} = -1. \tag{4}$$

(v) Under conditions quoted above and – namely – when the FE is fulfilled, an equilibrium exists between (the negative) *cosmological space tension* Σ and (the positive) *cosmological pseudo-pressure* P, with a, for the time being, unknown origin and character, so that the total *cosmological space stress* is equal to zero,

$$P + \Sigma = 0\ , \tag{5}$$

with possible exception for relatively small deviating oscillations [31, p. 339].

2. Spacetime curvature and *space-bending* in the *demonstration diagrams*

It is necessary and important to realize the principal difference between the spacetime curvature in the vicinity of a source of the local static gravitational field (we consider – for the sake of simplicity – the Schwarzschild field) and the curvature of the spacetime in the expanding/compressing[2] closed Universe:

(a) In the local static field the space-derivatives of the metric coefficients are non-zero, while their time-derivatives equal to zero.

(b) In the cosmic gravitational field the situation is the opposite: At a given cosmological epoch the space-derivatives of metric coefficients are equal to zero, while the same coefficients are changing with the cosmic time in the expanding/compressing Universe.

As we have serious objections against the relevance of the *embedding diagrams* frequently used in the GRT for the local gravitational fields (introduced by Misner [19, pp. 613–615]), we prefer to use so called *demonstration diagrams*, where the space-component of a null-geodesic is presented depending on how it appears for the distant (coordinate) observer; the relevant influence of the time metric coefficient (g_{tt}) is thus regarded implicitly[3]. In such a way, e.g., the photon horizon is

[2]We avoid here the notion *contraction* in order to respect the necessity to differentiate between the complex character of the phenomenon of *compressing* Universe and the usual relativistic contraction. Further, we differentiate between the notions *relaxation/constriction of the space* in the Universe and the *expansion/compression of the Universe*, but the difference will not be applied here.

[3]A *perfect demonstration diagram*, where the influence of metric coefficient g_{tt} would be taken into consideration, would necessarily have to be kinematic.

represented by a 2-sphere with its incident radius and the center at the origin of the Schwarzschild coordinate system.

For the demonstration diagram of the Universe we use the 4-dimensional Euclidean space, which, however, necessarily it must be dimensionally restricted for the practical use. Usually, the 2-sphere in the 3-dimensional Euclidean space is applied for such a purpose. There, for a given cosmological epoch, the *bending of the cosmic space*, being qualitatively different from the curvature of the spacetime in the local gravitational field, is sufficient; it is because in the local field the non-zero derivatives $\partial g_{tt}/\partial r$ and $\partial g_{rr}/\partial r$ [4] evidently are also deciding the shape of the formations in the demonstration diagrams, while the same derivatives are zero for the Universe at a given cosmological epoch τ. It is why we introduce the notion *bending of the cosmic space*, being relevant on the cosmological scale; in the dimensionally restricted demonstration diagram the bending of the space is easily and didactically represented by the simple classical bending of the respective 2-sphere. In Figure 1, a section through such a 2-sphere by the plane passing through its center and the place of the fundamental cosmological observer is shown.

Since our Universe is – as assumed – closed with trivial topology (i.e., it is an expanding 3-sphere), its bending is intrinsic. It should be emphasized that the dimensional analogy we use is exactly relevant to the real cosmological situation only for a universe with the trivial topology being closed (alternatively open and Euclidean), but not for open non-Euclidean models or for models with non-trivial topologies. The radius of the Universe (the quantity denoted r in the FE) is thus equivalent to the notion of the radius of the 2-sphere in the demonstration diagram. Most frequently, a form of the Friedmann-Robertson-Walker (FRW) metric of spacetime with three non-Euclidean space-coordinates is used for the Universe [18, Sections 60 and 61], but such a metric is equivalent to the one we use here (1).

In the FRW-metric, the curvature radius is considered to be just a parameter, not a vector, which is a logically necessary consequence in the (3+1)-dimensional curved spacetime where a fourth space dimension, relevant to the curvature radius, is a purely mathematical abstraction, while – in the Euclidean 4-space of the demonstration diagram – the radius-vectors of the Universe is orthogonal everywhere to its space, which is bent in the fourth dimension (i.e., the radius-vector is not 'inside our Universe'). The hypersphere radius presented above and curvature radius used in the concept avoiding the Euclidean 4-space are identical.

3. Character of the *cosmological space tension*

Cosmological space tension Σ has a very good analogy in the surface tension on the soap bubble. Except for the number of dimensions, the principal difference consists in the fact that the mediating interaction in the Universe is the gravitation, while, on the soap bubble the surface tension is caused by the intermolecular forces.

[4] ... for the anisotropic Schwarzschild metric; for an isotropized metric: "... non-zero derivatives $\partial g_{ij}/\partial r$, where $i = j$, ..."

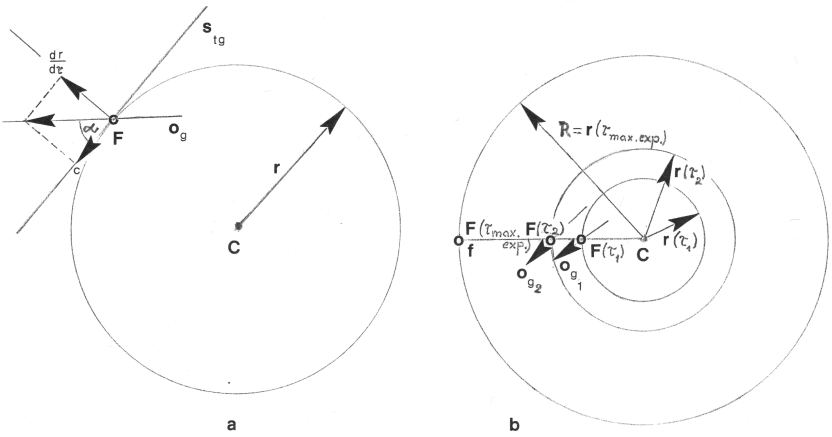

Figure 1: (a) The section through the restricted demonstration diagram of the Universe at a given epoch τ by a plane through its center C and fundamental cosmological observer F. The center is beside the space of the universe, both in the diagram and in our real closed Universe. For observer F, the closest local part of the circle, being the *space component* of a null-geodesic with tangent o_g, is coinciding with the Euclidean tangential straight line s_{tg}; for $c = 1$, $\mathrm{d}r/\mathrm{d}\tau = \tan\alpha$. (A planar section through the center of our real Universe would be identical to the one presented here, despite the different number of dimensions!) In an analogous 3-D demonstration diagram it would be possible to draw the planar pencil of the tangential straight lines forming the Euclidean tangential plane, touching the pencil of great circles in point F, i.e., touching the 2-sphere of the diagram. In the real space of the Universe, the spatial pencil (bundle) of the tangential straight lines can be drawn through the place of the fundamental observer, creating in such a way the Euclidean tangential space, touching in the point F the spatial pencil (bundle) of great circles in the *bent space*, i.e., touching the 3-sphere of the Universe with a common central point beside it. The section shown in the diagram is usually called the *world-map* of the Universe. Then, even though it is just a section through the 3-D demonstration diagram, it is – consistently seen – the very world-map of the real Universe as well.
(b) The 2-D set of all world-maps at different epochs we then call the *world-scheme* of the Universe. There, the straight radial line f is the world-line of fundamental observer F, while o_{g1} and o_{g2} are tangents to the null-geodesics of the photons passing in his vicinity at epochs τ_1 and τ_2, respectively. (Another – more didactic – manner would be to design the world-scheme in 3-D, with the single world-maps (planar sections) for different cosmic epochs being circles at planes parallel with the plane of projection (here, the paper), having their centers on the straight line of coordinate τ (i.e., on the τ-axis) passing through point C and being orthogonal to the plane of projection. Lines o_g, o_{g1} and o_{g2} in diagrams (a) and (b) are – more correctly – the time-parametrized orthogonal projections of the tangents to the null-geodesics from such a 3-D world-scheme onto the plane of the diagrams.)

Both for the soap bubble and the Universe, the rule holds that the smaller the radius of the bending, the stronger the '(self-)compressing tendency' of the formation [31].

In the opposite situation, the analogy of the necessary bending is very illustrative and adequate: An infinitely extended soap membrane cannot shrink, and – in an infinitely extended Euclidean (i.e. marginally open) universe – the gravitation cannot act dynamically on a cosmological scale. It is possible to show that the Euclidean universe, with a positive value of the critical mass-density, has zero *global mass-energy* density entering the field-equation; such a universe is then *formally* (i.e., in terms of mathematics) *empty* and thus the original static solution of Einstein (actually considered to be erroneous) can be taken as a relevant model [35].

4. Character of the *cosmological pseudo-pressure*

In the epoch of the Universe dominated by the matter a cosmologically significant classical pressure does not exist in the cosmic stratum.

In the currently accepted standard description of the closed FRW-model universe, one more or less tacitly presumes that the gravitational tension classically dynamically decelerates its expansion, i.e., that in such a process the adjacent gravitational force is in equilibrium with a cosmological inertia force originating in the matter of the cosmic stratum thanks to the deceleration. It is, however, a quite irrelevant description of the situation since:

(i) The expansion of the Universe is not a classical physical motion; it has the direction orthogonal to the physical cosmic space and actually still its *rate* $\mathrm{d}r/\mathrm{d}\tau > 1\ (= c)$.

(ii) The concept of a *cosmological inertia force* related to the *deceleration rate* $\mathrm{d}^2r/\mathrm{d}\tau^2$ of the cosmic expansion does not exist. The cosmic matter determining the origination of the inertia force in the sense of the Mach principle[5], see [29] and [30], is relativistically at rest relative to each of its own elements in the expanding cosmic stratum, since the matter itself participates in the expansion of the Universe. (Here it should be emphasized that the matter on the 'opposite side of the bubble' is influencing a given mass-particle gravitationally only along its hypersurface – not 'directly through the space of the bubble', which, in cosmology, means not directly through the Euclidean 4-dimensional hyperspace 'inside' the Universe being limited by its 3-sphere; the 4-dimensional interior does not belong physically to the Universe.)

The relevant description of the dynamics of the cosmic expansion is – in our opinion – that the gravitational space tension is in equilibrium with a cosmologically effective pressure P. Referring to the law of mass-energy conservation we can perform the following deduction:

[5]The Mach principle is not incompatible with the role of the Higgs boson.

For the mass-energy $m(\tau)$ of the cosmic stratum at epoch τ, defined as

$$m(\tau) = \rho(\tau)V(\tau), \tag{6}$$

where $V(\tau)$ is the volume of the 3-sphere of the closed Universe

$$V(\tau) = 2\pi^2 r^3(\tau) \tag{7}$$

and $\rho(\tau)$ is the average density of the matter and energy in the Universe at the same epoch, holds that

$$-\,\mathrm{d}m = P\mathrm{d}V \tag{8}$$

which is the Law of mass-energy conservation in a closed system (for $c = 1$) as used in thermodynamics [19, pp. 726–730]. The energy necessary for the expansion equals the decrement of the total mass-energy of the cosmic stratum. In the Law, the pressure has still the classical character and a performed physical work is usually presented as the work made by means of a force of pressure pushing on the surface of a piston. In the cosmology, the physical character of pressure P is not known *a priori*, but if it were unveiled that it is formally (i.e. mathematically) identical with the classical pressure, the respective mass-decrement $\mathrm{d}m$ necessarily remains to be determined in a quite unconventional way. Since 'no cosmic piston is pumping up' the Universe, the decrement of the bending of the space is offered as a hint when looking for something that fulfills its analogous function.

If the matter-energy of the cosmic stratum behaves in a Machian way (as presumed), i.e., as the energy of the ideal photon gas, then – recalling equation (7) – the numerical density of the photons

$$\rho_n(\tau) \propto V^{-1}(\tau) \propto r^{-3}(\tau), \tag{9}$$

while the representative frequency ν of a photon in the gas – and naturally its respective average energy as well – depends on $r(\tau)$ as

$$\nu(\tau) \propto r^{-1}(\tau), \tag{10}$$

being a consequence of relation (2). Further, evidently,

$$\rho(\tau) \propto \rho_n(\tau)\nu(\tau). \tag{11}$$

From the last three formulae it follows that

$$\rho(\tau) \propto r^{-4}(\tau) \propto V^{-4/3}(\tau). \tag{12}$$

Our aim is now to find the value of w in the Equation of state

$$P = w\rho. \tag{13}$$

From relations (6), (8), and (13) now follows that

$$\rho(\tau) \propto V^{-(w+1)}(\tau), \tag{14}$$

which, compared with relation (12), results in the conclusion that $w = 1/3$ or:

$$PV^{4/3} = const. \tag{15}$$

It means that the cosmic stratum apparently behaves as an ideal adiabatic gas with $\kappa = 4/3$ despite the very physical character of effective pressure P obviously cannot be considered as conventional, and it is why we call such a quantity *(cosmological) pseudo-pressure*. The FE as it is presented by means of relation (4) is then an energy-equation (compatible with relation (10)) valid for the whole evolution-history of the Universe, in spite of the currently generally accepted opinion is, that such a form of FE is *not* valid for the radiation-dominated phase of the Universe. Nevertheless, in the era of dominating radiation, a physically significant part of pressure P can be identified as a conventional pressure P_0 in the cosmic stratum (measurable as the pressure on the wall of a theoretically absolutely cold vacuum cell, considered that effects of the zero-point radiation can be neglected). It means that, in the early Universe, the conventional component P_0 of total pressure P plays a synergic role in the expansion, acting directly dynamically within its bent space filled with cosmic stratum. (In the soap-bubble analogy, pseudo-pressure P could be represented by a *fictive* 'surface pressure' determined by the horizontal elasticity of the bubble membrane, where the pressure is working against the surface tension, still under the condition that the bubble membrane is bent; *horizontal* here means: ... being in every point of the bubble orthogonal to its radius.)

Anyway, the cosmological pseudo-pressure – in its prevalent part $(P - P_0)$ – seems to have an unknown *abstract physical character*.

On this place it would be emphasized that not even the conventional pressure-component P_0 can act dynamically on the expansion of the Universe if its infinitely extended space were not bent; such a situation would be identical to the situation with cosmological space tension in a Euclidean universe, as mentioned in Section 3. The conventional pressure-component P_0 can perform cosmological physical work only in the bent space, which is why it is possible to include it – by definition – into the notion of *cosmological pseudo-pressure*, in spite of its *concrete physical character*.

5. Alternative explanations of the apparent acceleration of the cosmic expansion

First option explaining in an unconventional way the apparent acceleration of the expansion of the Universe, as ascertained from the observations of the distant supernovae of type Ia, is the possibility that it is a manifestation of the cosmic expansion combined with relatively small oscillations. (The idea of the Universe with oscillating expansion rate appeared already long ago [20].)

The expansion is modulated by the oscillations going on within the whole volume of the 3-sphere simultaneously (i.e., being the oscillations with modulus $l = 0$). We use the notion 'simultaneously' in place of the expression 'on the hypersurface of the homogeneity', considering that the expansion of the Universe *is not* a physical motion in the sense of the SRT: The *recession* is not any cause of the SRT-time dilation because the recession rate is not a conventional physical velocity; two cosmologically distant fundamental observers can – in principle – simply introduce a common cosmic time (τ) and establish their cosmologically synchronous cosmic clocks (although it is possible to make of them a common time standard only after a mutual contact has been established and rather complicated connection arrangements have been made).[6] These conclusions are just implications of Weyl's postulate [17, p. 241]. The quasi-contemporaneity of the above mentioned oscillations on the globally cosmological scale is determined by the common initial conditions in the process of the world-start, while the problem of the causal horizon is possible to overcome rather by means of the existence of the EPR-phenomenon already performed in laboratories than by the speculative mechanism of cosmic inflation. It is not excluded that higher modulating harmonics related to the considered oscillations exist [15].

One might object that a 'Universe with oscillations' is not described by the FE and thus the idea is only an unjustified speculation, but the similar problem arises considering that the Universe is not ideally homogeneous while the FE is commonly applied. It is quite possible that both aspects – the oscillations and the deviation from the ideal homogeneity – are mutually determined.

The second option is similar to the possible explanation published by Ellis [8].

Our modification of the mechanism presented there is founded on the Horák gravitational law in fluids [14]. The law is logically explaining the mechanism behind the formation of the 'honeycomb-structure' of the cosmic matter with agglomerations forming isles in the centra of the cells. In addition to this explanation, according to the same law, the test particle (a galaxy) inside a spherical void, not having the central position there, must be expelled radially with an acceleration increasing with the distance from the center of the void; for more details, see the subsequent text. If our peculiar velocity (relative to a momentary co-local fundamental observer) were interpreted as a statistical fluctuation, and/or as a consequence of our only slightly non-central position in the void, then there would not be a conflict with the Cosmological principle[7] [4, pp. 628–631]. The problem is, however, the absence of more observationally founded indications. Anyway, we would prefer such an explanation

[6] The SRT-Lorentz transformation can be easily modified in such a way that it becomes relevant for the cosmology in the expanding Universe (Voráček, in preparation).

[7] The recently published Letter [26] about the Laniakea supercluster of galaxies yields a new view on our cosmological position. The impression is that we are situated roughly centrally in a local dense conglomeration with a diameter of about 160 Mpc ($= 520 \times 10^6$ light years) in a huge void. Any conflict with the Cosmological principle need not exist, since the highest probability for us as observers is to be situated in the central agglomeration or – rather less probably – within the wall of a cell in the honeycomb-structure of the cosmic matter.

before the option explaining the acceleration of the cosmic expansion by means of oscillations, presented above.

Here it is important to mention that the article published by [6] is consistent with the possibility of the existence of a cosmic void with a (roughly) central agglomeration of matter, in combination with our recently ascertained position in the Laniakea supercluster. The authors claim that they have found "evidence for a low-redshift transition of the deceleration parameter indicating that the acceleration has passed a maximum around $z \approx 0.2$ and now evolves towards a deceleration phase in the near future."

The presented results are qualitatively compatible with the mentioned Horák gravitational law in fluids, since:

(i) The central region of the cosmic honeycomb cell with the agglomeration of matter is characterized by infall accelerations/velocities being opposite to the cosmic expansion. (The dispersion owing to peculiar velocities is high.)

(ii) Farther out, when the average density of the matter and energy becomes lower than the average density of the cosmic stratum, the gravitational attraction is changing to the effective radial repellence increasing with the radial distance from the center of the cell, thus apparently contributing to the cosmic expansion with the resulting phenomenon of its acceleration.

(iii) Approaching the cell wall, the dynamic influence of neighboring cells causes the successive weakening of the repellence.

(iv) At the cell-wall the galaxies from a neighboring cell are penetrating into our cell and then oscillate relative to the wall. The oscillations are strongly damped thanks to high viscosity of the matter in the wall. A weak, still significant, deceleration with the top at $z \approx 0.6$ to 0.7 is apparent. Clearly, such a damped oscillative movement in the direction towards us can be the cause.

We realize, however, that the qualitative concordance does not mean that the theoretical explanatory model is a guarantee for a quantitative match with reality as well: With the $z \approx 0.7$ for the cell wall, it means that its proper distance from us is 10.7×10^9 l.y. ($= 3.3\,\mathrm{Gpc}$). Is a void with such a huge radius possible? Nevertheless, with the actual radius of the Universe r_0 greater than 340×10^9 l.y. (i.e. with $\Omega_{\mathrm{crit.}} < \Omega_{\mathrm{tot}} < 1.0046\ \Omega_{\mathrm{crit.}}$, or $\mathrm{d}r/\mathrm{d}\tau > 14.8\ c$) such 'megavoids' would still present less than one percent of the circumference of the Universe, and then the criterion of its cosmological homogeneity could still be fulfilled.

Nonetheless, even if the question of the acceleration of the cosmic expansion were eliminated, the problem of the dark energy and the dark matter in the Universe still persists.

6. Cosmological pseudo-pressure as a manifestation of the existence of the *dimensionally-elastic energy* of the bent cosmic space, filled with the homogeneous matter and energy of the cosmic stratum, appearing as the *dark energy*

In 2004 Ambjørn, Jurkiewicz, and Loll published an essay [1], where under assumption of the existence of the (3+1)-spacetime in the local Lorentz frame of reference and of the validity of the Causality principle (including the absolute – i.e. light – velocity) on the Planck-scale, together with the chosen topology of a three-sphere (S^3), a model of the macroscopic world is deduced with the use of the *Causal dynamical triangulations* (CDT). The resulting dimensionality of its spacetime is then (3+1), which is not a self-evident consequence of the assumed (3+1)-dimensionality on the Planck-level; anyway, it is equal to that one of the real spacetime of our Universe. We consider that it is reasonable to assume that the space-dimensionality on the medium-macroscopic scale-level in the Universe is an optimal natural solution/choice under the really existing conditions. The result of the above quoted essay is thus putting the dimensionality choice, made on the Planck-scale-level, into the context with the physical reality characterized by the naturally optimal dimensionality of our world on the medium-macroscopic scale-level. As the chosen topology (S^3) is the same both for the quantum and macro worlds (inclusive the cosmological scale), the conclusion can be made that the used CDT-method is at least self-consistent. The assumption of the S^3-topology can however be legitimized as well, and thus, the status of the CDT can change from self-consistency to compatibility with reality. The justification of the assumption is based on theoretical deduction, which has been made by [12], [13] and successively developed and modified by us [30], [35][8], together with the result of the measurements of the Planck space telescope, revealing that no evidence for a multiply-connected topology has been found [23]. Moreover, as the authors of the essay mention, the Euclidean dynamical triangulations always gave results inconsistent with reality. It is important that the CDT-deduction also yields two other results: The first of them means that the pertinent model universe must be expanding, which is in accordance with the GRT (giving the Friedmann equation, which describes the expansion of the Universe), as well as with the observed reality. The second result has a quite new impact. It states that there exists the positive cosmological 'constant' of matter-energy quality, being 'consumed' in the process of the expansion. Such a conclusion is permitted by the GRT, yet it is not *obligatory* there, while the CDT makes it *necessary*.

We developed the explanatory model for the dark energy and the dark matter

[8]The closedness of the Universe can also easily be logically deduced from the quantum concept of the photon, which, however, is not generally sustained: A photon cannot be emitted if its future reception is not guaranteed (by entanglement?). Then, if our Universe were open, the engineers at any municipal street illumination central would take notice of that the electricity consumption is significantly lower at the nights with a clear sky than during nights when the sky is covered by clouds.

that uses the quoted results, namely the possible relation between the closedness of the Universe and the positive cosmological 'constant'.

On the medium-macroscopic scale-level, the (3+1)-spacetime of our Universe is practically flat; of course, only if the local gravitational fields are not considered. The S^3-topology has no measurable impact on the space geometry; the space on that level is thus practically perfectly Euclidean. On the cosmological level, however, as previously pointed out, in the closed Universe with the trivial topology, the necessity of the existence of the fourth spatial dimension for its adequate description appears explicitly (as the radius of the Universe) or implicitly (as the curvature radius of its space). Consequently, it means that the bending of the cosmic space into the fourth space-dimension is a deviation from the optimal number of space dimensions, which is three. (In other words, it is a deviation from the space-'Euclidicity'.) If the space of the Universe is filled with the matter and energy of the cosmic stratum, the situation necessarily leads to the origin of an elastic energy (the cosmological 'constant' of the CDT) and to a tendency to 'rectify' such a space in order to make it 3-dimensional and Euclidean. Such a tendency thus apparently has a character of cosmological pseudo-pressure P considered above. The positive *dimensionally-elastic energy* of the bent cosmic space filled by the matter and energy of the cosmic stratum, related to the pseudo-pressure is – as a consequence – the source of the gravitational field. On the scale-level of the homogeneity of the cosmic stratum it is possible to identify this energy as the enigmatic *dark energy* in the Universe.

In the 3-D demonstration diagram this energy would be represented as an energy of deformation of a matter-rich plane into the spherical shell. Such a practically technically hardly performable deformation is much more easily possible to represent by a slice being closely similar to its section by the plane (Fig. 1a), i.e. by an elastic blade closed into a circle (similar to a clock spring, but only with one winding – not a spiral), which struggles to rectify itself.

The situation in the smooth elastic bent blade, corresponding to the state in the phase of the early (radiation-dominated) Universe being highly homogeneous, is possible to demonstrate in such a manner that a certain part of the energy of the deformed spring is determined by a conventional pressure (caused, e.g., by its high temperature) that is isotropic in the horizontal plane of the blade. (Recall the fictive 'surface pressure' in the bubble model.) The adjacent pressure-energy in its hot material is analogously relevant to P_0, while its part relevant to pressure-component $(P - P_0)$ is caused by the very deformation, i.e. the bending of the blade into the circle in the cold state.

7. Appearance of the *dimensionally-elastic* energy as the *dark matter* in the Universe having a hierarchic structure

In the era of the matter-dominated Universe, characterized by the hierarchic heterogeneity, the omnipresent bending of the cosmic space is interacting with the hierarchic deviations of the local density of the matter from the average density of the

Universe, i.e. with deviations from its ideal homogeneity. The adjacent hierarchic dimensionally-elastic energy is then identifiable as the *dark matter*.[9] The mechanism of its behavior is not determined just by the magnitude of the deviation of the local matter and energy density from the average density of the Universe; it is much more complex, since the only possible link can be the local gravitational potential energy of the hierarchic deviation, which is determined by four – hitherto more or less unknown – rules:

(i) *The gravitational potential energy is related to that locality in the gravitational field, which is logically physically relevant to a given situation* [28].

The conclusion follows from the theory of GR-Hamiltonian (i.e. the total energy) of a test particle applied for mechanics of the free particle in a local gravitational field, where the potential energy would be related to the locality of a standard observer. In the case of a hierarchic matter-formation, being the deviation from the ideal homogeneity of the cosmological stratum, the potential gravitational energy of the matter in such a formation, with a density deviating from the cosmic average value, would be related to its center of gravity[10]; consequently, it is positive, with a value of zero in its center.

(ii) *The potential energy of a test particle in a gravitational field is localized in the particle* [7, p. 86, Section 6.4] – as a conjecture, or Voráček – as a hitherto unpublished proof).[11]

(iii) (a) *The hierarchic dimensionally-elastic energy – i.e., the dark matter – manifests first on such a distance-scale from the center of gravity of a hierarchic formation, which is significant in the context with the scale of effectivity of the determining bending of the cosmic space.*

(b) *On the other side, for the identical reason, the same energy manifests significantly locally in a sub-region of the hierarchic formation only if the sub-region has a sufficiently large space-extension.*

Sub-rule (a) is explaining why the dark matter manifests only outside the central regions of galaxies, while sub-rule (b) excludes the possibility that single stars, solar systems, or small star-groups could be connected with the dark matter in spite of their high baryon-density. Thus, both sub-rules together can answer the

[9]The idea that the phenomena of dark energy and dark matter have one common explanation appears also in the essay of [5]. In consistence with our solution presented here, Capozziello proposes the opinion that the cause need not be conventional energy and matter having the form of some "exotic ingredients", but that both are the curvature effects, and that the solution to the problem (being presented as well in the mentioned article) does not pertain into the frame of the actually presented form of the General relativity theory. In the rest of the essay, however, the key ideas of our solutions of the enigma are mutually quite different.

[10]We consider such an application of the rule above being a logically well-motivated conjecture.

[11]The rules (i) and (ii) together give a simple logical solution to the 'arch-problem' of localization of gravitational energy in the GRT.

question why the lumps of baryonic matter forming the relatively small galactic satellites and more external parts of spiral arms, both being more distant from the center of gravity of a galaxy, yet having enough significant space-extension, usually are rich in dark matter. The rules can also explain – quite logically – why the great sub-galactic agglomerations of apparently thin baryonic gas at great distances from the mother-galaxy become the dark matter-abundant formations. On the contrary, sub-rule (a) is explaining why the dark matter is not appearing gravitationally in the central regions of galaxies, despite the matter density being highest right there (Fig. 5) [12]. The query why the clusters of galaxies are – on average – evenly penetrated by the dark matter can be answered in such a way that it is generated by galaxies mutually gravitationally interacting on the huge distance-scale, while the intergalactic space in the cluster is practically baryonic matter-empty (picture reference 1: *El Gordo*). The gravitational potential in the group of galaxies has a high absolute value (when compared to the average cosmic value), but its space-gradient is low, namely in the central part of the group [25]. The single galaxies in the galaxy-clusters evidently have a much higher dark-matter density than the clusters on average; the cause is the value of underlying baryon-density and their sufficient space-extension.

(iv) *The basic explanation of the phenomenon of dark matter indicates that the mechanism of its origin is working in a convergent feedback.*

Such a feedback is local, which means it *seemingly* increases the local baryon-density at its locality, while the *cosmological bending of space is not influenced on the local scale-level*. (The feedback-influence on the bending of the space on the cosmological scale-level will be considered in the subsequent text.) At this place, the enigma of the Bullet Cluster [11], (picture reference 2: *Bullet Cluster*) and of the Musket Ball Cluster (picture reference 3: *Musket Ball Cluster*) is easily solvable: During the penetrative meeting of two groups of galaxies, the thin intergalactic gas in the groups collided, while their 'dark matter', together with the galaxies generating the same 'dark matter' passed without collisions. According to our view of the substance of the 'dark matter' in the galactic clusters, presented above, the absence of its interaction is quite logical.

It is possible to demonstrate the function of some of the rules above in a simple didactic manner using again the blade of the steel spring, where the thickness of its material represents the hierarchic density variations of the baryonic matter and energy in the cosmic stratum (Fig. 2, 3, 4, and 5).

In the qualitatively rough approach, it is possible to state that the *apparent distribution* of dark matter in the centrally spherical galactic cloud is compatible with the current knowledge of the galactic dynamics, if an axially symmetric ring of

[12]The apparent absence of dark matter in the galactic region of the Sun [2] might be explained by rules (a) and (b) together, considering that the distance from the center of the Galaxy is not too great and that the considered regions are not too large.

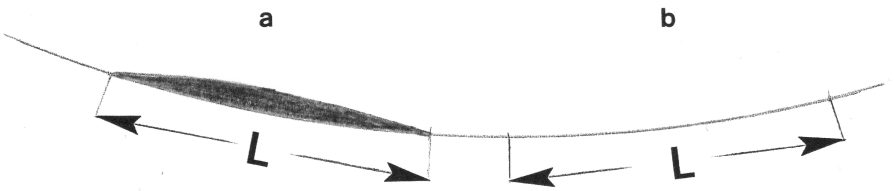

Figure 2: In situation (a) a much higher elastic energy is present on the length-scale L in the region with high local density of matter, determined by the hierarchic structure of cosmic stratum, than is the case on the same scale in situation (b) in the region with the homogeneous stratum having an average cosmological density. In both situations, the degree of the cosmological bending of the cosmic space is the same. (Yet, it must be pointed out that we realize that we are borrowing here the spatial hyperdimension in the demonstration diagram for an explanation of the role of the thickness of the steel blade.)

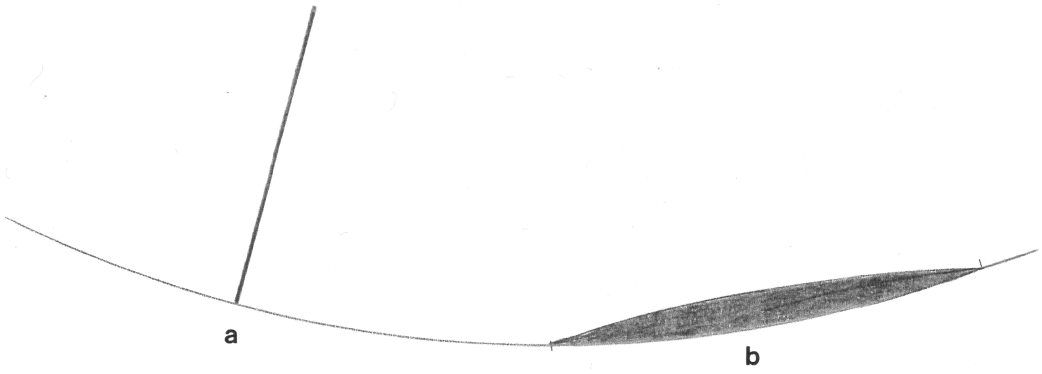

Figure 3: (a) The region of the sharply increased (needle-shaped) thickness of the spring blade contains less elastic energy than (b) the wide region with moderately increased thickness.

gravitationally effective dark matter is extending in the galactic plane from a certain radial distance outwards [3, Section 3.3].

The presented explanation of the phenomenon of dark matter is also consistent with the existence of extremely diffuse galaxies [27].

During the early epochs with a small radius of the Universe, i.e., with the higher degree of the bending of its space, the dark matter – quite logically – was bound much more 'eagerly' to the localities with relatively less outstanding positive density deviations (from the average value) in the baryonic matter. It means that then it is possible to explain why the conglomerates of the dark matter observed at great distances are smaller and more rich in details than those relatively close to us. It also explains the possible mechanism of the transfer of the energy of pseudo-pressure P into the dark matter and the rate of such a process: The small hierarchic inhomogeneities had a great qualitatively effective capacity to appear as holders of the

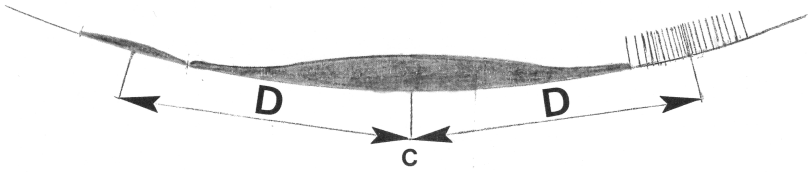

Figure 4: The galactic satellite with the hierarchic gravitational binding to a massive galaxy at great distance D from center of gravity C of the galactic system is demonstrated by a small, but still significant, increment of the thickness of the blade. The density of the baryonic matter in the galactic satellite is sometimes observed to be very low, while the dark matter-density is gravitationally significant [9]. Here it is also possible to explain (zoomed at right) why the stars in the galactic satellites (and – as a matter of fact – even the stars in galaxies) have not their adjacent dark matter components of their masses localized 'sharply' at their places: Consistently following such a (false) idea, it would be necessary to consider them as very long and thin needle-shaped isolated sources of gravitation as presented in Figure 3a; then, the single stars cannot cause a 'sharp' appearance of a significant quantity of dark matter, and this is why they play a relevant role solely in great quantities and then merely as extended diffuse objects.

dark matter already at the first stages of the matter-dominated era with a small radius of the Universe. Later, the bending of the space was diminishing owing to the expansion of the Universe, but the hierarchic inhomogeneities were increasing with time, as well as the contrasts of their baryonic matter-density. The actually observed picture of the early development thus appears as rather complex in order to be interpreted simply in an adequate manner; yet it is possible that the morphology of great hierarchic formations at huge distances is observed to be rather fuzzy and – as a consequence – the sub-groups of small distant hierarchic inhomogeneities with relatively low contrast, appear as coalesced into the huge 'monolithic' mega-formations. Another option is, that the ascertainment of huge monolithic conglomerations of dark matter at great distances is not charged by an observational fuzziness, but that it has a real ground in (i) their enormous space-extension and (ii) the high degree of the cosmic space-bending, while (iii) the deviation of their baryon-density from the average cosmological value were still very low (picture reference 4: *Three-Dimensional Distribution of Dark Matter in the Universe*).

8. The *cosmological feedback*

The dark matter and dark energy are the strong sources of the gravitational field of the Universe, i.e., they are strongly contributing to the effective average density of the cosmic stratum, and thus, they also *globally* determine the bending of the space in the Universe. As a consequence, in such a mechanism, they become the sources of the gravitational cosmic field in the feedback. Then, being both determined by the

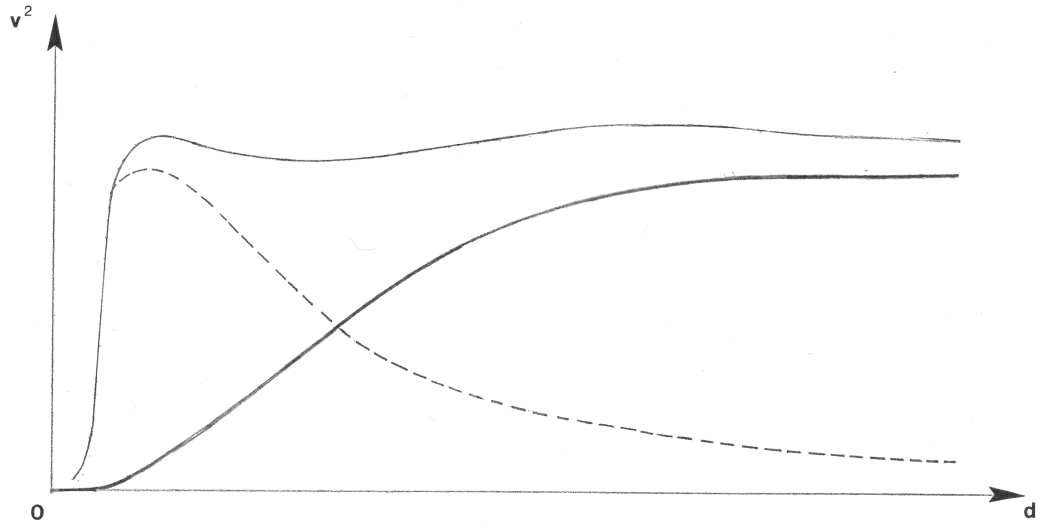

Figure 5: A qualitative diagram explaining the ascertained typical distribution of the total gravitational matter-energy in an 'average' galaxy. It is a composition of the appearance of a classical gravitational field of the baryonic matter and the influence of the cosmological bending of the space in the hierarchical environment of the galaxy appearing as the dark matter, with reference to rule (iii-a) above. In the diagram are plotted squares v^2 of the observed values of orbital velocities in the galactic disc (smooth line), their expected values (dashed line) and their respective differences caused by the presence of dark matter (bold smooth line), in relation to radial distance d from the galactic center.

same bending of the cosmic space, it is possible to describe them mathematically together by means of a sum of an infinite geometric series with quotient q:

$$\overline{\rho}_{tot.} = \frac{\overline{\rho}_{\mathrm{bar.}}}{1-q}, \tag{16}$$

where $\overline{\rho}$ are the average cosmological relative values ($\overline{\rho}_{tot.} = 1$) of the respective densities. Since $\overline{\rho}_{bar.}$ for our epoch has the value 0.049 (which means that 4.9% is the relative density of the baryonic matter), we obtain for feedback-quotient q the value equal to 0.951.

Any retardation of information about the state of the homogeneous Universe is (according to the Standard model) eliminated as:

(i) The cosmological space bending is for a given epoch τ the same in the whole Universe.

(ii) All hierarchic inhomogeneities have a scale lying under/within the causality horizon for every fundamental cosmological observer.

The dark energy and dark matter are determined by the bending of the cosmic space, i.e. – more generally – by the curvature of the spacetime of our Universe. Since the spacetime curvature is tightly related to the gravitation, it is possible to state that the gravitational interaction is the mediating agent in the phenomenon of appearance of both dark energy and dark matter.

9. Entropy of the dimensionally-elastic energy

In our previous paper [33] the entropy of the dimensionally-elastic energy was denoted (in a rather intuitive manner) as the entropy appertaining to the expansion of the Universe. Now we can present the same idea more precisely: It is the entropy appertaining to the energy that is the direct cause of the expansion of our Universe, which is possible to claim since the matter and energy are merely two qualitatively different forms of the same substance. Also, the conclusion was made that the *total generalized entropy* of a closed universe, being a totally isolated reversible and cyclic system, is constant. Its reversibility is determined, besides the closedness of the Universe, exclusively by the Planck density of the matter-energy, as the only parameter characterizing the cosmic stratum at the world-start (big bang) and world-end (big crunch). In the cosmology it is possible and useful to normalize such entropy to zero, as the mentioned parameter is unique for the Universe[13].

Thus, in the same manner as total entropy $\mathscr{S}$, the *specific entropy*, defined as

$$\mathscr{S}_0 = \mathscr{S} V^{-1}, \tag{17}$$

is consequently normalized. In the formula, V is the volume of a closed compact universe, as specified by relation (7). (In cosmology it is reasonable to relate specific entropy $\mathscr{S}_0$ to volume V as the sole – for the intended purpose available – parameter, being well-defined during the whole process of evolution of the Universe; thus, specific entropy $\mathscr{S}_0$ becomes the *generalized entropy-density*.) Actually, the total generalized entropy of the cosmic stratum filling the cosmic space consists only of two components, one being the entropy of the dimensionally-elastic energy and the second, the entropy of the baryonic matter with all possible conventional forms of energy pertaining to it. Their sum is the *generalized entropy*, which is the constant equal – as we choose – to zero, while the entropy of the baryonic matter-component is positive.

Then, the entropy of the dimensionally-elastic energy necessarily must be negative. Yet, from our perspective it is impossible to decide whether the absolute values of the entropy-components are increasing or decreasing with the cosmic expansion. (In [33] it was assumed that they are decreasing, but today we realize that such an assumption was not reserved enough.) It is however plausible to claim that the

[13]We consider that the volume of the Universe at its start has a value resulting from the laws of the GRT and quantum physics. A thorough explanation of the idea, however, lies outside the frame of this essay. (Here it can only be said that the validity of the Law of mass-energy conservation is the starting point of the explanation.)

absolute values of respective entropy-densities are decreasing. Such an outstanding character of those densities is determined by the fact – being special for cosmology – that for the rate of expansion of the Universe the condition $\mathrm{d}r/\mathrm{d}\tau \gg 1$ (where $c = 1$) is valid in the decisive stages of its evolution; actually, the rate is still greater than one[14]

10. Course of the generalized total entropy and its components during the evolution of the Universe until now

(a) During the short era of the very beginning of the Universe, its stratum consisted exclusively of unified bosons, which can be called 'hyper-photons'; in terms of thermodynamics, it consisted of the ideal adiabatic photon-gas, which is extremely ultra-relativistic and homogeneous. The pressure of the gas during those short moments is possible to identify with concrete conventional pressure P_0, being at that time the only component of total cosmological pseudo-pressure P. The pressure-energy of the photon-gas may be of use in the process of expansion only in the positively bent cosmic space, i.e. in the closed Universe, while the same energy is determined by the pertinent bending. (For more details, see [35].) In this sense, the pressure-energy of the photonic gas could still be considered (which we will anyhow avoid in the subsequent text) as a kind of dimensionally-elastic energy, even though it can be specified to be the sum of the energies of the single photons; regarding the cosmic expansion, it is possible to claim that "the space, in such a special manner, struggled to establish its optimal dimensionality (i.e. the 'Euclidicity')". The pressure-energy of the photonic gas had been consumed during that era solely for the compensation of the negative[15] cosmological potential energy of (as assumed) closed Universe in the process of the cosmic expansion; the mechanism is quite similar to the gravitational redshift of the photons moving outwards in a local gravitational field, when a photon is moving from one place to another with a successively diminishing absolute value of the (negative) gravitational potential at the respective places.

From the viewpoint of thermodynamics, the energy consumed for the expansion of the Universe is analogous to the work done be the expanding ideal gas pushing on a piston in an adiabatic process. *If* the stratum of the Universe forever remained *only* in the form of homogeneous photon-gas, its pressure P_0 (with

[14]The value of $\mathrm{d}r/\mathrm{d}\tau$ can actually be equal, very roughly, to 21 ± 2, if the results from the Planck space telescope are regarded. Assuming a closed Universe, the result of the Planck space telescope by itself limits this value to be greater than 19 [22], [23]. Thus, since the positive entropy-density component of the cosmic stratum is decreasing owing to the expansion of the Universe, the conditions are given for the origination of local sources and sinks of energy, as well as for the formation of the hierarchic systems on subsequently increasing space scales, i.e., of the process of *self-organization* of the baryonic matter filling our Universe.

[15]In consistence with the FE (4), the cosmological potential energy is negative when it is related to the epoch of the maximal expansion, while the FE is considered to be the Law of mass-energy conservation applied to the Universe.

the physical character described above) would be non-negligible even at the epoch of maximal expansion, being still/constantly in equilibrium with the space tension Σ, while $\mathrm{d}r/\mathrm{d}\tau$ momentarily would be equal to zero. Neither dark energy nor dark matter would exist.

Knowing the character of the adiabatic photon-gas, as described in Section 4, its picture presented there is hereby completed; the usual concept of entropy of the cosmic stratum, being hitherto constant, need not yet be generalized. We put that entropy equal to zero, which was motivated in Section 9; its value is usually considered to be quite arbitrary, or it has another fixed value motivated in another way [10, p. 99]. Anyway, from the Planck era the photonic gas is starting with an entropy, which is the maximal possible in the given situation.

(b) The character of the composition of the cosmic stratum, however, began to change already in the consecutive – still very early – stage of the expansion of the Universe. The original pressure-energy of the photonic gas (being *always* equal to the sum of the energies of the single photons), besides the overwhelming consumption of it by the above mentioned energetically 'voracious' expansion of the Universe, began to transform to *baryonic matter*. (The notion 'baryonic matter' – as it is used in this paper – comprises all non-photonic elementary particles[16] together with their kinetic energies relative to a fundamental cosmological observer, as well as their mutual binding energies.) Together with the origination of the baryonic matter the adjacent dark energy (together with its feedback component) was also arising, undoubtedly in a process of transformation from the pressure-energy of the photon-gas. Further, it is needed to take note that in the era we consider, the cosmic stratum was still highly homogeneous on the scale-level higher than that of elementary particles, and thus, the dark matter was not yet present; the very dimensionally-elastic energy consisted exclusively of dark energy. That era could possibly be called the 'era of mixed photon-baryon Universe'.

Pressure P_0 of the photon-gas was becoming less and less significant and the value of the constant on the right-hand side of equation (15) was diminishing, caused by the decrement of the total number of photons in the Universe. In spite of this, the remaining photon-gas was still adiabatic (as is the state of the CBR, which actually has a cosmologically quite negligible total energy). Then, the entropy of the remaining photonic gas is not changing, i.e., it is constantly equal to zero, as originally chosen. It is so, because at any epoch, with a given value of the right-hand side of equation (15), the process is – at least potentially – reversible (which means – if the conversion to baryonic matter was stopped at the same moment).

[16]The term 'non-photonic elementary particles' here refers to particles not moving at the absolute velocity c. The term 'baryonic matter' is used because we could not find a proper established adequate term.

Now the notion of the total entropy of the Universe needs to be generalized. It split into three components with the sum equal to zero, as explained in Section 9. The concept of the (zero-)entropy of the remaining photon-gas need not be changed, as already indicated above, while the positive entropy of the baryonic matter must be generalized, because its form can differ very strongly from the aggregation state of a gas. The same conclusion is applicable for the dimensionally-elastic energy, since its form is quite abstract; anyway, its generalized entropy-component is necessarily negative.

(c) The end of the mixed photon-baryon era is characterized by the decrease of photon pressure P_0 to the values so low that the relevant energy-component becomes cosmologically negligible. After the establishment of the baryon-dominated Universe, the whole effective pressure P has the form of the abstract representative pseudo-pressure. The extremely high expansion rate $\mathrm{d}r/\mathrm{d}\tau$ of the Universe manifested itself in the earliest eras in form of enormous recession rate already on the scale of elementary particles, which probably made the process of photon transformation into baryonic matter quite necessary. The expansion, still having the high rate, caused rather later that statistical fluctuations in the density of the baryonic matter could not dissipate, yet — just oppositely – they diverged. It resulted necessarily in the dehomogenization of the cosmic stratum on a successively increasing scale of extension in the space, from the scale of elementary particles in the earliest beginning-epochs to the scale of super-groups of galaxies much more later.

In the angle of view of thermodynamics, the divergent fluctuations in the density of the baryonic matter created local sources of energy – the stars, together with the effective energy-sinks (for the radiation produced by the stars) in the form of cavities – the voids. In such a way, the local regions arose where the respective local thermodynamic systems became open and where the cosmic baryonic stratum were not in a state of thermodynamic equilibrium. As a consequence, the conditions for validity of the second law of thermodynamics were not fulfilled there, which means that deviations from the validity of the law could appear there, and thus, the entropy in the considered regions could locally decrease. The process (still actually) manifests as *self-organization* of baryonic matter. In conventional physics, such a process in one locality must be followed by an increase of entropy in another place. In cosmology, however, the process of the hierarchic self-organization of the cosmic stratum is determined by the very special condition of the high expansion rate of the Universe, together with the (not just locally, but on average) decreasing entropy-density of the baryonic matter. Thus, a local entropy-decrement at the given place, which is a manifestation of the process of self-organization in the baryonic matter of the cosmic stratum, need not have, as a consequence, any local entropy increment in some other place. Nonetheless, the local entropy decrement (being practically the same notion as the decrement of the entropy-density) of the baryonic matter is compensated at

a given place by the *co-local* increment of the *negative* entropy (being practically the same notion as the increment of the entropy-density) of the dark matter.

In the hierarchically dehomogenized cosmic stratum, the energy of pseudo-pressure P consists only of the dimensionally-elastic energy in the forms of the dark energy and dark matter together.

The last logical query at this moment is: From what source came the dark matter that arose in the era when the pool of energy of photon-gas, with photons of significant individual energies and of sufficient numerical density, was already empty? Only two possible sources existed: (i) The pool of dark energy, which was partially consumed in the pertinent process, and/or (ii) a part of the already existing baryonic matter. In spite of the fact that no mechanism of transformation of the baryonic matter into dark matter is mentioned in the – for us known – literature, we consider that the existence of such a mechanism is not completely excluded. For instance, a new description of the physics at the event horizon of black holes [34], and/or the impact of the expansion of the Universe on peculiar velocities in its stratum [32, pp. 405–408] or – equivalently – [16, formula (2.30), p. 38], seems to us a possible, though rather complex, solution to the present query.

References

[1] Ambjørn, J., Jurkiewicz, J., and Loll, R.: 2004, "Emergence of a 4D World from Causal Quantum Gravity", arXiv:hep-th/0404156v4, 16 Sep 2004.

[2] Bidin, C. M., Carraro, G., Méndez, R. A., and Smith, R.: 2012, *Astrophys. J.* **751**, 30.

[3] Binney, J. and Tremaine, S.: 1987, *Galactic Dynamics*, Princeton University Press, Princeton, New Jersey.

[4] Blanchard, A.: 2010, *Astron. Astrophys. Rev.* **18**, 595.

[5] Capoziello, S.: 2012, *Mem. Soc. Astr. It.* **83**, 1054.

[6] Cárdenas, V.H., Bernal, C., and Bonilla, A.: 2013, *Mon. Not. R. Astron. Soc.* **433**, 3534.

[7] Cooperstock, F.I.: 2009, *General Relativistic Dynamics*, World Scientific, New Jersey.

[8] Ellis, G.: 2011, *Classical and Quantum Gravity* **28**, 164001.

[9] Geha, N., Willman, B., Simon, J.D., Strigari, L.E., Kirkby, E.N., Law, D.R., and Strader, J.: 2009, *Astrophys. J.* **692**, 1464.

[10] Gorbunov, D.S. and Rubakov, V.A.: 2011, *Introduction to the Theory of the Early Universe: Hot Big Bang Theory*, World Scientific.

[11] Harvey, D., Massey, R., Kitching, T., Taylor, A., and Tittley, E.: 2015, *Science* **347**, 1462.

[12] Horák, Z.: 1963a, *Bull. Astron. Inst. Czech.* **14**, 117.

[13] Horák, Z.: 1963b, *Bull. Astron. Inst. Czech.* **14**, 119.

[14] Horák, Z.: 1984, *Bull. Astron. Inst. Czech.* **100**, 1.

[15] Karlsson, K.G.: 1971, *Astron. Astrophys.* **13**, 333.

[16] Kolb, E.W. and Turner, M.S.: 1990, *The Early Universe*, Addison-Wesley Publishing Comp., Redwood City, California.

[17] Lambourne, R.J.A.: 2010, *Relativity, Gravitation and Cosmology*, Cambridge University Press, New York.

[18] Lawden, D.F.: 1982, *An Introduction to Tensor Calculus, Relativity and Cosmology*, John Wiley & Sons, Chichester.

[19] Misner, C.W., Thorne, K.S., and Wheeler, J.A.: 1973, *Gravitation*, W.H. Freeman and Co., San Francisco.

[20] Morikawa, M.: 1991, *Astrophys. J.* **369**, 20.

[21] Perlmutter, S.: 1999, *Astrophys. J.* **517**, 565.

[22] Planck Collaboration: 2014a, *Astron. Astrophys.* **571**, A16.

[23] Planck Collaboration: 2014b, *Astron. Astrophys.* **571**, A26.

[24] Riess, A.: 1998, *Astron. J.* **116**, 1009.

[25] Sarli, E., Meyer, S., Meneghetti, M., Konrad, S., Majer, C.L., and Bartelmann, M.: 2014, *Astron. Astrophys.* **540**, A9.

[26] Tully, R.B., Courtois, H., Hoffman, Y., and Pomarede, D.: 2014, *Nature* **513**, 71.

[27] Van Dokkum, P. G., Abraham, R., Merritt, A., Zhang, J., Geha, M., and Conroy, C.: 2015, *Astrophys. J. Lett.* **798(2)**, L45.

[28] Voráček, P.: 1979, *Astrophys. Space Sci.* **65**, 397.

[29] Voráček, P.: 1983, *Astrophys. Space Sci.* **91**, 5.

[30] Voráček, P.: 1985, *Astrophys. Space Sci.* **116**, 197.

[31] Voráček, P.: 1986a, *Astrophys. Space Sci.* **122**, 327.

[32] Voráček, P.: 1986b, "The Relativistic Retardation of Deviations from the Hubble Flow in Early Epochs of the Closed FRW-Universe: A Possible Mechanism" in *Proceedings of the 26th Liège International Astrophysical Colloquium, July 1-4, 1986: "Origin and Early History of the Universe"*, Université de Liège, Cointe-Ougrée.

[33] Voráček, P.: 1991, *Astrophys. Space Sci.* **186**, 157.

[34] Voráček, P.: 1997, "Planck membrane - a domain of co-existence of the GRT and quantum physics – substituting the event horizon of the black hole taking the form of a 'frozen star'.", Contribution to *Gravity Research Foundation* contest.

[35] Voráček, P.: 2008, *Bull. Czech. Soc. Mech.* **2**, 21 (in Czech).

Picture references

1 "El Gordo" Galaxy Cluster
`http://www.nasa.gov/press/2014/april/nasa-hubble-team-finds-monster-el-gordo-galaxy-cluster-bigger-than-thought/`

2 Bullet Cluster
`http://chandra.harvard.edu/photo/2006/1e0657/`

3 Musket Ball Cluster
`http://chandra.harvard.edu/photo/2012/musketball/`

4 Three-Dimensional Distribution of Dark Matter in the Universe
`http://hubblesite.org/newscenter/archive/releases/2007/01/image/e/`

Conference *Cosmology on Small Scales 2018*
Michal Křížek and Yurii Dumin (Eds.)
Institute of Mathematics CAS, Prague

SURROUNDING MATTER THEORY

Frederic Lassiaille

Nice, France
frederic.lassiaille@yahoo.fr

Abstract: S.M.T. (Surrounding Matter Theory), an alternative theory to dark matter, is presented. It is based on a modification of Newton's law. This modification is done by multiplying a Newtonian potential by a given factor, which is varying with local distribution of matter, at the location where the gravitational force is exerted. With this new equation the model emphasizes that a gravitational force is roughly inversely proportional to mass density at the location where this force is applied. After presentation of the model, its dynamic is quickly applied to cosmology and galaxy structure. Some possible caveats of the model are identified. But the simple mechanism described above suggests the idea of a straightforward solution to the following issues: virial theorem mystery, the bullet cluster (1E 0657-56 galaxy clusters) issue, the strong relative velocity of its sub-clusters, the value of cosmological critical density, the fine tuning issue, and expansion acceleration. Nucleosynthesis is not explained and would require a different model for radiation era. But a de Sitter Universe is predicted, this means that the spatial curvature K is 0, and today's deceleration parameter q is -1. The predicted time since last scattering is $68\,h^{-1}$ Gyr. With this value SMT explains heterogeneities of large scale structure and galaxy formation. Each kind of experimental speed profile is retrieved by a simulation of a virtual galaxy. In the simulations, ring galaxies are generated by SMT dynamic itself, without the help of any particular external event. Those studies give motivation for scientific comparisons with experimental data.

Keywords: gravitation, dark matter, dark energy, galaxy

PACS: 95.35+d, 98.80.-k, 98.35.Hj

1. Introduction

This article presents Surrounding Matter Theory (SMT), and is a very quick survey of its predictions and results. This model is an alternative to dark matter in solving today's gravitational mysteries. The solving principle is a modification of Newton's law. SMT is composed of 1 equation and 2 parameters. This simplicity allows a robust survey of the model, and restricts enormously the amount of possible

regression on other parts of physics. Stated in one sentence, the whole behavior of those equations is that a gravitational force is inversely proportional to matter density at the location where the force is exerted. The first motivation is an old one: Machs principle [1]. Here an attempt is made to express fully this principle by getting the ratio of inertial to gravitational mass, or let us say a $\ll$ modified $G \gg$, directly coupled to matter. And to avoid any resulting changes in the local behaviour of matter, and the local equations of motion, the first idea is to restrict this variation to large distances only. The second idea is a novelty: relating this G variation only to matter located at the location where the force is exerted. This will keep valid linearity with attracting matter. The second motivation concerns General Relativity (GR). Indeed, in GR, the Bianchi identity and the resulting null covariant divergence $\nabla G_{\mu\nu} = 0$ of the Einstein tensor is linked directly to energy conservation $\nabla T_{\mu\nu} = 0$ of $T_{\mu\nu}$, the stress-energy tensor, via Einstein equation. But one could notice that the first one comes from pure geometry, whereas the second one comes from physics, namely energy conservation physics principle. This leads me to consider the possibility that those 2 equations are not directly binded together, but could rely on one another through a more complex relation. In particular, I allowed for the Einstein tensor not to be proportional to the stress-energy tensor but rather to be a more general function of it. Furthermore, for reasons such as linearity with respect to energy, I was led to the form $G_{\mu\nu} = \kappa C^{\rho}_{\mu} C^{\sigma}_{\nu} T_{\rho\sigma}$. Here κ is the multiplicative constant of Einstein equation. Furthermore C^{ν}_{μ} is a mixed tensor which remains to be calculated using the GR case and the non relativistic limit. For the latter this modification undergo to the simple modification of a gravitational potential. This led to $\Phi = C_{SMT}\Phi_n$, where Φ is the final gravitational potential, Φ_n is a Newtonian potential and C_{SMT} is a varying factor, being a function of matter density at the location where the force is exerted. Today's gravitational mysteries are solved or partially solved using various different theories, for example in [2]–[8]. After the SMT description, its dynamic will be illustrated in the context of the appearance of those mysteries.

2. The model

As introduced above, the starting point is the following gravitational potential equation

$$\Phi_n = -\frac{MG}{x}, \tag{1}$$

where x is the distance from an attracting infinitesimal object, M the mass of this object and G is gravitational constant. The model consists of modifying this equation. Three more variables are added. The first one is ρ, mass density calculated in a sphere of ray $r_{\max}$ around the location where the force is applied. This sphere will be called the $\ll$SMT sphere$\gg$: in this document. There is $r_{max} = 10\,h^{-1}\,\mathrm{kpc}$, h being Hubble constant in units of $100\,\mathrm{km\,s^{-1}\,Mpc^{-1}}$. Using $H_0 = 68\,\mathrm{km\ s^{-1}\,Mpc^{-1}}$, there is $r_{\max} \simeq 15\,\mathrm{kpc}$. It is this r_{max} value which will be used in this document.

ρ_0 is today's value of ρ in the vicinity of the Sun. It will be used: $\rho_0 = 0.98\,\mathrm{km/m^3}$. The modified potential equation is the following

$$\Phi = -\frac{MG}{x} C_{\mathrm{SMT}} = -\frac{MG}{x} \frac{\alpha_0 \rho_0 + \rho_{u0}}{\alpha \rho + \rho_u}. \tag{2}$$

The second variable is ρ_u, the Universe mass density. ρ_{u0} is today's value of ρ_u. The third variable is α, which can be set to 2 values only. There is $\alpha = \alpha_0 = 1.6 \times 10^{-5}$ inside the galaxies, and $\alpha = 1$ outside any galaxy. Those values are stated to be independent of Universe expansion.

3. Relativistic version

In the equation giving C_{SMT}, through a Lorentz transform, each parameter on the numerator evolves exactly the same way as its corresponding counterpart in the denominator. The result is that C_{SMT} is a Lorentz invariant.

The first remark before searching for a relativistic version is the role of M in equation (1) and (2). Since C_{SMT} depends only on matter at the location, where the force is exerted, it does not depend directly on M. Therefore, like equation (1), equation (2) shows acceleration as being linear with respect to attracting matter (M). This is a distinctive characteristic of SMT as a modification of Newton's law. Only variations with distance (x), and G (in some sense, because it is in fact $C_{\mathrm{MT}}G$) are modified, not variation with M. One could even guess that this characteristic would hold with the relativistic version of SMT. Now modifying Einstein equation with a metric related scalar would not give back equation (2) as the non relativistic limit. It would be the same with any scalar-tensor theory [9], which would finally add a scalar tensor to the physical stress-energy tensor. Einstein modified equation would not show its left-handed term as being strictly linear with respect to attracting energy. Any modification acting on Lagrangian level would probably result in the same caveats, except if modifying the scalar curvature itself in GR Lagrangian. SMT Lagrangian will be given below, but only after calculation of the modified Einstein equation. For this calculation the algebraic constraints are the following.

- Bianchi identity,
- stress-energy tensor conservation,
- variation of C_{SMT},
- linearity of curvature with respect to attracting matter.

The latter implies that any added term is forbidden. Therefore, a simple solution is to replace C_{SMT} by its space-time tensorial expression. Here C_{SMT} is replaced by $C^{\rho}_{\mu} C^{\sigma}_{\nu}$, where C^{ν}_{μ} is a mixed multiplying tensor, allowing a different factor than C_{SMT} to be applied to the space components of $T_{\mu\nu}$. Since the result must retrieve equation (2) in the non-relativistic case, there is $(C^0_0)^2 = C_{\mathrm{SMT}}$ in the co-moving bases. Bianchi identity and energy conservation along with C_{SMT} variation imply a separate variation of each C^{ν}_{μ} factor in front of its corresponding component

in the stress-energy tensor. Now this factor depends on the component being multiplied, that is, it depends on μ and ν. These constraints lead to the generalization of $R_{\mu\nu} - \frac{1}{2}Rg_{\mu\nu} = \frac{8\pi G}{c^4}T_{\mu\nu}$ by the following group of equations.

$$\begin{aligned} R_{\mu\nu} - \frac{1}{2}Rg_{\mu\nu} &= \frac{8\pi G}{c^4}S_{\mu\nu}, \\ S_{\mu\nu} &= C^{\rho}_{\mu}C^{\sigma}_{\nu}T_{\rho\sigma}, \\ C^{\nu}_{0} &= \sqrt{C_{\mathrm{SMT}}}\delta^{\nu}_{0}, \\ C^{\nu}_{i} &= \sqrt{s}\delta^{\nu}_{i} \end{aligned} \tag{3}$$

where c is the speed of light, $R_{\mu\nu}$ is the Ricci tensor, $g_{\mu\nu}$ is the metric, R is the trace of $R_{\mu\nu}$, δ^{ν}_{μ} is Kronecker's symbols and i indice is varying between 1 and 3. Equations (3) shows that C^{ν}_{μ} is a time dilation by the C_{SMT} factor, and a space dilation by the s factor, s being a positive scalar. For calculating s, $\nabla G_{\mu\nu} = 0$ implies the following

$$\begin{aligned} 2\partial_0(C_{\mathrm{SMT}}\rho) + (C_{\mathrm{SMT}}\rho + sT^i_i)g^{ii}\partial_0 g_{ii} = 0, \\ 2\partial_i(sT^i_i) + (C_{\mathrm{SMT}}\rho + sT^i_i)g^{00}\partial_i g_{00} + s(T^i_i - T^k_k)g^{kk}\partial_i g_{kk} = 0. \end{aligned} \tag{4}$$

Here it has been supposed $c = 1$ for simplification. The notation $\partial_\mu = \partial/\partial x^\mu$ has been used. The calculation is done in co-moving bases such as $g_{\mu\nu}$ matrices are diagonal, and supposing no shear forces in $T_{\mu\nu}$. Therefore, $T_{\mu\nu}$ matrices are also diagonal. Here the non SMT case $C_{\mathrm{SMT}} = 1$ is simply solved by setting $s = 1$. In the general case equations (4) allow a calculation of a finite s, but only under the supposition of a non null pressure $T^i_i \neq 0$. Otherwise it corresponds to the more general hypothesis of a null stress tensor. And this can be argued as being never completely physically relevant. A static Universe is also forbidden for calculating s (exactly there must be $\partial_0 g_{ii} \neq 0$). And it can be argued also that a static Universe is never physically relevant.

Nevertheless, for avoiding those slight caveats, another solution is the following. As mentioned in the motivation, let us postulate that the null covariant divergence $\nabla G_{\mu\nu} = 0$ of the Einstein tensor is independent of energy conservation $\nabla T_{\mu\nu} = 0$, in the general case. This can be modeled by a $S_{\mu\nu}$ isotropic space part, independent of $T_{\mu\nu}$. In this case $\nabla S_{\mu\nu} = 0$ yields the following, using again the co-moving bases and searching for a diagonal $S_{\mu\nu}$ matrix, but now without any supposition on $T_{\mu\nu}$,

$$\begin{aligned} 2\partial_0(C_{\mathrm{SMT}}\rho) + (C_{\mathrm{SMT}}\rho + P_{\mathrm{SMT}})g^{ii}\partial_0 g_{ii} = 0, \\ 2\partial_i P_{\mathrm{SMT}} + (C_{\mathrm{SMT}}\rho + P_{\mathrm{SMT}})g^{00}\partial_i g_{00} = 0. \end{aligned} \tag{5}$$

It has been written $P_{\mathrm{SMT}} = S_{11} = S_{22} = S_{33}$. This should allow to calculate P_{SMT} in any cases. But here the non SMT case $C_{\mathrm{SMT}} = 1$ implies either an unrealistic simplification of the physical stress tensor, or its independence from space-time curvature. Therefore, the validation of GR equation in the particular context of a non

null space part of the stress-energy tensor must be searched for, in order to possibly invalidate this last solution, and then choose the other one. This completes the construction of equations (3). Finally, those equations must be validated backward. And the result is that they fulfill each of their initial constraints. In the specific case of today's solar system, SMT prediction is exactly GR. More generally, GR is retrieved in the ≪constant $C_{\mathrm{SMT}} = 1$ ≫: case. This is of course mandatory. Equation (2) is retrieved in the non-relativistic case. But in the other cases, differences with GR must be analyzed.

4. Possible regressions

In the ≪constant C_{SMT} ≫: case, GR is not exactly retrieved: if $C_{\mathrm{SMT}} \neq 1$, there is also $s \neq 1$, with $s \neq C_{\mathrm{SMT}}$. Therefore, not only G appears to be different, but also a dilatation factor appears on the space part of the stress-energy tensor. This implies that some PPN formalism parameters will be different from their GR values. But comparing those new predicted values with reality would require testing gravity today 15 kpc beyond the solar system, or inside the solar system but more than 50 000 years in the past (since there is 15 kpc $\simeq$ 50 000 ly). At first glance those experiments seems difficult to realize. Even the ≪varying C_{SMT} ≫: case in which matter density is varying consistently, must be thoroughly analyzed. In particular, a possible time variation of C_{SMT} in the solar system must be studied. The resulting apparent G variation must be calculated from matter density variation in the SMT sphere around the Sun, and then compared to experimental data. The case of binary stars and exoplanets will be addressed further in this document. An important case is the spherically symmetric Universe. The Schwarzschild metric behaves like the classical one but with a different G value. Here emptiness $T_{\mu\nu} = 0$ leads to a radically unrealistic situation: there is a singularity everywhere in the Universe. And this is, now, compatible with Mach's principle. The cosmological case will be addressed below.

5. Lagrangian version

Let us review GR Lagrangian: $L_{GR} = \int \sqrt{-g} R dx^4 + L_M$, where g is the metric determinant and L_M the energy Lagrangian such as $T_{\mu\nu} = -\frac{1}{8\pi G}\frac{\delta L_M}{\delta g^{\mu\nu}}$. Now let us calculate L_{SMT}, the SMT Lagrangian replacing L_{GR}. Writing D^ν_μ such as

$$D^\nu_\lambda C^\lambda_\mu = C^\nu_\lambda D^\lambda_\mu = \delta^\nu_\mu, \quad R_{\mathrm{SMT}} = g^{\mu\nu} D^\rho_\mu D^\sigma_\nu R_{\rho\sigma},$$

and L_{CSMT} such as

$$L_{\mathrm{CSMT}} = -\int \sqrt{-g} X dx^4,$$

X being a scalar such as $\frac{\delta X}{\delta g^{\mu\nu}} = g^{\rho\sigma} R_{\lambda\delta} \frac{\delta (D^\lambda_\rho D^\delta_\sigma)}{\delta g^{\mu\nu}}$, there is:

$$L_{\mathrm{SMT}} = \int \sqrt{-g} R_{\mathrm{SMT}} dx^4 + L_M + L_{\mathrm{CSMT}}. \tag{6}$$

It looks like GR Lagrangian. Here R has been replaced by R_{SMT}, which can be interpreted as R modified by C_{SMT}. An added term, L_{CSMT}, has appeared. It can be interpreted as the Lagrangian corresponding to C_{SMT}. The following suppositions have been done in order to yield equation (6).

- The mean value of C_{SMT} has been supposed constant over the Universe, this ≪mean≫: value being calculated over a given distance greater than the visible Universe size.
- C_{SMT} is supposed to vary around this mean value regularly (that is, with a frequency bounded by a minimum value).

6. Gravitational mysteries

6.1. Aim of these overviews

Some gravitational mysteries will be studied in this document. This will be done in a very quick, mostly qualitative, and careful manner. These studies are not scientific comparisons. They are only very quick applications of SMT to some particular contexts. Their aim is only to reveal some interesting characteristics of SMT dynamic.

6.2. Critical Universe density

In the context of Friedmann-Lemaître-Robertson-Walker (FLRW) metric, there is $\rho = \rho_u$. This is imposed by Universe homogeneity in this case. First of all, let us calculate the first Friedmann-Lematre (FL) equation.

$$H^2 + \frac{Kc^2}{a^2} = \frac{8\pi G}{3} C_{\mathrm{SMT}}\, \rho_u. \tag{7}$$

This result is independent of the choice of the model, that is, the choice between equations (4) or equations (5). Here H is the Hubble parameter, a is the scale factor, and K is space curvature. In FLRW metric context, there is $\alpha = 1$ therefore equation (2) shows that $C_{\mathrm{SMT}}\rho_u$ is constant. This will produce dramatic simplifications of cosmological model. Indeed, writing $P_{\mathrm{SMT}} = w_{\mathrm{SMT}} C_{\mathrm{SMT}} \rho$, the classical version of energy conservation under FLRW metric implies $w_{\mathrm{SMT}} = -c^2$ and $K = 0$: FL equations yield a de Sitter Universe. And once again, this result is independent of the choice of the model, that is, the choice between equations (4) and equations (5). Let us notice that another possible solution from any chosen group of equations, (4) or (5), could be a static Universe with a positive space curvature. But this is physically irrelevant. The result is that w_{SMT} has no interesting physical meaning. In FLRW co-moving bases $S_{\mu\nu}$ is simply $-\rho_c c^2$ times the Minkowski metric diagonal matrix $\eta_{\mu\nu}$, such as $\eta_{0\nu} = -\delta_{0\nu}$ and $\eta_{i\nu} = \delta_{i\nu}$ for ν between 0 and 3. Because of the well-suited tensor product of equations (3), the physically meaning state equation $\rho = wP$, P being $T_{\mu\nu}$ pressure, has no specific effect on space-time curvature. Everything acts as if

$T_{\mu\nu}$ has been replaced by $S_{\mu\nu}$, having a constant matrix in FLRW co-moving bases. Now, equation (7) can be written:

$$H^2 = \frac{8\pi G}{3}\rho_c. \tag{8}$$

This equation is valid from last scattering until today. Before last scattering, SMT is no longer valid. The solution of this de Sitter universe is the following

$$a = a_0 \mathrm{e}^{H_0 t}. \tag{9}$$

It will be supposed $a = a_0 = 1$ at present time. The predicted elapsed time since last scattering, T_{LS} is given by the following equation, using $a_{ls} = \frac{1}{1+z_{ls}}$.

$$T_{LS} = \frac{\ln(a_{ls}^{-1})}{H_0} = 68\, h^{-1}\mathrm{Gyr}. \tag{10}$$

This is in strong disagreement with ΛCDM model value of $13.798 \pm 0.037\,\mathrm{Gyr} = 9.35\,\mathrm{h}^{-1}\,\mathrm{Gyr}$ (using $H_0 = 67.80\,\mathrm{km\,s^{-1}\,Mpc^{-1}}$). It could be allowed by a much longer dark age period. But such a duration explains the formation of galaxies. For example, now a galaxy such as UGC 2885 [10] will have more than $(68/9.35) \times 12 \simeq 87$ revolutions to create, since last scattering, in place of only 12 revolutions with ΛCDM value. Also, the localization of UDFJ-39546284 [11], [12] at $z \simeq 12$ is possible in the context of SMT. The important result of this chapter is that the issue of critical Universe density [13], [14], is solved directly and in a simple manner by SMT. No more cosmological constant is needed.

6.3. Nucleosynthesis, fine tuning, singularity, particle's horizon and acceleration of Universe's expansion

In the context of SMT, there is no fine tuning issue, since matter density has been simplified during the modification of FL equations. At first glance, particles horizon issue is solved by the disappearance of any time limit in the past, ensuring the Universes homogeneity and isotropy, and ≪big-bang≫: singularity is solved altogether. These are direct consequences of the previous calculations.

But primordial nucleosynthesis is not explained by SMT: the predicted Deuterium abundances are incorrect. It would probably require microscopic scale, or high energy specific predictions for studying radiation-dominated era. And this is a domain in which SMT is probably inoperative. Therefore, particles horizon and ≪big-bang≫: singularity would need different or refined explanations.

Let us write the deceleration parameter q such as $q = -\frac{\ddot{a}a}{\dot{a}^2}$, $\dot{a} = \frac{da}{dt}$, $\ddot{a} = \frac{d^2a}{dt^2}$. From equation (8), we have

$$q = -1. \tag{11}$$

This is in accordance with experimental data [15], Table 8. SMT predictions, $K = 0$ and equation (11), are compatible with today's measured values [15], [16].

6.4. Heterogeneity of large scale structure

The problem of heterogeneities of large scale structure [17] can first be addressed with Jeans instability. Let us start from the classical collapse time t_j, valid under Newton's law

$$t_j = \frac{1}{\sqrt{G\rho_u}}. \tag{12}$$

This value in the context of SMT is also calculated from hydrodynamic and is the following

$$t'_j = \frac{1}{\sqrt{G\rho_c}} = 28\,h^{-1}\mathrm{Gyr}. \tag{13}$$

Equations (12) and (13) are valid in a homogenous Universe, at any time. But equation (13) shows a very important difference: SMT collapse calculation is no longer driven by Universe's expansion, like Newton's law collapses are. Using $c_s = 5\,\mathrm{km/s}$ for the sound speed just after decoupling, the Jeans length is the following

$$l'_j = c_s t'_j = 140\,h^{-1}\mathrm{kpc}. \tag{14}$$

This allows for the creation of voids and walls structures.

Now let us suppose a wall, located between $x = 0$ and $x = x_{\mathrm{wall}} > 0$, parallel to the $y - z$ plane, at today's time. From equation (2), if $\vec{a}$ is the SMT acceleration corresponding to any $\vec{a}_n$ Newtonian acceleration, there is:

$$\vec{a} = \frac{2\rho_c}{\rho_{u0} + \rho}\left(1 + \frac{r}{\rho_{u0} + \rho}\frac{\partial\rho}{\partial r}\right)\vec{a}_n, \tag{15}$$

where r is the distance between the infinitesimal object generating $\vec{a}_n$, and the location where it is exerted. The distance between two walls is always far greater than the Jeans length given by equation (14). Therefore, any hydrodynamic equilibrium will be driven by equation (15) only. The astonishing prediction is that no more counteracting pressure is required in order to achieve a hydrodynamic equilibrium. And this is even independent of the exact wall and filament structure. Between the filaments and walls, if one neglect the matter density with respect of matter density of the wall and filaments, there exist a completely new, stable equilibrium, given by the following equation. It expresses the distribution of matter density, valid, for example, on the right-hand side of this wall,

$$\rho = (\rho_{\mathrm{wall}} + \rho_{u0})\,\frac{x_{\mathrm{wall}}}{x} - \rho_{u0}, \tag{16}$$

where ρ_{wall} is the matter density of the wall. The approximations driving this equation were $x \gg x_{\mathrm{wall}}$, and only small perturbations allowed with $\rho \ll \rho_{\mathrm{wall}}$. Supposing also $\rho_{\mathrm{wall}} \gg \rho_{u0}$, equation (16) shows the void falling into complete emptiness at this x_e coordinate,

$$x_e \simeq \frac{\rho_{\mathrm{wall}}}{\rho_{u0}} x_{\mathrm{wall}}. \tag{17}$$

This repartition of matter remains to be compared with experimental data [18]. But the novelty here is the existence of this stable equilibrium. It has no equivalent in the context of Newton's law. Of course, once the equilibrium obtained, the classical hydrodynamic equations still drive the behavior of matter for small and local perturbations. Anyhow in a void, gravitational force is much stronger than that predicted by Newton's law. Supposing $\rho \gg \rho_{u0}$, equation (2) yields:

$$C_{\mathrm{SMT}} \simeq \frac{\alpha_0 \rho_0 + \rho_{u0}}{\rho_{u0}} = \frac{2}{\Omega} = 40. \tag{18}$$

The result is an evacuation of voids as soon as they are created. Collapse time in a void is now $t''_j = 20\, h^{-1}\mathrm{Gyr}$. As an intermediate conclusion, with SMT equations, the gravitational collapses are unaffected by expansion. The collapse time (equation (13)) is 2.4 times weaker than the predicted elapsed time, since last decoupling (equation (10)). A stable equilibrium and an evacuation of voids are also predicted. This gives a possible explanation of the heterogeneities of large scale structure.

6.5. Galaxy dynamic

This well-known mystery is, for example, evident in [19]. Simulations has been executed, based on [20] and [21]. Exactly the same initialization has been set, except that a greater initial mass and a smaller ray has been used in place of those used in [20]. Simulating immediately SMT model from [21] initial state results in a burst which greatly increases the disparity of stars velocities. To avoid this, SMT model is implemented progressively in the simulations, starting from Newton's model. The available data for calculating C_{SMT} on each point of the galaxy, is the number of simulated stars NbP, which are located in the ≪SMT disk≫: of ray $r_{\max}$, centered on this point. And since the width of the galaxy is not easily available, the simulated volume matter density is not known. That is why the computed equations are the following

$$\begin{aligned} NbP_{\mathrm{added}} &= \frac{m_0}{m}\frac{h}{h_0} NbP_0, \\ NbP_m &= \max\left(NbP, \frac{7}{39} NbP_{\mathrm{added}}\right), \\ C_{\mathrm{SMT}} &= \frac{40 NbP_{\mathrm{added}}}{39 NbP_m + NbP_{\mathrm{added}}}, \end{aligned} \tag{19}$$

where NbP_{added} is the constant which corresponds to 39 times ρ_{u0} in equation (2) and which has been progressively decreased during the simulations, starting from a very high value. This progression is described below: NbP_m corresponds to matter density in a galaxy, which is not exactly proportional to NbP, because ρ_{IGM}, IGM (intergalactic medium) matter density must be taken into account outside of the galaxy. It has been used $\rho_{\mathrm{IGM}}/\rho_{u0} = 7$, and this specific value will be explained below in the study of virial theorem mysteries, m is the mass of a simulated star,

m_0 is the mass of a star which is used in the simulation of the Milky-Way, and which is therefore in accordance with Milky-Way's mass, h is the width of the simulated galaxy disk, supposed proportional to the size of the galaxy. h_0 is the width of the Milky-Way's disk. NbP_0 is the number of stars located in the SMT disk, at the Sun's galactocentric distance of 8 kpc. Its value, 76 000 , has been measured on the corresponding curve during the permanent regime of the Milky-Way simulation.

The program execution is divided into 2 phases. The first one is usual simulation of a virtual galaxy using Newton's law. This is done exactly like in [20], starting with the initialized galaxy described by the paragraph untitled ≪Initial conditions≫: in [21]. The end of this phase occurs after 50 galactic revolutions. At this time the 2nd phase begins, in which Newton's law is replaced progressively by SMT. For ensuring this progressivity, the following equation is used, modifying equations (19).

$$C_{\mathrm{SMT}} = \frac{39NbP_{\mathrm{added}} + NbP_{\mathrm{prog}}}{39NbP_m + NbP_{\mathrm{prog}}}. \tag{20}$$

At the beginning of this 2nd phase, a very strong value (19 500 000) is given to NbP_{prog}. Therefore, at this time the simulation does not yield a great modification of the whole galaxy. The galaxy's shape is still very similar to the Newton's law permanent regime. Then, very slowly, NbP_{prog} is decreased. Therefore, the shape of the simulated galaxy slowly changes. This decrease stops as soon as $NbP_{\mathrm{prog}} = NbP_{\mathrm{added}}$ is reached, after 750 revolutions. Therefore, at this time the full equations (19) are finally computed. Figure 1a shows the results. For comparison, Figure 1b shows exactly the same initial galaxy, after the same number of revolutions, but always simulating Newton's law. The galactic center shows the apparition of a ring [22]. This is discussed below. Newtonian logarithmic matter density profile is curved positively, from 0 to 50 kpc galactocentric distances. But SMT one is a straight line between 20 and 70 kpc. This is more compatible with experimental data. But of course, below 20 kpc, the curve is no longer a straight line due to the existence of the ring. Radial and tangential speed dispersions are 2 or 3 times worse than the one obtained with Newton's law. No stable spiral arms are noticed, like in [20]. Like in [20], they can appear only from time to time and are not stable structures. But the kind of apparition of arms shown by Figure 2 seems to be provoked by the overall increase of C_{SMT} though the whole galaxy. A Kepler-like speed profile is of course shown under Newton's law (Figure 1a). Those speed profiles are completely ruled out by experimental data, as commonly accepted. But SMT speed profiles are much closer to flat curves. Of course this comes from the ≪smoothing≫: behavior of SMT model, on velocities: C_{SMT} increases with distance from the galactic center, due to matter density decrease. The galaxy speed profile of Figure 1b has a shape which can be easily compared to the Milky-Way speed profile shape, for example. The speed profiles yielded by SMT are always far closer to experimental ones than those yielded by Newton's law. This was true for each executed simulation, which were done using various values of SMT parameters (an NbP_{added} different value, and also other constants than 7/39, 40, 39). The values of those parameters in equations (19)

are predicted by SMT but are not the most appropriate in order to yield the best profiles when comparing to experimental data. Nevertheless in this document, the simulations are always computing equations (19), except when expressly mentioned. Assuming different values for the parameters than those in equations (19), an almost perfectly flat speed profile can be obtained, for giant galaxies. This is also very much compatible with experimental data. Indeed, such a flat profile is observed in the case of UGC 2885 [23], NGC 801, or NGC 2403, for instance. Assuming different values for the parameters a typical ≪increasing bell shape≫: profile can also be obtained, for smaller galaxies. This is obtained in particular when the ring is weak, or absent. Finally, a little ≪wave≫: is often noticed at the beginning of the speed profiles, which is often present in experimental speed profiles. For example, on Figure 1b this wave is located around 10 kpc from the galactic center. Galaxy stability is increased in lower density environments for medium- or large-sized galaxies. Indeed, it has been supposed when calculating equations (19), that IGM matter density is equal to $\rho_{IGM} = 7\rho_{u0}$. But supposing $\rho_{\mathrm{IGM}} = 0$ implies a modification of equations (19), such as $NbP_m = \max(NbP, (7/39)NbP_{\mathrm{added}})$ is replaced by $NbP_m = NbP$. This increases the maximum C_{SMT} possible value from 5 to 40. This multiplication of gravitational forces by a factor of 8, valid only when located out of the galaxy (or at the edge of it) will of course increase its stability. This has been confirmed by simulations (under the $h = h_0$ hypothesis) and might be in accordance with experimental data [24]. In this $\rho_{IGM} = 0$ case, after its slow dissolution, a giant galaxy yields a very faint large galaxy, which can be easily compared with a LSB galaxy. But this does not occur under the $\rho_{\mathrm{IGM}} = 7\rho_{u0}$ supposition, in which case this galaxy is only dissolving faster, without any remaining structure. The computational flexibility is low and the liberty degrees are in the galaxy characteristics input. The first characteristic is the simulated matter density with respect to ρ_0, in other words NbP with respect to NbP_0. This depends on parameters such as the width and volume matter density in a galaxy, with respect to its size. The second characteristic is the exact knowledge of gas and star distribution in the galaxies. This gas distribution was not taken into account in those simulations. Hopefully, in spiral galaxies the gas density is only a few percent of that of stars, and in elliptical galaxies it is even lower. Therefore, this error might have no strong effects. But this might not be true for simulating a standalone dwarf galaxy. Anyhow this gas behavior simulation would require a specific kind of computation. The issue of this chapter is the most difficult and delicate. It would need a huge amount of work. But even without such a workload, here the SMT results speak for themselves.

6.6. Dwarf galaxies

The simulations show an occasional generation of dwarf galaxies, orbiting around the main galaxy. But this occurs only when simulating under SMT model. When simulating Newton's law, no dwarf galaxies were noticed. Dwarf galaxies are almost systematically generated during the burst which occurs at the start of the simulation, when SMT model is immediately fully calculated, without beginning with

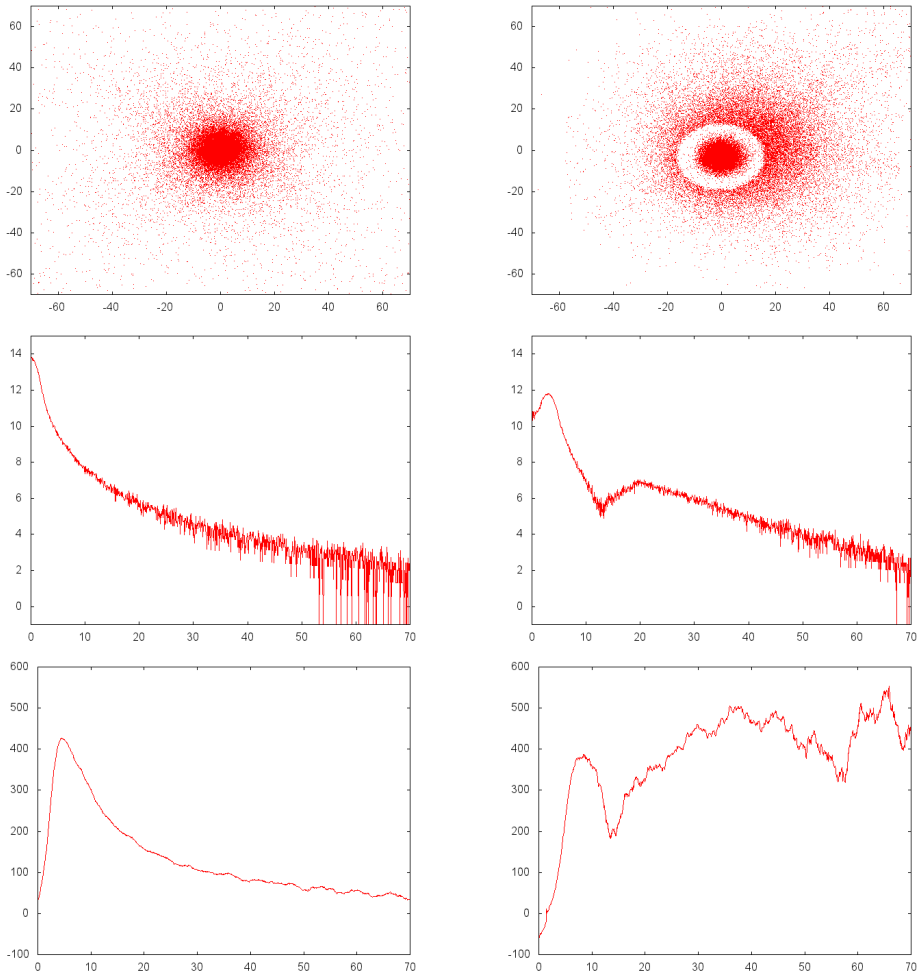

Figure 1: On the left (a) are shown the results of a simulation executed under Newton's law. The simulated galaxy is the same as in [20] after 750 revolutions, except that the galaxy mass is equal to 1.8×10^{12} Sun's masses, the initial galaxy ray is equal to 1.4 kpc. 10^5 stars has been simulated in a 256×256 grid calculation over a $67 \times 67\,\mathrm{kpc}^2$ square. On top the 2D localization of the stars is drawn. In the middle $8 + \log(\rho)$ is drawn, where ρ is the mean value over 13 kpc of galactic surface matter density and ρ unit is $\mathrm{kg/m}^2$. On the bottom the tangential speed of the stars in km/s is drawn. For those three drawings, horizontal values (and vertical values for the top drawing) are galactocentric distances, with unit in kpc. On the right of (b) are shown the results of another simulation, which is the same as the one represented on the left, except that SMT model has been progressively introduced in place of Newton's law. Finally those results are obtained, after 750 revolutions, with an exact SMT simulation (equations (19)). The same axis and units are used as on the left.

a first phase in which Newton's law is active. Dwarf galaxies may also be generated with a simulation using a progressive installation of SMT model calculation. In this case, they can appear just at the beginning of the second phase of the simulation, which is executing progressively SMT model. A faint galaxy, because it is faint, is probably located in a low or very low matter density environment. Therefore, C_{SMT} is strong and the perceived gravitational attraction is high (may be up to 40 times greater than Newton's law attraction). As a result, the existence of this faint dwarf is more understandable under SMT than under Newton's law, as well as its important velocity in its revolution around a main galaxy. In front of this, faint and ultra-faint galaxies existence could be an issue under MOND theory [25]. The same mechanism might explain the mystery of ≪the lower the surface brightness of a system, the larger its mass discrepancy≫: [26]. Indeed, low surface brightness galaxies are mainly isolated field galaxies. As such, they might also be located in a low matter density environment. Those dwarf galaxies 2D generations are in accordance with experimental data. Indeed, studies of M31 [27], of the Milky-Way [28], and even of globular clusters and streams around the Milky-Way [28] has shown a systematic preferred location of dwarf galaxies along a common disk. Of course, it would be better to simulate in 3D, but the existence of 2D generations itself might be a result since no such dwarf galaxies were generated by the same simulations under Newton's law. After a while they often dissolved progressively by themselves. When the main galaxy contains a ring, those dwarf orbiting galaxies are generated only outside of this ring, therefore at more than 15 kpc from the galactic center. It was noticed also that they are often encountering the galactic center along their trajectory. But when this center contains a ring, which is often the case, they cannot dissolve themselves into it. They are systematically bouncing on the ring edge, forbidding any merge. This might result in a better stability of dwarf galaxies, with SMT, than with Newton's law. By other means, the location of the Milky-Way on the plane containing the dwarf orbiting galaxies around M31 [27] is not explained by the model and would need a 3D simulation.

6.7. Ring galaxies

During the simulations a surprising result was found. Ring galaxies are oftenly generated by the SMT dynamic itself, without the help of any particular external event. They appear to be self-generated and stable structures. There is no longer the need to imagine any collision scenario between galaxies in order to explain their existence. And this is in complete accordance with experimental data. For instance, in a region called ≪the general field galaxy population lying behind the Tucana dwarf galaxy≫: [29], an ≪unexpectedly large number of ring galaxies≫: is found. This number is inconsistent with the hypothesis of ring galaxies generated only by collision. SMT might predict this abundance directly, without supposing any ≪steeply increasing galaxy interaction rate with red-shift≫: [30]. Also, it could be difficult to understand why those ring galaxies are so young [31]. But this mean age of 1 Gyr might be understood by the simulations. Indeed, several dislocations of rings

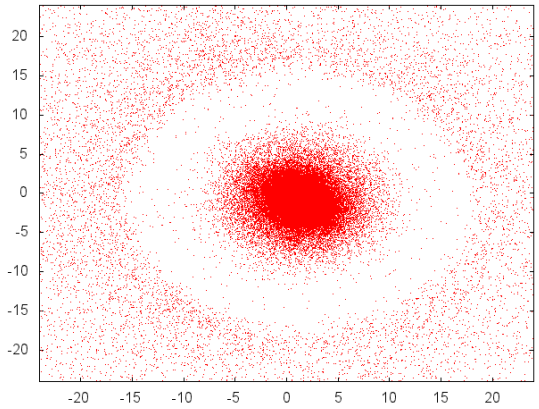

Figure 2: A simulated ring galaxy

were noticed during the simulations. Those dislocations were always very quick and resulted in the same galaxy but without any more ring. This could indicate that nevertheless this stability is fragile, and therefore could explain this relatively young age. Even our Milky-Way galaxy has been recently found to host a ≪ring of stars≫: [22]. When simulating a galaxy with the same characteristics (mass, star velocities, diameter) as the Milky-Way, this ring is found. It has a radius of 18 kpc, which is exactly the experimentally observed ring radius. Also, the simulations has shown multi-ring stable structures. When simulating equations (19) they are noticed for big galaxies (having a ray greater than 50 kpc). This is confirmed by experimental data. For example NGC 2859 double ring is obvious. The simulated ring shows strong matter density values also beyond the ring itself. This is not consistent with the visible rings of observational data. But as explained in [32], there is probably a low luminosity gaseous disk in ring galaxies. The simulations seem to show that SMT prediction is the following. The width of the empty ring could not be greater than $r_{\max}$. Moreover, it should be often below or just below this value. The simulations, for example the one of Figure 2, shows a ring diameter of 34 kpc, composed of a nucleus diameter of 10 kpc, and an empty ring width of 12 kpc (just below $r_{\max}$ value). Those dimensions are similar to the Cartwheel galaxy dimensions, for example.

The galaxy simulations shows that the ring's ray of the simulated galaxies, when they contain a ring, is always just below $r_{\max}$. Therefore, an attempt could be to retrieve on existing galaxies the statistical distribution of such a ray. The simulation has shown that the particular truncated shape of the observed bars in the galaxies, along with the particular enrolled shape of arms around it, can result from the existence of a ring in those galaxies. For instance, on Figure 3 the length of the bar is roughly equal to 35 kpc. This bar is the nucleus of an ancient ring galaxy. This nucleus started to deform itself and to rotate quickly. As a result the generated arms quickly enrolled around it. The result is then shown on the figure.

The similarity with observations is noticeable. And this was not obtained when

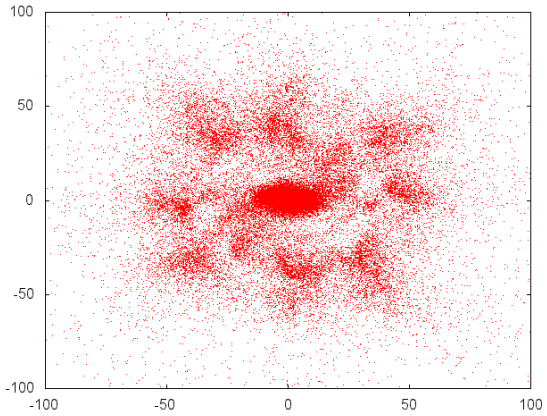

Figure 3: This galaxy shape appears when executing equations (20) with $NbP_{\text{prog}} = 705\,000$, $NbP_m = NbP$, and equations (20) with $h = h_0$. At this time NbP_{prog} is decreasing at a pace of 15 600 per galactic revolution. The central bar is rotating quickly, enrolling 2 arms around it. The simulated galaxy has a mass equal to 1.5×10^{14} Sun's masses, and an initial ray equal to 1.9 kpc.

simulating Newton's law with the same program. With Newton's law, the bar and its arms always showed a ≪slow S≫:, as in [19]. This particular observed shape described above was never noticeable neither for the bar nor for the arms, under Newton's law. Finally another weird prediction of the simulations is that the rotational speed of the stars located in the nucleus is sometimes opposite to the speed of the stars located outside of the ring. This prediction is validated by NGC 7217 speed profile. Of course, this work is still in progress. A 3D simulation is needed, in order to know if the exact prediction is a ring, or a radial hole. And this simulation must be done using real galaxy data, and then compared with observations. Finally, comparing this with the corresponding MOND and ΛCDM model predictions would be very interesting.

6.8. Galaxy mass and scale

The observational fact that galaxy masses are proportional to their size [33], is not predicted immediately by the model. It would require a deeper understanding of galaxy dynamics in the context of SMT.

6.9. Virial theorem

Let us try to quantify what predicts the model in the cases studied by [34], [35] (gravitational forces greater than expected in Virgo or Coma clusters, among others). It will be assumed that $\rho_{IGM}/\rho_{u0} = 7$, which is roughly the lowest of the commonly accepted bounds [36] for this ratio. Equation (2) yields the following value for the SMT increase of gravitational forces in IGM:

$$C_{\text{SMT}} = \frac{\alpha_0\rho_0 + \rho_{u0}}{\rho\text{IGM} + \rho_{u0}} = 5. \tag{21}$$

This equation yields the measured value of 5. Therefore with SMT it might be possible to explain the virial theorem classical mystery. Also, other gravitational anomalies like the bending of light, or the Great Attractor [37] anomalies might be explained, exactly the same way.

6.10. Bullet cluster

This is ≪1E 0657-56≫: galaxy cluster [38], [39], [40]. Possible explanations of its strange dynamic have been given for example in [41] and [42]. The main cluster's length is around 700 kpc. With $r_{\max} = 15\,\text{kpc}$, this makes a relative value of 2%. That's why the probability of intersection of a galaxy with the SMT sphere has been approximated to 0. But of course this must be confirmed based on a detailed information about the bullet cluster. Hence, only the gas cloud has been taken into account for evaluating ρ in equation (2). A simulation of SMT prediction has been executed. It has been supposed a plane distribution of matter (on the plane which is perpendicular to the line of sight). Therefore only a 2D simulation has been executed. Of course a 3D simulation would be better. But this simplification allows the SMT dynamic to be easily perceived in such a case. A Gaussian distribution of matter has been used for each of the two clusters, and for the gas distribution. The fitted standard deviations of the gas cloud and the clusters distributions has been set respectively to 560 kpc and 130 kpc. Their fitted relative amplitude has been set respectively to 1 and 0.3. The distance between the centers of the two clusters has been set to 750 kpc. For simulating equation (2), the simulated matter density has been multiplied by a fitted constant. It has been supposed also that $\rho_u = \rho_{u0}$. Then, the calculation of the algorithm was the following. Based on those mass distributions, the acceleration potential is calculated. In the case of Figure 4, it is Newton's potential. In case of Figure 5, it is SMT potential given by equation (2). Then, mass distributions are calculated (back) again, based on those potentials. But now for Figures 4 and 5, those mass densities are calculated supposing that the potential Φ is a Newtonian potential. A precise FFT is not available, therefore, the usual Poisson formulation of Newton's law is used: $\Delta\Phi = 4\pi G\rho_f$, where ρ_f is the final mass density shown on the figures. The numerical calculation of this $\Delta\Phi$ Laplacian uses the following matrix:

$$A = \begin{pmatrix} 0.4 & 0.2 & 0.4 \\ 0.2 & -2.4 & 0.2 \\ 0.4 & 0.2 & 0.4 \end{pmatrix}. \tag{22}$$

This is calculated with a 64 bits floating point format on a 256 grid covering the bullet cluster. It yields visible errors in the final result. But on Figure 4 this calculated mass distribution is qualitatively the same as the initial one, and the interesting result is obtained when comparing Figure 4 with Figure 5. Figure 5 reveals the following SMT mechanism. Mainly, C_{SMT} is inversely proportional to local gas matter density. In the clusters, since there is almost no more gas among the galaxies, this factor is strong. Conversely, between the two clusters, in the gas

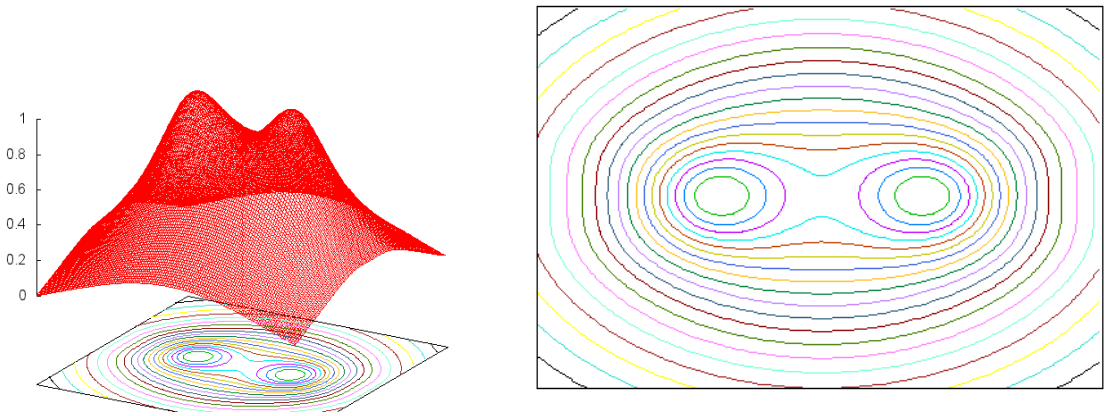

Figure 4: On the left is drawn in 3D the surface from which the contours are shown on the right. It represents a modelled mass distribution of the bullet cluster. Three gaussian distributions have been used for modelling the two galaxy clusters and the gas cloud. The result shown is the calculated Laplacian of the potential. This potential has been calculated using Newton's law, based on this mass distribution. This figure is here for comparison with Figure 5. This final result is slightly different from initial mass distribution due to program execution precision errors. Vertical units are relative matter density.

cloud, it is lower. This explains qualitatively the bullet cluster weak lensing mass distribution. More precisely, based on equation (2), SMT predicts that $\Phi_g(M)$, the SMT acceleration potential generated by the gas cloud only, and applied on a given point, is proportional to the following expression.

$$\Phi_g(M) \propto \frac{\frac{G}{D(M,N)} * \rho_g(N)}{D_M(N) * \rho_g(N)}, \tag{23}$$

where $\rho_g(N)$ is the gas density located on a given N point, $d(M,N)$ is the distance between M and N, $D_M(N)$ is equal to 1 if $d(M,N) < r_{\max}$, else it is equal to 0.

When comparing Figure 5 with Figure 1a of [38], the 2D whole profiles are qualitatively the same and many similarities are noticed. On those two figures the gas cloud seems to generate no Newton-like gravitational attraction. This is predicted by equation (23), because $G/d(M,N)$ and $D_M(N)$, as functions of N, are symmetrically centered, and thin. This is also because $\rho_g(N)$ varies on a 700 kpc scale, and $r_{\max} \ll 700\,\text{kpc}$. The result is that equation (23) shows nearly no variation of $\phi_g(M)$. Due to this specific quotient of convolutions yielding $\phi_g(M)$, it might even be predicted other similarities with the experimental figure. Noticeably, on Figure 1b of [38], the mass contours on the left are following the end of the gas cloud limits. Also, the mass contours tend to surround closely the two bowls of gas (in black). This could be predicted because $G/d(M,N)$ and $D_M(N)$, although symmetric and thin, are nevertheless different. Noticeably, $D_M(N)$ has finite support

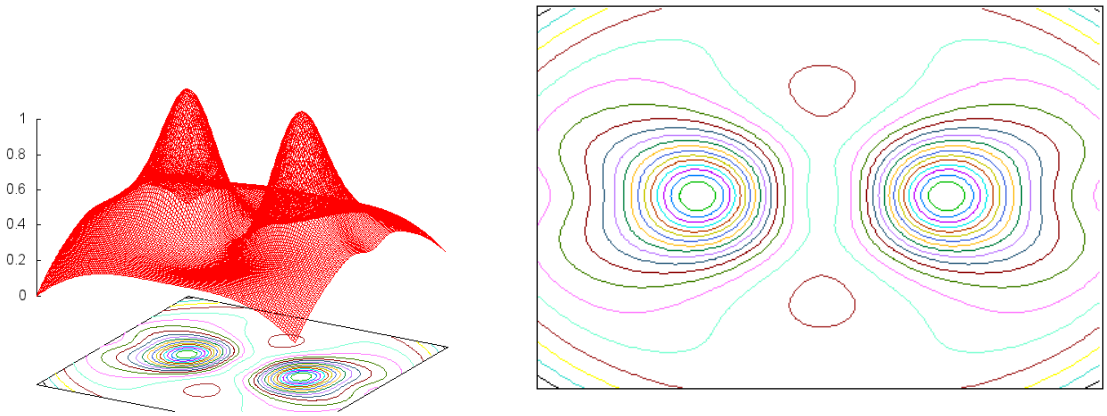

Figure 5: On the left is drawn in 3D the surface from which the contours are shown on the right. The same initial mass distribution has been used as for drawing Figure 4. The shown result is the calculated Laplacian of acceleration potential. This potential has been calculated using SMT, based on this initial mass distribution. This figure must be compared with Figure 4 and uses the same units.

whereas $G/d(M,N)$ has not. Moreover, on the left of the right part of Figure 5, the mass contour predicted by SMT draws an $\ll \varepsilon \gg$: shape. This shape is quite similar on Figure 1b of [38]. Finally, a small valley can be seen, between the two clusters (top center of Figure 1a of [38]). This valley is also present in Figure 5, as well as another one just below. Different simulations shows that those two symmetrical valleys are a systematic result of SMT when varying the parameters of the modelled mass distribution. Of course, this simulation would better be executed in 3D. It would better use real experimental data, such as real matter densities, as well as the exact galaxy locations and dimensions. But the overall result is that SMT suggests a possible explanation of bullet cluster weak lensing mass reconstruction. Concerning the strange relative velocity of the clusters [43], [44], equation (18) shows that gravitational acceleration can increase by a C_{SMT} factor of up to 40. This value, valid inside a void, is much greater than the corresponding values of ΛCDM and MOND models [44], which are in the range (2–6). For example, a cluster located in a void can be strongly accelerated by the neighboring walls, during the predicted evacuation of the void. Therefore, this cluster will receive an acceleration much greater than the one coming only from any other cluster. In fact, this acceleration is generated by the attracting walls, not only by the other cluster. And, also, $C_{\mathrm{SMT}} \simeq 40$ is valid in this case. The result is that the relative velocity between the two clusters might be much greater than the one generated only by their own masses, and much greater than Newton's law prediction. Therefore, the SMT predicted velocity might be in accordance with the observed value of 4700 km/s [44]. And for the same reasons, SMT might predict that such a cluster velocity would not be a rare event [43]. But of course this has to be confirmed by precise calculations or simulations.

6.11. Tully-Ficher law

Trying to explain Tully-Ficher law [45] in the context of SMT leads to the conclusion that α in a galaxy depends on the galaxy characteristics. This is of course not satisfying. But a slight modification of the model is possible, yielding the exact Tully-Ficher relation. This work is in progress.

6.12. Miscellaneous

The tremendous amount of gravitational mysteries [46], [47], is not easy to address in one article. For example, simulation of the galaxy interactions and mergers, such as the Antennae [25], would be interesting. But some issues listed in [47] are already qualitatively answered in the context of SMT. Among others, each of the following issues might be explained simply by some of the basic SMT mechanisms which have been described in this document.

- Features in the baryonic distribution imply features in the rotation curve.
- The bulk flow challenge.
- The high-z clusters challenge.
- The Local Void challenge.
- a_0/G as a critical mean surface density for stability.
- a_0 as a transition acceleration.

The issue titled ≪Features in the baryonic distribution imply features in the rotation curve≫: seems easy to solve in the context of SMT since it is a modified gravity theory, not a Dark Matter theory. The ≪bulk flow challenge≫: might be qualitatively answered exactly the same way as above, for the measured relative velocity of the sub-clusters of the bullet cluster. The ≪high-z clusters challenge≫: is answered simply by equation (10): the time since last scattering is $68/9.35 \simeq 7$ times greater than ΛCDM one. Existence of big structures at high red-shift is possible with SMT. The ≪Local Void challenge≫: issue, which asks why the local void, located around the Milky-Way, has so few galaxies, has a simple direct explanation in the context of SMT. Indeed, as stated above, in a void, the applied gravitational force is up to 40 times greater than Newton's one. Therefore, the remaining galaxies are strongly attracted to each other, resulting in a quicker creation of giant galaxies. Another SMT behavior is that those giant galaxies are more stable in a low matter density environment. This mechanism has been explained above. Also, the main proportion of matter in a giant galaxy is not located on its edge. Therefore, C_{SMT} can stay close to 1 in an inner and major part of the galaxy. As a consequence, a giant galaxy might not follow the evacuation of a void, which drives only sparsely distributed and isolated objects. The final result is a low number of galaxies, and a higher proportion of giant galaxies predicted by SMT in low matter density environments. And exactly this is shown by experimental data [24]. The issue untitled $\ll a_0/G$ as a critical mean surface density for stability≫: has been partially explored when simulating the galaxies. Indeed, Figures 1 and 2 shows that matter density of the same virtual galaxy in a Newton's context has its maximum more than 10^2 times

greater than the corresponding one in SMT. This is due to the strong SMT decrease of gravitational forces at locations where matter density is strong. This creates a cutting off behavior of SMT for strong matter density values. And it might be guessed that this implies a decrease of a galaxy mean surface density between the two models. This might give a first answer to this issue. The issue untitled $\ll a_0$ as a transition acceleration$\gg$: is well resumed by Figure 48 of [47]. It shows that the mean acceleration inside galaxies and clusters stays roughly constant, independent of the scale. This might be a consequence of the existence of the cutting-off value, suggested above. By the way, GR singularities and closed time-like curves can be addressed by SMT for the same reason. Indeed, under SMT context, very high matter densities are much harder to occur than under GR, because of the cutting-off value suggested above. SMT predicts also a varying, or, different orbital period for binary stars and exoplanets (different from Newton's law prediction). This must be calculated, using a measurement of the surrounding matter density in each case. But this might give an explanation of the issue of the strange variation of orbital period of black hole X-ray binaries [48].

7. Violation of momentum conservation at large scale

In the context of SMT, the principle of momentum conservation is violated at large scale. Indeed, equation (2) shows that two mutually attracted objects might not exert on one another exactly opposing gravitational forces. But this prediction concerns only objects attracted to one another that are more than 15 kpc apart. Comparing this prediction with observational data, for example in the case of clusters of galaxies, is extremely important. But this violation appears only when matter density is varying consistently. Hence it would need precise calculations based on detailed information on gas and stars distributions.

8. Testing the model

8.1. Intragalactic

This test consists in continuing the simulation of a galaxy under the SMT model. A specific focus on flat profiles of giant galaxies might be done.

8.2. Extragalactic

One test could be to measure matter density and a possible increase of gravity, outside of any galaxy. Indeed, the following equation is the rewriting of equation (2) for extragalactic spaces.

$$\frac{G'}{G} = 2\frac{\rho_c}{\rho + \rho_u} \tag{24}$$

Let us remind the notations:

G is the gravitational constant.

G' is the equivalent value of G as predicted by the model. Therefore G'/G is the increase of the gravitational force, but at a given M space-time location, as predicted

by the model. M must be located outside of any galaxy. It is the increase of G which must be used for calculating any exerted force in M. It is not a generated one, because the generated ones are simply using G, that is, unmodified Newton's law.

- ρ is the matter density calculated in a 10 h^{-1}kpc ray sphere centered in M.
- ρ_u is the mean matter density of the Universe at the time of the M event.
- ρ_c is Universe critical matter density. This equation shows a big difference with ΛCDM, in the case of voids: $G'/G \simeq 40$ if $\rho = 0$. More generally, the model predicts a difference with Newton's law in areas in which $\rho = \rho_{IGM}$ varies consistently.

8.3. Large scale structure

This is the test of the very SMT specific stable equilibrium. It is predicted by SMT over large scale structure. Either equation (16) or equation (17) might be used. The test might consist in measuring the observed matter density distributions which are used in those equations, and then to check if those equations are retrieved.

9. Conclusion

SMT is composed of equation (2) and of 2 parameters, $r_{\max}$ and α. Each gravitational mystery, or any gravitation behavior acting below $r_{\max} \simeq 15\,\text{kpc}$ from the Sun does not have to be checked by the model. Indeed, for those cases the model behaves exactly like Newton's law. The overall behaviour of this model shows gas and dust playing a major role in the strength of the perceived gravitational force. First of all they generate Newton-like gravitational attraction like any other energy. This is done at the location where gravitational force is created (generated). But also, the presence or absence of gas or dust at the location where gravitational force is applied (exerted), respectively decreases or increases its strength. This is the main novelty of this model. It might explain, in a simple manner and quite directly, the virial theorem mystery, and the bullet cluster issue. It might explain also the strong relative velocity of the sub-clusters of the bullet cluster, and similar issues. On cosmological scale SMT predicts a correcting factor of gravitational forces which is inversely proportional to Universe density. This leads to a de Sitter Universe with $K = 0$ and $q = -1$, which is compatible with measured values. The value of critical Universe density, fine tuning, and the issue of particle's horizon are in accordance with this de Sitter behaviour. Large scale singularities are avoided by SMT. Complete emptiness, or infinite matter densities lead to an infinite equivalent G for the former case, and to a null equivalent G for the latter case. This appears to be compatible with Mach's principle. But primordial nucleosynthesis is not predicted by SMT. This shows that, however, a more sophisticated model could be required in order to model the microscopic scale. SMT might explain heterogeneities of large scale structure and galaxy formation. This is because the predicted time since last scattering is 7 times greater than with ΛCDM. But this is mostly because with SMT, the effect of matter density is independent of the scale factor. An explanation of the voids emptiness might also be given by the prediction of a specific equilibrium. Galaxy

speed profiles are complex to work on because they need an important and detailed experimental data. They also require a huge amount of work. But the predicted speed profiles seems to be closer to experimental ones than Newton's law prediction. Varying SMT parameters, each kind of experimental speed profile might be actually retrieved by a simulation of a virtual galaxy. Even very flat curves of giant galaxies seems to be retrieved. The structure and dynamic of the galaxies seem compatible with experimental data. An unexpected prediction is also found by the model's simulations: ring galaxies are easily created by SMT specific dynamic, in a stable state. Their structure, frequency and age might be in accordance with experimental data. The ≪Local Void≫: challenge might be solved qualitatively as well as the ≪lower the surface brightness of a system, the larger its mass discrepancy≫. SMT predicts exactly the same behavior as GR, but with a possibly different and constant value of G, in each cases where matter density stays constant (evaluated in the 15 kpc ray SMT sphere). Conversely in each case in which this matter density consistently varies, SMT predicts a variation of G. In those cases the variation of a dilatation factor is also predicted, acting on the space components of the stress-energy tensor. This remains to be thoroughly calculated and compared with experimental data. The only required test in solar system is testing the variation of G over more than 50 000 years. Outside the solar system, testing any modified G must be done only 15 kpc beyond solar system. The Tully-Ficher law and the linear variation of galaxy mass with size are not explained. A scientific comparison of the model's predictions with experimental data must be done. And this has not even been started here. But nevertheless this work could suggest that the new kind of dynamic yielded by SMT might help to understand some of the today's gravitational mysteries.

Acknowledgements

I acknowledge discussions with Craig Sarazin.

References

[1] Brans, C. H.: The roots of scalar-tensor theory: an approximate history. arXiv:gr-qc/0506063v1 (2005).

[2] Susskind, L.: String theory. Found. Phys. 43, 174–181 (2013).

[3] Gaitskell, R. J.: Direct detection of dark matter. Ann. Rev, Nuc. Part. Sci. 54, 315–359 (2004).

[4] Sanders, R. H., MacGaugh, S. S.: Modified Newtonian dynamics as an alternative to dark matter. Ann. Rev. Astron. Astrophys. 40, 263–317 (2002).

[5] Bekenstein, J. D.: Relativistic gravitation theory for the modified Newtonian dynamics paradigm. Phys. Rev. D 70, 083509 (2004).

[6] Bekenstein, J. D., Sanders, R. H.: Gravitational lenses and unconventional gravity theories. Astrophys. J. 429, 480–490 (1994).

[7] Roychoudhuri, C.: Next Frontier in physics-space as a complex tension field. J. Modern Phys., 3(10), 1357–1368 (2012).

[8] Leibovitz, J.: Dark energy as a property of dark matter. J. Modern Phys. 2(12), 1470–1479 (2011).

[9] Salgado, M., Martinez-del Rio, D.: The initial value problem of scalar-tensor theories of gravity. J. Phys.: Conference Series 91, 012004 (2004).

[10] Canzian, B., Allen, R. J., Tilanus, R. P. J.: Spiral structure of the giant galaxy UGC 2885 – H-alpha kinematics. Astrophys. J., Part 1, 406), 457–469 (1993).

[11] Bouwens, B. et al.: Photometric constraints on the redshift of z $\sim$ 10 candidate UDFJ-39546284 from deeper WFC3/IR+ACS+IRAC observations over the HUDF1. arXiv:1211.3105 [astro-ph.CO] (2013).

[12] Brammer, G. B. et al.: A tentative detection of an emission line at 1.6 μm for the $z \sim 12$ candidate UDFj-39546284. Astrophys. J. Letters, 765:L2 (2013).

[13] Gott, J. R., Gunn, J. E., Schramm, D. N., Tinsley, B. M.: An unbound Universe? Astrophys. J. 194, 543–553 (1974).

[14] de Bernardis, P. et al.: First result from the BOOMERanG experiment. Am. Inst. Phys. Conf. Proc. 555, 85–94 (2000).

[15] Riess, A. et al.: Observational evidence from supernovae for an accelerating Universe and a cosmological constant. Astron. J. 116, 1009–1038 (2009).

[16] de Bernardis, P. et al.: A flat Universe from high-resolution maps of the cosmic microwave background radiation. Nature 404, 955–959 (2000).

[17] Shectman, S. A., Landy, S. D., Oemler, A., Tucker, D. L., Lin, H., Kirshner, R. P., Schechter, P. L.: The Las Campanas redshift survey. Astrophys. J. 470, 172–188 (1996).

[18] Tully, R. B.: The local void is really empty. In IAU Symposium, J. Davies, M. Disney, (eds.), vol. 244 of IAU Symposium, 146–151 (2008).

[19] Van Albada, T. S., Sancisi, R.: Dark matter in spiral galaxies. Phil. Trans. Royal Soc. London, Ser. A 320, 447–464 (1986).

[20] Hohl, F., Hockney, W.: A computer model of disk of stars. J. Comput. Phys. 4, 306–324 (1969).

[21] Hohl, F.: Numerical experiments with a disk of stars. Astrophys. J. 168, 343–359 (1971).

[22] Yanny, B. et al.: A low-latitude halo stream around the Milky Way. Astrophys. J. 588:824–841 (2003).

[23] Rubin, V. C. et al.: Rotational properties of 21 Sc galaxies with a large range of luminosities and radii, from NGC 4605 ($R = 4\,\mathrm{kpc}$) to UGC 2885 ($R = 122\,\mathrm{kpc}$). The Astrophys. J. 238, 471–487 (1980).

[24] Peebles, P. J. E., Nusser, A.: Nearby galaxies as pointers to a better theory of cosmic evolution. Nature 465, 565–569 (2010). doi:10.1038/nature09101

[25] Tiret, O., Combes, F.: Interacting galaxies with modified Newtonian dynamics. In: Formation and Evolution of Galaxy Disks (Funes, J. G., Corsini, E. M., eds.), ASP Conf. Ser., Vol. 396, 259 (2008).

[26] de Blok, W. J. G., McGaugh, S. S.: Testing modified Newtonian dynamics with low surface brightness galaxies: Rotation Curve Fits. Astrophys. J. 508, 132 (1998).

[27] Ibata, R. A.: A vast, thin plane of corotating dwarf galaxies orbiting the Andromeda galaxy. Nature 493, 62–65 (2013).

[28] Kroupa, P. et al.: Local-group tests of dark-matter concordance cosmology. Towards a new paradigm for structure formation? Astron. Astrophys. 523, A32 (2010).

[29] Pawlowski, M., Pflamm-Altenburg, J., Kroupa, P.: The VPOS: a vast polar structure of satellite galaxies, globular clusters and streams around the Milky Way. Mon. Not. R. Astron. Soc. 423, 1109 (2012).

[30] Lavery, R. J. et al.: Distant ring galaxies as evidence for a steeply increasing galaxy interaction rate with redshift. Astrophys. J. 467, L1–L4 (1996).

[31] Whitmore, B. C., Lucas, R. A., McElroy, D. B. et al.: New observations and a photographic atlas of polar-ring galaxies. Astron. J. 100, 1489 (1990).

[32] Whitmore, B. C.: The shape of the dark halo in polar-ring galaxies. Astrophys. J. 314, 439–456 (1987).

[33] Ostriker, J. P., Peebles, P. J. E., Yahil, A.: The size and mass of galaxies, and the mass of the Universe. Astrophys. J. 193, L1–L4 (1974).

[34] Zwicky, F.: Die Rotverschiebung von extragalaktischen Nebeln. Act. Helv. Phys. 6, 110–127 (1933).

[35] Zwicky, F.: On masses of nebulae and clusters of nebulae. Astrophys. J. 86, 217–246 (1937).

[36] Fang, T. et al.: Confirmation of X-Ray absorption by warm-hot intergalactic medium in the sculptor wall. arXiv:1001.3692 [astro-ph.CO] (2010).

[37] Kraan-Korteweg, R. C.: Galaxies behind the Milky Way and the great attactor. arXiv:astro-ph/0006199 (2000).

[38] Markevitch, M., Gonzalez, A. H., Clowe, D., Vikhlinin, A., Forman, W., Jones, C., Murray, S., Tucker, W.: Direct constraints on the dark matter self-interaction cross-section from the merging galaxy cluster 1E0657–56. Astrophys. J. 606, 819 (2004).

[39] Clowe, D., Gonzalez, A. H., Markevitch, M.: Weak lensing mass reconstruction of the interacting cluster 1E0657-558: direct evidence for the existence of dark matter. arXiv:astro-ph/0312273v1 (2003).

[40] Clowe, D., Bradac, M., Gonzalez, A. H., Markevitch, M., Randall, S. W., Jones, C., Zaritsky, D.: A direct empirical proof of the existence of dark matter. Astrophys. J. 648, L109 (2006).

[41] Brownstein, J. R., Moffat, J. W.: The bullet cluster 1E0657-558 evidence shows modified gravity in the absence of dark matter. Mon. Not. R. Astron. Soc., 382, 29–47 (2007). doi:10.1111/j.1365-2966.2007.12275.x.

[42] Bradac, M. et al.: Strong and weak lensing united. III. Measuring the Mass Distribution of the Merging Galaxy Cluster 1ES 0657-558. Astrophys. J. 652, 937 (2006).

[43] Hayashi, E., White, S.: How rare is the bullet cluster? Mon. Not. R. Astron. Soc. 370, L38 (2006). doi:10.1111/j.1745-3933.2006.00184.x

[44] Angus, G. W., McGaugh, S.: The collision velocity of the bullet cluster in conventional and modified dynamics. Mon. Not. R. Astron. Soc. 383, 417–423 (2008). doi:10.1111/j.1365-2966.2007.12403.x.

[45] Tully, R. B., Fisher, J. R.: A new method of determining distances to galaxies. Astron. Astrophys. 54, 661–673 (1977).

[46] Famaey, B., McGaugh, S.: Modified Newtonian dynamics (MOND): Observational phenomenology and relativistic extensions. arXiv:1112.3960 [astro-ph.CO] (2012).

[47] Famaey, B., McGaugh, S.: Challenges for CDM and MOND. J. Phys.: Conf. Ser. 437, 012001 (2013).

[48] González Hernández, J. I., Rebolo, R., Casares, J.: Fast orbital decays of black hole X-ray binaries: XTE J1118+480 and A0620−00. Mon. Not. R. Astron. Soc. 438, L21 (2014).

LIST OF PARTICIPANTS

Ali Hussain Abdullah
College of Technological Studies, Bayan P.O. Box 66238, Kuwait 43753,
State of Kuwait
dralihussain(at)gmail.com

Chemseddine Ananna
Universite Abderrahmane Mira de Bejaia, Cooperative des artistes,
Sidi Ahmed Bejaia, 06000 Algeria
ananna.chemseddine(at)gmail.com

Thomas B. Andrews
1348 Grand St., Westbury, NY 11590, U.S.A.
tba(at)xoba.com

Francesco Bajardi
University of Naples "Federico II", 90145 Palermo (PA), Italy
Bajardi(at)na.infn.it

Matúš Benko
Institute of Computational Mathematics, Johannes Kepler University,
Johann-Wilhelm-Klein Strasse 64, 4040 Linz, Austria
MatusBenko(at)hotmail.com

Michal Bílek
Astronomical Institute, Czech Academy of Sciences, Boční II, CZ-141 31 Prague 4,
Czech Republic
bilek(at)asu.cas.cz

Hana Bílková
Institute of Computer Science, Czech Academy of Sciences,
Pod Vodárenskou věží 2, CZ-182 07 Prague 8, Czech Republic
hanka(at)cs.cas.cz

Łukasz Bratek
Institute of Nuclear Physics, Polish Academy of Sciences,
Radzikowskego 152, 31342 Kraków, Poland
lukasz(at)ifj.edu.pl

Salvatore Capozziello
Department of Physics, University of Napoli, Via Cinthia, Ed. N., I-80126 Napoli,
Italy
capozziello(at)na.infn.it

Giovanni Carraro
Padova University, Vicolo Osservatorio 3, I-35122 Padova, Italy
giovanni.carraro(at)unipd.it

Joerg Dabringhausen
Astronomical Institute, Faculty of Mathematics and Physics, Charles University, V Holešovičkách 2, CZ-180 00 Praha, Czech Republic
joerg(at)sirrah.troja.mff.cuni.cz

Federico Dávila Kurbán
Observatorio Astronómico de Córdoba, Laprida 854, (X5000BGR) Córdoba, Argentina
fdavilakurban(at)gmail.com

Yurii V. Dumin
P.K . Sternberg Astronomical Institute of M. V. Lomonosov Moscow State University, Universitetskii pr. 13, 119992 Moscow, Russia; Space Research Institute, Russian Academy of Sciences, Profsoyznaya str. 84/32, 117997 Moscow, Russia
dumin(at)sai.msu.ru, dumin(at)yahoo.com

Antonín Dvořák
Kovoprojekta Brno a.s., Poznaňská 22, CZ-616 00 Brno, Czech Republic
antonin.dvorak(at)centrum.cz, advorak(at)kovoprojekta.cz

Encieh Erfani
Department of Physics, Institute for Advanced Studies in Basic Sciences, No. 444, Prof. Yousef Sobouti Blvd., P.O. Box 45195-159, Zanjan, Iran
erfani(at)iasbs.ac.ir

Benoit Famaey
Observatoire Astronomique de Strasbourg, Université de Strasbourg, CNRS UMR 7550, 11, rue de l'Université, F-67000 Strasbourg, France
benoit.famaey(at)astro.unistra.fr

Michael R. Feldman
Southwest Research Institute, 7111 Santa Monica Blvd, STE B #265, San Antonio, Texas, U.S.A.
mrf(at)m--y.us

Michal Galba
Raiffeisenbank CZ, Humpolecká 1937/6, CZ-140 00 Prague 4, Czech Republic
michal.galba(at)gmail.com

Itzhak Goldman
Afeka Engineering College and Tel Aviv University, Mivtza Kadesh 38, Tel Aviv, Israel
goldman(at)afeka.ac.il

Rajendra Gupta
Macronix Research Cooperation, 9 Veery Lane, Ottawa, Canada
sonice810(at)gmail.com

Isuf Guri
Kristal University, L. 4, P. 9, Shk. 2, Ap. 6, Kukes, Albania
isuf.guri(at)yahoo.com

Moritz Haslbauer
Argelander Institute for Astronomy, University of Bonn, Auf dem Huegel 71, D-53121 Bonn, Germany
mhaslbauer(at)astro.uni-bonn.de

Clémentine Hauret
STAR-OrCA, University of Liège, Quartier Agora, 19c, Allée du 6 Août - Bat. B5c, 4000 Liège (Sart Tilman), Belgium
clementine.hauret(at)uliege.be

Maryam Hami
AstroMundus, 1134 Crest Ave, Pacific Grove, CA 93950, U.S.A.
Maryam.Hami(at)student.uibk.ac.at

David Kaftan
Nad Soutokem 1418/9, CZ-143 00 Prague 4, Czech Republic
david.kaftan(at)post.cz

Igor Dmitrievich Karachentsev
Special Astrophysical Observatory, Russian Academy of Sciences, Nizhnij Arkhyz, Zelenchukski region, Karachai-Cherkessian Republic, R-369 167 Russia
ikar(at)sao.ru

Olga Kashibadze
Special Astrophysical Observatory, Russian Academy of Sciences, Nizhnij Arkhyz, Karachai-Cherkessian Republic, R-369167 Russia
phiruzi(at)gmail.com

Claus Kiefer
Institut für theoretische Physik Universität zu Köln, Zülpicher Strasse, D-77 50937, Köln, Germany
kiefer(at)thp.uni-koeln.de

Jaroslav Klokočník
Astronomical Institute, Czech Academy of Sciences, CZ-251 65 Ondřejov, Czech Republic
jklokocn(at)asu.cas.cz

Vladimír Kocour
Faculty of Transportation Sciences, Czech Technical University, Konviktská 20, CZ-110 00 Prague 1, Czech Republic
kocouvl(at)fd.cvut.cz

Michal Křížek
Institute of Mathematics, Czech Academy of Sciences, Žitná 25, CZ-115 67 Prague 1, Czech Republic
krizek(at)cesnet.cz, krizek(at)math.cas.cz

Pavel Kroupa
University of Bonn, Helmholtz-Institut für Strahlen- und Kemphysik, Nussallee 14–16, D-53115 Bonn, Germany
pavel(at)astro.uni-bonn.de

Frederic Lassiaille
Polytech Nice Sophia, University of Nice Sophia Antipolis, Nice, France
lumimi2003(at)hotmail.com

Federico Lelli
European Southern Observatory, Headquarters Germany, Karl-Schwarzschild-Strasse 2, D-85748 Garching, Germany
flelli(at)eso.org

Eric J. Lerner
LPPFusion, Inc., 128 Lincoln Blvd., Middlesex, NJ, 08846-1022 U.S.A.
eric(at)lppfusion.com

František Lomoz
Sedlčany Astronomical Observatory, CZ-115 67 Sedlčany, Czech Republic
F.Lomoz(at)seznam.cz

Martín López-Corredoira
IAC, C/.Vía Láctea, s/n, E-38205 La Laguna, Tenerife, Spain
martinlc(at)iac.es

André Maeder
Geneva Observatory, 19, chemin des Marais, CH-1234 Vessy, Switzerland
Andre.Maeder(at)unige.ch

Pierre Magain
University of Liege, Allée du 6 Aout, 19, B-4000 Liege, Belgium
Pierre.Magain(at)uliege.be

Dmitry Makarov
Special Astrophysical Observatory, Russian Academy of Sciences, Nizhnij Arkhyz, Zelenchukski region, Karachai-Cherkessian Republic, R-369 167 Russia
dim(at)sao.ru

Lidia Makarova
Special Astrophysical Observatory, Russian Academy of Sciences, Nizhnij Arkhyz, Zelenchukski region, Karachai-Cherkessian Republic, R-369 167 Russia
lidia(at)sao.ru

Tomáš Málek
Institute of Mathematics, Czech Academy of Sciences, Žitná 25,
CZ-115 67 Prague 1, Czech Republic
malek(at)cesnet.cz

Leonid Marochnik
University of Maryland, 6277 Cobbler Ct., Columbia MD, 21045, U.S.A.
lmarochnik(at)gmail.com

Jan Maršák
Pedagogical Institute, Prague, Czech Republic
jmarsak(at)seznam.cz

C. Johan Masreliez
3209 W. Lk. Sammamish Pkwy. NE, Redmond, Washington, D.C., 98052, U.S.A.
jmasreliez(at)estfound.org

Jan Mazanec
Vyškov Observatory, Czech Astronomical Society, Novoměstská 17, CZ-621 00 Brno, Czech Republic
jmazanec(at)email.cz

Stacy McGaugh
Department of Astronomy, Warner & Swasey Observatory,
Case Western Reserve University, 10900 Euclid Avenue, Cleveland, OH 44106, U.S.A.
ssm69(at)case.edu

Attila Mészáros
Astronomical Institute of Charles University, V Holešovičkách 2, CZ-180 00 Prague 8, Czech Republic
meszaros(at)cesnet.cz

Ondřej Michálek
Faculty of Mathematics and Physics, Charles University, V Holešovičkách 2, CZ-180 00 Prague 8, Czech Republic
ondra.mich(at)seznam.cz

Jaroslav Mlýnek
Department of Mathematics, Technical University of Liberec, Studentská 2, Liberec, Czech Republic
Jaroslav.Mlynek(at)tul.cz

Klaus Morawetz
Münster University of Applied Sciences, Stegerwaldstrasse 39, D-48565 Steinfurt, Germany; Max Planck Institute for the Physics of Complex Systems, D-01187 Dresden, Germany
morawetz(at)fh-muenster.de

Vladimír Novotný
Cosmological Section of the Czech Astronomical Society, Jašíkova 1533/4, CZ-149 00 Prague 4, Czech Republic
nasa(at)seznam.cz

Marek Nowakovski
Departamento de Fisica, Universidad de los Andes, Cra 1E, 18A-10, Bogota, Colombia
mnowakos(at)uniandes.edu.co

Wolfgang Oehm
An Quirinusbrunnen 14, D-53129 Bonn, Germany
physik(at)wolfgang-oehm.com

Tomáš Ondro
Constantine the Philosopher University in Nitra, Tr. A. Hlinku 1, SK-949 74 Nitra, Slovak Republic
tomas.ondro(at)ukf.sk

Sohyun Park
Institute of Physics, Czech Academy of Sciences, Na Slovance 1999/2, 182 21 Praha 8, Czech Republic
park(at)fzu.cz

Jaidev B. Parmar
39, Chitle Marg, Opposite Nirmal Apts, Dhantoli, Nagpur, 440012 India
jparmar(at)gmail.com

Marcel S. Pawlowski
Department of Physics & Astronomy, University of California Irvine,
2182 Frederick Reines Hall, Irvine, CA 92697, U.S.A.
marcel.pawlowski(at)uci.edu

Milan Práger
Institute of Mathematics, Czech Academy of Sciences, Žitná 25,
CZ-115 67 Prague 1, Czech Republic
prager(at)math.cas.cz

Thomas Prevenslik
QED Radiations, Kelheimer Strasse 8, Berlin, D-10777 Germany
thomas.prevenslik(at)gmail.com

Salvador J. Robles-Perez
Estación Ecológica de Biocosmología Pedro de Alvarado, 14, 06411 Medellín, Spain
Departamento de matemáticas, IES Miguel Delibes, Miguel Hernández 2,
28991 Torrejón de la Calzada, Spain
salvador.robles@educa.madrid.org

Petr Sadílek
Cosmological Section of the Czech Astronomical Society, Prague, Czech Republic
petr.sadilek(at)post.cz

Karel Segeth
Institute of Mathematics, Czech Academy of Sciences, Žitná 25,
CZ-115 67 Prague 1, Czech Republic
segeth(at)math.cas.cz

Francesco Sinigaglia
Università degli Studi di Padova, via Bracciano 12, Selvazzano Dentro, 35030,
Padova (PD), Italy
francesco.sin.96(at)gmail.com

Lawrence Somer
Department of Mathematics, Catholic University of America, Washington, D.C.,
20064, U.S.A.
somer(at)cua.cz

Alessandro D. A. M. Spallicci
Université d'Orléans, Observatoire des Sciences de l'Univers, Campus CNRS, 3A Av. de la Recherche Scientifique, F-45071 Orléans, France
spallicci(at)cnrs-orleans.fr

Alexei A. Starobinsky
L. D. Landau Institute for Theoretical Physics, Russian Academy of Sciences, 2, Kosygina, 119 334 Moscow, Russian Federation
alstar(at)landau.ac.ru

Ksenia Telikova
Ioffe Institute, Sector of Theoretical Astrophysics, 26 Politekhnicheskaya, St. Petersburg, 194021 Russian Federation
ks.telikova(at)mail.ru

Oleg Tsupko
Space Research Institute, Russian Academy of Sciences, Profsoyznaya str. 84/32, 117997 Moscow, Russia
tsupko(at)iki.rssi.ru

Tomáš Vejchodský
Institute of Mathematics, Czech Academy of Sciences, Žitná 25, CZ-115 67 Prague 1, Czech Republic
vejchod(at)math.cas.cz

Pavel Voráček
Lund Observatory, Box 43, SE-221 00 Lund, Sweden
postmaster(at)astro.lu.se (with Subject: Pavel)

Vladimír Wagner
Nuclear Physics Institute, Czech Academy of Sciences, Hlavní 130, CZ-250 68 Řež, Czech Republic
wagner(at)ujf.cas.cz

Agata Maria Wislocka
University of Innsbruck, Austria,
Nikodima Milasa 8/58, 11120 Belgrade, Serbia
agata.wislocka(at)student.uibk.ac.at

Radoslaw Jan Wojtak
Dark Cosmology Centre, Niels Bohr Institute, University of Copenhagen, Juliane Maries Vej 30, 2100 Copenhagen, Denmark
wojtak(at)dark-csomology.dk

Jana Žďárská
K Panskému poli 274, CZ-251 01 Světice, Czech Republic
jazdar(at)seznam.cz

CONFERENCE PROGRAM

Wednesday, September 26

8:00–9:00 Registration

9:00–9:10 Opening

9:10–9:15 **Michal Křížek**, Laudation to Professor Lawrence Somer on his 70th birthday

Chair: Igor Karachentsev

9:15–10:00 **Pavel Kroupa**, Modern progress in understanding the astrophysics of galaxies

10:00–10:45 **Martin López-Corredoira**, Problems with the dark matter and dark energy hypotheses, and alternative ideas

10:45–11:15 Coffee Break

Chair: Alessandro D. A. M. Spallicci

11:15–12:00 **Salvatore Capozziello**, Beyond Einstein's gravity: Addressing the missing matter problem in galaxies through a new fundamental gravitational radius

12:00–12:20 **Marcel S. Pawlowski**, Structures in the phase-space distribution of satellite galaxies as challenges to the LCDM model

12:20–14:00 Lunch Break

Chair: Lawrence Somer

14:00–14:45 **Federico Lelli**, The empirical laws of galactic rotation

14:45–15:30 **Itzhak Goldman**, Primordial cosmic turbulence : generation and implications

15:30–15:50 **Wolfgang Oehm**, Constraints on the existence of dark matter haloes by the M81 group and the Hickson compact groups of galaxies

15:50–16:20 Coffee Break

Chair: Itzhak Goldman

16:20–16:40 **Joerg Dabringhausen**, Early-type galaxies without non-baryonic dark matter

16:40–17:00 **Moritz Haslbauer**, Galaxies lacking dark matter in the Illustris simulation

17:00–17:20 **Yurii V. Dumin**, Can the dark-matter deficit in the high-redshift galaxies explain the persistent discrepancy of Hubble constants?

17:20–17:40 **Michael Feldman**, Pushing PPN

17:40–18:00 **Eric J. Lerner**, Observations in multiple data sets vs concordance cosmology

18:00–18:20 **Michal Křížek**, Ten arguments against dark matter

---

Thursday, September 27

Chair: André Maeder

9:00–9:45 **Alexei A. Starobinsky**, Inflationary models: present status and future perspectives

9:45–10:30 **Leonid Marochnik**, Dark energy and inflation from gravitational waves

10:30–10:55 Coffee Break

Chair: Alexei A. Starobinsky

10:55–11:15 **Yurii V. Dumin**, Cosmological inflation from the quantum-mechanical uncertainty relation

11:15–12:00 **Salvador J. Roblez-Perez**, Effects of inter-universal entanglement on the state of the early universe

12:00–12:20 **Klaus Morawetz**, Nonlocal quantum kinetic theory and dynamical constraints on phase transitions in the early universe

12:20–14:00 Lunch Break

Chair: Martín López-Corredoira

14:00–14:45 **Benoit Famaey**, Alternatives to CDM in the light of the mass discrepancy-acceleration relation

14:45–15:30 **Igor Karachentsev, Ksenia Telikova**, Stellar and dark matter density in the local universe

15:30–16:00 **Lidia Makarova**, Dwarf satellites in the Local Universe: insights to the cosmology

16:00–16:30 **Dmitry Makarov**, Multiparametric Tully-Fisher relation for late type edge-on galaxies

16:30–17:00 Coffee Break

Chair: Michal Křížek

17:00–18:00 **André Maeder**, Glaciers, geysers, dry rivers, volcanoes on Mars. Was there a beginning of life? **(Public lecture)**

Friday, September 28

Chair: Pavel Kroupa

9:00–9:45 **Alessandro D. A. M. Spallicci**, Perspectives for astrophysics and cosmology from non-Maxwellian light

9:45–10:30 **Łukasz Bratek**, Lower bound estimates for the Milky Way mass from various observables

10:30–11:00 Coffee Break

Chair: Lidia Makarova

11:00–12:00 **André Maeder**, Scale invariant theory and dark matter, observational tests

12:00–12:15 **Pierre Magain, Clémentine Hauret**, Could the dark matter problem be solved without dark matter nor alternative theories?

12:15–14:00 Lunch Break

Chair: Dmitry Makarov

14:00–14:45 **Stacy McGaugh**, Cosmic signatures of scale-invariant dynamics

14:45–15:15 **Oleg Tsupko**, Analytical investigation of black hole shadow

15:15–15:30 **Thomas Prevenslik**, Cosmology and redshift in cosmic dust

15:30–15:45 **Radoslaw Jan Wojtak**, Observational constraints on redshift remapping and its correspondence to conformally Friedmann-Lemaître-Robertson-Walker cosmologies

15:45–16:00 **Attila Mészáros**, Classification of distances in cosmology

16:00–16:30 Coffee Break

Chair: Yurii V. Dumin

16:30–16:45 **Frederic Lassiaille**, Surrounding matter theory

16:45–17:00 **Olga Kashibadze**, Kinematic study of the local supercluster plane

17:00–17:15 **Sohyun Park**, Nonlocal gravity for dark energy and/or dark matter

17:15–17:30 **Pavel Voráček**, Possible common solution to the problems of dark energy and dark matter in the Universe

17:30–17:45 **Rajendra Gupta**, Determination of the Mach effect contribution to the redshift

17:45–18:00 **Francesco Bajardi**, Alternative theories of gravity: gauge theories, topological theories, affine and metric theories

18:00–18:15 **Encieh Erfani**, Primordial black holes as dark matter

18:15–18:30 **Chemseddine Ananna**, Local expansion of the universe

Saturday, September 29

9:00–12:00 Excursion to the astronomical and cosmological sights of Prague guided by **Michal Křížek**. We will meet at 9:00 in front of the main gate of the Institute of Mathematics at Žitná 25.

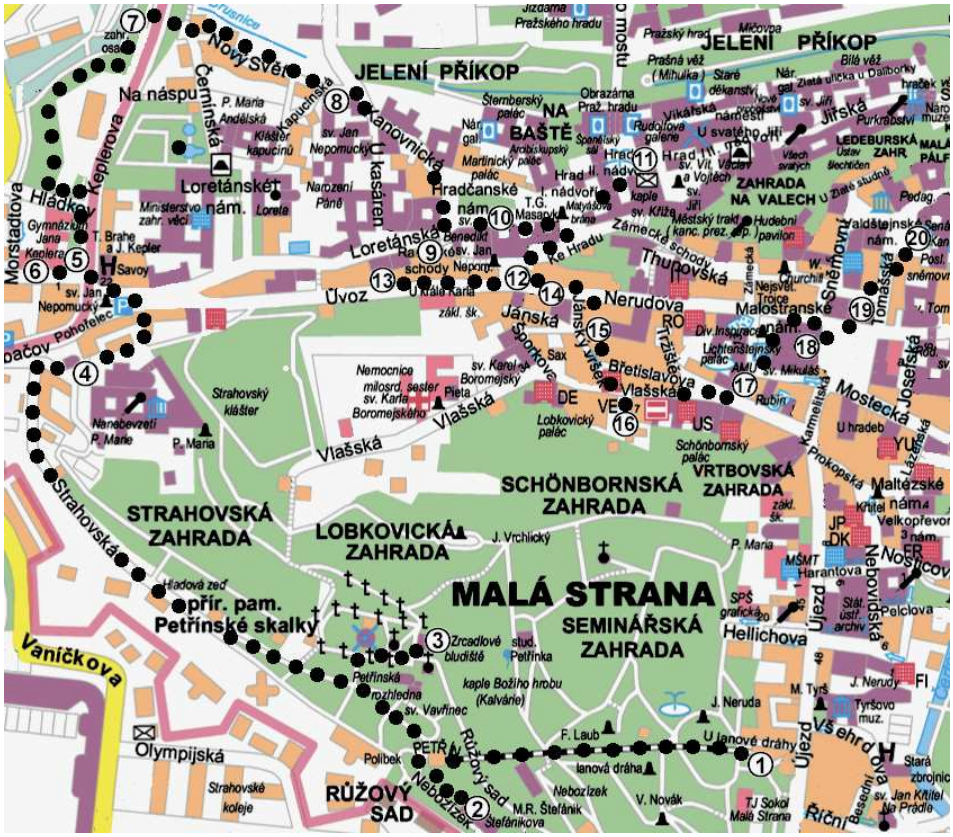

Map of the proposed walk through the astronomical and cosmological sightseeings of Hradčany and Malá Strana:

1. Funicular to the hill Petřín (formerly water funicular)
2. Štefánik Astronomical Observatory with analemma
3. Mirror Labyrinth
4. Strahov Monastery
5. Group of statues of Tycho Brahe and Johannes Kepler
6. Kepler's Gymnasium
7. Tomb of Josef Jüttner
8. Plaque of Tycho Brahe
9. Prague's Elbow Standard
10. Schwarzenberk Palace, where Tycho Brahe had his last dinner
11. Mathematical Tower
12. Sundials from 1567
13. Busts of Luna and Sun

14. House of the two Suns in Neruda street 47/233
15. Observatory of the alchemist Edward Kelley
16. Memorial Plaque of the Czech Nobel Prize Winner Prof. Jaroslav Heyrovský
17. House 21/259, where the Danish astronomer Theodor Brorsen lived
18. Faculty of Mathematics and Physics of Charles University no. 5/240
19. Sundials in the Malostranské Square
20. Astronomical corridor in the Valdštejn Square

For more details see A. Šolcová and M. Křížek: Pokroky Mat. Fyz. Astronom. **52** (2007), 127–141, available at `www.dml.cz`.